



HAL
open science

Thermo-elasto-plastic uncoupling model of width variation for online application in automotive cold rolling process

Quang Tien Ngo

► **To cite this version:**

Quang Tien Ngo. Thermo-elasto-plastic uncoupling model of width variation for online application in automotive cold rolling process. Mechanics of materials [physics.class-ph]. Université Paris-Est, 2015. English. NNT : 2015PESC1063 . tel-01220524

HAL Id: tel-01220524

<https://pastel.hal.science/tel-01220524>

Submitted on 26 Oct 2015

HAL is a multi-disciplinary open access archive for the deposit and dissemination of scientific research documents, whether they are published or not. The documents may come from teaching and research institutions in France or abroad, or from public or private research centers.

L'archive ouverte pluridisciplinaire **HAL**, est destinée au dépôt et à la diffusion de documents scientifiques de niveau recherche, publiés ou non, émanant des établissements d'enseignement et de recherche français ou étrangers, des laboratoires publics ou privés.

Paris-Est University

Doctoral School of Sciences, Engineering and Environment

Thesis

for obtention of Doctor of Science of Paris-Est University

<p>Thermo-elasto-plastic uncoupling model of width variation for online application in automotive cold rolling process</p>

presented on 30th March 2015 by

NGO Quang Tien

to the jury composed of

Pierre MONTMITONNET	<i>Professor, CNRS Research Director Cemef - MINES ParisTech</i>	President
Habibou MAITOURNAM	<i>Professor, Mechanical Unit Director ENSTA ParisTech</i>	Rapporteur
Ahmed BENALLAL	<i>Professor, CNRS Research Director LMT - ENS Cachan</i>	Rapporteur
Nicolas LEGRAND	<i>PhD, Research & Development Engineer ArcelorMittal USA</i>	Examiner
Alain EHRLACHER	<i>Professor, GMM department Director ENPC ParisTech</i>	Director

Abstract

In order to save material yields in cold rolling process, the thesis aims at developing a predictive width variation model accurate and fast enough to be used online. Many efforts began in the 1960s in developing empirical formula. Afterward, the Upper Bound Method (*UBM*) became more common. [Oh 1975]'s model with 3D "simple" velocity field estimates well the width variation for finishing mill rolling conditions. [Komori 2002] proposed a combination of fundamental ones to obtain a computer program depending minimally on the assumed velocity fields. However, only two fundamental fields were introduced and formed a subset of the "simple" family. [Serek 2008] studied a quadratic velocity family that includes the "simple" one and leads to better results with a higher computing time.

Focusing on *UBM*, the first result of the thesis is a 2D model with an oscillating velocity field family. The model results to an optimum velocity that oscillates spatially throughout the roll-bite. The optimum power and the velocity field are closer to *Lam3-Tec3* results than the "simple" one. For 3D modelling, we chose the 3D "simple" *UBM* and carried a comparison to the experiments performed at ArcelorMittal using narrow strips [Legrand 2006]. A very good agreement is obtained. Further, a new *UBM* model is developed for a crowned strip with cylindrical work-rolls. It shows that the width variation decreases as a function of the strip crown and the results match well those of *Lam3-Tec3*. However, the *UBM* considers only a rigid-plastic behaviour while in large strip rolling, the elastic and thermal deformations have important impacts on the plastic one. There exist some models considering these phenomena [Counhaye 2000, Legrand 2006] but they are all time-consuming. Thus, the idea is to decompose the plastic width variation into three terms: total, elastic and thermal width variations through the plastic zone that are determined by three new models. The simplified roll-bite entry & exit models allow estimating the elastic and plastic width variations before and after the roll-bite. They give equally the longitudinal stresses defining the boundary conditions for the roll-bite model which is indeed the 3D "simple" *UBM* approximating the total width variation term. Moreover, with the plastic deformation and friction dissipation powers given by the same model, the thermal width variation term is also obtained. The width variation model, called *UBM-Slab combined* is very fast (0.05s) and predicts accurately the width variation in comparison with *Lam3-Tec3* (<6%).

Résumé

Dans le but d'optimiser la mise aux milles au laminage à froid, la thèse consiste à développer un modèle prédictif de variation de largeur à la fois précis et rapide pour être utilisable en temps réel. Des nombreux d'efforts ont commencé en 1960s en développant des formules empiriques permettant d'estimer la variation de largeur au laminage. Mais par la suite, la Méthode des Bornes Supérieures (MBS) est devenue la plus connue grâce à sa simplicité et efficacité. A ce sujet, il sera un manque de ne pas parler de [Oh 1975] avec le champ de vitesse 3D "simple", [Komori 2002] avec une méthode de combinaison des champs de vitesse et [Serek 2008] avec le champ de vitesse quadratique.

En approfondissant la méthode, le premier résultat obtenu dans la thèse est un modèle 2D (MBS) avec des champs de vitesse oscillante. Ce champ de vitesse particulier a abouti à des résultats (puissance, vitesse...) plus proches de ceux de *Lam3-Tec3* que d'autres champs de vitesse étudiés dans la littérature. Pour une modélisation de variation de largeur, j'ai choisi la MBS avec la vitesse 3D "simple" et obtenu un très bon accord avec les expériences réalisées sur des produits étroits à ArcelorMittal [Legrand 2006]. En outre, un nouveau modèle MBS est développé pour une bande bombée et des cylindres droits. Les résultats montrent que la variation de largeur diminue avec la bombée de la bande et correspondent bien à ceux de *Lam3-Tec3*. Cependant, la MBS admet un comportement rigide-plastique tandis qu'au laminage des bandes larges les déformations élastique et thermique ont des impacts importants sur la déformation plastique. Afin d'obtenir un modèle rapide, l'idée a été de décomposer la variation de largeur plastique en trois termes: les variations de largeur totales, élastique et thermique et les déterminer par trois nouveaux modèles simplifiés. Les deux premiers permettent d'estimer les variations de largeur élastique et plastique en amont et en aval de l'emprise. Ils donnent aussi les conditions aux limites au modèle d'emprise qui est en effet la MBS avec le champ de vitesse 3D "simple" permettant d'estimer la variation de la largeur totale. En outre, avec les puissances de déformation et de dissipation plastique de frottement données par le même modèle, la variation de largeur thermique est également obtenue. Le modèle de variation de largeur est donc appelée *UBM-Slab combiné*, très rapide (0,05 s) et prédit avec précision la largeur de variation par rapport à *Lam3-Tec3* (<6%).

Thanks

I would like to acknowledge everyone who has assisted me throughout my doctoral studies over the years.

Firstly, I would like to give special thanks to my thesis director, professor Alain EHRLACHER (Navier laboratory - ENPC, Paris-Tech) who accepted me to perform this thesis in a particular financial condition. Then, he always directed and advised me with excellently creative ideas allowing me to advance on the topic. In addition, I am extremely grateful to him for his the encouragements at numerous difficult moments during the thesis. Without such supports I could have never completed the thesis successfully as it is.

A sincere thank to my industrial advisor Nicolas LEGRAND (ArcelorMittal Global Research & Development) for his guidance and orientation that inspired my works and developments. He is also the person who initiated, constructed the subject and supported me to perform this thesis.

I would like to appreciate Pierre-Stéphane MANGA, manager of *Cold plant* service and Marie-Christine REGNIER, manager of *Downstream Processes* department who always made the best conditions for me to work on the thesis. My sincere thanks to my previous managers Akli ELIAS and Daniel LAUNET as well as to ArcelorMittal direction for their agreement and support to this project. Thanks to Camille ROUBIN, Maxime LAUGIER and Eliette MATHEY and all my other colleagues for their prestigious technical exchanges which strongly enriched me about rolling process culture.

I highly appreciated professor Ahmed BENALLAL at LMT - ENS Cachan, CNRS Research Director and professor Habibou MAITOURNAM, Mechanical Unit Director at ENSTA for accepting to be my thesis rapporteurs as well as for their careful lecture and very worthy recommendations. I would like to acknowledge professor Pierre MONTMITONNET, CNRS Research Director, Cemef - MINES ParisTech for agreeing to be the committee president.

Very special thanks to my parents, my sisters and my brother as well as all my friends for their inducement and expectation that became my great motivation to become doctor.

I express, finally my all appreciation to my wife and my two daughters for supporting all my endeavours. They are my daily inexpiable sources of motivation.

THANKS

THANKS

Long abstract

Objective

Cold rolling of flat products is nowadays one of the main forming processes in metallurgical industry. The process geometry seems simple but its control requires the understanding of intricate thermo-mechanical aspects. In cold rolling process, due to the reduction in thickness the strip width is also changed. It is observed that in most of the cases the strip width decreases. And this width variation can be up to more than 10mm while it is not predicted in the production plants. By consequence, the plants produce usually an over-width in order to ensure the customer requirement and this over-width leads to an important over-cost of the production.

One solution to reduce the over-width consists in using a predictive model of width variation for each process in general and for cold rolling in particular. Such a model enables to determine the necessary width at the entry of cold rolling process to produce the required width. However, the over-width is not eliminated. It is still necessary to take an over-width due to the uncertainty of the model. Therefore, the more accurate the model the lower the unavoidable over-width. That means, even with a predictive model the production is set up to get an over-width in most of the cases and an under-width otherwise. In addition, products provided by hot rolling mill have usually different width in comparison with what the cold rolling mill requires and it varies all along the product. It is, thus also benefiting to adjust online the width in cold rolling process by varying some rolling parameters. For these reasons, the thesis aims at developing a predictive width variation model for cold rolling process which is accurate and fast enough to be used in real-time production.

Bibliographic reviews

2D simplified models in literature

In the beginning of the 20th century when the computer science notion had never ever existed, there were many efforts to develop analytical rolling models. The two famous families of models are slab method based on the well-known equilibrium equations pioneered by [113] in 1925 and Orowan's theory [86] considering the inhomogeneity of stresses across strip thickness. Around the 1950s, simplified methods were introduced in order to take into account the strip elastic deformation [16, 17] before that Cosse [27] proposed the first complete elasto-plastic model in 1968.

In parallel with the developments of models for strip deformation, there exist equally diverse models for the work-roll deformation. The very first one, Hitchcock's model [46] considers that the deformed work-roll remains circular with a higher diameter. This model is still used today by a large number of models for industrial rolling preset. It is modified in 1952 by [17] to take into account influence of the elastic deformation areas. Later, in 1960 [52] proposed to determine the deformation of each point on the surface of the roll by a sum of influence function of each finite element with a specific pressure distribution. The method approaches accurately the work-roll profile. Fleck and Johnson [36] investigated on thin strip rolling and were the firsts who consider the existence of elastic deformation areas inside the roll-bite (the strip deformation is elastic and plastic alternatively) as well as the existence of a neutral zone instead of a neutral point previously. This model is a significant progress to approach rolling process of very thin strip such as packaging products.

With variation models in literature

Concerning existing models of width variation in rolling process, important effort began in the area of the 1960s in developing empirical formula to predict the width variation - [115, 104, 43, 14]. Afterward, with the appearance of computer science there existed many analyses using *FEM* for flat and shape rolling such as [77, 78, 54] where the shape and the spread are predicted and [76] where a complete thermo-mechanical solution could be found. In order to reduce the computing time certain authors, based on the Upper Bound Method (*UBM*), developed numerical method for integration which is similar to *FEM*, [58, 1]. The *UBM* became more and more common to approach the width variation problem thanks to its simplicity and rapidity. In addition, unlike the empirical models mentioned above, the *UBM* is physical and fully predictive.

2D *UBM* models for rolling process

As for *UBM*, that is an extremum principle for perfectly plastic solids formulated by [91] which states that among all kinematically admissible strain rate fields the actual one minimizes the potential power. This method is largely used to obtain approximate solution to forming processes problems. By nature, the *UBM* result depends strongly on the choice and the construction of velocity fields. In the literature, there exist two categories of velocity fields. The first one considers rigid bodies motions (called also slip lines) and the second one includes continuous velocity fields to model the plastic deformation zone. In 1973, Johnson and Mellor [51] analyzed strip rolling by the unitriangular velocity field based on the curvilinear triangle, opening a new avenue of approach for the *UBM*. In 1986, Avitzur and Pachla [10] introduced the concept of neighboring rigid body zones which were applicable to strip drawing, extrusion, forging, rolling, drawing, cutting processes. Camurri and Lavanchy [22] developed in 1984 a velocity fields with multitriangles slip lines. This model has been reanalyzed by Avitzur, Talbert and Gordon [12] by using the concept presented in [10]. With multitriangular velocity field, the meaning of the neutral region becomes evident. That is one of triangular regions that rotates with the same rotational velocity as the work-roll. This model allows improving the optimum power but the resolution of optimization problem becomes however much more complicated in comparison with the unitriangular one.

On the subject of continuous category, around 1963 Avitzur [5, 6, 7] proposed the "eccentric" velocity field. The author defined the arcs connecting any two symmetrical points on the opposing rolls. These arcs are eccentric and each one meets the roll surfaces at right angles. The velocity of each material point on an arc is on the direction of the its radius. With this velocity field, Avitzur obtained an analytical solution to the power optimization problem by assuming small angle approximation. In 2001, Dogruoglu [31] based on flow function concept, introduced a method for constructing kinematically admissible velocity field by pre-assuming the form of the flow lines. In one of his applications, the flow lines are chosen being "elliptical" and led to an optimum power that is smaller (better) than that obtained by the eccentric velocity field. Later, Bouharaoua and al [18] by assuming that a material cross section stays vertical all along the roll-bite (equivalent the slab method assumption), obtained a velocity field called "simple" one. In the present thesis, we demonstrate that this field and the elliptical one are exactly the same in the case of circular work-roll.

Rigid-plastic 3D *UBM* models for prediction of width variation

In 1975, Oh & Kobayashi [83] are two of the pioneers who applied the *UBM* to 3D rolling process analysis. The authors supposed a 3D "simple" velocity field which is in the analogy of the 2D "simple" one. The longitudinal velocity is constant on an across section and the vertical and lateral velocities are linear in the thickness and width directions correspondingly. In 2002, K. Komori [59] proposed to represent the velocity field as a linear combination of predefined fundamental ones. With this new method of analysis, the structure of the computer program depends minimally on the assumed kinematically admissible velocity fields. Nevertheless, it is not so easy to propose fundamental velocity fields. In the article, only two fundamental fields are mentioned for demonstration. Moreover, in the present thesis, we brought out that Komori's velocity field [59] is indeed included in the "simple" family. Later, Serek [99] proposed a method for constructing kinematically admissible velocity fields by means of Dual Stream Function (DSF). This DSF was introduced by [117] allowing to express the three velocity components as functions of two scalar fields and the incompressibility condition is satisfied. The rigid plastic boundary at the inlet zone is quadratic instead of a plane section by the "simple" velocity field. The results obtained from the analysis are compared with experimental results and a good agreement is found confirming the *UBM* efficiency to approach the width variation in rolling.

Achievements

2D *UBM* analysis and oscillation phenomenon of mechanical fields in rolling process

As mentioned above, Dogruoglu's method allows determining the velocity field based on the predefined stream lines. However, it is very difficult to imagine a very good and complete flow lines. For this reason, until today, except circular and elliptical flow lines, there does not exist any other imagined flow lines pattern to approach rolling process. In the chapter 4 we presented a method for constructing kinematically admissible velocity fields based on the DSF method. Any kinematically admissible velocity field can be given as the sum of the "simple" (or elliptical) one and an additional term. By observing that the equations of kinematically admissible conditions of the additional term are closely similar to the wave propagation ones, we proposed a new family of "oscillating" velocity fields. Further, applying the *UBM* to this new velocity family results to an optimum velocity that oscillates spatially throughout the roll-bite with pseudo-period equal to the local strip thickness. The rolling power obtained with this oscillating velocity field is smaller than the one with the simple (elliptical) velocity field. The results of this model match very well those obtained by *Lam3-Tec3* in terms of velocity field, plastic deformation zone and flow lines. As a result of the *UBM* model as well as *Lam3-Tec3*, the mechanical fields heterogeneity is non-linear, quasi-sinusoidal across the strip thickness. Whilst this heterogeneity remains little investigated.

Rigid-plastic 3D *UBM* model for flat strip

Applying the method proposed in the chapter 4 any 3D velocity field is also composed of 3D "simple" one and an additional term. The characteristics of this additional term are analyzed. Nevertheless, in order to keep a fast computing time of the power optimization resolution, we carried out the study of width variation using the 3D "simple" velocity field. The integrations are done using Gauss's method allowing accelerating the computing time. A comparison with experiments has showed a very good coherence. These experiments have been performed in ArcelorMittal pilot mill with relatively narrow strips ($w_e \simeq 60 - 70mm$).

In addition, with this 3D "simple" *UBM* model, an analysis has been realized and pointed out the effect of rolling parameters on the strip width spread. As results for a narrow strip, the width spread increases strongly with an increase in the reduction and falls down exponentially as a function of the strip entry width. It grows almost linearly as the roll radius increases and decreases with an increase in the entry or exit tensions. These results are coherent with existing works in the literature.

Rigid-plastic 3D *UBM* models for crown strip

Some studies using a mixture of analytical and numerical methods [109, 73, 3, 30, 29] pointed out that for thin strip rolling, the spread is small. Nevertheless, these studies showed out that the exit thickness profile of the strip (closely linked to the strip flatness) can influence the strip lateral spread.

Interested in this phenomenon, a new *UBM* approach is developed for cold rolling of strip with initial thickness crown while the work-roll is considered rigid and perfectly cylindric. First, an analysis is proposed to study kinematically admissible velocity fields in supposing some hypotheses. As the geometry of the strip is more complex than the case of flat strip rolling, the roll bite is divided into three areas in which the velocity field is different. The model shows that the width variation decreases with an increase in the strip initial crown. These results match very well those obtained with *Lam3-Tec3*. Moreover, as can be noted, the strip crown increases the strip thickness reduction is higher at the strip center than at the edges that leads to a flatness defect called "center wave". Thus, the more the strip crown, the more "center wave" and the smaller the strip spread that can even be negative (necking).

UBM - Slab combined model to predict thermo-elasto-plastic width variation in industrial conditions

As previously seen, the *UBM* model for flat and crowned strip in rolling process match well the experiments on pilot mill as well as *Lam3-Tec3*. However, it is worth to highlight that the *UBM* assumes a rigid-plastic behavior of the strip that is justified for narrow strip rolling because the elastic width variation are negligible. On the opposite, in automotive industrial rolling condition the strip is large and the elastic width variation which is proportional to the strip width is no longer negligible. This elastic deformation is reversible but it has important impact on the plastic one. In addition, friction and plastic deformation powers heat up the strip. The material is, thus dilated in the width direction

but it can not because of the contact friction with the roll. That creates compression plastic deformation - called thermal contraction. After a bibliography review a new width variation model for online applications is developed taking into account the effects of elastic and thermal deformations in addition to the width variation of *UBM* for flat strip rolling mentioned above.

An analysis of *Lam3-Tec3* simulations about the impact of elastic and thermal deformation leads to a conclusion that the elastic deformation as well as the thermal dilatation of the strip in the roll-bite create a plastic deformation of a same amplitude but with an opposite sign. By consequence, the plastic width variation can be decomposed by three terms: the total width variation in the roll-bite, the elastic and the thermal width variations between the first and last points of plastic deformation. In order to determine these three terms, we develop simplified models for the entry, exit and inside the roll-bite as follows.

Simplified models for the entry and exit of the roll-bite: By assuming a homogeneous stress in thickness as the slab method, new simplified models are developed and allow to approximate the solution of strip deformation before and after the roll-bite. In other words, the models give us the spring back width variation at the roll-bite exit and the compression width variation at the entry. They give equally an approach of longitudinal stress just before and after the roll-bite area defining the boundary conditions for the roll-bite model.

Simplified model for the roll-bite: Thanks to the understanding of the impact of elastic and thermal deformation, the total width variation in the roll-bite is estimated close to the rigid-plastic width variation. This term can be, thus determined by the rigid-plastic *UBM* with 3D "simple" velocity field developed in the previous chapter. The boundary conditions (longitudinal stress tensor) at the roll-bite entry and exit are given by the roll-bite entry and exit models instead of entry and exit tensions initially imposed. Moreover, as the plastic deformation and friction dissipation powers are also determined by this model, the increase of strip temperature and the thermal width variation term are therefore determined. The width variation model is hence completed. This simplified thermo-elasto-plastic width variation model is called the **UBM-Slab combined model**.

Fast computing time enables online applications: As the model for roll-bite entry is completely analytical and the exit one is quasi-analytical, the main computing time is related to the roll-bite model - the rigid-plastic *UBM*. Thanks to the analytical development of the powers computation the total computing time of the width variation model (in C++) is less than 0.05s (CPU: Intel Core I5-4200M, 250GHz) enabling online applications such as preset or dynamic control.

Good prediction width variation: A comparison between the UBM-Slab combined model and *Lam3-Tec3* is performed and a very good agreement is observed. The total plastic width variations obtained with the two models are very closed (less than 6% for stands 1, 2 & 3 and about 10% for the last stand making very small reduction). Finally, the UBM-Slab combined model allows studying the influence of rolling parameters not only on the final width variation but also on each contributing terms (roll-bite width variation, elastic or thermal deformation contributions) for a deeper understanding. The results match really well the tendencies observed in industrial data presented by some studies existing in literature [64].

Nomenclature

Symbols	Meaning
ν_r, ν	Poisson's coefficient of the roll and the strip
E_r, E	Young modulus of the roll and the strip
h_e, h_s	Strip half thickness before and after the roll-bite
$\delta = h_e - h_s$	Absolute thickness reduction
$r = 1 - \frac{h_s}{h_e}$	Relative thickness reduction
h_e^{relax}, h_s^{relax}	Strip half thickness before and after roll-bite if there is no stress in the strip
h	Strip half thickness function in the roll-bite
h_e^{relax}, h_s^{relax}	Strip half width before and after roll-bite if there is no stress in the strip
w_e, w_s	Strip half width before the roll-bite
w	Strip half width function in roll-bite
S_e, S_s	Strip cross section before the roll-bite
S	Strip cross section in the roll-bite
x_e, x_s	x-position of entry and exit section
x_n	x-position of the neutral point
h_n	Strip half thickness at the neutral point
θ	Position angle
θ_e, θ_n	Position angle at roll-bite entry and at neutral point
V_e, V_s	Strip velocity before the roll-bite
V_c	Peripheral velocity of the roll
F_e, F_s	Entry and exit tensions (N)
T_e, T_s	Entry and exit average stress (Mpa)
t_e, t_s	Entry and exit adimensional average stress
R, R_{def}	Work-roll initial and deformed radii
μ, m	Coulomb and Tresca friction coefficients
$\sigma_0, k = \frac{\sigma_0}{\sqrt{3}}$	Strip yield stress and shear yield stress
σ_n	Contact normal pressure (positive value by convention)
τ	Contact shear stress - friction stress
C_{vol}	Material volume flow rate
L	Contact length
F	Roll force by an unit of width (N/mm)
f_s	Forward slip (%)
Tq	Roll torque by an unit of width (N.mm/mm=N.m/m)
$\underline{\xi}, \underline{u}$	Vector of displacement and vector of velocity
$\underline{\sigma}$	Stress tensor
$\underline{\epsilon}, \underline{\dot{\epsilon}}$	Strain and strain rate tensors
J_{fric}	Power consumed by friction
J_{def}	Power consumed by plastic deformation
$J_{\dot{\epsilon}}$	Power consumed by plastic deformation in the continuous velocity zones
$J_{\Delta u}$	Power consumed in the surfaces of discontinuity of velocity
J_{ten}	Power of entry and exit tensions
J	Total power
Γ_e, Γ_s	Surface of velocity discontinuity at roll-bit entry and exit
x, y, z	3 Direction coordinates : longitudinal, lateral and vertical

Contents

Abstract	0
Thanks	i
Long abstract	i
Nomenclature	v
1 Width variation problematic in steel rolling	1
1.1 Introduction to steel	2
1.2 Typical steel production route	3
1.3 Width variation problematic in cold rolling process	15
1.4 Thesis objective and approaches	19
2 Rolling process modeling reviews	21
2.1 General description of rolling problem	22
2.2 Typical tribological models	28
2.3 Typical strip models	31
2.4 Typical work-roll deformation models	45
2.5 Discussions	49
3 Upper Bound Method applied in rolling process	51
3.1 Principle of the <i>UBM</i>	52
3.2 Velocity fields with rigid bodies motions	56
3.3 2D continuous velocity fields	62
3.4 Discussions	69
4 Oscillation of mechanical fields in roll bite	71
4.1 Introduction	72
4.2 Method for constructing velocity field	72
4.3 An oscillating velocity field proposal	76
4.4 <i>UBM</i> with the oscillating velocity field	79
4.5 Comparison with <i>Lam3-Tec3</i> and other <i>UBM</i> models	86
4.6 Conclusions and perspectives	93

5	Rigid-plastic <i>UBM</i> model for width spread	97
5.1	Statistical models for width spread	98
5.2	3D rigid-plastic <i>UBM</i> for width variation analysis	99
5.3	Chosen rigid-plastic model of width variation in rolling	105
5.4	Conclusions and perspectives	117
6	<i>UBM</i> for crowned strip rolling	123
6.1	Velocity field proposition	124
6.2	Calculation of the powers	129
6.3	Numerical resolution	131
6.4	Comparison between <i>UBM</i> and <i>Lam3-Tec3</i>	132
6.5	Conclusion	133
7	A thermal-elastic-plastic width model	135
7.1	Bibliographic review on width variation in industrial cold rolling	136
7.2	Analytical thermal-elastic-plastic width variation model	143
7.3	A simplified entry elasto-plastic compression model	151
7.4	A simplified elastic spring back model - elastic slab method	153
7.5	A simplified model for roll-bite	158
7.6	Summary	160
8	The <i>UBM</i>-Slab combined model validation	163
8.1	Simplified model algorithm and programming	164
8.2	Validation by comparison with <i>Lam3-Tec3</i>	165
8.3	Validation by comparison with industrial observations	168
8.4	Conclusions	171
9	General conclusions and perspectives	175
9.1	Conclusions	175
9.2	Perspectives	176
	Appendix	178
A	Numerical Gauss-Legendre integration	179
A.1	Principle	179
A.2	Applications	181
B	Calculation of powers	183
B.1	Calculation of power of plastic deformation $J_{\dot{\epsilon}}$ for the simple 2D velocity field	183
B.2	Calculation of powers for the simple 3D velocity field	185

C Experiment on narrow strips	189
C.1 Rolling parameters	189
C.2 <i>Lam3-Tec3</i> modeling	190
References	193

Chapter 1

Width variation problematic in steel rolling

The present chapter is an introduction to the subject of the thesis. In the first two sections the steel production route is presented briefly. That points out where hot and cold rolling processes are found, clarifies their roles and reason for existence. The third part presents the width variation problematic in the whole production route and the importance of predictive models for the setup of the strip width during its production. The material yield caused by over-width is the main issue for what a rapid and predictive model of width variation in cold rolling is developed. That is the goal of this study presented in the fourth section of the chapter together with the development methodology. In the last place, the fifth section demonstrates the structure of the thesis.

Contents

1.1	Introduction to steel	2
1.1.1	Steel applications	2
1.1.2	Steel and metallurgy history	2
1.2	Typical steel production route	3
1.2.1	Liquid steel	3
1.2.2	Secondary metallurgy and casting	7
1.2.3	Hot rolling plant	8
1.2.4	Cold rolling plant	10
1.3	Width variation problematic in cold rolling process	15
1.3.1	Industrial observation	15
1.3.2	Width specification using prediction models	15
1.3.3	Over-width material yield	17
1.3.4	Two ways reducing material yield	18
1.4	Thesis objective and approaches	19
1.4.1	Thesis objective - predictive model for cold rolling process	19
1.4.2	Approaches	19

1.1 Introduction to steel

1.1.1 Steel applications

Steel is one of the materials the most used over the world. Talking about steel induces thinking of strength, durability, safety and cleanliness. That is why we can find steel anywhere in our daily life. The steel applications field can be classified into five main domains.

1. **Automotive industry:** Car white body is composed of thin, flat carbon steel. High strength steel and stainless steel are used for structure, reinforcement and safety parts. Wheel and suspension parts are also made by strength steel while engine is long product steel. We can also find steel in many other pieces of a car as: tyre reinforcement (steel cord), exhaust system and decoration (stainless, aluminized or chromium steel). More than a half of car weight is made from steel.
2. **Packaging:** food containers, drink cans, liquid and gas containers. These consumable products are made from steel partly because of the steel high recyclability. It is incredibly true that drink cans made from steel could be recycled infinite of times. For this application, we use mostly thin low carbon steel resisting to high pressure. High quality of surface is required because steel is coated (health safety) and painted.
3. **Household appliances:** Many kitchen objects as oven, refrigerator, washing machine, sink... are made from painted low carbon steel, enameling steel and stainless steel. And thanks to its health safety, cleanliness and very high strength, stainless steel is most used for cooking utensils and cutlery.
4. **Construction and mechanical industry:** Thanks to very interesting ratio strength/weight and high durability, steel always keep its place in construction market among numerous number of materials. Many bridges, offshore platforms, boats and sheet pilings are made from heavy steel plates, high strength beam and wires. All rails are high carbon long steel product. Steel is also used to produce: tubes, pipes, tanks for petrol, chemical and food industries as well as transportation or specific products like pressure vessels and springs...
5. **Building:** There are more and more building with steel structure using steel beam (long product), flat panels, roofs. Different from other material stainless steel or painted and coated steel are used for decoration.

In the present thesis, we are interested in rolling process of flat carbon steel for automotive and packaging applications. Thus, after a brief history of metallurgy, the production route of these kinds of steels, considered representative for general steel production, will be presented.

1.1.2 Steel and metallurgy history

The discovery of steel: By the 11th century BC it has been discovered that iron can be much improved. If it is reheated in a furnace with charcoal (containing carbon), some of the carbon is transferred to the iron. This process hardens the metal. In addition this effect is considerably greater if the hot metal is rapidly reduced in temperature, usually achieved by quenching it in water. The new material is steel. It can be worked just like softer iron, and it will keep a finer edge, capable of being honed to sharpness. Gradually, from the 11th century onwards, steel replaces bronze weapons in the Middle East, birthplace of the **Iron Age**.

The first cast iron: Thus far in the story iron has been heated and hammered, but never melted. Its melting point (1528°C) is too high for primitive furnaces, which can reach about 1300°C and are adequate for copper (melting at 1083°C). This limitation is overcome when the Chinese develop a furnace hot enough to melt iron, enabling them to produce the world's first cast iron - an event traditionally dated in the Chinese histories to 513 BC. In this they are a thousand and more years ahead of the western world. The first iron foundry in England, for example, dates only from AD 1161. By that time the Chinese have already pioneered the structural use of cast iron, using it sometimes for the pillars of full-size pagodas.

Ironmasters of Coalbrookdale: Until the early 18th century the working of iron has been restricted by a practical consideration. The melting of iron requires large quantities of charcoal, with the result that ironworks are usually sited inaccessibly in the middle of forests. And charcoal is expensive. In 1709 Abraham Darby, an ironmaster with a furnace at Coalbrookdale on the river Severn, discovers that coke can be used instead of charcoal for the smelting of pig iron. This Severn region becomes Britain's centre of iron production in the early stages of the **Industrial Revolution**. Its pre-eminence is seen in the Darby family's own construction of the first iron bridge, and in the achievements of John Wilkinson.

Ironbridge 1779: In the space of a few months in 1779 the world's first iron bridge, with a single span of over 100 feet, is erected for Abraham Darby (the 3rd of that name) over the Severn just downstream from Coalbrookdale. Work has gone on for some time in building the foundations and casting the huge curving ribs. But in this new technology little time need be spent in assembling the parts - which amount, it is proudly announced, to 378 tons of metal.

Puddling and rolling 1783-1784: In successive years Henry Cort, an ironmaster with a mill near Fareham in Hampshire, patents two processes of lasting significance in the story of metallurgy. One is the technique which becomes known as puddling. Cort's innovation is a furnace which shakes the molten iron so that air mingles with it. Oxygen combines with carbon in the metallic compound, leaving almost pure iron. Unlike the brittle pig iron (or cast iron), this purer metal is malleable. Capable of being hammered and shaped, it is a much more useful metal in industrial processes than cast iron.

In the previous year Cort has also patented a machine for drawing out red-hot lumps of purified metal between grooved rollers, turning them into manageable bars without the laborious process of hammering. **His device is the origin of the rolling mills** which subsequently become the standard factories of the steel industry.

Steel growth since the last century: The world-wide steel industry has tremendous growth during the 20th century, from an annual production of 20 million tons of steel in 1900 to more than 1.2 milliard tons nowadays. The most important growth rate has been performed in the 50s and 60s after the Second World War when the reconstruction as well as the economy and military concurrence in many countries required more and more steel. Another fast growth period is since 2000 when emerging countries as China, India... realize incredible economic growth. During this period the steel technology has been developed with a drastic rate as the evolution of sciences, engineering technologies and computer science. It is uncountable the number of scientific articles, books, thesis as well as numerous number of patents about the steel compositions and production processes.

1.2 Typical steel production route

1.2.1 Liquid steel

There are two ways to produce liquid steel, a classic way called "primary steel route" using iron ore and the other using steel scrap called "recycling route". This section has objective to introduce typical processes of steel production, their roles and particularities explaining their existence. The physical or chemical principle of certain processes are only shortly and roughly explained but not detailed.

1.2.1.a Primary route

Coke oven and sinter plant

In a classic production route, raw iron ore follows first a sintering process to be purer. Today, after sintering the average iron ore charge varies from 70% up to 90%.

About coke, most of coke is man-made and obtained by pyrolysis of coal in regrouped furnaces in absence of air. This process, realized at about 1000°C, is called coke-making providing coke with high carbon content and few impurities. The coke is essential fuel for blast furnace thanks to its solidity, able to support charge and porosity allowing the transfer of gas and liquid through.

Blast furnace (BF) - Pig iron

BF operates on the principle of chemical reduction whereby carbon monoxide, having a stronger affinity for the oxygen in iron ore than iron does, reduces the iron to its elemental form. Chemical reactions, control of temperature and the circulation of materials in the furnace are in fact complicated. Avoiding details of what happens, a very short description can be given as follows.

The main chemical reaction producing the molten iron, that might be indeed divided into multiple steps, is:



The iron ore and coke are supplied through the top of furnace in successively forming alternative layers while the gas is flowed into furnace at the bottom (see Figure 1.1). Going up, the gas is efficiently in contact with solids all along the furnace height. As output, the *pig iron* obtained and extracted at the bottom of the furnace contains generally *Fe* (93-95%), *C* (3-5%), *Si* (0.2-0.8%), *Mn* (0.2-2%) and also *Al*, *S*, *P*...

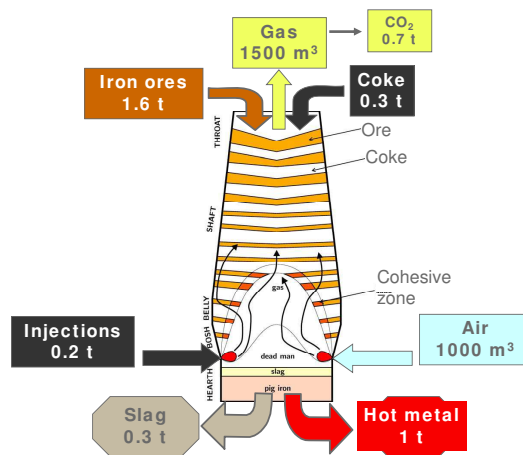
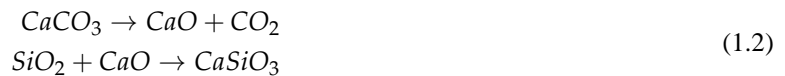


Figure 1.1: Blast furnace scheme and an approximated balance to obtain 1 ton of pig iron.

Limestone ($CaCO_3$) is provided into the top side in order to remove some impurities contained in iron ore notably silica *Si*. At the middle of the furnace, limestone is decomposed by reaction with CO_2 and then the calcium oxide obtained reacts with various acidic impurities (silica for example), to form a fayalitic calcium silicate.



Slag is the liquid mainly composed of remaining of limestone decomposition and impurities of iron CaO , SiO_2 , Al_2O_3 and MgO as well as silicates of calcium ($CaSiO_3$) of other metals ... The liquid slag floats on top of the liquid iron since it is less dense and is removed continuously from the furnace bottom. At the furnace top side, the monoxide and dioxide of carbon are evacuated in the waste gas. Figure 1.1 gives approximated quantity of main inputs and outputs corresponding to a ton of hot metal (pig iron).

Basic oxygen furnace (BOF) - converter

BF pig iron, containing 3-5% C, can be used to make cast iron but more often refined further to make steel (much less C content). Liquid steel needs to contain lower contents of C, *Mn*, *Si*. Table 1.1 shows an example of composition of input pig iron and desired composition of liquid steel.

	T	C	Mn	Si	P	S	O
	°C	%	%	%	%	%	%
Liquid pig iron	1370	4.70	0.23	0.26	0.08	0.02	0.00
Liquid steel	1650	0.05	0.10	0.00	0.02	0.02	0.05

Table 1.1: Example of composition of pig iron supplied to BOF and liquid steel obtained.

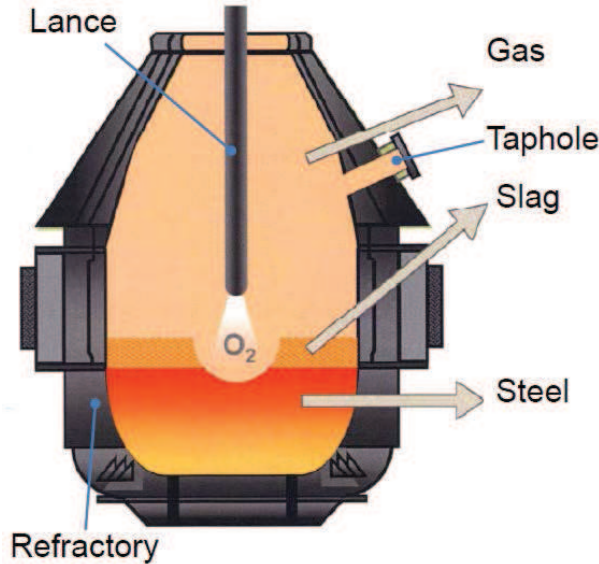


Figure 1.2: Schema of BOF principle components. BOF allows refining C content of pig iron at high temperature using oxygen.

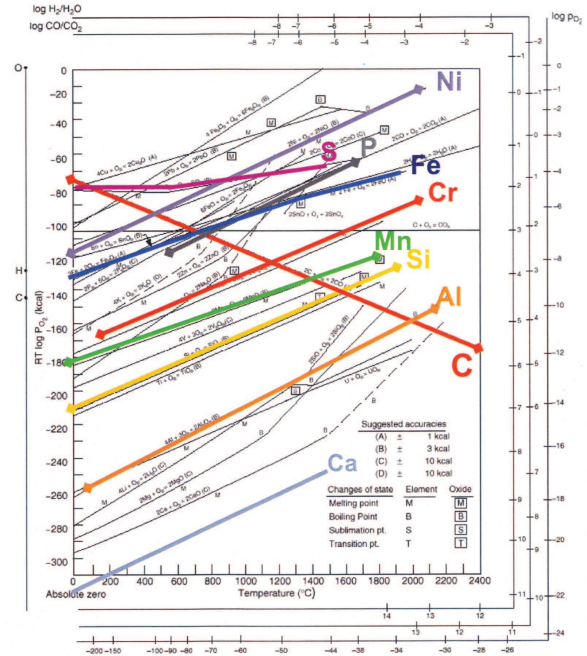
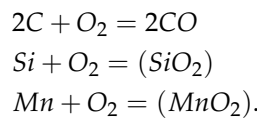


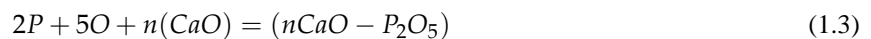
Figure 1.3: Ellingham diagram: dependence of affinity for oxygen of different elements. Carbon affinity for oxygen increases with an increase in temperature while that of metals decreases.

To do that, the molten pig iron is poured into a Basic Oxygen Furnace (BOF) where most of the remaining carbon will be removed. In a BOF, pure oxygen is blown through a long tube, or lance inserted into the furnace top side. Sometimes, for higher stirring (to get lower C content), oxygen is blown from the bottom side (see Figure 1.2).

As can be seen in Figure 1.3 that the affinity for oxygen of C at high temperature is much higher than that of Fe. Because other elements present in pig iron as Al, Mn, Si, Cr have also higher affinity for oxygen than Fe, they are equally almost removed from liquid pig iron by combining with oxygen to form oxide and stay in slag floating on the steel liquid such as:



Since S and P have similar affinity for oxygen as Fe (see Figure 1.3) they are more difficult to be removed. The solution is to add limestone to supply CaO born after decomposition of CaCO₃ (see equation 1.2). The basic reaction to eliminate P is:



a stable oxide in slag. And the desulphurization is based two reactions



1.2.1.b Recycling route

For a recycling route, the main raw material is no longer iron ore (oxide of Fe) but steel scrap with various compositions. Reducing oxides of Fe in BF and reducing C (and other impurities) in BOF are no longer necessary. Thus, instead of BF and BOF, Electric Arc Furnace (EAF) is used to melt scrap and produce directly liquid steel.

The cost of an EAF is about 8M€ (Alternating Current - AC EAF) or 23M€ (Direct Current - DC EAF) much lower than that required to build a BF (about 300M€). With lower productivity (about 0.7Mt per year), EAF is suitable for mini-mills. Invented in 1900, it had been used mainly for long products (bars, rods and small profiles) production. Today, EAF is also used to make flat carbon (thin slab casting) or heavy section products. Typically, better grades of steel products come from virgin iron ore and are rolled a great deal to fully develop internal quality and grain structure. In the market for midquality steels, the integrated can offer perhaps more than enough quality but often at too high cost. The mini-mills, in contrast, may have the right cost structure but not necessarily the right quality. By choosing suitable production route, companies can achieve a better pairing of cost and quality.

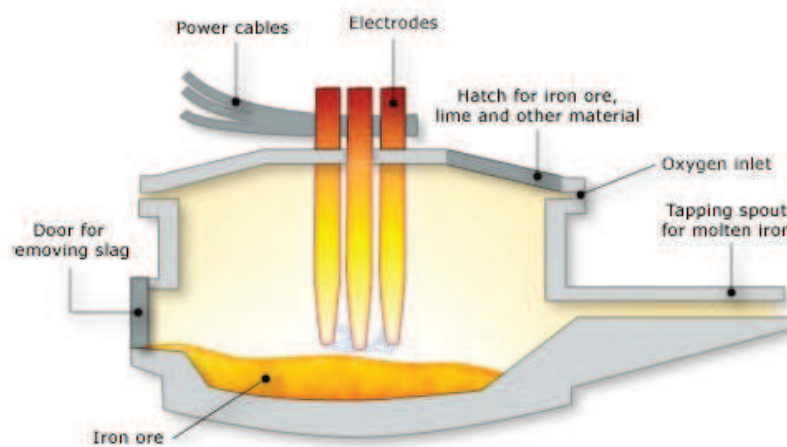


Figure 1.4: Illustrating the Electric Arc Furnace which uses scrap steel to produce pure steel.

Raw materials and elaboration

For the production of steel in a EAF, the following principal raw materials are used as feedstock:

- Recycled steel scrap
- Hot metal
- Pig iron
- Reduced iron

In general, three first materials (scrap, hot metal, pig iron) are charged into EAF before the actual elaboration starts and the reduced iron is continuously fed into the vessel during elaboration to adjust the target composition.

Heating

The EAF principle is to heat material by electric arc through the metal between a graphite electrode inside and another at the bottom of the furnace thanks to a high voltage of about 1300V ((see Figure 1.4). The heating can be divided into two steps: meltdown and super-heating. During the first phase, the electrode starts from the top of the scrap charge, goes down close to the bottom to melt little quantify of scrap and form small metal bath. The electric

energy continues to melt scrap until obtaining flat bath (end of meltdown). After this meltdown phase, there remains some unmelted scrap, the superheating (refining) consists in melt them by moving the electrode inside the furnace and use lower level of power.

Almost all materials charged into the furnace can be oxidized and hence release some energy. Iron and tramp elements when oxidized are transferred from the steel bath to the slag while carbon containing elements are converted to furnace off-gas. Chemical energy is also entered using external divides as natural gas burners to assist meltdown avoiding cold spots in the vessel and oxygen & carbon lances providing oxygen for oxidation and post combustion.

Metallurgical results obtained at the EAF

The remaining tramp elements (*Cu, Sn, Ni, Mo, Sb...*) in liquid steel depends on the scrap composition (scrap yard) while carbon and phosphorus content is result of the process (oxygen injection). Table 1.2 gives a rough idea about the composition of liquid steel obtained by EAF.

Process	Scrap charge	<i>Cu</i>	<i>Sn</i>	<i>S</i>	<i>P</i>	<i>N</i>	<i>C</i>
		ppm	ppm	ppm	ppm	ppm	ppm
EAF	Low quality	250	50	50	40	70-90	40-50
	Standard quality	150	20	30	15	70-90	
	High quality	50	10	10-20	<10	70-90	
	Scrap + few iron	<50	<10	10-20	<10	40-50	
BOF	Pig iron	20	<5	10-20	<10	<20	10-40

Table 1.2: Comparison of chemical composition of liquid steel obtained by EAF and BOF

1.2.2 Secondary metallurgy and casting

Secondary metallurgy

After BOF or EAF, the liquid steel enters into the refining process called secondary metallurgy which has primary objective to finely adjust chemical composition of steel in controlling impurities and metallic inclusions. This secondary steelmaking process is most commonly performed in ladles. The necessary alloying elements are added while the impurities are removed by deoxidation (*Al, Si*), metal/slag reaction and vacuum degassing. Tight control of ladle metallurgy is associated with producing high grades of steel in which the tolerances in chemistry and consistency are narrow.

The second objective of the process is to prepare the right temperature of liquid steel just before casting process typically about 20°C more than liquidus temperature. A too low temperature may cause risk of solidification in the ladle or tundish while a too high temperature would make uncomplete solidification producing break at the casting machine exit. The ladles are commonly equipped of small electric arc furnace that is used to regulate the liquid steel temperature, for instance to re-heat the liquid steel when the casting process is delayed.

Continuous casting

Figure 1.5 shows standard components of a casting machine. The ladles containing liquid steel are charged on the top side of the machine (feeding zone) where a rotating system allows replacing a full ladle into the position of an empty "in casting" ladle at the end of each casting "sequence". The liquid steel flows from the ladle to a tundish where the steel is well protected thermally and chemically. The tundish aims at feeding several strands in liquid steel and is a buffer tank during ladle change. It enables to control and regulate the steel flow rate in molds.

After the feeding zone, the steel comes in the molds, head zone, where heat is extracted to form primary solidified shell and give suitable geometry. Out of mold, the steel comes into solidification zone with many rolls guiding the change of direction from vertical to horizontal. The steel is solidified completely with position of the end of solidification depends on steel grade and process parameters. After an oxy-cutting process, solid steel slabs are produced with a dimension required by hot rolling plant.

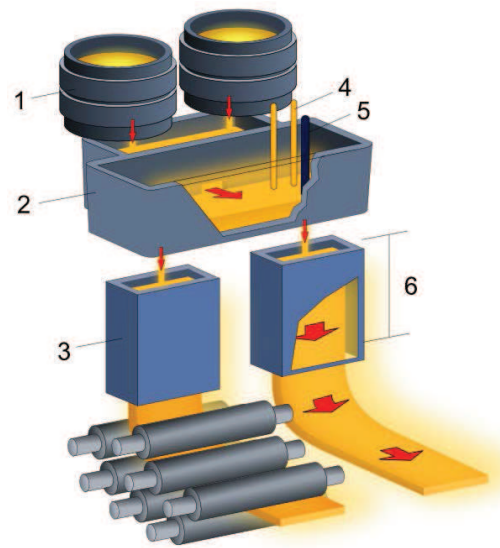


Figure 1.5: Continuous casting machine: 1-Ladle, 2-Tundish, 3-Mold, 4-Plasma torch, 5-Stopper, 6-Straight zone.

After casting machine, automotive and packaging product slabs have generally a dimension of about 5-15m (Length) x 800-2000mm (Width) x 220-260mm (Thickness) weighting from 20 to 35tons. In a same casting sequence, the slabs have same width and thickness. **It is necessary to note that casting machine only produces certain values of width, for example 800mm, 1200mm, 1600mm and 2000mm but not any desired one.**

1.2.3 Hot rolling plant

The objective of a Hot Strip Mill (HSM) is to reduce the product thickness and width while controlling the product surface quality and mechanical properties. Different installations of a HSM can be described as follows (see Figure 1.6). Hot rolling is also called hot metalworking process which consists in deforming product above the phase transformation temperature of the material because:

- at austenite phase, material is much softer
- at higher temperature, the grains deform during rolling, they recrystallize, which maintains an equiaxed microstructure and homogenous grains size.
- the phase transformation needs to be precisely performed to get desired mechanical properties. This is done the most commonly during the natural cooling at the coil park after coiling process.

In general, to maintain a safety factor a finishing temperature (end of finishing mill) is usually defined about 100°C above the phase transformation temperature.

1.2.3.a Reheating furnaces

The reheating furnace function is to heat slabs up to enough high temperature (about 1100-1300°C) depending on the steel grade by using natural and coke furnace gases. A HSM can work with 2,3 or 4 furnaces in function of the productivity. A furnace has a power of about 120MW and a capacity of about 350t/h (heating time of a slab is about 2-3h).

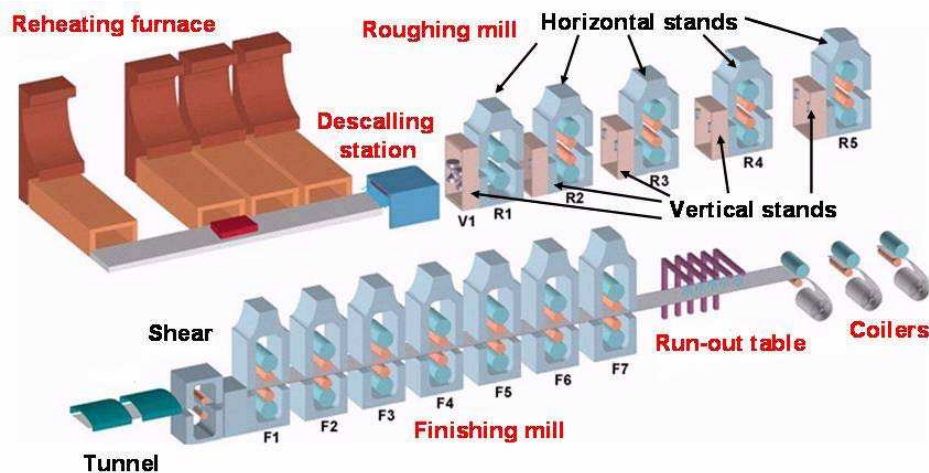


Figure 1.6: Schema of a Hot Strip Mill.

1.2.3.b Roughing mill

Before the rolling process, a descaling is necessary to remove the scale (oxide layer) forming on the slab surface in the reheating furnace. Because a thick scale layer would be broken and inserted into the steel causing surface quality defect. The slab passes firstly under two pairs of powerful spray headers that blast high-pressure water to remove the 3mm-thick scale layer. Shortly after, a relatively small 2-High rolling mill called a scalebreaker reduces slightly slab thickness to break up any scale that remains. Then sweep sprays clean away any loosened scale that remains on the slab surfaces. The transfer bar will be descaled once or twice more during roughing to remove the scale that has grown back over the some minutes spent in the roughing mill.

The roughing mill can compose of more or less five stands through which the slab goes in keeping a same direction. Sometimes, it is a reversible stand where the slab passes an impar number of times (five times for example). In any case, a roughing stand is a combination of a vertical rolling stand called **edger** aiming at reducing the slab width and a horizontal stand reducing the slab thickness. After roughing mill, the slab thickness usually decreases to about 60mm and is elongated to about 40m. **We remark that the product width is only rolled in roughing mill when the product is thick enough and in the later rolling processes variation of width is a consequence but not an objective.**

After the roughing mill, the slab is transferred to the finishing mill with a low velocity on a segment of free or motorized small rolls that is called waiting table or rollers table. And the slab is now called a transfer bar. In some necessary cases, in order to prevent the slab from radiation thermal lost we switch down a tunnel to cover entirely or partly this segment.

1.2.3.c Cropping machine

Then, the transfer bar is descaled once more to eliminate most of scale grown during transfer time and just before the finishing mill it passes into a cropping machine. Because a bad quality head-end (oval form or with ski-effect) is critical to properly threading the finishing mill and the downcoiler, and an fish-tail tail-end can mark work-roll surface, the head and tail-ends of nearly every transfer bar are cropped by a pair of large steel drums each with a shearblade extending along its length. With the bar crawling along the roller table at around 0.5-0.7m/s, some sensors detect its position and speed in order to time the crop shear drums to optimize the amount cropped.

1.2.3.d Finishing mill

One of a finishing mill functions is to reduce the product thickness to a predefined (targeted) value. As the transfer bar is enough long and it will be longer and longer (for example 600m for an exit thickness of about 3mm), the product

can be rolled at the same time in several stands increasing the productivity. In general, a finishing mill is a system including seven (more or less) successive 4-High stands forming a tandem. Between stands, there are tensiometers which allows to control the strip tension between stands making rolling process stable. A measurement of thickness is usually available at the exit of finishing mill allow to control and regulate the thickness by acting on the roll force (if hydraulic technology stand) or screw position (mechanical technology stand) to vary thickness reduction of one or more stands.

Another objective of finishing mill is to get a right temperature at its exit (entry of run-out table). That is why the exit strip temperature is measured and enables to adjust the rolling speed. In average, the rolling time of a strip is about 60-100s. It is easy to remark that the tail-end of strip is therefore colder than the head-end of about 50-70°C. In order to obtain a homogenous temperature along the strip, the finishing mill increases continually its rolling speed. This is a very common practice to compensate the temperature lost.

1.2.3.e Run-out table

Metallurgically critical to the properties of hot-rolled steel is the coiling temperature, as the coil will cool from this temperature to ambient over the course of three days, a heat treatment comparable to annealing. Coiling temperature is specified by product metallurgists to search optimal mechanical properties. Therefore the objective of the run-out table is to cool the strip from the temperature at the exit of the finishing mill to optimal coiling temperature.

The run-out table is composed of many water valves regrouped in different segment spraying the water at low pressure on the strip. Because the temperature at the exit of finishing mill can be fluctuating all along the strip. At the same time the strip speed is not controlled in the run-out table but by the finishing mill, an automatic system opening/closing the valves enables to regulate the number of opened valves to meet targeted temperature through the coil length.

1.2.3.f Coiling process

Out of the HSM, the strip is about 400-700m long and is coiled to be easily transported. Coiling temperature is a key element for metallurgical properties of material and can vary from 550°C to 800°C depending on grade.

Commonly a HSM relies on two coilers working alternatively avoiding long waiting time. A coiler begins with a pair of pinch rolls that catch the strip head-end. The head-end is deflected by a gate down to a mandrel and is guided around the mandrel, laps begin to build around the mandrel, forcing away the wrapper rolls. Once the head-end is cinched and friction and tension prevent the wraps of steel from slipping relative to the mandrel, the wrapper rolls disengage from the growing coil of steel. Before the strip tail is pulled through the pinch rolls, the wrapper rolls are reengaged. A hydraulic coil car moves into place beneath the coil, and, after rising up to support the coils bulk, strips the coil from the mandrel and places it in position. The coil is ready to be pickled and sent to customer (hot rolled product) or transported to cold rolling process (cold rolled product).

1.2.4 Cold rolling plant

Cold rolling mill has main objectives to reduce the product thickness with high surface quality, good flatness and mechanical properties. Figure 1.7 describes different processes and necessary installations of a cold rolling plant which allow to obtain these objectives.

1.2.4.a Pickling line

At the end of HSM products, coiled at high temperature (550°C-800°C) develop scale layer during the cooling time in air. Depending on the coiling temperature that the scale thickness can vary from 5µm to 20µm. In order to avoid incrustation of this scale into the steel during rolling, it is necessary to move it out thanks to acid tanks. The usual acids in pickling line are *HCl* at about 85°C or *H₂SO₄* at about 100°C.

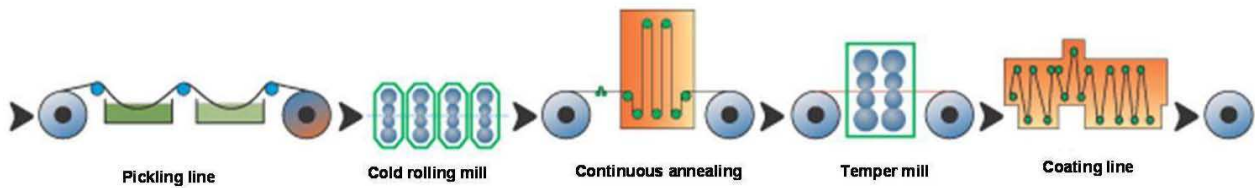


Figure 1.7: Different processes of a cold rolling plant.

At the beginning of the pickling process, a tension leveller aims at breaking the scale layer facilitating efficiency of the acid action. The tension leveller introduces tensions and alternative bending movements to deform plastically the strip. In general, the strip is elongated of about 0.5-2.0% barking more or less scale layer. An elongation of about 2% can allow to decrease twice the necessary pickling time.

1.2.4.b Side trimming

In order to eliminate edge defects that potentially make strip break in cold rolling, strip is often side trimmed before the rolling mill. And depending on steel grade and product dimension, high quality of strip edges is required to reduce the risk of work-roll mark in rolling process. The side trimming lets equally to obtain homogenous width along the strip length. However, this operation requiring a minimum cut-off width is a significant material yield source. Side trimming operation can be therefore skipped off when the risks mentioned above are estimated negligible. For automotive steel production about 60% of products are side trimmed before cold rolling mill.

1.2.4.c Cold rolling

Main objective - Thickness reduction

The main functionality of cold rolling mill is to reduce the strip thickness to the final one while providing high surface quality. The most common flat product cold rolling mills contain from 4, 5 or 6 4-High or 6-High rolling stands. For automotive product, the entry thickness varies from 2mm to 6mm for a total reduction of 40-85%.

For packaging product, the reduction in cold rolling needs to be well defined in order to reduce the planar anisotropy after annealing. This anisotropy generates a famous type of defect, called earing defect, in deep drawing process as can drawing. The anisotropy increases as a function of cold rolling reduction, then decreases and becomes zero at very high reduction. So depending on grade (especially on Carbon content) the suitable cold rolling reduction is defined, usually between 86 and 92%. After the annealing, if the cold rolled thickness is still higher than the commanded one, the strip thickness is reduced once more at the skin-pass process (see section 1.2.4.e). Many packaging products follow this production route that is called double reductions. The 1st reduction is done at the tandem cold rolling mill (before annealing process) and the 2nd reduction is done at the skin-pass rolling mill (after the annealing).

Flatness

In rolling, the strip can be deformed heterogeneously in width direction, meaning that the reduction is not homogenous. In this case, it is elongated more or less at the strip center and edges and after rolling the strip can contain important residual stress and **flatness defects**. There may be many reasons for these defects:

The first one is the very important roll force, 1000 to 3000tons that deforms the work-rolls, which are in contact with the strip, in deflexion mode, and can make reduce more thickness at strip edges than at the strip center. The material is, hence more elongated at the edge than the center which generates flatness defect called "long edge". To limit amplitude of flatness defects, bigger work-rolls should be a solution. However, that increase the contact area with the strip and increase the necessary roll force for a same thickness reduction. More clever solution is to use back-up rolls which are bigger and in contact with the work-rolls to prevent them from deflexion deformation. A stand with only a pair of work-rolls is called 2-High stand, with a pair of back-up rolls likewise is 4-High stand. The 4-High

stand is able to use smaller work-roll and therefore needs lower roll force than the 2-High one. That is the reason why in industrial flat rolling, the common stand technology is 4-High or 6-High stands. For stainless steel (very hard steel), there may be used 20-High stand, called Sendzimir stand, with several time smaller work-rolls than a typical automotive 4-High stand.

Additionally, to correct the "long-edger" flatness defect, bending force could be used to separate the ends of top and bottom work-rolls (see Figure 1.8). On the contrary, negative bending exerted to bring the work-rolls ends together should be used to correct "long-center" defect.

Another solution consists in using work-rolls designed initially with small positive (higher diameter at the center than two ends) or negative crown allowing to correct "long-edge" and "long center" defects. More recently, smart crown technology is developed to control faster and more efficiently the flatness defect. That consists in designing an intelligent work-roll profile: continues variable crown (CVC) as shown in Figure 1.9. By shifting the work-rolls, it is possible to change the gap between them and that enables to control the flatness efficiently.

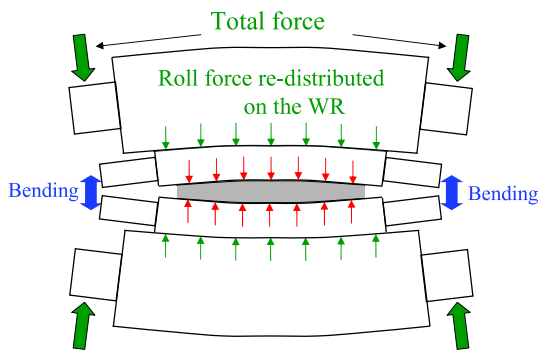


Figure 1.8: Positive bending forces are exerted to separate work-rolls ends.

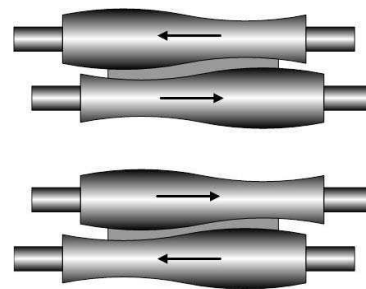


Figure 1.9: CVC rolls allow to control strip flatness.

Lubrication

In cold rolling, lubrication is an essential factor allowing to obtain a good strip surface. An insufficient quality or quantity of lubricant could create scratch defect. By decreasing the roll-strip contact friction the lubrication reduces the un-useful energy dissipated by contact friction and slows down the work-roll wear. In cold rolling process, two common techniques to apply the lubricant are direct and recirculated applications. The direct application uses less stable oil and reject it after while the recirculated system uses more stable oil and reuse it after a retreating process.

Cooling

During rolling, the electricity consumed is mostly transformed into heat distributed to the strip and the tools (work-roll, back-up roll...). In average, a cold rolling mill consumes from 15 to 20MW and is able to heat the strip and work-roll of several hundred °C. That is the reason why it is very important to cool down the work-rolls as well as the strip. Most common technology is water nozzles sprays. The work-roll cooling can be at the entry (before the roll-bite) or/and at the exit (after the roll-bite). The strip cooling is done between two stands (interstand). A bad cooling system leads to too high temperature degrading work-roll surface and creating heating mark defect on strip. That is also origins of work-roll thermal crown (more dilatation at medium of work-roll) causing "long-center" flatness defects.

Roughness control

One of qualities required by customers or by next process (galvanizing for example) is that the strip surface roughness need to be in a certain range. A too low roughness (smooth surface) makes the strip not adherent enough to paint layer. A too high roughness could increase paint consumption. In order to obtain roughness, the last stand work with rough work-rolls with a roll force defined to obtain right roughness. This stand does not aim at making reduction but at

producing strip roughness and regulating strip flatness. In the contrary, in a tin-plate tandem mill (packaging product), the last stand uses low roughness work-roll and makes high reduction.

Coupling line

The pickling and cold rolling lines can be completely separated. The coil coming from HSM is uncoiled, pickled and recoiled at the pickling line before being transported to the cold rolling mill (CRM). Then in the CRM it is uncoiled again, cold rolled and recoiled. Or the two processes are sometimes coupled where the coils are uncoiled, welded successively, head to tail, and then continually pickled and then cold rolled before being recoiled. As coupling line allows to increase productivity and decrease the transport, waiting time and other management cost, it becomes more and more frequent since the last decades.

1.2.4.d Annealing - material drawability

After being deformed in the cold rolling, the strip material is strongly work-hardened and the microstructure grains are sharply reduced in thickness direction and elongated in rolling direction. The material becomes anisotropic, hard and fragile. However, customers need high drawability steels supporting forming processes to make car pieces. Therefore, after cold rolling, the annealing is necessary to recrystallize the material making it less brittle and more workable.

Batch annealing (BA)

In BA, the coils are heated intact in small furnaces over approximately 3 days. They are usually stacked four or five high on fixed bases, covered, as shown in Figure 1.10. To prevent oxidation of the strip, the atmosphere around the strip inside the furnaces is a controlled mixture of H₂ and N₂ although hydrogen only is sometimes used because of its increased conductivity. It is usually used for packaging steels.

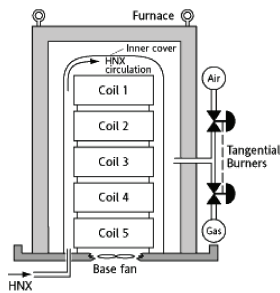


Figure 1.10: Typical batch annealing base.

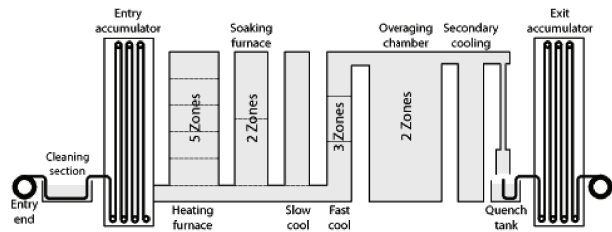


Figure 1.11: Typical continuous annealing line.

Continuous annealing line (CAL)

The CAL subjects rolled strip product to a sequence of furnaces to elevate and profile the strip temperature according to grade and dimension. Unlike BA, in CAL the strip is uncoiled, treated and recoiled in approximately 15 minutes.

Figure 1.11 shows a typical example of CAL installation. Accumulators provide storage areas between static steel coils and continuous strip running through the furnace sections. Different furnaces are necessary to give steel the desired properties by heating to particular temperatures. In the heating furnace, the product is heated to the highest temperature. Then the soaking furnace is required to maintain strip temperature that allows to finish recrystallization of the material forming more homogenous and bigger grains size. The strip is cooled down slowly and fast in the first and secondary primary cooling sections before going into the overaging chamber where the strip is maintained at an intermediate temperature eliminating carbon precipitates.

1.2.4.e Skin-pass rolling

After the annealing process, many products have abnormal work-hardening behavior with an yield plateau as shown in Figure 1.12. At the beginning of plastic deformation, the material is work-softened and not work-hardened up to certain plastic deformation. If the steel is sent directly to customers, during their forming process, the material will be deformed. In the steel, some local points will be deformed first and because of its work-softening, there will be a strong local concentration of deformation at these points. That creates heterogenous thickness in the structure and apparent surface defects when painted. Lüders defect is the demonstration [38].

Therefore, the primary functionality of a skin-pass mill called also temper mill is to suppress the yield point plateau of annealed steel by doing relatively small but enough plastic deformation in the strip. This elongation is to be defined as a function of steel grade and annealing cycle. It varies commonly from 0.5 to 2.5%.

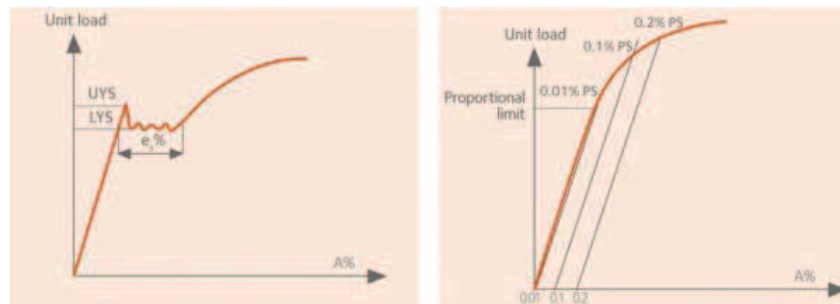


Figure 1.12: Tensile yield stress curve of an annealed steel before (left) and after skin-pass process (right).

The second objective of skin-pass rolling is to provide a strip roughness required by the customer varying from 1 to $3\mu\text{m}$. The work-rolls roughnesses are quite important and the roll force is calculated coil-to-coil (it can not be too low or too high) to succeed the roughness transfer. A temper mill aims equally at improving strip flatness thanks to small deformation that it offers to the strip and a bending system.

For automotive steel, skin-pass mill can be 1-stand mill called also stand-alone. The skin-pass mill can roll one by one the coils coming from BA and is called offline skin-pass line. And when it is combined with and continually fed by a CAL, it is called CAL skin-pass line. The skin-pass is also used in galvanizing line after galvannealing process.

On the other side, packaging products are often highly drawable after annealing. It is, thus possible to reduce their thickness to reach lower thickness range and work-harden them to get higher yield stress by having always a good final drawability. That is why the packaging skin-pass mill is usually 2-stand mill able to make from 1 to 55% of reduction to obtain the final customer thickness and provide good roughness and flatness.

1.2.4.f Coating

This is the last process giving additional properties to products as anti-corrosion, adhesion and aesthetic appearance required by every steel market. There exist different kinds of coating lines adapted to different steels and customers. Most of automotive products are treated in two common Hot Dip Galvanizing GI (Zn with 0.2 to 0.3% of Al) and GA ($ZnFe$ with 0.1 to 0.135% of Al) are to deposit $Zn - Al$ layer on the steel surface. Packaging products are electro-coated, organic coated or tinned.

1.3 Width variation problematic in cold rolling process

1.3.1 Industrial observation

1.3.1.a Scattering of width variation

Strip width decrease called width necking, according to Legrand, Becker and Roubin [64], may reach over 20mm through different steel production processes of a cold plant, which are introduced in the section 1.2.4. Continuous annealing and galvanizing (or annealing) furnaces, temper mills and tension levellers are known to have influence on strip width variations. Between these processes, tandem cold mill is considered as the most influent factor on that phenomenon. For instance, Figure 1.13 shows the strip width variation of about 6000 automotive steel products rolled at the 4-stand cold rolling tandem mill of ArcelorMittal Florange. It can be seen that in this tandem mill, strip width variations are mostly negative (width necking) and can be up to 15mm or more.

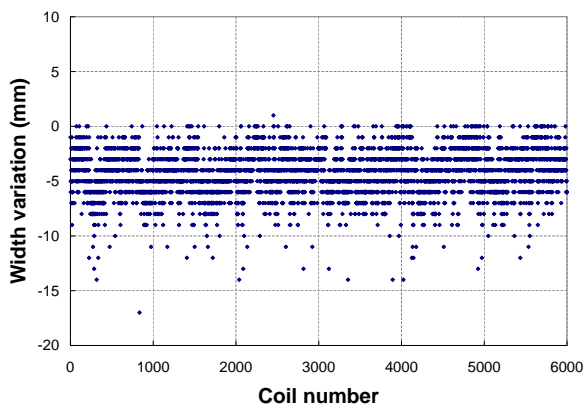


Figure 1.13: Width variation observed for 6000 coils rolled at ArcelorMittal Florange 4-stand cold rolling tandem.

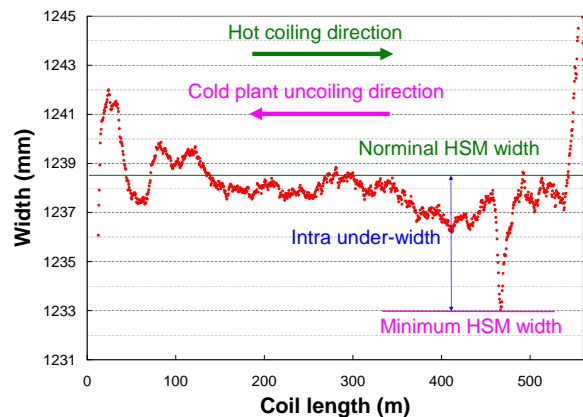


Figure 1.14: Typical strip width profile provided by HSM to cold plant at ambient temperature.

These width contractions (showed in Figure 1.13) are scattered and badly estimated nowadays. Consequently, that could lead to producing under-width coils unsatisfying customer requirements and the coils are therefore downgraded or rejected. To compensate for these width variations, cold plants use to order to hot strip mills coils with significant over-widths, these over-widths are often overestimated. The hot finishing strip mill, with its own width scatter, tends to increase also the width ordered by cold mills. All these over-widths and the associated side trimming operation produce an important and non optimized yield all along the production route.

1.3.1.b Heterogenous width profile at entry of cold plant

It is usually observed that the width is not homogenous along a coil. In particular, at the entry of the cold plant, the width profile has a minimum which can be up to 10mm less than the width average and concentrate locally near to the tail end of the coil (about 90m in the example given by 1.14). A typical width profile obtained after HSM is given in the graphic 1.14. We remark that the tail end at pickling line of the cold plant corresponds to the hot coil head end. It remains being the tail at CRM for a coupling (pickling - CRM) line or becomes the head end for uncoupled line.

1.3.2 Width specification using prediction models

1.3.2.a Taking into account width variation in each process

The width specification is an industrial terms meaning the determination of targeted width of each product along the production route from the known customer one. The schema 1.15 shows typical methodology about how a cold plant

determines the necessary entry width allowing to produce final customer width. The targeted width at the entry of each process is based on targeted one at the entry of the next downstream process and an estimation of width variation in this process itself. In the other words, firstly the entry width of the last process (skin-pass rolling in this example) is calculated from customer width and an estimation of width variation in the skin-pass. Similarly, the entry thickness of annealing is that at the entry of the skin-pass adjusted by an estimated width variation of the annealing process. The same operation is repeated for cold rolling mill, tension leveller (at entry of pickling line), until the side trimmer to obtain the targeted cold plant entry width. The cold plant orders the HSM to provide the concerned product with this width. For the HSM, the cold plant is customer. The first over-width in HSM is to compensate the thermal contraction related to the difference of temperature, about 600°C at HSM coiler, and ambient temperature at the entry of cold plant. And the second is an over-width for width variation in the finishing mill. Up to the roughing mill, the edgers, mentioned in the section 1.2.3.b, where the processes are controlled to produce the targeted width for the Finishing Mill.

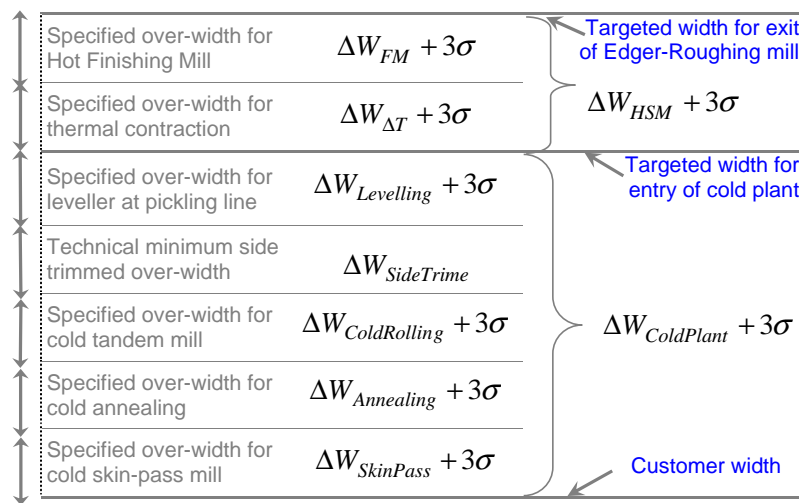


Figure 1.15: Schema of the determination of targeted width for different processes before manufacturing.

It is important to highlight that, in a process if the width variation is positive or in other words a width spread, the necessary entry width is smaller than the targeted exit one of the process. However, in reality almost every process produces a width necking for most of products passing through. That are the reasons why an over-width for each process is to be determined during specification.

The side trimmer is particular where the width is trimmed to be homogenous at both edges. To ensure good cutting quality this operation requires a minimum trimmed width that is more or less 5mm per edge (fixed or varied as a function of strip thickness) meaning 10mm of width trimmed. It is an important material yield compared to other processes. Thus, only a special part of production passe though this process.

1.3.2.b Taking into account width variation along the coil

As discussed in the section 1.3.1.b the HSM produces today varying strip width profile with a local minimum. Therefore, in the specification strategy, the HSM takes into account this fact simply by targeting to provide the coils with the minimum width equal or higher than that required by the cold plant. That means, the HSM specified over-width is higher (than if width profile is homogenous) to compensate in addition the local under-width.

1.3.2.c Safety margin and uncertainty of predictive models

For cold plant as well as for hot plant, a width compensation is needed to compensate width decrease in different processes. This is estimated by predictive models that have certain level of accuracy. The uncertainty of prediction

models is not only due to the own quality of the models themselves but also the uncertainty of the models inputs. In other words, the processes parameters (models inputs) forecasted during specification phase are also different from the real production ones. Consequently, because of models uncertainty the production line would provide some times over width and other times under width.

The over width could increase the production cost and reduce benefice but it is usually accepted by customer or can be easily side trimmed to right width just before expedition. In the contrary, the under width is usually unacceptable. The customer refuse the coils and there may be even consequence of commercial agreement. Therefore, the production line avoids under-width by taking a **safety margin**.

This safety margin can be taken constant or calculated in function of the predictive models error following the strategy of plants. To facilitate the discussion we take an example where the safety margin of each process is equal to three times the standard deviation of models error denoted σ : Safety margin = 3σ . This strategy promotes over-width strategy in order to avoid under-width problem. If the prediction error follows the normal Gaussian distribution, such a safely margin results to under width for 0.135% and over width for 99.865% of products. We note that the average error of predictive models is small because the models are tuned and adapted to the measured data. Thus the models average error is negligible before their standard deviation, meaning the predictions are well centered.

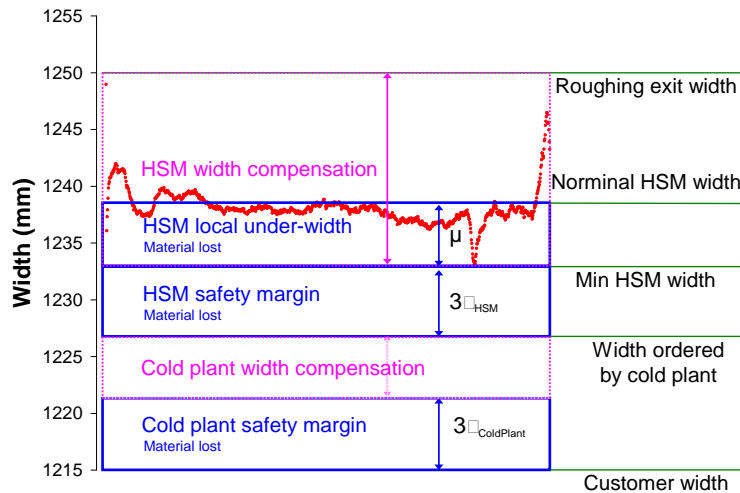


Figure 1.16: Summary of width specification of HSM and cold plant.

The specification method illustrated in Figure 1.15 can be summed up the schema 1.16. The HSM calculate the HSM width compensation to compensate the width variation at all Hot Plant process from the roughing mill exit width to finishing mill and thermal contraction for the local minimum width point. And the HSM safety margin is equal to three times the total of standard deviation of predictive models of all these HSM processes. Similarly, the cold plant width compensation is the total of width necking in all cold plant process calculated by predictive models and cold plant safety margin is also equal to three times the standard deviations of all these models.

1.3.3 Over-width material yield

1.3.3.a Material yield due to predictive models uncertainty

As can be seen in previous section, a such specification strategy leads to about 99.865% of products having over-width and 0.135% having under-width. This is true for every process if each process adopt this same strategy. The under-width products are usually rejected and becomes scrap to come back to liquid steel production. Sometimes, they are only downgraded and sale at lower price. The other products, most of production, with over-width are side trimmed before being sent to the customer. They are also in some cases sent to the customer without being paid. Thus,

in any case, the over-width is a material yield. These over-width products (99.865% of the production) have an average over-width a little higher than but very closed to 3σ , the safety margin. Therefore, it is reasonable to consider that the average over-width is equal to the safety margin.

Hence, the material yield related to predictive models error is equal to $3\sigma_{ColdPlant}$ for cold plant and $3\sigma_{HSM}$ for hot plant (including thermal contraction between HSM and cold plant).

1.3.3.b Material yield due to width heterogenous profile

As discussed above, the strip width provide by the HSM is heterogenous and the specification aims at ensuring that the minimum width is higher than the width required by cold plant (see Figure 1.16). That results to the fact that the material at the edgers where the strip width is higher than the minimum width is not serviceable. And this is and represent material yield for HSM. All along of a coil, the useless part has an average width equal to the intra-coil under-width defined as the difference of the coil nominal width (average width) and the minimum one. And for the whole production (many coils) the average of this useless part is equal to the average of intra-coil under-width.

Finally, if the material yield is defined as the useless part width averaged on a many-coil production, it is approximated by the sum of cold plant safety margin, HSM safety margin and the average intra-coil under-width of products provided by the HSM to the cold plant. It is necessary to note that, this estimation is true if the safety margin is high enough so that most of products are produced with an over-width. This hypothesis is verified as shown in the example above because the plants aim at avoiding providing under-width products to customer.

1.3.4 Two ways reducing material yield

1.3.4.a Improving accuracy of predictive models

According to a strategy described above the safety margin and material yield depend directly on the uncertainty of width variation predictive models, obviously improving accuracy of the predictive model of any process allows to save the material yield.

1.3.4.b Using process actuators

Coil-to-coil width correction

Following the specification strategy described above, arriving at the cold plant, a product provided by the HSM has a higher width than that required in most of the times. This entry over-width varies from a product to another. As the width variation in a cold plant is about several millimeters for a width of more than one meter, meaning less than one percent. The entry over-width will be changed of about less than one percent. In other word, the entry over-width is almost kept unchanged and is transformed to an final over-width. If there exists an actuator of which an variation will cause a change of the width variation in the cold plant, it should be able to play with this actuator to make more width necking in the cold plant and therefore reduce the material yield. The new value of this actuator parameter is chosen in function of the entry over-width measured to compensate it. An process actuator is efficient when its variation makes sensible change of the width variation in the process.

The actuator is even more important in the case of under-width because it generates a significant lost. Moreover, as an under-width is usually small, it is more possible to be adjusted by an actuator.

Intra-coil width correction

At the coil-to-coil scale, the actuator is chosen for the minimum width point of each coil. At the scale of a coil, the other point all along a coil will be in over-width, the interest is of course to reduce this over width by setting varying value of the actuator parameter. This material is elongated and transformed in to the coil length direction and is thus saved.

1.4 Thesis objective and approaches

1.4.1 Thesis objective - predictive model for cold rolling process

The primary objective of the thesis is to develop a rapid and accurate predictive model of width variation in cold rolling process.

The phenomena contributing to the width variation of strip in cold rolling will be presented in detail in the chapter 7. It will be shown that the subject has been studied by different studies such as [48], [59], [94], [49], [53], [114]... Many of them brought out phenomena involving in the width variation for flat bar rolling with small ratio width-thickness (less than 10 in general). For flat sheet rolling where the width-thickness ratio varies from 200 to 1500 for automotive and up to more than 5000 for packaging products, there are very few existing studies. Between them the two typical ones are [64] and [23]. In this rolling configuration, the width variation is a thermo-mechanical problem that Finite Elements Method (*FEM*) calculations like *Abaqus*, *Lam3-Tec3* are able to simulate and give satisfying predictive results. However, these methods are very expensive in terms of computing time (from several hours to few days). Another method named stream lines method [23] allows also to model the width variation problem accurately but the computing time remains in the order of few hours. These models are of course not applicable to the width specification and even less serviceable for online control of strip width.

On the other hand, some statistic and neural networks models exist and can be easily developed and tuned to industrial database [65], [26]. They are extremely rapid but poor in physical comprehension and accuracy. Thus, the present thesis aims at developing a physical model by introducing some simplifying hypotheses and analytical methods as far as possible to obtain accurate predictive results with reasonable calculation time.

Success criterion: Such a model is considered successful when its accuracy is higher than that of statistical models, closed as much as possible to that of *FEM* models and has a computing time of order of a second.

1.4.2 Approaches

Issued from a bibliographic study about width variation of flat product in rolling process which is presented in the next chapters, the Upper Bound Method, an approach based on the velocity field seems to be an adequate method to develop fast model of width variation. Hence, the present thesis is based on this method to start with. According to this model, it is the plastic lateral flow of material that creates the width variation. The obtained results are in excellent agreement with other existing models and experiments performed in within ArcelorMittal laboratory pilot rolling mill.

However, it is necessary to highlight that the strips width the experiments is quite narrow. The width-thickness ratio is lower than 60. Very quickly, when applying this model to automotive product with typical width-thickness ratio of about 1000, the width variation obtained is always positive (width spread) unlike the industrial measurements showing negative width variation. The *FEM* calculations with *Abaqus* and *Lam3-Tec3* are therefore performed in this rolling condition in order to bring out physical phenomena involving in the width variation. Despite of its reversibility, the elastic deformation has an important impact on the final width variation. That is also proved that the thermal deformation influence in a similar way the plastic deformation generated in the roll-bite and thus contributes to the final width variation. The amplitude of both phenomena increases while the lateral flow decreases sharply with the strip width. Therefore, the influencing phenomena in the width variation and above all their coupling become really complicated. Developing rapid or analytical model is therefore extremely delicate.

Thus, the methodology is to analyze width variation phenomena by *FEM* in order to find good simplifying hypotheses and appropriate way to introduce them to the new predictive model. The *FEM* results are also used for validation of the rapid model.

Chapter 2

Rolling process modeling reviews

To answer the needs for research and industrial applications, there have been developed numerous of rolling models with various levels of complexity and rapidity. This chapter firstly aims at giving a general point of view on rolling process and modeling. Afterwards, some typical models are presented separately for work-roll elastic deformation, tribology of roll-strip contact and strip elasto-plastic deformation. We privilege the discussions on analytical or semi-analytical models. The main physical understandings and equations are detailed for the two famous families of rolling models, slab method for homogeneous deformation and Orowan theory taking into account inhomogeneity of strip deformation across the thickness. The developments concerning introduction of elastic deformation are as well mentioned. These elements help to develop a new elastic-plastic plane deformation model introduced in a later chapter. This new model aims at approximating the width variation.

Contents

2.1	General description of rolling problem	22
2.1.1	Main characteristics of rolling process	22
2.1.2	Main objects to be modeled in rolling	24
2.1.3	A well-posed problem of rolling	24
2.1.4	Rolling model - A coupling of separated models	28
2.2	Typical tribological models	28
2.2.1	Dry friction	29
2.2.2	Lubricated friction	29
2.2.3	Friction in cold rolling	30
2.3	Typical strip models	31
2.3.1	0D and 1D models - Analytical models	31
2.3.2	2D models	44
2.3.3	3D models	45
2.4	Typical work-roll deformation models	45
2.4.1	Bending and flattening in width direction Oyz - 3D modeling	46
2.4.2	Flattening models for 2D modeling	46
2.5	Discussions	49

2.1 General description of rolling problem

2.1.1 Main characteristics of rolling process

In the section 1.2 of the previous chapter, all processes of a production route are presented. That brings out the main aims of hot rolling as well as of cold rolling processes. The hot rolling (see 1.2.3) aims at reducing strip width and thickness and controlling outlet temperature in order to get targeted mechanical properties. On the other hand, during cold rolling (see 1.2.4) only strip thickness is reduced while the width variation is a consequence. And unlike the hot rolling, the cold rolling objective is to obtain a very good surface and flatness.

A definition of rolling process: There exist many definitions of this process in the literature. Here following is presented one of them. According to [75] this operation is defined as follows: In metallurgic industry, rolling is an operation having objective to reduce one or more dimensions of a long product thanks to a system of two or several axisymmetric tools rotating around their axis. It is the rotation of these tools which drives the product move toward the roll-bite thanks to the presence of work roll - strip contact friction, see Figure 2.1.

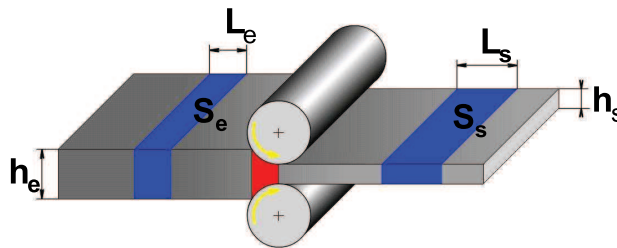


Figure 2.1: Rolling process usually consists in reducing strip thickness and elongate its length by consequence.

2.1.1.a Steady state or transient rolling and modeling

Industrial rolling process can be performed constantly in transient phase, especially in hot slab rolling. In a roughing mill for instant, product is rolled one by one separately and rolling of product extremities has transient nature, i.e rolling parameters (strip deformation, roll force, velocity...) vary during time. In this process, the product is not long enough to establish steady state rolling.

Unlikely, in a cold rolling, the product is very long compared to its width and work-roll size, the rolling is mostly performed at a steady state. The establishment of mechanical steady state is quite fast. In general, after a rolled length of several times of the widths mechanical fields becomes constant during time. In particular, for 2D (plane strain hypothesis) it is even faster. Rolling several times of roll-bite length is already sufficient to get steady state. Nevertheless, the thermal steady state requires longer time. Just after being changed, work-rolls start with homogenous temperature equal to ambient one. It is heated by exchanged heat with products and by friction dissipation. This heating process requires many rotations, sometimes only after rolling several product, the thermal steady state is established.

Time-dependent or incremental methods

Correspondingly to these possible phases of rolling process, there exist two categories of models. The first one contains time-dependent models allowing to understand what happens during transient phases. The incremental or *Lagrangien* models integrate the equations in function of time. The product geometry is known at the given time, and its evolution in time is calculated by integrating the velocity field in a same way for the strip and the tool (see Figure 2.2). These methods allow to model not only the transitory states but also the equilibrium ones by integrating the equations long time enough until obtaining stable situation. However the calculation time is important. Typical applications of incremental method are for the roughing mill where the extremities (head and tail) deformations and the threading issues should be studied. These models are also used to model unstable phases as flatness issues or vibrations problems for both hot and cold rolling.

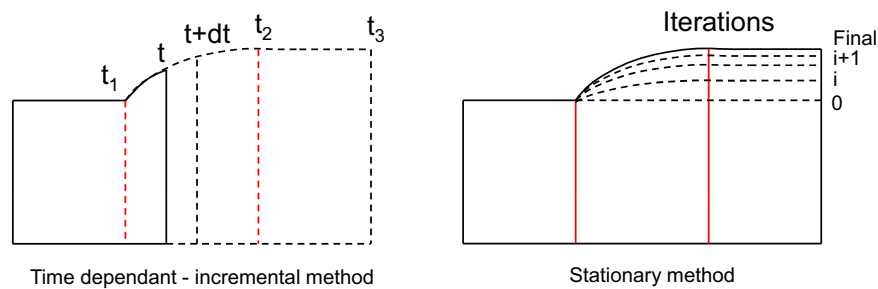


Figure 2.2: Incremental and stationary methods.

Stationary or steady state methods

Stationary models are constructed by eliminating the time in all equations sometime called the *Eulerian* models. This method represent certainly an attempt to develop but in return, many substantial advantages. In particular, they decreases the computing time by more than ten or even hundred times in some cases. The principal difficulty is that the calculation domain *i.e* the geometry of the product and tool during and after deformation become an additional unknown of the problem because of the free surfaces where no displacement boundary conditions are present [25]. In general, this difficulty is translated into a calculation by iteration (see Figure 2.2).

Remark: The main objective of the thesis is to model the width variation during cold rolling. Of course, during this process, the product thickness and mechanical properties are not homogenous from at head to the tail end. But very commonly these variations are small and negligible. And when these variations occur on a long part of the product (low frequent variations) the process is considered as quasi steady state rolling, meaning that the time depending solution is a succession of many steady state solutions of the inputs that are time-dependent. **That is why henceforth only steady state models will be mentioned.**

2.1.1.b Symmetric or asymmetric rolling

Operator-motor sides asymmetry: An example of asymmetries is tilting problem when roll gap is not constant along the rolls axe (the strip width direction). The strip is therefore deformed more at one edge side than the other. By consequence, one of the strip edges is more elongated making the strip direction be curved at the exit of rolling stand and causing strip steering problem. Many other reasons could also make asymmetries in width direction. For example, inhomogeneous lubrication can create inhomogeneous friction along the strip width direction. Or an heterogenous work-roll cooling can also make an varying temperature distribution along the work-roll axe. And as a result of thermal dilatation, the work-roll apparent diameter is not constant and can make a various roll-gap...

Anyway, every asymmetry in width direction is not desired. Therefore, automatic control system attempts to eliminate apparent asymmetric defects on the strip (anti-tilting for example). In other words, the rolling process is controlled to be as symmetric in width direction as possible.

Top-bottom asymmetry: The rolling can be top-bottom asymmetric due to many reasons such as a difference of top and bottom work-rolls diameter, surface or roughness, a difference of their speed during rolling... One of the obvious origins for the top-bottom asymmetry is the gravity. Because the strip is horizontal, the lubricant and coolant are stored more easily on the top strip surface than on the bottom side. Thus, the roll-bite friction and the heat exchange coefficients are often top-bottom asymmetric.

This kind of asymmetry could generate appearing defects on the strip like ski-effect in hot rolling or bow-flatness defect in cold rolling (the strip is curved in rolling direction). Rarely but there exist desired top-bottom asymmetries in rolling unlike the operator-motor sides asymmetries. T.Hoang [47] develops an allowing to quantify the ski-effect amplitude du to top-bottom asymmetries. The author brings out that the rolling with different work-rolls diameter

should allow to decrease both roll force and power compared to symmetric rolling with a same average work-roll diameter.

Remark: Only symmetric rolling is considered in this thesis because asymmetric defects are not what the present study searches for. Even though asymmetric defects may influence the width variation, our objective, they are not the principle motivations.

2.1.2 Main objects to be modeled in rolling

The rolling process contains essentially a product, tools (including two work-rolls, two back-up rolls...), a lubrication system and a cooling system as can be shown in a simplified way by Figure 2.3.

Strip - Roll-bite and out of roll-bite: As the objective of rolling is to reduce the thickness, the strip is deformed plastically due to the pressure exerted by the work-rolls. The strip part under contact is called the roll-bite. It is obvious that what happens in the roll-bite is the main goal of any model but the elastic deformation out-side the roll bite can be also important. For example the distribution of tension in width direction representing flatness varies significantly out side of the roll-bite. According to Saint Venant's principle, the length of extending parts on both sides is comparable to the strip width. In brief, it is necessary to model the strip before, in side and after the roll-bite as shown in Figure 2.3.

Tool: The tool is usually modeled as a system of a pair of work-rolls and/or another of back-up roll. Obviously, only elastic deformation are expected in the tool at least in macroscopic scale. The micro plastic deformation is inevitable because of the rough surfaces contact between strip and work-roll, and between work-roll and backup-roll. In macroscopic scale, the work-roll is deformed in two different modes called respectively flattening (radial and tangential direction) and deflexion (roll axes direction). The modeling of the work-roll deformation will be more explained in a later section 2.4.

Contact surface - lubricant: The contact nature depends much on the presence or absence of lubricant. In many hot rolling processes, no lubricant is injected to the strip and work-roll contact. In these cases, the roll-bite is lubricated by the work-roll scale layer and the strip scale layer due to oxidation of their surfaces at high temperature. Otherwise, the hot rolling process is sometimes lubricated. Certainly due to the strip high temperature, the oil is burn rapidly once in contact with the strip and only a very thin film of residual oil particles stays and lubricates the roll-bite. This film is extremely thin but could change completely the contact nature and decrease drastically the friction coefficient. In both cold or hot rolling the contact tribology is complicated and require sophisticated models depending on the study objective. In the section 2.2, some typical models for cold rolling will be mentioned.

Cooling system - Thermal phenomena: As mentioned in the section (see 1.2.4), the cooling system including work-roll cooling and strip cooling is necessary to keep the temperature of the tool and the strip at reasonable levels. However, it is not in a rolling model that the cooling system is modeled in detail. It is simply modeled as a heat exchange fluxes on the cooling zones. And the heat exchange coefficients are usually identified independently.

2.1.3 A well-posed problem of rolling

The mathematical term well-posed problem stems from a definition given by J.Hadamard [41]. He believed that mathematical models of physical phenomena should have the properties that: A solution exists. The solution is unique and the solution behavior changes continuously with the initial conditions. In continuum mechanics, a problem is call well-posed when:

1. In side modeled objects, the volume charges are given

2. On all external surfaces of the modeled objects the boundary conditions are given and complete. On a surface, the boundary conditions are considered as complete when there are three boundary conditions on the velocity or (and) the stress corresponding to the three space directions. In other word, the velocity and stress boundary conditions are complementary on this surface.
3. Constitutive equations related to the materials behavior are defined. That includes elastic constitutive equation, plasticization criterion and flow equations.

And in general, a well-posed mechanical problem results to a unique stress solution while the velocity solution is not necessarily when the rigid body movements are possible.

Hereby, we will describe the rolling problem in a very general case and with all necessary conditions to be a well-posed one.

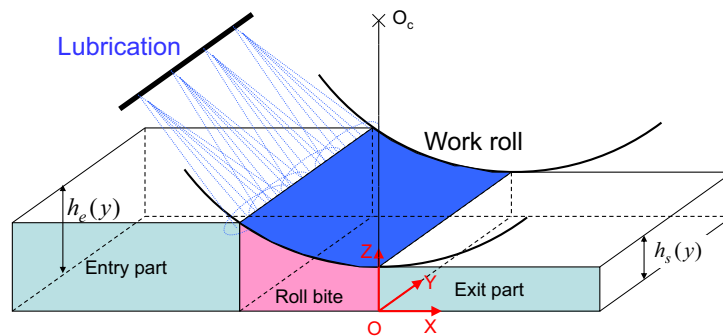


Figure 2.3: For symmetric rolling, only a quarter geometry, a half of the thickness and a half the width, is necessary to be modeled.

2.1.3.a Equilibrium

By neglecting the volume gravity force before the stress and variation of stress, the equilibrium equations in both the strip and the roll are:

$$\underline{\nabla} \underline{\sigma} = 0 \quad (2.1)$$

2.1.3.b Boundary conditions

Thanks to the symmetry hypotheses in both strip thickness and strip width directions, only a quarter of the total geometry is necessary to be modeled as shown in Figure 2.3.

Work-roll boundary conditions

The work roll is driven by a motor. Its peripheral velocity V_c is given and controlled while the driving torque provided by the motor, denoted *Torque*, is a consequence. Not only in contact with the strip, the work-roll is also in contact with the back-up roll for a 4-High stand. In point of view of the work-roll, the stresses on the contact surface with the strip are given, they are consequence of the strip behavior being deformed. The remaining surface is free mechanically. The work-roll is blocked in rolling direction Ox and strip width direction Oy . Its center position is adjusted in Oz by an automatic gauge control (AGC) in order to obtained the targeted strip exit thickness h_s .

The thermal conditions are the heat exchange of different natures in the whole surface of the roll: steel-steel contact heat exchange with the strip and back-roll, heat exchange with work-roll coolant (water or emulsion¹), heat exchange

¹A mix of water with oil at more or less 1-2% of oil concentration, used also to lubricate the roll-bite.

with air otherwise. The radiation is negligible. On the contact surface, the friction is a heat generation source. In general, the friction power is shared one part to the work-roll, the other to the strip with a given sharing coefficient. This coefficient, very difficult to be identified is commonly equal to 0.5.

Strip boundary conditions

Strip entry section: The entry section is the initial form of the strip before rolling. It can be rectangular with given thickness h_e and given width b_e . And if the strip has an initial crown, its thickness profile is given instead of h_e . On this section the material moves with a homogenous velocity in rolling direction, meaning:

$$\underline{u}|_{S_e} = V_e \cdot \underline{e}_x.$$

V_e is an unknown of the problem but the total entry tension (resulting on S_e) is given as $T_e \cdot S_e$ where T_e is the average specific entry tension. All other stresses components are null, in other words:

$$\int_{S_e} \underline{\underline{\sigma}} \cdot \underline{e}_x \, dS = T_e S_e \underline{e}_x.$$

Strip exit section: Similarly to the entry section, the velocity at the exit section is also homogeneous and unknown. The nominal (average) exit thickness is given but unlike the entry section, the exit thickness profile and exit width are unknown. And the exit total tension is given:

$$\begin{cases} \underline{u}|_{S_s} = V_s \cdot \underline{e}_x \\ \int_{S_s} \underline{\underline{\sigma}} \cdot \underline{e}_x \, dS = T_s S_s \underline{e}_x. \end{cases}$$

It is notable to remind that both velocities V_e and V_s are not given and to be determined as results of the problem.

Boundary condition on symmetry plane $z = 0$: If the whole strip is modeled, by definition, a top-bottom symmetric velocity field verifies three followings conditions for every strip material point:

$$\begin{cases} u_x(x, y, z) = u_x(x, y, -z) \\ u_y(x, y, z) = u_y(x, y, -z) \\ u_z(x, y, z) = -u_z(x, y, -z) \end{cases} \quad (2.2)$$

$\forall x, y, z$. These equations imply that $\forall x, y$ when $z \rightarrow 0$:

$$\begin{cases} \frac{\partial u_x}{\partial z}(x, y, z = 0) = 0 \\ \frac{\partial u_y}{\partial z}(x, y, z = 0) = 0 \\ u_z(x, y, z = 0) = 0 \end{cases} \quad (2.3)$$

When only top half of the geometry is modeled, the velocity needs to verify 2.3 and the velocity of the bottom half is simply deduced using 2.2. In other words, the symmetry conditions on symmetry plane $z = 0$ is given by 2.3.

It is remarkable that the first two equations of 2.3 can be also obtained by symmetry conditions on the rotation rate saying that on this symmetric surface the rotation rate in x and y direction are null. To demonstrate that, it is enough to rewrite the definition of rotation rate tensor and multiply it to the normal vector of symmetry surface $-e_z$ to obtain the rotation rate vector. The first two components of this vector must be 0. Then using the third equation of 2.3, we obtain the same equations as 2.3.

Boundary conditions on symmetry plane $y = 0$: The same, the boundary condition on $y = 0$ symmetric plane can be written as: $\forall x, z$,

$$\begin{cases} \frac{\partial u_x}{\partial y}(x, y = 0, z) = 0 \\ u_y(x, y = 0, z) = 0 \\ \frac{\partial u_z}{\partial y}(x, y = 0, z) = 0 \end{cases} \quad (2.4)$$

Strip edge surface $y = b(x, z)$: From the entry to the exit section through the roll-bite the width function changes and in a general case, strip edge can be different from a straight section, meaning that b is a function of both x and z . This is a free surface on which that all stress field components are null:

$$\underline{\underline{\sigma}}(x, y = b(x, z), z) \cdot \underline{\underline{n}} = \underline{\underline{0}} \quad \forall x, z. \quad (2.5)$$

Furthermore, at steady state the width surface is also stream lines. Thus, in terms of velocity field, the boundary conditions can be written as:

$$\begin{cases} u_y(x, y = b(x, z), z) = \frac{\partial b}{\partial x}(x, z) \cdot u_x(x, y = b(x, z), z) \\ u_z(x, y = b(x, z), z) = \frac{\partial b}{\partial z}(x, z) \cdot u_x(x, y = b(x, z), z) \end{cases} \quad (2.6)$$

Strip top surface $z = h(x, y)$: The thickness profile at the entry section is given as $h_e(y)$, then $h(x, y)$ becomes unknown and varies during the area before the roll-bite. In the contact area $h(x, y)$ is imposed by the work-roll shape (within a constant because the work-roll position needs to be determined to obtain the strip exit thickness). After the contact $h(x, y)$ becomes free again and varies to the exit section where its nominal value is equal to targeted exit thickness h_s .

The boundary condition on this surface is as follows: before and after the contact, the strip top surface is free:

$$\underline{\underline{\sigma}}(x, y, h(x, y)) \cdot \underline{\underline{n}} = \underline{\underline{0}} \quad \forall x, y. \quad (2.7)$$

Contact surface: In the contact area, the first boundary condition is that the strip thickness is imposed by the work-roll shape $h(x, y)$ issued from a work-roll deformation model (see the section 2.4 for typical ones). This condition fixes the deformation of the strip in the normal direction but is not enough because it does not describe what happens in the tangential directions. Therefore, complementary boundary conditions take over the two tangential stresses. These conditions are given by a tribological model where the friction coefficient can be isotropic or not, dependent of normal stress or not or can vary as a function of sliding velocity or not... (see some typical model in the section 2.2).

2.1.3.c Material constitutive equations

For the roll, the constitutive equation is simple because there is only elastic deformation. For the strip, many models build with rigid-plastic (RP) or slightly-compressive rigid-plastic [77] to avoid difficulties related to the incompressibility in flow formulation. Some others use elastic-viscoplastic (EVP) or thermal-EVP behavior. The thermal effects are not only important for hot rolling through thermo-mechanical coupling (influence of temperature on yield stress) and also its influence on microstructure. For cold rolling, these effects are less primordial.

The constitutive equation is thus a key point of each model allowing to take into account or to simplify the physic of strip deformation. We will see in the section 2.3 some typical strip models.

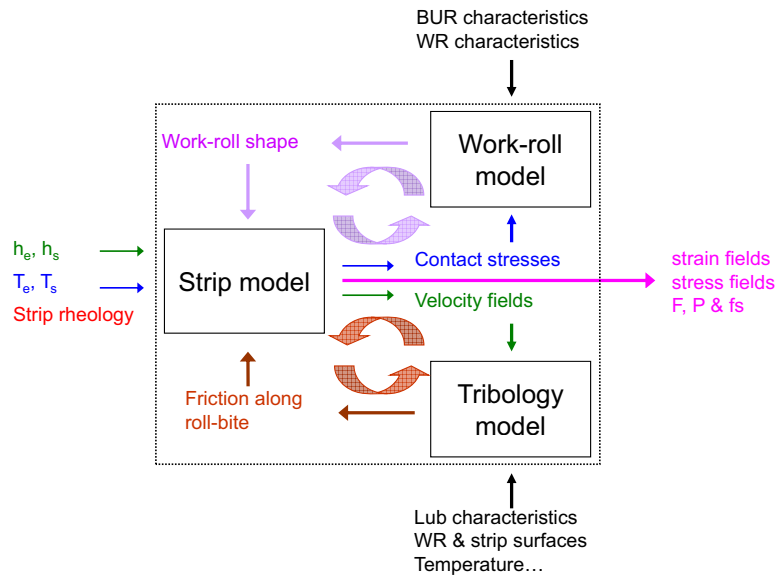


Figure 2.4: Illustration of the coupling of strip, work-roll and tribology models.

2.1.4 Rolling model - A coupling of separated models

As described above, a rolling problem contains mainly three objects to be modeled with very different natures of involving physical phenomena. Until today there exist no coupled model that resolves all coupling equations at the same time. But each object is modeled separately and the whole model is a weak coupling of them.

Figure 2.4 shows the principle of coupling. Being more or less sophisticated but almost every models in the literature are built in this way. The strip model needs the entry thickness profile $h_e(y)$, exit targeted nominal thickness h_s , entry and exit average tensions T_e , T_s , material rheology and behavior law but also the work-roll shape and friction coefficient. For the first iteration, we can assume a simple work-roll shape and a constant friction coefficient. This model computes the contact geometry, the contact stresses and temperature, velocity, stress and temperature fields inside the strip. Then, the work-roll model uses the contact geometry, stresses and temperature given by the strip model to evaluate the work-roll shape. The tribological model uses also the contact pressures, contact velocity fields and temperature to estimate the macroscopic friction coefficient along the roll-bite. We can hence feed the strip model with this newly obtained work-roll shape and friction coefficient and start the second iteration... The convergence will be reached when the evolution of work-roll shape, contact geometry and stresses, friction coefficient are enough stable from one interaction to the next one.

2.2 Typical tribological models

Let start with tribological models for two reasons. The first is that the equation giving the shear stress on the contact surface is necessary for the understanding of the resolution of strip models. Thus, for each presented strip model a friction one will be cited. The second reason is that, tribological model can become very rapidly complicated if we want to determine the friction stress based on the what happens on the contact surface in the roughness scale. These problems can be in no way treated shortly in this section. Therefore, only some typical facts about friction models will be cited here without much details.

2.2.1 Dry friction

2.2.1.a Coulomb friction model

The classic rules of sliding friction were discovered by Leonardo da Vinci (1452-1519), but remained unpublished in his notebooks. They were then rediscovered by G. Amontons (1699) and the understanding of friction was further developed by C-A. De Coulomb (1785). The sliding or kinetic friction were expressed as three empirical laws:

1. Amontons' first law: The force of friction is directly proportional to the applied load.
2. Amontons' second law: The force of friction is independent of the apparent area of contact.
3. Coulomb's law of friction: Kinetic friction is independent of the sliding velocity.

These laws led to popular Coulomb dry friction model for sliding contact as follows:

(2.8)

where the "-" means that the friction force is in the opposite direction of the relative sliding velocity denoted v . The Coulomb friction model can, when the sliding happens be written by a relation between the normal and tangential stresses σ_n and τ as follows:

$$\tau = -\mu\sigma_n \text{sign}(v) \quad (2.9)$$

where μ is the Coulomb friction coefficient. This friction model is most commonly used and usually referred to as dry friction although it is used for dry contacts as well as boundary and mixed lubricated contacts.

2.2.1.b Asperity contact theory of adhesive friction

Inelastic adhesion concept of friction - Bowden and Tabor 1954 Considering that the classical frictional law of Amontons was based on the projected or apparent area, Bowden and Tabor (1954) were concerned with the real area over which the two sliding bodies are in contact. The real area of contact is made up of a large number of small regions of contact, called asperities or junctions of contact, where atom-to-atom contact takes place. Bowden and Tabor showed that the force of friction between two sliding surfaces is strongly dependent on the real area of contact. Assuming during a frictional sliding process a fully plastic flow situation of all asperities, friction is found to change linearly with the applied load as demanded by Amontons 1st Law.

Elastic adhesion concept of friction Archard 1953 Bowden and Tabor investigated on friction for a purely elastic sliding process. They used a simplified single asperity model of contact based on the Hertzian elastic theory, and found a non-linear friction-load dependence ($F = N^{2/3}$), which clearly contradicted Amontons 1st Law and the experiments. It was Archard (1953), who recognized that there was indeed no contradiction. Instead of assuming a constant number of asperities as Bowden and Tabor did, Archard assumed a load dependent number of asperities. With this assumption the controversy between the elastic multiple asperity hypothesis and Amontons 1st Law could be resolved.

2.2.2 Lubricated friction

2.2.2.a Viscous friction model

Until lubrication was studied pragmatically, it was Nikolai Pavlovich Petrov and Osborne Reynolds around 1880, who recognized the hydrodynamic nature of lubrication, and introduced a theory of fluid-film lubrication. Still today, Reynolds' steady state equation of fluid film lubrication given by:

$$\tau = -\frac{\eta}{h_{lub}}v. \quad (2.10)$$

is valid for hydrodynamic lubrication of thick films where the frictional stress is proportional to both the sliding velocity v and the bulk fluid viscosity η and inversely proportional to the film lubricant thickness h_{lub} .

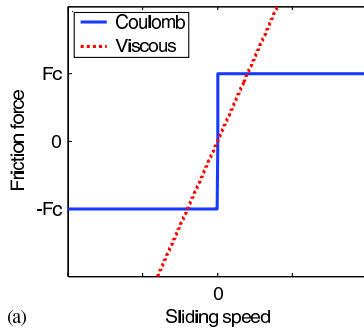


Figure 2.5: Coulomb and viscous friction as a function of sliding speed (source [4]).

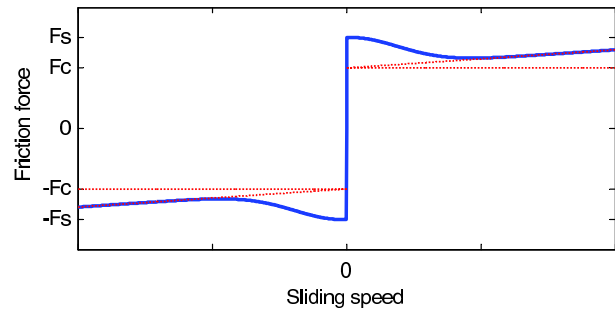


Figure 2.6: Relation between friction stress and sliding speed according to Stribeck model (source [4]).

2.2.2.b Stribeck friction model

The hydrodynamic theory breaks down below a critical thickness threshold that is expressed in the Stribeck-Curve [107]. Stribeck does not only take into account the fact that the static friction is higher than the sliding friction but also the dependence on sliding speed.

$$\tau = -\text{sign}(v) [\tau_c + (\tau_s - \tau_c)] e^{(-\gamma v)^i} - \frac{\eta}{h_{lub}} v \quad (2.11)$$

where τ is the friction stress, v the sliding speed, τ_c the Coulomb sliding friction stress, τ_s the maximum static friction stress, γ the sliding speed coefficient and i an exponent. The Stribeck friction model is illustrated in Figure 2.6. The Stribeck friction model can provide very good representation of the friction between sliding surfaces. It covers everything from Coulomb friction to viscous depending on the choice of parameter values.

2.2.3 Friction in cold rolling

2.2.3.a Cold rolling lubrication

Lubrication in cold rolling is mandatory to obtain high strip surface quality and protection from wear. Thus, most of cold rolling processes of automotive and packaging steels, except some skin-pass rolling, are lubricated using different lubricant types and technologies. A cold rolling lubrication can be classified into three regimes, as illustrated in Figure 2.7:

1. Hydrodynamic regime happens when the oil film is thick enough to separate mostly the roughness of the work-roll and that of the strip. In this regime, the strip surface is rather freely deformed so there is an apparition of grain poly-crystallin structure on the strip surface after rolling. The friction coefficient is very low in this regime.
2. Limit regime is the one when the oil film is very thin and there is a strong steel-steel interaction between strip and work-roll leading to very high friction coefficient. In this case, the work-roll roughness is printed or transferred onto the strip surface. After rolling, the grooves appear on the strip surface with roughness pattern similar to that of the work-roll.
3. Mixed regime with intermediate oil film thickness. There exist alternatively the limit and hydrodynamic contacts. The friction coefficient is medium and the obtained strip surface is a mix of groove and bump areas.

In general, the cold rolling process aiming at making quite high reduction and providing good strip quality is in mixed regime for the best compromise between high quality surface and low friction coefficient. At the last stand of automotive steel rolling when the strip roughness need to be controlled, the limit lubrication is required by using very high work-roll roughness. This limit regime allows a good transfer of work-roll roughness onto the strip. Skin-pass rolling is also usually in this regime for the same reason.

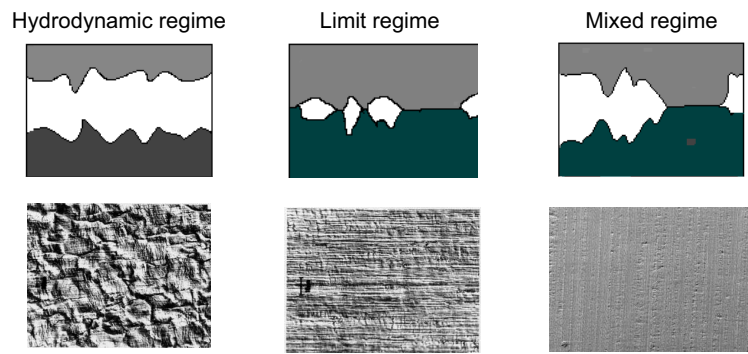


Figure 2.7: Three regimes of cold rolling lubrication correspond to three strip surface qualities.

2.2.3.b Adopted friction models for cold rolling

As mentioned above, the objective of this study concerns especially the rolled strip and work-roll deformation but less the tribology model. And in the point of view of strip model, the tribology model is an input giving the distribution of the friction stress along the contact area. Then, if someone is interested in modeling of the whole system, with any disposed tribology, it is possible to couple the three models as showed in the section 2.1.4. In the present thesis any friction model can be classified into two families.

Load-linear-dependent friction model

$$\tau(\underline{x}) = -\mu(\underline{x})\sigma_n(\underline{x})\text{dir}(\underline{v}(\underline{x})) \quad (2.12)$$

that includes the Coulomb's friction law stating that μ is constant as a function of sliding velocity.

Load-independent friction model

$$\tau(\underline{x}) = -m\underline{x}\sigma_0(\underline{x})\text{dir}(\underline{v}(\underline{x})) \quad (2.13)$$

where $\text{dir}(\underline{v})$ is the unity direction vector of the sliding velocity \underline{v} at the point \underline{x} . This model includes Tresca friction law.

The coefficients distributions $\mu(\underline{x})$ and $m(\underline{x})$ can be more or less complicated. However, they are given by tribological models as an input of our developed models.

2.3 Typical strip models

2.3.1 0D and 1D models - Analytical models

In the beginning of the 20th century when the computer science notion had never ever existed, there were many efforts to develop analytical rolling models with objective to estimate macroscopic rolling parameters such as roll force and torque. The 0D models are those with analytical solution of roll pressure and friction distribution. This solution is sufficiently simple that the roll force and torque calculated by the integration of the roll pressure and friction can be obtained analytically. Otherwise, when it is necessary to solve numerically the differential equations concerning roll pressure along the roll-bite, they are 1D models. In those models, the same physical simplifications such as plane strain deformation, rigid-plastic behavior with constant stress, dry slipping friction are generally used. Many of them use also the hypothesis of homogeneous deformation (slab method base) except the Orowan's theory [86] and derived models. And it is then in the nature of mathematical approximations that these various slab method based models differ.

In order to understand the simplifications adopted by different analytical models, let's study in the first place the 1D theory based on slab method.

2.3.1.a Homogeneous deformation - Slab model

Hypotheses and simplified constitutive equation:

The first hypothesis is plane strain deformation implying that there is no deformation in width direction and other strain components as well as strain rate and stress fields are constant in strip width direction Oy . This hypothesis includes of course that the roll profile is straight or the roll-gap is constant in width direction. The problem is thus a 2D one where all mechanical fields depend on x and z direction. The plane strain condition can be written as follows, $\forall x, z$:

$$\begin{cases} \epsilon_{yy}(x, z) = 0 \\ d_{yy}(x, z) = 0 \end{cases} \quad (2.14)$$

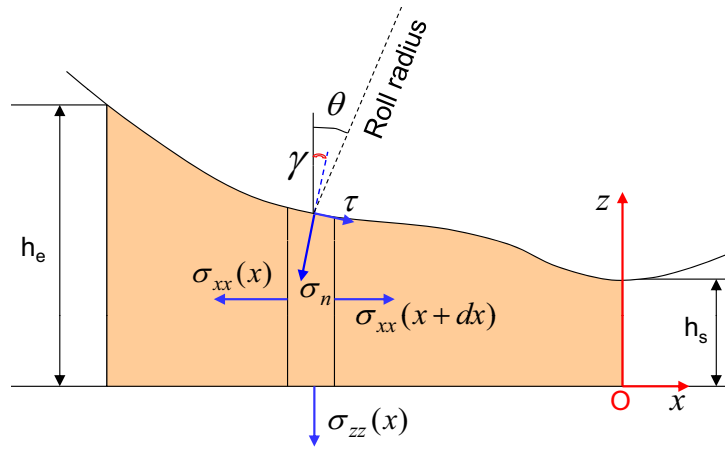


Figure 2.8: 2D illustration of slab method for a general work-roll shape.

The second hypothesis considers that the deformations are homogeneous in the thickness direction all along the roll-bite which implies therefore all mechanical fields are constant strip thickness direction. In other words, a material vertical slab will stay vertical all along the roll-bite. And this is the reason why the method is called "slab method". Furthermore, combining with plane strain hypothesis, we deduce that all mechanical fields are only x -dependent. This model becomes, thus a 1D model.

The third hypothesis consists in neglecting all shear stresses. The stress tensor is, hence:

$$\underline{\underline{\sigma}} = \begin{bmatrix} \sigma_{xx}(x) & 0 & 0 \\ 0 & \sigma_{yy}(x) & 0 \\ 0 & 0 & \sigma_{zz}(x) \end{bmatrix}. \quad (2.15)$$

The hydrostatic and deviatoric tensors related to this stress tensor are:

$$\underline{\underline{P}} = \frac{1}{3} [\sigma_{xx}(x) + \sigma_{yy}(x) + \sigma_{zz}(x)] \underline{\underline{I}} \quad (2.16)$$

$$\underline{\underline{S}} = \frac{1}{3} \begin{bmatrix} 2\sigma_{xx}(x) - \sigma_{yy}(x) - \sigma_{zz}(x) & 0 & 0 \\ 0 & 2\sigma_{yy}(x) - \sigma_{xx}(x) - \sigma_{zz}(x) & 0 \\ 0 & 0 & 2\sigma_{zz}(x) - \sigma_{xx}(x) - \sigma_{yy}(x) \end{bmatrix}. \quad (2.17)$$

The fourth hypothesis says that the strip behavior is rigid-plastic with an yield stress depending on the strain and strain rate. As these fields depend only on x , then $\sigma_0(\epsilon, \dot{\epsilon}) = \sigma_0(x)$ or $k(\epsilon, \dot{\epsilon}) = k(x)$. The hypothesis announces also that the material behavior verifies Von-Mises plastic criterion. Thus, under the roll-bite we can write:

$$\underline{\underline{S}} : \underline{\underline{S}} = \frac{2}{3} \sigma_0^2(x) = 2k^2(x). \quad (2.18)$$

The Von Mises flow criterion says that:

$$\underline{\underline{S}} = \lambda \underline{\underline{d}} \quad (2.19)$$

This equation and the 2nd equation of 2.14 (plane strain deformation hypothesis) imply that $S_{yy} = 0$, thus:

$$\sigma_{yy}(x) = \frac{\sigma_{xx}(x) + \sigma_{zz}(x)}{2} \quad (2.20)$$

Finally, under these forth hypothesis, the stress tensor can be simplified as:

$$\underline{\underline{\sigma}}(x, y, z) = \begin{bmatrix} \sigma_{xx}(x) & 0 & 0 \\ 0 & \frac{1}{2} [\sigma_{xx}(x) + \sigma_{zz}(x)] & 0 \\ 0 & 0 & \sigma_{zz}(x) \end{bmatrix} \quad (2.21)$$

and the deviatoric tensor becomes:

$$\underline{\underline{S}} = \frac{1}{2} \begin{bmatrix} \sigma_{xx}(x) - \sigma_{zz}(x) & 0 & 0 \\ 0 & 0 & 0 \\ 0 & 0 & \sigma_{zz}(x) - \sigma_{xx}(x) \end{bmatrix} \quad (2.22)$$

By consequence, the Von Mises plastic criterion (2.18) deduces that:

$$[\sigma_{xx}(x) - \sigma_{zz}(x)]^2 = 4k^2(x)$$

And noting that the strip material is compressed more in thickness direction than longitudinal one, i.e $\sigma_{xx}(x) - \sigma_{zz}(x) > 0$, we obtain as follows the simplified constitutive equation of the slab method:

$$\sigma_{xx}(x) - \sigma_{zz}(x) = 2k(x) \quad (2.23)$$

The stress tensor can be finally expressed by only one 1-variable function as follows:

$$\underline{\underline{\sigma}} = \begin{bmatrix} \sigma_{xx}(x) & 0 & 0 \\ 0 & \sigma_{xx}(x) - k(x) & 0 \\ 0 & 0 & \sigma_{xx}(x) - 2k(x) \end{bmatrix} \quad (2.24)$$

Equilibrium equations

The equilibrium in x direction of a slab under contact (see Figure 2.8) is written as:

$$d[\sigma_{xx}(x).h(x)] = (\sigma_n(x) \sin \gamma - \tau(x) \cos \gamma) \frac{dx}{\cos \gamma}$$

then

$$\frac{d}{dx} [\sigma_{xx}(x).h(x)] = \sigma_n(x) \tan \gamma - \tau(x) \quad (2.25)$$

where γ is the angle between the local normal vector \underline{n} of contact surface and the vertical direction Oz , positive by convention. As the roll shape $h(x)$ is given, γ can be also calculated as:

$$\tan \gamma = -h' \quad (2.26)$$

Therefore, we can rewrite 2.25 as follows:

$$\boxed{\frac{d}{dx} [\sigma_{xx}(x).h(x)] = -\sigma_n(x)h'(x) - \tau(x)} \quad (2.27)$$

The equilibrium in z direction of the same slab leads to:

$$\sigma_{zz}(x) dx = -(\sigma_n(x) \cos \gamma + \tau(x) \sin \gamma) \frac{dx}{\cos \gamma}$$

that deduces:

$$\sigma_{zz}(x) = -\sigma_n(x) + \tau(x)h'(x) \quad (2.28)$$

By substituting 2.28 into 2.23 we obtain:

$$\boxed{\sigma_{xx}(x) = 2k(x) - \sigma_n(x) + \tau(x)h'(x)} \quad (2.29)$$

Friction law

As discussed previously, two families of friction models are studied: load dependent represented by 2.12 including Coulomb's dry model and load independent given by 2.13 containing Tresca's friction model. By definition, the neutral point is the point where the tangential velocity of strip surface velocity is equal to the roll one. Thus, before the neutral point, the roll velocity is higher than that of the strip and the friction is conventionally positive and inversely it is negative after.

Load dependent friction model:

Using 2.12 and the convention above, the friction can be written as:

$$\tau(x) = \pm\mu(x).\sigma_n(x) \quad (2.30)$$

where: + before and – after the neutral point. A friction coefficient issued from a general tribological should be in general form as $\mu(x, y)$. Nevertheless in plane strain deformation, all mechanical fields are independent of y , the friction does either: $\mu = \mu(x)$. We will keep this expression of $\mu(x)$ in the latter equations even if in practice, all 0D and 1D existing models consider a constant friction along the roll-bite due to the complexity of contact lubrication modeling (see section 2.2).

Using the equation 2.30 and by eliminating then σ_n in the equations 2.27 and 2.29, we can obtain the following ordinal differential equations of $\sigma_{xx}(x)$:

$$\begin{array}{l} \text{before neutral point: } \frac{d}{dx} [\sigma_{xx}(x).h(x)] = [\sigma_{xx}(x) - 2k(x)] \frac{\mu(x) + h'(x)}{1 - \mu(x)h'(x)} \\ \text{after neutral point: } \frac{d}{dx} [\sigma_{xx}(x).h(x)] = [\sigma_{xx}(x) - 2k(x)] \frac{-\mu(x) + h'(x)}{1 + \mu(x)h'(x)} \end{array} \quad (2.31)$$

Load independent friction model

Similarly, with 2.13 and the convention above, the friction is given by:

$$\tau(x) = \pm m(x).\sigma_0(x). \quad (2.32)$$

Also by eliminating σ_n in the equations 2.27 and 2.29, the final ordinal differential equations of $\sigma_{xx}(x)$ for load-independent friction model (Tresca's friction law) 2.32 are obtained as follows:

$$\begin{array}{l} \text{before neutral point: } \frac{d}{dx} \sigma_{xx}(x) = \frac{2k(x)}{h(x)} \left[-h'(x) - m(x) \frac{1 + h'^2(x)}{2} \right] \\ \text{after neutral point: } \frac{d}{dx} \sigma_{xx}(x) = \frac{2k(x)}{h(x)} \left[-h'(x) + m(x) \frac{1 + h'^2(x)}{2} \right] \end{array} \quad (2.33)$$

Boundary conditions and resolution algorithm

With the hypothesis that the stresses are homogeneous in the thickness in the roll-bite, we deduce that at the entry and exit of the roll-bite:

$$\begin{cases} \sigma_{xx}(X_e) = T_e \\ \sigma_{xx}(0) = T_s. \end{cases} \quad (2.34)$$

The equations 2.31 or 2.33 and the boundary conditions 2.34 allow to determine completely the two curves of $\sigma_{xx}(x)$, one before and the other after the neutral point. The intersection of these two curves determines the neutral point.

This resolution is in our days very easy thanks to finite different method and the obtained calculation time could be much less than few milliseconds with hundreds of slabs in the roll-bite. Nevertheless, the numerical resolution of the previous equations seemed to be impossible during many years before the existence of computer. For this reason, there were many attempts to simplify them in order to develop analytical solutions.

2.3.1.b Rigid-plastic slab based models

The very first investigation in rolling process is Karman's study [113] in 1925. He is the first who wrote out the equilibrium of slabs under a form of differential equation as 2.25. Karman is then considered as the pioneer and founder of slabs method. Various simplification methods of von Karman equation lead to various solutions accordingly. Using small angle approximation, Tselikov [110] deduced a simplified integration considering entry, exit tensions and a rigid perfectly plastic material without work-hardening. Unfortunately, when comparing the roll force with the measurements, he used too high Coulomb friction coefficient of 0.6. Nadai [81] also used small angle assumption but applied for different friction laws: Coulomb, constant and slip velocity dependent.

We can obviously remark that, depending on the complexity of the function $h'(x)$ that the differential equations 2.31 and 2.33 may have or not analytical solutions. Hence, one of the most common simplification assumption is to consider that the roll is circular so that the function $h'(x)$ can be expressed simply as: $h'(x) = -\tan \theta$ where θ is the angle position (see Figure 2.8). Before 1935, Karman [113], Siebel [100] and Ekelund [34] considered rigid roll with initial radius R while other authors, after 1935 mostly used Hitchcock's circular roll deformed radius R_{def} [46] depending on the roll force (see section 2.4). In some cases, as the strip model is simplified it can be coupled with Hitchcock's model analytically or otherwise by iteration method as explained in the section 2.1.4.

To understand more in detail the foundation of these models, let's study the two analytical models proposed by Bland & Ford [16] and by Alexander [2] correspondingly to Coulomb's and Tresca's friction laws.

Bland and Ford model

In 1948, Bland and Ford [16] proposed an analytical solution in the case of circular work-roll, homogenous deformation, small angle assumption and Coulomb's law with a constant friction coefficient all along the roll bite. Under the circular work-roll deformation and small angle assumptions, we note that:

$$\begin{cases} x = -R \sin \theta \\ dx = -R \cos \theta d\theta \simeq -R d\theta \\ h = h_s + R(1 - \cos \theta) \simeq h_s + \frac{R}{2}\theta^2 \\ h' = -\tan \theta \simeq -\theta \end{cases} \quad (2.35)$$

And the equation 2.28 implies that:

$$\sigma_{zz} = -\sigma_n + \tau.h'(x) \simeq -\sigma_n(1 + \mu\theta) \simeq -\sigma_n.$$

Then, by replacing σ_{xx} from 2.23 into the final equation 2.31 corresponding to Coulomb's friction law, we obtain (only the equation before the neutral point is studied because the one after will be deduced easily then):

$$\frac{d}{-R d\theta} [(2k + \sigma_{zz}).h] = \sigma_{zz} \frac{\mu - \theta}{1 + \mu\theta} \quad (2.36)$$

The left side term of this equation can be developed as:

$$\frac{d}{d\theta} \left[2kh \left(1 + \frac{\sigma_{zz}}{2k} \right) \right] = \frac{d}{d\theta} (2kh) \left(1 + \frac{\sigma_{zz}}{2k} \right) + 2kh \frac{d}{d\theta} \left(\frac{\sigma_{zz}}{2k} \right). \quad (2.37)$$

In the condition of small angle, the author highlighted that the first term of the right hand side of the equation 2.37 is negligible before the second one. By the way, as the term $\mu\theta \ll 1$, it is neglected in the equation 2.36 and this equation is then simplified as:

$$2kh \frac{d}{d\theta} \left(\frac{\sigma_{zz}}{2k} \right) = -R\sigma_{zz} (\mu - \theta).$$

We can rewrite this equation as:

$$\frac{d}{d\theta} \left(\frac{\sigma_{zz}}{2k} \right) = \frac{\sigma_{zz}}{2k} \frac{R(\theta - \mu)}{h_s + \frac{R}{2}\theta^2} \quad (2.38)$$

or

$$\frac{d\left(\frac{\sigma_{zz}}{2k}\right)}{\frac{\sigma_{zz}}{2k}} = \frac{R\theta d\theta}{h_s + \frac{R}{2}\theta^2} - \frac{R\mu d\theta}{h_s + \frac{R}{2}\theta^2}. \quad (2.39)$$

Finally:

$$\frac{d\left(\frac{\sigma_{zz}}{2k}\right)}{\frac{\sigma_{zz}}{2k}} = \frac{dh}{h} - 2\mu\sqrt{\frac{R}{2h_s}} \frac{\sqrt{\frac{R}{2h_s}} d\theta}{1 + \frac{R}{2h_s}\theta^2}. \quad (2.40)$$

This equation has following analytical solution:

$$\begin{aligned} &\text{before neutral point: } \sigma_{zz} = -2kh.K_e e^{-\mu.H} \\ &\text{after neutral point: } \sigma_{zz} = -2kh.K_s e^{\mu.H} \\ &\text{with } H = 2\sqrt{\frac{R}{2h_s}} \arctan\left(\theta\sqrt{\frac{R}{2h_s}}\right). \end{aligned} \quad (2.41)$$

K_e and K_s are two constants defined by the two boundary conditions at entry and exit as a function of entry and exit tensions and flow stresses. The neutral point is then determined by the equality of the two curves of σ_{zz} before and after neutral point given by 2.41. As can be seen, Bland and Ford solution is analytical for both longitudinal and vertical stresses as well as the contact pressure distribution along the roll bite. However, the roll force and torque can not be obtained analytically and need approximating numerically.

Alexander model

Always keeping the circular work-roll hypothesis but unlike Bland and Ford, Alexander [2] discards the assumption of small angle and considers Tresca's friction law (also with constant friction coefficient along the roll bite) and a rolled material with constant yield stress (without work-hardening). Using 2.35 but without small angle approximation, the equation 2.33 becomes (before neutral point):

$$\frac{d\sigma_{xx}}{-R \cos \theta d\theta} = \frac{2k}{h} \left[\tan \theta - \frac{m}{2 \cos^2 \theta} \right]$$

which implies:

$$\frac{d\sigma_{xx}}{d\theta} = -\frac{2kR}{h} \sin \theta + \frac{mkR}{h \cos \theta}$$

or

$$\frac{d\sigma_{xx}}{d\theta} = -\frac{2k}{h} \frac{dh}{d\theta} + \frac{mk}{\left(1 + \frac{h_s}{R}\right) \cos \theta - \cos^2 \theta}. \quad (2.42)$$

Finally by integrating analytically from the entry and similarly from the exit, Alexander obtains an analytical solution as follows:

$$\begin{aligned} &\text{before neutral point: } \sigma_{xx} = T_e - 2k \ln \frac{h}{h_e} + mk [G(\theta) - G(\theta_e)] \\ &\text{after neutral point : } \sigma_{xx} = T_s - 2k \ln \frac{h}{h_s} - mkG(\theta) \\ &\text{with } G(\theta) = \frac{R}{R + h_s} \left\{ \ln \left[\tan \left(\frac{\theta}{2} + \frac{\pi}{4} \right) \right] + \frac{2}{\sqrt{\left(1 + \frac{h_s}{R}\right)^2 - 1}} \arctan \left(\tan \frac{\theta}{2} \sqrt{1 + \frac{2R}{h_s}} \right) \right\} \end{aligned} \quad (2.43)$$

The contact pressure can be calculated from this solution and the equation 2.29.

2.3.1.c Inhomogeneous deformation - Orowan theory

Unlike previous models, Orowan [86] discarded constant yield stress assumption and introduced strain-stress curve through $\sigma_0(\theta)$. Especially, he attempted to consider inhomogeneity of deformation in thickness direction based on Prandtl's [92] and Nadai's theory [80]. According to Prandtl's analytical stresses solution for the problem of plane strain compression between two parallel plates with sticking friction, the shear stress is distributed linearly in the slab thickness and therefore the relation between longitudinal and vertical components is:

$$\begin{cases} \sigma_{xz} = -\frac{\sigma_0}{\sqrt{3}} \frac{z}{h} \\ \sigma_{xx} = \sigma_{zz} + \frac{2}{\sqrt{3}} \sigma_0 \sqrt{1 - \frac{z^2}{h^2}}. \end{cases} \quad (2.44)$$

And Nadai's solution for plane strain compression between inclined plates with a sticking friction is quite similar but he used polar co-ordinates instead of cartesian ones:

$$\begin{cases} \sigma_{xz} = -\frac{\sigma_0}{\sqrt{3}} \frac{\vartheta}{\theta} \\ \sigma_{xx} = \sigma_{zz} + \frac{2}{\sqrt{3}} \sigma_0 \sqrt{1 - \frac{\vartheta^2}{\theta^2}}. \end{cases} \quad (2.45)$$

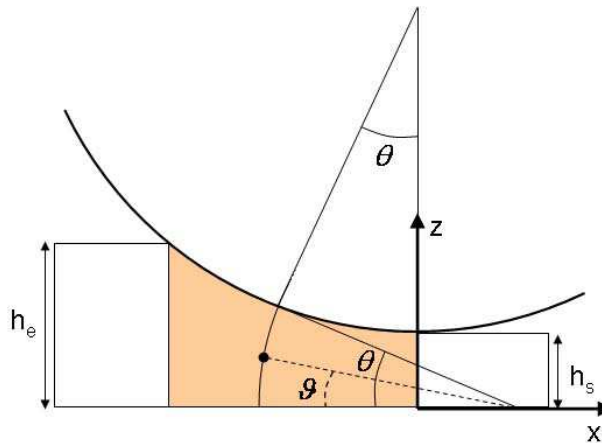


Figure 2.9: Illustration of Orowan model.

Orowan assumed that the rolling deformation resembled the compression between inclined plates to take into account heterogeneity of deformation in rolling. Moreover, he adapted Nadai's solution for a general, slipping-sticking friction law that is defined as follow:

$$\begin{cases} \lambda = \min \left(1, \frac{\sqrt{3}\mu\sigma_n}{\sigma_0} \right) \\ \tau = \pm \lambda \frac{\sigma_0}{\sqrt{3}}. \end{cases} \quad (2.46)$$

He obtained finally:

$$\begin{cases} \frac{d}{d\theta} (\bar{\sigma}_{xx} \cdot h) = R_{def} \sigma_n \sin \theta \pm R_{def} \tau \cos \theta \\ \bar{\sigma}_{xx} = \sigma_n - \frac{2\sigma_0}{\sqrt{3}} W(\lambda, \theta) \pm \tau \left(\frac{1}{\theta} - \frac{1}{\tan \theta} \right) \end{cases} \quad (2.47)$$

where $\bar{\sigma}_{xx}$ is defined as the average of σ_{xx} in the strip thickness and $W(\lambda, \theta)$ is a geometrical function given by:

$$W(\lambda, \theta) = \frac{1}{\sin \theta} \int_0^\theta \sqrt{1 - \lambda^2 \left(\frac{\xi}{\theta}\right)^2} \cos \xi \, d\xi.$$

Discussions

It is important to note that with this friction law, Orowan's theory is able to model both slipping or sticking areas alternatively along the roll-bite and that makes Orowan theory advantageous compared to previous ones. In general, when the sticking friction occurs, it is first at the neutral point corresponding to the maximum pressure and expands with increasing of friction coefficient to the entry and exit. Further, as can be seen, with the inhomogeneity of the plastic flow taken into account the differential equations 2.47 are not more complicated than with assumption of homogeneous compression (slab method). The resolution algorithm is therefore the same. The model showed excellent results compared to Siebel and Lueg's measurements [102].

However, the computing time is significantly higher due to the integration computation of $W(\lambda, \theta)$. That is why during several decades, being used as a standard against which many other models are often compared, Orowan's theory has not been applied to mill design and operation because of expensive time needed for calculations.

Regarding inhomogeneity of deformation, it is certainly difficult to judge if the rolling compression is similar to that of inclined compression plates problem. It is however interesting to just highlight that in the chapter 4, a new model of inhomogeneous and non-linear plastic deformation will be introduced. The deformation is supposed oscillation mode, implying that the shear stress is strongly non-linear and oscillates with a period equal to strip thickness function $h(x)$. These oscillation are obtained by careful *Lam3-Tec3*, finite-element method calculations as well as by *UBM*. The shear stress variation in thickness direction is indeed, more complicated than a linear relation.

2.3.1.d Orowan-based models

Since the publication of the Orowan model in 1943, a lot of work was carried out to explore or simplify its application for gains of computing time [35, 111, 112, 39, 82, 84]. Here following are presented two examples. The first one, Sims's model, with full sticking friction is very famous and largely used in industrial rolling process control. The other, recently developed attempts to keep more originalities of Orowan theory concerning mixed friction and work-hardening effect.

Sims model

Assuming full sticking with constant yield stress and small angle approximation, Sims [103] solved Orowan's differential equation analytically and derived algebraic formulae for roll pressure distribution, neutral angle, roll force and torque as follows ²:

$$\begin{cases} F = \frac{2}{\sqrt{3}} \sigma_0 \sqrt{2R_{def} \delta} Q_f \\ Q_f = \sqrt{\frac{h_s}{\delta}} \left[\frac{\pi}{2} \arctan \sqrt{\frac{\delta}{h_s}} - \sqrt{\frac{R_{def}}{2h_s}} \left(\frac{1}{2} \ln \frac{h_e}{h_s} - \ln \frac{h_n}{h_s} \right) \right] - \frac{\pi}{4} \\ Torque = \frac{2}{\sqrt{3}} \sigma_0 R_{def} R (\theta_e - 2\theta_n). \end{cases} \quad (2.48)$$

²The formula is slightly different from that of [103] because of different notations

Li's model

In 2006, based equally on the Orowan theory but unlike Sims, Li *et al* [67] discards the assumption of sticking friction. They also use the small angle hypothesis and by assuming that the function $W(\lambda, \theta)$ is independent of θ that seem to be justified (see the graphic of W in the p. 20 of [86]). This function becomes a simple function of λ , $W = W(\lambda)$. By consequence algebraic equations of roll pressures in the forward and backward slip zones have been derived by solving the two Orowan equations 2.47 analytically. The roll force and torque are then integrated numerically and the model is already fast because no integration of w is needed. Further, by approaching the roll pressure distribution as a quadratic function of θ by part (before and after the neutral point), its is only necessary to compute the roll pressure at 5 points (2 before, 2 after and the neutral point) to get a quadratic approximation. The roll force and torque are then analytical integration from this approximated solution. Finally this quadratic approximation requires extremely low calculation time while its errors compared to Orowan's exact solution are lower than 1% for rolling conditions of a 7-stand and 3-stand aluminium mills.

2.3.1.e Taking into account elasticity - Bland and Ford 1952

After the Orowan theory and the simplification developments, some latter studies brought out the inaccuracy of these models despite of their sophistication allowing for inhomogeneous deformation and slipping-sticking friction. This inaccuracy is indeed due to the elastic deformation and can be important for estimation of both roll force and much more in the case of roll torque. It is predominately significant for small thickness reduction ratio, less than 10%. Ford *et al* [37], Bland & Ford [17] and Bland & Sims [15] made considerable modifications to the simplified theory of cold rolling developed by Bland & Ford [16]. Until the work of Bland and Force in 1952 [17], non of the theories of rolling, nor the calculations of roll force and torque have taken into account the effect of the elastic zones. While these elastic zones do not only have direct influence on the roll force and torque but also change the entry and exit tensions of the plastic zone. Bland and Ford proposed a method for approximating these contributions of entry and exit elastic zones to the roll force and torque.

Elastic recovery: Let study first their analysis for the elastic recovery zone at the exit. At first, the authors assume plane strain deformation for all plastic and elastic zones, even if this hypothesis leads to a discontinuity of stresses due to the difference of Poisson's coefficient $\nu = 0.3$ in elastic zone and 0.5 in yield criterion. They consider in elastic recovery zone the longitudinal stress (tension) changes but not much and can be approximated constant and equal to T_s . The vertical stress varies from a certain value at the lowest point of the work-roll and becomes 0 at the last point of contact $x = a$. The lowest point is also the last point of plastic deformation. All shear stresses are neglected.

Bland and Ford consider in this elastic zone that: $\sigma_{yy} = \nu (\sigma_{xx} + \sigma_{zz})$ then by Hooke's generalized law:

$$\begin{aligned}\epsilon_{zz} &= -\frac{\nu(1+\nu)}{E}\sigma_{xx} + \frac{1-\nu^2}{E}\sigma_{zz} \\ \sigma_{zz} &= \frac{E}{1-\nu^2}\epsilon_{zz} + \frac{\nu}{1-\nu}\sigma_{xx}.\end{aligned}$$

We remark that in fact this hypothesis is too strict because at the last point of contact $x = a$ the plane strain deformation is not really verified. This point will be discussed more in the latter chapter 7, section 7.4.1. In fact, in this zone only the variations of stresses verify plane strain hypothesis, meaning:

$$\Delta\epsilon_{zz} = -\frac{\nu(1+\nu)}{E}\Delta\sigma_{xx} + \frac{1-\nu^2}{E}\Delta\sigma_{zz}.$$

If the reference is chosen at the point $x = a$ where $\sigma_{zz} = 0$ and reminding that $\Delta\sigma_{xx} \simeq 0$, we have:

$$\Delta\epsilon_{zz} = \frac{1-\nu^2}{E}\sigma_{zz}. \quad (2.49)$$

We will continue to use this weaker hypothesis instead of plane strain one because indeed it does not change the results of Bland and Ford analysis.

If Δu_z denotes the variation of vertical displacement on the upper surface with respect to the reference point $x = a, z = h_s$, as the upper surface is in contact with the work-roll we have:

$$\Delta u_z = -\frac{1}{2R_{def}} (a^2 - x^2). \quad (2.50)$$

And by definition,

$$\Delta u_z = \int_0^h \Delta \epsilon_{zz} dz. \quad (2.51)$$

By substituting the equations 2.49 and 2.50 into 2.51 and using $h \simeq h_s$, σ_{zz} is constant in the thickness, we get:

$$u_z = -\frac{1}{2R_{def}} (a^2 - x^2) = \int_0^h \frac{1 - \nu^2}{E} \sigma_{zz} dz \simeq h_s \frac{1 - \nu^2}{E} \sigma_{zz}$$

which deduces finally:

$$\sigma_{zz} = -\frac{E}{2(1 - \nu^2) R_{def} h_s} (a^2 - x^2). \quad (2.52)$$

Now, the yield criterion at the $x = 0$ implies:

$$\sigma_{xx}(x = 0) - \sigma_{zz}(x = 0) = k(0) = k_s \Rightarrow \sigma_{zz}(x = 0) \simeq T_s - k. \quad (2.53)$$

By comparing two equations 2.52 and 2.53, we can determine a as follows:

$$a^2 = \frac{2(1 - \nu^2) R_{def} h_s}{E} (k - T_s). \quad (2.54)$$

The contribution of this elastic zone to the roll force, torque and tension can be estimated by:

$$\begin{aligned} P_s^{elas} &= - \int_0^a \sigma_{zz} dx = \frac{Ea^3}{3(1 - \nu^2) R_{def} h_s} \\ G_s^{elas} &= -\mu R P_s^{elas} \\ T_s^{plas} &= T_s - \frac{\mu P_s^{elas}}{h_s}. \end{aligned} \quad (2.55)$$

Elastic compression at entry: With a similar analysis the authors obtain equally a parabolic distribution of vertical stress (similar to 2.52) as follows:

$$\sigma_{zz} = -\frac{E}{2(1 - \nu^2) R_{def} h_e} (L^2 - x^2) \simeq -\frac{E.L}{(1 - \nu^2) R_{def} h_e} \delta x. \quad (2.56)$$

The first point of yield criterion is determined by $\sigma_{zz} = T_e - k$, thus:

$$\delta x_e = \frac{(1 - \nu^2) R_{def} h_e}{E.L} (k - T_e) \quad (2.57)$$

where L is the contact length. The contribution of this elastic compression zone to the roll force, torque and tension are given by:

$$\begin{aligned} P_e^{elas} &= - \int_0^{\delta x_e} \sigma_{zz} d\delta x = \frac{E.L}{2(1 - \nu^2) R_{def} h_e} \delta x_e^2 = \frac{(1 - \nu^2) R_{def} h_e}{2E.L} (k - T_e)^2. \\ G_e^{elas} &= \mu R P_e^{elas} \\ T_e^{plas} &= T_e - \frac{\mu P_e^{elas}}{h_e}. \end{aligned} \quad (2.58)$$

Discussions: This very first work taking into account the elasticity in rolling showed out that the elastic zones (especially the exit one) have an appreciative effect on the total roll force and torque. And these results of Bland and Force being completely analytical are largely used for online applications. Nevertheless, this is not the exact solution of slab method for elastic behavior because of many approximations (small angle even for entry elastic compression zone, small perturbations...). And the most important point that the authors also brought out is that in the plastic zone the elastic component of strain is not taken into account by their model and it has never been done previously. Until 1968, Cosse et al [27] solved this problem by building the most complete model based on slab method for elasto-plastic behavior.

2.3.1.f Elasto-plastic slab model - Cosse et al 1968

Cosse et al [27] assume the main hypotheses of slab method such as plane strain, homogenous deformation in thickness. They consider Coulomb slipping friction (no sticking) law with a constant friction coefficient along the roll bite. On the other hand, they introduce elasto-plastic behavior of rolled material by using the complete Prandtl-Reuss equations [45]. The material behavior law depends equally on strain rate allowing to model influence of rolling speed. Moreover, the authors attempted to develop the most general theory as possible by using non-circular work-roll deformation model based on the influence functions method allowing good performances even in the conditions small reduction rolling.

Material mechanical behavior:

Based on literature studies, the authors use an analytical form that takes into account work-hardening effect as follows:

$$\bar{\epsilon} = \frac{\sigma_0}{E} + \left(\frac{\sigma_0}{B}\right)^n = \frac{\sigma_0}{E} + |\sigma_0|^{n-1} \frac{\sigma_0}{B^n}. \quad (2.59)$$

The dynamic effect can be taken into account through the parameter B without impact on the resolution of equations system.

Equilibrium equation:

The equilibrium equations for a slab are the same as 2.27 and 2.28. As a reminder, the definition of the angle γ representing the local normal vector of strip surface as $\tan \gamma = h'$. According to us Cosse et al made small mistake in their equilibrium equations using θ instead of γ ($\gamma \neq \theta$ for non-circular work-roll, see Figure 2.10) as follows:

$$\begin{aligned} \frac{d}{dx} [\sigma_{xx} \cdot h] &= \sigma_n \tan \theta - \tau = \sigma_n (\tan \theta - \mu) \\ \sigma_{zz} &= -\sigma_n - \tau \tan \theta = -\sigma_n (1 + \mu \tan \theta). \end{aligned} \quad (2.60)$$

However, this is not a big issue and could be easily corrected. Indeed, this fact does not influence the great interest of this model which is how to deal with elasto-plastic behavior. Let follow the authors original equations.

The roll profile is represented by a various radius function $R'(\theta)$ which, unlike the Hitchcock curved radius R_{def} , is the real distance from a point on the roll surface to its center. To understand the calculation of thickness, let h_2 is the targeted value of the minimum height of the roll gap (in this article, h_2 is given but not the outgoing height h_s as in other ones). The question is how to set the work-roll center vertical position in order to get this targeted minimum gap as the roll is deformed. At first let fix the center so that the non-deformed half of roll gap is equal to h_2 , meaning the distance between the two rolls centers is $2(h_2 + R)$ and as the roll is deformed the minimum height is equal to h_4 . So to get the minimum height of h_2 we need to set a new position of the roll so that the half of roll gap with non-deformed roll is:

$$h_0 = 2h_2 - h_4. \quad (2.61)$$

. Finally, the strip thickness can be calculated as follows:

$$h = 2h_2 - h_4 + R - R'(\theta) \cos \theta. \quad (2.62)$$

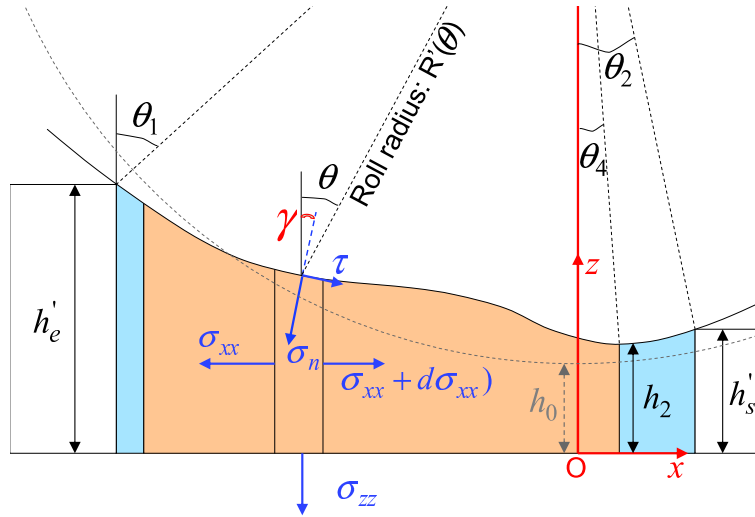


Figure 2.10: Cosse et al slab model for elasto-plastic strip behavior and non-circular work-roll deformation.

By neglecting $\mu \tan \theta$ in the 2nd equation of 2.60 and substituting it into the 1st one, the authors obtain following equilibrium equation:

$$\frac{d\sigma_{xx}}{d\theta} = \frac{1}{h} \left[R' \sigma_{zz} (\sin \theta - \cos \theta) - \sigma_{xx} (R' \sin \theta - \cos \theta \frac{dR'}{d\theta}) \right]. \quad (2.63)$$

Elasto-plastic compression:

This zone extends from the entry of the strip between the rolls (θ_1) and the minimum height in the gap (θ_4). The general equations relating stresses and strains are those of Prandtl-Reuss [45]:

$$\begin{aligned} \delta\epsilon_{xx} &= \frac{1}{E} [\delta\sigma_{xx} - \nu (\delta\sigma_{yy} + \delta\sigma_{zz})] + \frac{\delta\bar{\epsilon}_p}{\sigma_0} \left[\sigma_{xx} - \frac{1}{2} (\sigma_{yy} + \sigma_{zz}) \right] \\ \delta\epsilon_{yy} &= \frac{1}{E} [\delta\sigma_{yy} - \nu (\delta\sigma_{zz} + \delta\sigma_{xx})] + \frac{\delta\bar{\epsilon}_p}{\sigma_0} \left[\sigma_{yy} - \frac{1}{2} (\sigma_{zz} + \sigma_{xx}) \right] \\ \delta\epsilon_{zz} &= \frac{1}{E} [\delta\sigma_{zz} - \nu (\delta\sigma_{xx} + \delta\sigma_{yy})] + \frac{\delta\bar{\epsilon}_p}{\sigma_0} \left[\sigma_{zz} - \frac{1}{2} (\sigma_{xx} + \sigma_{yy}) \right] \end{aligned} \quad (2.64)$$

The plane strain condition is:

$$\delta\epsilon_{yy} = 0. \quad (2.65)$$

In addition to the Prandtl-Reuss relationships, Von Mises plasticity criterion is chosen. This criterion is, in the condition of no shear stresses, given by:

$$\sigma_0 = \sqrt{\frac{(\sigma_{xx} - \sigma_{yy})^2 + (\sigma_{yy} - \sigma_{zz})^2 + (\sigma_{zz} - \sigma_{xx})^2}{2}}. \quad (2.66)$$

The strip material behavior 2.59 implies that:

$$\delta\lambda = \frac{\delta\bar{\epsilon}}{\sigma_0} = \frac{n}{B^n} |\sigma_0|^{n-1} \frac{d\sigma_0}{\sigma_0}. \quad (2.67)$$

By definition:

$$\epsilon_{zz} = \ln \frac{h}{h_e} \quad (2.68)$$

Not showing here the details of calculations, we highlight only that the authors obtain from the equations above the three final differential equations as follows:

$$\begin{cases} \frac{dS_x}{d\theta} = \frac{R'(S_z + S_y)(\sin\theta - \mu \cos\theta)}{h} - A(S_x + S_y) - \frac{dS_y}{d\theta} \\ \frac{dS_y}{d\theta} = \frac{A}{G_1} - \frac{G_1 - FS_x(2S_z - S_x)}{3G_1} \frac{dS_z}{d\theta} + \frac{G - G_1 + FS_x(2S_x - S_z)}{3G_1} \frac{dS_x}{d\theta} \\ \frac{dS_z}{d\theta} = \frac{A}{G + FS_z(S_z - S_x)} - \frac{FS_z(2S_x - S_z)}{G + FS_z(2S_z - S_x)} \frac{dS_x}{d\theta} \end{cases} \quad (2.69)$$

where

$$\begin{cases} G = (1 + \nu)E \\ G_1 = (1 - 2\nu)E \\ S_x = \sigma_{xx} - \sigma_{yy} \\ S_y = \sigma_{yy} \\ S_z = \sigma_{zz} - \sigma_{yy} \\ F = \frac{3n}{4B^n} (S_x^2 + S_z^2 - S_x S_z)^{\frac{n-3}{2}} \\ A = \frac{R' \sin\theta - \frac{dR'}{d\theta} \cos\theta}{h} \\ S_x^2 + S_z^2 - S_x S_z = S_y^2 = \sigma_0^2 \end{cases} \quad (2.70)$$

The equations 2.69 are solutions for the elasto-plastic zone corresponding to the part before the neutral point. For the other part, the sign of friction coefficient inverses.

Elastic recovery: This zone extends from θ_4 to the exit of the contact θ_2 . In this zone, the material behavior follows Hooke's law:

$$\begin{aligned} d\epsilon_{xx} &= \frac{1}{E} [d\sigma_{xx} - \nu (d\sigma_{yy} + d\sigma_{zz})] \\ d\epsilon_{yy} &= \frac{1}{E} [d\sigma_{yy} - \nu (d\sigma_{zz} + d\sigma_{xx})] \\ d\epsilon_{zz} &= \frac{1}{E} [d\sigma_{zz} - \nu (d\sigma_{xx} + d\sigma_{yy})] \end{aligned} \quad (2.71)$$

and the plane strain condition implies $d\epsilon_{yy} = 0$, hence:

$$d\sigma_{yy} = \nu (d\sigma_{zz} + d\sigma_{xx}). \quad (2.72)$$

Then, substituting 2.72 into the third equations of 2.71, we have:

$$\frac{d\epsilon_{zz}}{d\theta} = \frac{1}{E} \left[(1 - \nu^2) \frac{d\sigma_{zz}}{d\theta} - \nu(1 + \nu) \frac{d\sigma_{xx}}{d\theta} \right]. \quad (2.73)$$

Noting that the strip thickness is imposed by the work-roll shape along this elastic zone, then:

$$\frac{d\epsilon_{zz}}{d\theta} = \frac{1}{h} \frac{dh}{d\theta}. \quad (2.74)$$

The equation 2.73 becomes:

$$\frac{d\sigma_{zz}}{d\theta} = \frac{E}{1 - \nu^2} \frac{1}{h} \frac{dh}{d\theta} + \frac{\nu}{1 - \nu} \frac{d\sigma_{xx}}{d\theta}. \quad (2.75)$$

The equilibrium equation 2.63 and the equation 2.75 form a system of two differential equations which represent the solution in the elastic recovery zone.

Roll flattening by influence functions method: The authors use the method proposed by Jortner [52], see the section 2.4.2.b.

Resolution: Here following is the principles of numerical resolution:

1. In the first iteration, the roll is considered to be non-deformed and the $h_0 = h_2$. In subsequent iterations, the deformation of the roll corresponding to the pressure distribution found in the preceding iteration is calculated. The angle θ_4 as well as the minimum height h_4 are then determined. The new position of the roll is estimated with $h_0 = 2h_2 - h_4$.
2. Determine entry angle θ_1
3. Chose initial value of neutral angle θ_N .
4. Solve the system of differential equations 2.69 for the elasto-plastic compression zone using initial conditions at $\theta = \theta_1$ as $\sigma_{xx} = T_e$ and $\sigma_{yy} = \sigma_{zz} = 0$. The system is solved numerically according to an improved Runge-Kutta method [24]. In each step, the instantaneous strain rate is calculated first and then the material law parameters B and/or n are deduced. The θ is compared to θ_N to decide the sign of the friction. This sequence of calculations is repeated until θ_4 .
5. Solve the differential equations 2.63 and 2.75. The initial conditions at $\theta = \theta_4$ are the stresses σ_{xx} and σ_{zz} issued from the exit of the elasto-plastic zone. The neutral point can also be present in this zone so the thickness h is compared to the thickness h_N to decide the sign of friction in the equation 2.63. This operation is repeated until the value of σ_{zz} reaches 0, to within certain accuracy. The angle θ_2 as well as σ_{xx} and σ_{zz} are thus defined.
6. Compare the tension $\sigma_{xx}(\theta_2)$ obtained to the exit tension T_s . If they are not identical, it means that the value θ_N is not correct. Chose a new value of θ_N and restart the calculations from the step 4 (elasto-plastic zone) to step 6 until $\sigma_{xx}(\theta_2) = T_s$ within a given accuracy.
7. Calculate the foll force and compare to the values obtained by two previous iterations. If they are less different than a given precision, the solution is obtained. If not, restart from step 1 with new contact stresses distribution.

Discussions:

Cosse and al proposed a very general theory for cold rolling with minimum as possible of assumptions both in the strip and the roll. This elasto-plastic solution allows to overcome many questions previously put out, such as the discontinuity of σ_{yy} at the limit between elastic and plastic zones because of the Poisson's coefficient of 0.3 (for elastic zone) and 0.5 (for plastic zone) in plane strain conditions. Moreover, unlike Bland & Ford, the plane strain is correctly written using the variation of strain is equal to zero. The model can also be accommodated for any material behavior law as well as any friction law (Tresca or Coulomb, contact or variable along the roll bite...).

However, it is important to highlight that both Bland & Ford and Cosse et al models neglect shear stress (issued from assumption of homogeneous deformation) in the entry elastic compression zone. That should not be correct. Indeed, at the first contact point du to the brutal change of thickness the shear stress can be very important despite it can be concentrated in a really small zone. It could even be the main reason for the plastic yield at this point. That is why we will propose a very new and simple model for this in the section 7.3. The elastic recovery will be re-studied in the same chapter because these elastic zones have primordial influence on the width variation of the strip that is the objective of the thesis. Cosse model will be the base for our developments concerning the influence of elasticity on the width variation.

2.3.2 2D models

In cold temper rolling processes (skin-pass), as thickness reduction is usually very small, deformation is strongly z -dependent with a concentration near the strip/roll contact). The same is true in hot strip rolling, in particular in the roughing mill because of significant ratio thickness to contact length. In the finishing section, the strains and stresses

are more or less z -independent in the last stands, but the strong temperature coupling brings the z -coordinate back in. 2D models are particularly required when we are interested in flatness defects like longbow and crossbow in a top-bottom asymmetric rolling (see Figure 2.11). The longbow defect corresponding to a curvature along the strip is caused by inhomogeneous longitudinal heterogeneous residual stress σ_{xx} and crossbow representing by a curvature across its width is due to heterogeneous residual stress σ_{yy} . In such cases, 1D approaches are inadequate and must be replaced by plane strain 2D models, whereby fields depend on 2 space variables x and z .

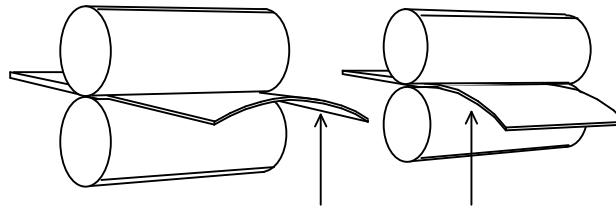


Figure 2.11: Crossbow (left) and longbow (right) defects due to homogeneous residual stress in strip thickness.

In the literature, several types of methods are able to make these requirements met. The first one is Finite Difference Methods (*FDM*) [23] and [85]. Of course *FEM* [63, 61] are useful to quote pioneering work. *FEM* models are generally quasi-static implicit [66], sometimes dynamic explicit [62]. And recently, the Element-Free Galerkin method [116]. These methods may use any kind of constitutive equations. The last commonly used method for 2D rolling is the Upper-Bound or Upper-Bound-like methods with velocity fields based on streamlines generally, using either visco-plastic or rigid-plastic slightly compressible. *UBM*-based 2D models will be presented in the chapter 3.

Unlike 1D models, 2D ones could approach physical solutions of shear strains and stresses without any assumption as proposed by Orowan. The z -dependence of velocity, strain, stress and temperature are equally modeled and this fact enables to predict profiles of residual stress distribution in strip thickness as well as profiles of temperature and microstructure. Moreover, they are able to deal with extremity effects as well as unsteady state while 1D models are confined to stabilized state. On the other hand, these models are more time-consuming and there is not really significant development of simplified solutions of 2D models except some *UBM*-based ones.

2.3.3 3D models

When objective of the study concern residual stresses, flatness defects or when we are interested in the distribution of any parameters in width direction Oy , 3D models become necessary. These models are also required otherwise for any case where the plane strain deformation is no longer valid, for example rolling process of relatively narrow and thick products. Obviously, for the width variation, 3D models should be inevitable. The methods include generalized Upper Bound Methods, such as Finite Strip Methods with rigid plastic behavior [69]. 3D models are often *FDM* [23, 85], and widely *FEM* with dominantly implicit ([68] and many others) or sometimes dynamic explicit formulations.

2.4 Typical work-roll deformation models

For a 4-High stand, the most commonly used in automotive and packaging steel rolling, the roll force is usually applied at the ends of the backup-rolls. The work-rolls are at the same time under the contact pressure with the backup-rolls and the strip. The roll torques are very often driven directly on the work-rolls. The work-roll deformation can be separated into two modes. The first one, called bending is the roll deformation in the transverse-vertical plane Oyz , as can be seen in Figure 1.8. The deformation of the roll axis generally can be calculated by beam theory. That can result to a deformed strip thickness profile with a maximum at the center and a slight decreasing toward the edges.

The second mode caused by strip contact pressure is called flattening. That is the local deformation of the roll in the plane Oxz reducing in fact the distance of the work-roll surface material point to its axis. In addition, at the strip edges the roll profile is locally reflected in the transverse vertical plane Oyz because of the discontinuity of contact

pressure (see Figure 2.12). By consequence, the strip thickness is reduce more at its edges, called often **edge drop** phenomenon.

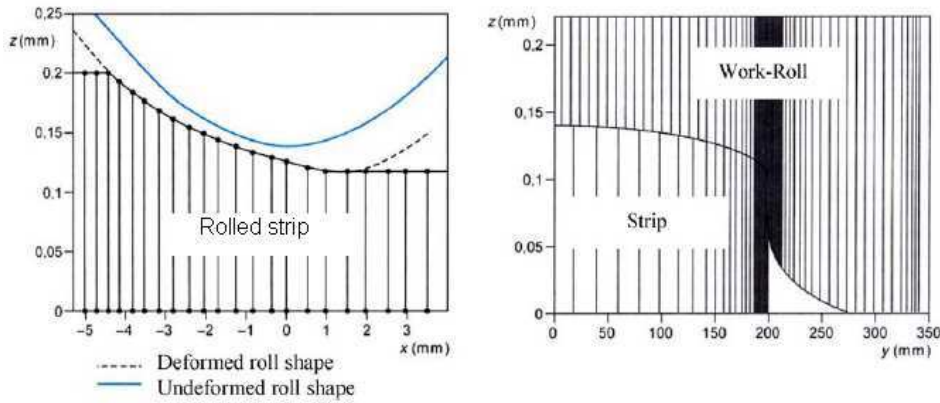


Figure 2.12: Work-roll flattening respectively in plane xz called non circular deformation along the roll-bite and yz called edge drop.

2.4.1 Bending and flattening in width direction Oyz - 3D modeling

As mentioned above, 2D and 3D modeling is not the main subject of the thesis, then it is so for the work-roll deformation in 3D modeling. That is why although there exist many interesting works using *FDM*, *FEM* and analytical methods to model the bending and flattening at the edge of the strip, they are not presented in this document.

On the other hand, we present only in some words about Tec3 a work-roll deformation model developed by Arcelor-Mittal. Beam + influence functions for flattening in both planes xz and yz . The combination of *Lam3* and *Tec3* becomes referent model and will be used to estimate performance of models developed in this thesis.

2.4.2 Flattening models for 2D modeling

2.4.2.a Hitchcock model

The very first exiting model of roll deformation is Hithcock's one [46] for roll flattening. Based on the analysis of the elastic Hertz contact, he considers the flattened roll stay circular in the roll-bite but with an increased radius. This deformed radius is explicitly given by:

$$R_{def} = R \left[1 + \frac{1 - \nu_r^2}{\pi E_r} \frac{F}{\delta} \right]. \tag{2.76}$$

Thanks to simplicity, satisfying results and the fact that the deformed roll is always circular allowing many simplifications of strip models, this formula is largely used 1D and 2D models.

Latter, taking into account the elasticity in the deformation of the strip *see* te section 2.3.1.e, Bland & Ford [17] introduced two additional contact arcs at entry and exit of the roll bite under which the strip is only deformed elastically. Due to these elastic arcs the contact length is higher and by consequence the roll is less deformed for a same given roll force. That is why they proposed to correct Hitchcock's formula as follows:

$$R_{def} = R \left[1 + \frac{1 - \nu_r^2}{\pi E_r} \frac{F}{(\sqrt{\delta} + \delta_1 + \delta_2 + \sqrt{\delta_2})^2} \right]. \tag{2.77}$$

where δ_1 and δ_2 are defined as follows:

$$\begin{cases} \delta_1 = \frac{\nu_r(1 + \nu_r)}{E_r} (T_s h_s - T_e h_e) \\ \delta_2 = h_s \frac{1 - \nu_r^2}{E_r} (k_s - \sigma_s) \end{cases} \quad (2.78)$$

Hitchcock’s model more and more valid if the rolled material is softer or the ratio thickness over roll diameter is higher or the reduction is larger. This model is very commonly used in hot rolling domain including roughing as well as finishing mills. For cold rolling, it is only valid the firsts stands of automotive tandem mills. For rolling of packaging products (very low thickness down to 0.17mm) the roll is strongly deformed and can not be approached by this model. An other case where this model reaches is not accurate is skin-pass rolling where the reduction is generally from 0.2% to 3%.

2.4.2.b Jortner model - Influence functions

Jortner model [52] closely approximates the condition found in a 4-high mill where the back-up roll supplies the balancing load. Making use of St. Venant’s principle, it is assumed that the actual location and distribution of the back-up pressure will have a negligible effect on the radial deformations of points on the contact arc. Thus, this model was based on the elementary problem of a cylinder subjected to diametrical concentrated loads . Based on the exact elastic deformation solution of this problem given by Timoshenko and Goodier [108], Jortner integrated the radial strain along a radius to obtain the radial deformation of an arbitrary point $S(R, \theta)$ as follow:

$$u_r(R, \theta) = \frac{P}{\pi \cdot E_r} \cdot \left\{ (1 - \nu_r^2) \left[\cos \theta \ln \frac{1 - \cos \theta}{1 + \cos \theta} + 2 \right] - (1 - \nu_r - 2\nu_r^2) \sin \theta \left[\arctan \frac{1 + \cos \theta}{\sin \theta} + \arctan \frac{1 - \cos \theta}{\sin \theta} \right] \right\} \quad (2.79)$$

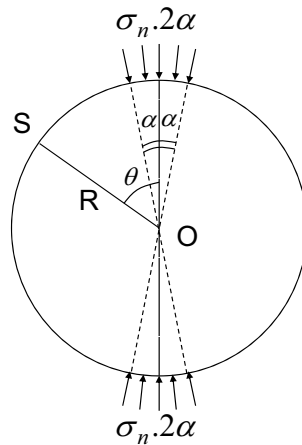


Figure 2.13: Plane-strain problem of a cylinder subjected to diametrically applied pressures over finite angle.

Replacing of the concentrate force by a continuous pressure σ_n over the small finite angle 2α as shown in Figure 2.13, not only eliminates the infinite stresses and strains under the point load but also permits an arbitrary pressure distribution to be expressed in terms of finite increments. Performing the integration involving equation 2.79 yields the

following result when the point S is outside the pressure area, $|\theta| > \alpha$:

$$\begin{cases} u_r(R, \theta, \alpha) = \frac{\sigma_n \alpha}{\pi \cdot E_r} \cdot [M(\theta + \alpha) - M(\theta - \alpha) + N(\theta + \alpha) - N(\theta - \alpha)] \\ \text{with:} \\ M(\xi) = (1 - \nu_r^2) \sin \xi \ln \frac{1 - \cos \xi}{1 + \cos \xi} \\ N(\xi) = (1 - \nu_r - 2\nu_r^2) \cos \xi \left[\arctan \frac{1 + \cos \xi}{\sin \xi} + \arctan \frac{1 - \cos \xi}{\sin \xi} \right]. \end{cases} \quad (2.80)$$

When the point S is inside the pressure area, $|\theta| < \alpha$, it is necessary to integrate from both sides but not going through the point S . The final result is:

$$\bar{u}_r(R, \theta, \alpha) = u_r(R, \theta, \alpha) - \frac{\sigma_n \alpha}{\pi \cdot E_r} (1 - \nu_r - 2\nu_r^2). \quad (2.81)$$

Finally, with the influence function established the deformation of a point on the surface of the roll due to a specific pressure distribution can be determined by a sum of finite increments.

In the same article, Jortner has coupled this roll deformation model with a strip model based on Bland & Ford [17] by iterative method as explained in the section 2.1.4. By comparing the roll and torque with sixteen experiments, he obtained quite low errors but it is difficult to judge if the accuracy of the prediction is better than previous models. However, it is felt that this method is at least as accurate and considerably more general than other methods in use.

Remark: *It is important to note that the author considered that tangential shearing stresses on the contact arc have a negligible effect on the radial deformations. Therefore, only the radial deformation of the work-roll caused by radial stress (main contributing factor) is considered in this article.*

2.4.2.c Fleck and Johnson - Neutral zone existence

In the domain of thin metallic foil cold rolling (typically packaging product), according to slab method 2.3.1.a, the evolution of normal stress along the roll bite is proportional to $1/h(x)$ and becomes therefore important for thin strip especially around the neutral point. With classic sliding friction, tangential stress is also important and itself makes the normal stress increase more after resolution. Finally, the normal and tangential stresses are artificially increased around the neutral point. After, Fleck and Johnson [36], this phenomenon does not really exists because the work-roll should be deformed under this concentrated contact stresses. They consider that there exist a region at the middle of the roll bite where the strip thickness is not reduced. This problem was previously recognized by Quan [93] but Quan assumed that the rolls remain circular.

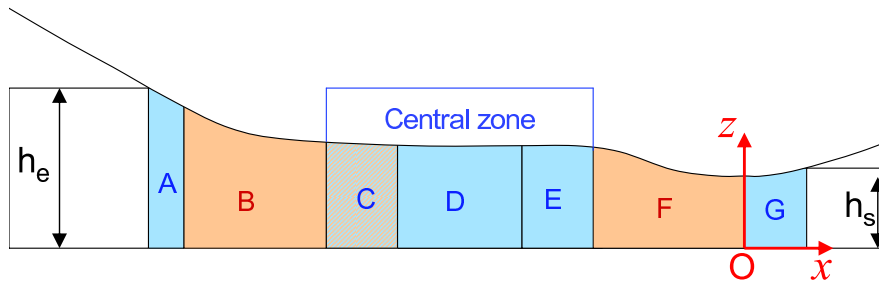


Figure 2.14: The roll bite is divided into 7 zones: Entry elastic zone (A), entry plastic reduction zone (B), plastic contained without reduction & slipping (C), elastic without slipping (D), elastic with slipping (E), exit plastic reduction zone (F) and exit elastic unloading (G).

In Fleck and Johnson theory, the work roll is allowed to deform to a non-circular profile and the plastic reduction occurs near entry and near exit of the roll bite, separated by a central region where the strip does not suffer reduction and does not slip relative to the work roll, see Figure 2.14.

For the work-roll deformation, based on Johnson and Bental [50] study for the case of zero reduction, Fleck and Johnson postulated that:

$$\sigma_n(x) = p_0 \sqrt{1 - \frac{x^2}{L}} - K_n (h_e - h(x)) \quad (2.82)$$

where p_0 is the maximum normal stress. This expression is Hertzian solution adjusted by a "elastic foundation" perturbation due to the local plastic reduction $h_e - h(x)$ of the foil at considered point. And K_n is a "foundation modulus" constant chosen to give a good match with the true deformation. The resolution method consists in writing in each zone the governing equation of stresses and continuous conditions through successive zones. Iterative calculations are required to determine p_0 , position and length of each zone.

Remark: This model is the first that introduce the presence of non-reduction zone allowing to approach thin and very thin rolling. However, it is not really advantageous because the strip thickness evolution is almost imposed and because the model does not take neither into account the entry and exit tensions nor the strip material work-hardening.

2.4.2.d Matsumoto

Matsumoto [72] is an elastic-plastic model with presence of a neutral zone. The difference compared to Fleck and Johnson model is that, Matsumoto considers that the neutral zone is also the non-reduction one. The roll bite is therefore composed of 5 zones instead of 7 by Fleck and Johnson model. In addition, he points out that in this zone, the plastic thickness is constant by the real apparent thickness is variable due to the stress and elastic deformation variation, meaning the work-roll shape is not really constant, see Figure 2.15.

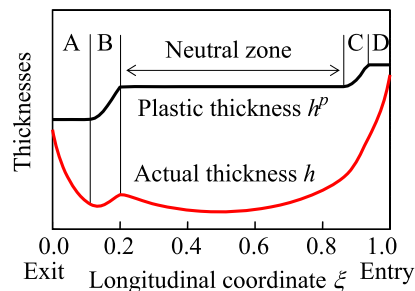


Figure 2.15: In this figure, the roll bite entry is in the right side. According to Matsumoto, the roll bite is divided into 5 zones: Entry elastic (D), entry plastic (C), neutral zone without slip and without plastic deformation, exit plastic (B) and exit elastic (A).

Matsumoto's model based on influence function model for the work-roll deformation and Orowan model for the strip. But allowing to occur the neutral zone, Matsumoto obtained a quite general rolling model for both cold and temper rolling. His model is robust even for very low reduction such as 0.1% or even lower. He introduces equally a numerical method using a fixed number of elements in the roll bite at a coordinate ζ that is standardized always 0 at exit and 1 and the entry. With this method, he obtains an influence matrix (calculated only once) instead of influence function allowing to improve the computing time to less than one hundred ms.

2.5 Discussions

Online process control Although being developed long time ago, these analytical models thanks to their advantage rapidly, are very largely used for industrial rolling process preset and control. For example, Sims's model with sticking friction usually coupled with the Hitchcock's model is very commonly used and gives excellent performances

in strip or plate hot rolling where a high friction coefficient occurs. However, when lubricant is applied, a significantly lower friction occurs, that has been observed in hot rolling of steel [97], [105] and [88]. There were many developments of simplified models and there will be more allowing to improve more and more quality of online process control.

In cold rolling mill, in order to cover high range of reduction (low reduction for hard and wide products) the elastic spring back (elastic recovery zone) needs taking into account. The models such as Bland & Ford [17], [17] and Bryant & Osborn [19], [20] are generally used.

For skin-pass rolling with relatively high friction and small reduction (about 0.2-3.0%) the elastic deformation becomes extremely important. Sometime, the elastic deformation may appear inside the roll-bite, *i.e* the material deformation is elastic and plastic alternatively. In addition, due to a very small contact length the work-roll deformation is strongly non-circular. By consequence, the models taking into account strip elasticity and non-circular deformation of the work-roll such as [36, 72] could be enough accurate for this process.

Offline applications The 2D and 3D models are of course extremely important understanding of physical phenomena and to explore more in detail where the measurements are not accessible. These model are, therefore generally used for pioneering studies of new subjects, or as a standard to validate simplified models. They are sometimes used for finding the causes of certain defects allowing then to propose corrections process actions.

Chapter 3

Upper Bound Method applied in rolling process

This chapter presents in the first place the extremum principles. The Upper Bound Method (UBM) is one of these principles that is very largely used to model metal forming processes. The second section presents the typical applications of the UBM to rolling process in plane strain condition (2D). The application pointed out the main advantages of UBM to be analytical (or almost), fast and give interesting results. All along the chapter, the reader will see that the principal difficulty of the method is how to build suitable kinematically admissible velocity field for the considered problem. There exist two families of velocity fields: one with rigid body (slip lines) and the other with continuous velocity field in the plastic deformation zone. The UBM, allowing to estimate the velocity field, is furthermore frequently used to model the width variation in rolling. Such 3D UBM models will be presented in a later chapter 5.

Contents

3.1 Principle of the UBM	52
3.1.1 Extremum principles	52
3.1.2 UBM applied to rolling process	55
3.2 Velocity fields with rigid bodies motions	56
3.2.1 Simulated sliding theory and experiments	56
3.2.2 Concept for analysis of linear and rotational velocity fields	58
3.2.3 Unitriangular velocity field	58
3.2.4 Multitriangular velocity field	61
3.3 2D continuous velocity fields	62
3.3.1 Continuous eccentric velocity field	62
3.3.2 Continuous simple velocity field	64
3.3.3 Improved velocity field	66
3.3.4 Circular stream lines velocity field	66
3.3.5 Elliptical stream lines velocity field	67
3.4 Discussions	69

3.1 Principle of the UBM

3.1.1 Extremum principles

Prager and Hodge [91] formulated in 1951 the lower and upper bound theorems for perfectly plastic solids obeying two flow laws Mises and Prandtl-Reuss. These theorems became extremely powerful to obtain approximate solution to complicated boundary problems. It is largely used to model metal forming processes such as drawing, extrusion, rolling... As the foundation of the theorems is similar for Mises and Prandtl-Reuss material behaviors and it is the Mises one that is used in this thesis, here will be presented the mentioned extremum principles for Mises material behavior law.

3.1.1.a Description of plastic problem

Let consider a domain Ω deformed plastically with boundary conditions as shown in Figure 3.1: The material particles on the portion S_u of the surface S are made to move with given velocity \underline{u}^d while the remainder S_T of the surface S is subjected to given surface stress \underline{T}^d . Assuming that the whole domain Ω is in a state of plastic flow and we desire to determine the stress field $\underline{\underline{\sigma}}$ or strain rate $\underline{\underline{\dot{\epsilon}}}$ throughout Ω .

A stress field defined throughout Ω is *statically admissible* if it satisfies

- the equilibrium condition $\nabla \cdot \underline{\underline{\sigma}} = 0$ (equation 2.1)
- the plastic yield condition

$$\underline{\underline{S}} : \underline{\underline{\dot{\epsilon}}} = \frac{2}{3} \sigma_0^2 \text{ in } \Omega \tag{3.1}$$

- and the boundary condition

$$\underline{\underline{\sigma}} \cdot \underline{n} = \underline{T} \text{ on } S_T. \tag{3.2}$$

A strain rate field $\underline{\underline{\dot{\epsilon}}}$ defined throughout Ω is *kinematically admissible* if it is derived from a velocity field which satisfies

- the condition of incompressibility

$$\text{div } \underline{u} = \text{tr } \underline{\underline{\dot{\epsilon}}} = 0 \text{ in } \Omega \tag{3.3}$$

- and boundary condition

$$\underline{u} = \underline{u}^d \text{ on } S_u. \tag{3.4}$$

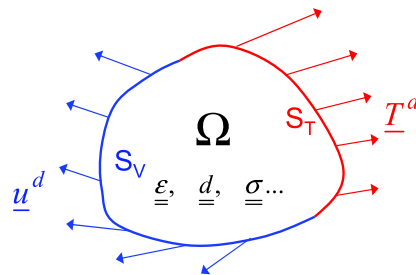


Figure 3.1: The problem on the body Ω deformed plastically under velocity boundary condition on S_u and stress (or tension) condition on S_T . $\underline{\underline{d}} = \underline{\underline{\dot{\epsilon}}}$.

3.1.1.b Extremum theorems

Theorem 1: Among all statically admissible stress fields $\underline{\underline{\sigma}}$ the actual one $\underline{\underline{\sigma}}^a$ maximizes the expression

$$I = \int_{S_u} \underline{\underline{\sigma}} \cdot \underline{\underline{n}} \cdot \underline{\underline{u}}^d \, dS. \quad (3.5)$$

Demonstration: First of all, we will remind the principle of virtual work. Let consider the integral

$$\int_{\Omega} \underline{\underline{\sigma}} : \underline{\underline{\epsilon}} \, dV. \quad (3.6)$$

where $\underline{\underline{\epsilon}}$ is a virtual strain derived from a virtual displacement field $\underline{\underline{\zeta}}$ by

$$\underline{\underline{\epsilon}} = \frac{1}{2} \left(\underline{\underline{\text{grad}}}_{\underline{\underline{\zeta}}} + \underline{\underline{\text{grad}}}^T \underline{\underline{\zeta}} \right). \quad (3.7)$$

Since the stress tensor is symmetric, the integrand of 3.6 can be written as $\underline{\underline{\sigma}} : \underline{\underline{\text{grad}}}_{\underline{\underline{\zeta}}}$. Application of Green's theorem leads to:

$$\int_{\Omega} \underline{\underline{\sigma}} : \underline{\underline{\epsilon}} \, dV = \int_{\Omega} \underline{\underline{\sigma}} : \underline{\underline{\text{grad}}}_{\underline{\underline{\zeta}}} \, dV = \int_S \underline{\underline{\sigma}} \cdot \underline{\underline{n}} \cdot \underline{\underline{\zeta}} \, dS - \int_{\Omega} \nabla \cdot \underline{\underline{\sigma}} \cdot \underline{\underline{\zeta}} \, dV. \quad (3.8)$$

We can deduce from this equation by using the equilibrium condition 2.1 that

$$\int_{\Omega} \underline{\underline{\sigma}} : \underline{\underline{\epsilon}} \, dV = \int_S \underline{\underline{\sigma}} \cdot \underline{\underline{n}} \cdot \underline{\underline{\zeta}} \, dS. \quad (3.9)$$

In the analogy of this result we can write also

$$\int_{\Omega} \underline{\underline{\sigma}} : \underline{\underline{\dot{\epsilon}}} \, dV = \int_S \underline{\underline{\sigma}} \cdot \underline{\underline{n}} \cdot \underline{\underline{u}} \, dS. \quad (3.10)$$

where $\underline{\underline{\dot{\epsilon}}}$ is the strain rate associated with any virtual velocity field $\underline{\underline{u}}$.

To prove the *Theorem 1*, let consider the difference $I^a - I$ where I is defined by 3.5 associated with some statically admissible $\underline{\underline{\sigma}}$ and I^a associated with the actual stress $\underline{\underline{\sigma}}^a$. Since both stress tensors satisfy 3.2 we can write this difference as follows

$$I^a - I = \int_{S_u} (\underline{\underline{\sigma}}^a - \underline{\underline{\sigma}}) \cdot \underline{\underline{n}} \cdot \underline{\underline{u}}^d \, dS = \int_S (\underline{\underline{\sigma}}^a - \underline{\underline{\sigma}}) \cdot \underline{\underline{n}} \cdot \underline{\underline{u}}^a \, dS \quad (3.11)$$

where $\underline{\underline{u}}^a$ denotes the actual velocity field. Applying the principle of virtual work, 3.10, we obtain

$$I^a - I = \int_{\Omega} (\underline{\underline{\sigma}}^a - \underline{\underline{\sigma}}) : \underline{\underline{\dot{\epsilon}}}^a \, dS \quad (3.12)$$

with $\underline{\underline{\dot{\epsilon}}}^a$ is the actual strain rate field. Since $\text{tr} \underline{\underline{\dot{\epsilon}}} = 0$ (3.3) on account of the incompressibility of the material and according to Mises' material flow law

$$\underline{\underline{\dot{\epsilon}}} = \lambda \underline{\underline{S}} \quad (3.13)$$

with certain coefficient $\lambda > 0$, we obtain

$$I^a - I = \int_{\Omega} (\underline{\underline{S}}^a - \underline{\underline{S}}) : \underline{\underline{\dot{\epsilon}}}^a \, dS = \int_{\Omega} \lambda (\underline{\underline{S}}^a - \underline{\underline{S}}) : \underline{\underline{S}}^a \, dS = \int_{\Omega} \lambda (\sigma_0^2 - \underline{\underline{S}} : \underline{\underline{S}}^a) \, dS. \quad (3.14)$$

Now, by Schwarz' inequality (see for example [28])

$$\underline{\underline{S}} : \underline{\underline{S}}^a \leq \sqrt{\underline{\underline{S}} : \underline{\underline{S}}} \sqrt{\underline{\underline{S}}^a : \underline{\underline{S}}^a} = \sigma_0^2 \quad (3.15)$$

where the equality sign can hold only if $\underline{\underline{S}} = c \underline{\underline{S}}^a$. Since both $\underline{\underline{S}}$ and $\underline{\underline{S}}^a$ satisfy the yield condition 3.1 we deduce then $c = 1$. Finally, we conclude that

$$I^a - I \geq 0 \quad (3.16)$$

where the equality can hold only if $\underline{\underline{S}} = \underline{\underline{S}}^a$ which implies that the stress fields $\underline{\underline{\sigma}}$ and $\underline{\underline{\sigma}}^a$ can differ at most by a constant hydrostatic pressure. The boundary condition 3.2, however, rules out such a difference. Thus, the relation $\underline{\underline{S}} = \underline{\underline{S}}^a$ implies that $\underline{\underline{\sigma}} = \underline{\underline{\sigma}}^a$ except in the case where S_u comprise the entire S .

Theorem 2: Among all kinematically admissible strain rate fields $\underline{\dot{\epsilon}}$ the actual one $\underline{\dot{\epsilon}}^a$ minimizes the expression

$$J = \sqrt{\frac{2}{3}}\sigma_0 \int_{\Omega} \sqrt{\underline{\dot{\epsilon}} : \underline{\dot{\epsilon}}} dV - \int_{S_T} \underline{T}^d \cdot \underline{u} dS. \quad (3.17)$$

Demonstration: Let consider

$$J - J^a = \sqrt{\frac{2}{3}}\sigma_0 \int_{\Omega} \left(\sqrt{\underline{\dot{\epsilon}} : \underline{\dot{\epsilon}}} - \sqrt{\underline{\dot{\epsilon}}^a : \underline{\dot{\epsilon}}^a} \right) dV - \int_{S_T} \underline{T}^d \cdot (\underline{u} - \underline{u}^a) dS. \quad (3.18)$$

By transforming this difference in a manner similar to that used in proving *Theorem 1*, we find

$$J - J^a = \sqrt{\frac{2}{3}}\sigma_0 \int_{\Omega} \left(\sqrt{\underline{\dot{\epsilon}} : \underline{\dot{\epsilon}}} - \sqrt{\underline{\dot{\epsilon}}^a : \underline{\dot{\epsilon}}^a} \right) dV - \int_{\Omega} \frac{1}{\lambda} \underline{\dot{\epsilon}}^a (\underline{\dot{\epsilon}} - \underline{\dot{\epsilon}}^a) dV. \quad (3.19)$$

Since Mises' law 3.13, the coefficient λ can be obtained by

$$\lambda = \sqrt{\frac{\underline{\dot{\epsilon}}^a : \underline{\dot{\epsilon}}^a}{S^a : S^a}} = \sqrt{\frac{\underline{\dot{\epsilon}}^a : \underline{\dot{\epsilon}}^a}{\frac{2}{3}\sigma_0^2}}. \quad (3.20)$$

Substituting this into 3.19 we have

$$J - J^a = \sqrt{\frac{2}{3}}\sigma_0 \int_{\Omega} \frac{\sqrt{\underline{\dot{\epsilon}} : \underline{\dot{\epsilon}}} \sqrt{\underline{\dot{\epsilon}}^a : \underline{\dot{\epsilon}}^a} - \underline{\dot{\epsilon}} : \underline{\dot{\epsilon}}^a}{\sqrt{\underline{\dot{\epsilon}}^a : \underline{\dot{\epsilon}}^a}} dV. \quad (3.21)$$

According to Schwarz' inequality, the numerator of the integrand in 3.21 can not be negative, meaning that

$$J - J^a \geq 0. \quad (3.22)$$

The equality can hold only if $\underline{\dot{\epsilon}} = c\underline{\dot{\epsilon}}^a$ where c is a scalar factor of proportionality. In certain cases, such as where the surface S_T comprises the entire surface S or $\underline{u}^d = \underline{0}$ on a non-empty S_u ... the strain rates are determined only to within an arbitrary constant factor.

Discussion: *Theorem 1* was first proved by Hill [44] for the special case where the velocities were prescribed over the entire surface and *Theorem 2* is due to Markov [70]. Both principles were preceded historically by Sadowsky's heuristic principle of "maximum plastic resistance" [95] stating that among all statically admissible stress distributions the actual one requires a maximum external effort to maintain the flow. This principle led to correct results in certain special cases. Hill has stated that in these cases, Sadowsky's principle coincides with Hill's principle and in general case it will not lead to correct results even if ambiguity can be avoided in defining the term "effort".

Combination of both principles: The two theorems may be combined to yield upper and lower bounds. Indeed, using Mises flow equation 3.13, yield condition 3.1 and 3.20 we find

$$\underline{S}^a : \underline{\dot{\epsilon}}^a = \sqrt{\frac{2}{3}}\sigma_0 \sqrt{\underline{\dot{\epsilon}}^a : \underline{\dot{\epsilon}}^a}. \quad (3.23)$$

Thus,

$$\sqrt{\frac{2}{3}}\sigma_0 \int_{\Omega} \sqrt{\underline{\dot{\epsilon}}^a : \underline{\dot{\epsilon}}^a} dV = \int_{\Omega} \underline{S}^a : \underline{\dot{\epsilon}}^a dV = \int_{\Omega} \underline{\sigma}^a : \underline{\dot{\epsilon}}^a dV = \int_S \underline{\sigma}^a \cdot \underline{n} \cdot \underline{u}^a dS \quad (3.24)$$

which implies then

$$J^a = \sqrt{\frac{2}{3}}\sigma_0 \int_{\Omega} \sqrt{\underline{\dot{\epsilon}}^a : \underline{\dot{\epsilon}}^a} dV - \int_{S_T} \underline{T}^d \cdot \underline{u}^a dS = \int_S \underline{\sigma}^a \cdot \underline{n} \cdot \underline{u}^a dS - \int_{S_T} \underline{\sigma}^a \cdot \underline{n} \cdot \underline{u}^a dS = \int_{S_u} \underline{\sigma}^a \cdot \underline{n} \cdot \underline{u}^a dS = I^a. \quad (3.25)$$

Theorems 1 and *2* can therefore be combined as follows

$$I \leq I^a = J^a \leq J. \quad (3.26)$$

3.1.2 UBM applied to rolling process

Theorem 2 is largely used for metal forming processes like extrusion, drawing or rolling in order to find an upper bound estimation of external charge (tension or torque). To apply this extremum principle to rolling process, the following assumptions are necessary.

3.1.2.a Assumptions

1. *Rigid work-roll*: The work-roll is considered rigid and its shape (circular or not) is given as an input of the problem.
2. *Rigid-plastic strip*: The strip mechanical behavior is considered rigid-plastic which implies that all elastic deformations are neglected. This is an important hypothesis that simplifies what happens out of the roll-bite. As a consequence of this assumption, the strip entry and exit parts before and after the roll-bite have no deformation and move as rigid bodies. In other words, the velocity field is homogenous and constant throughout these parts. Thus, there are two surfaces of velocity discontinuity before and after the plastic deformation zone Ω . The surfaces are denoted Γ_e and Γ_s (see Figure 3.2). Their shape is not predetermined but depends on the choice of plastic velocity field. And the dissipation due to the discontinuity of velocity on these surfaces are added into the plastic deformation of the function J in theorem 2.
3. *Tresca friction law*: The studied problem includes both the strip and the work-roll. The friction between them is then an internal force. The Tresca friction law 2.13 is often used because the friction stress is known as a function of the material yield stress. Therefore, its dissipation can be added into the function J in a similar way as the dissipations on Γ_e and Γ_s .

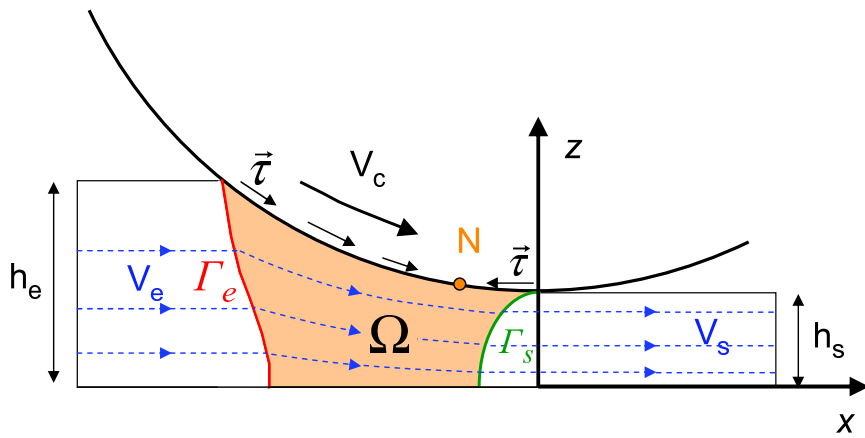


Figure 3.2: 2D modeling of rolling with UBM . The plastic area Ω (clear-brown) is limited by the discontinuity surface Γ_e , Γ_s , contact surface and symmetry plane $z = 0$. The form of this area and the discontinuity surfaces depends on the choice of velocity field in this area. They are outputs (results) of the model.

3.1.2.b Statement of the UBM for rolling process

With the previous assumptions, *theorem 2* (3.17) states that among all kinematically admissible velocity fields \underline{u} the actual one minimizes the expression:

$$J(\underline{u}) = \int_{\Omega} \sigma_0 \dot{\epsilon}(\underline{u}) \cdot d\Omega + \int_{S_d} \frac{\sigma_0}{\sqrt{3}} \cdot \|\Delta \underline{u}\| \, dS + \int_{S_c} \tau \cdot \|\Delta \underline{u}_c\| \, dS - \int_{S_{ext}} \underline{T}^d \cdot \underline{u} \, dS \quad (3.27)$$

where J represents the externally supplied power on the roll, σ_0 is the yield stress, $\frac{\sigma_0}{\sqrt{3}}$ is shear yield stress, $\dot{\epsilon}$ is equivalent strain rate, $\Delta \underline{u}$ is the velocity discontinuity on the surfaces S_d of the strip material including Γ_e and Γ_s , $\Delta \underline{u}_c$ the difference between strip material velocity and work-roll velocity on the contact surface S_c . The first term of the right side of 3.27 corresponds to the power of plastic deformation due to the continuous deformation inside Ω , denoted $J_{\dot{\epsilon}}$. The second term is the power of plastic dissipation on the surfaces of velocity discontinuity, denoted $J_{\Delta u}$. Sum of these two terms is the total plastic deformation power $J_{def} = J_{\dot{\epsilon}} + J_{\Delta u}$. The third one is the friction dissipation power, J_{fric} and the last term is the external work power (entry and exit tensions), J_{ten} .

3.1.2.c 2D rolling UBM -based models in literature

As the set of the kinematically admissible forms an infinite-dimension space, the optimization problem (Theorem 2) to find out the optimum velocity field needs simplifying. In practice, a family of velocity fields with few parameters is studied of which the velocity field minimizing the power function defined by 3.27 is the best approximation of the real one. The UBM result depends, thus strongly on the choice and construction of velocity fields. In literature, the authors apply this method to rolling using different families of velocity fields. It is possible to classify them into two categories of velocity fields. The first one consider rigid bodies velocity field (called also slip lines because the deformation concentrates on some shear lines) and the second one analyzes the plastic deformation zone with continuous velocity field.

3.2 Velocity fields with rigid bodies motions

3.2.1 Simulated sliding theory and experiments

Most of metals have a crystalline microstructure, the behaviour of which in plastic deformation consists of glide packages having slipped inside a grain. Deformation occurs almost entirely on slip surfaces while the material between them remains practically unaffected. This theory of simulated sliding in microscopic scale has already been applied for a long time in continuous plastic deformation of metal. In 1976, Piispanen [89] stated also that the plastic deformation of rigid plastic material is also macroscopically inhomogeneous. The author performed experiments on hot rolling process using miniature rollers. The bar was rolled until continuity is attained in the strain process. After the rolling test, the rolled bar emerging surface was polished but not etched so that only marks from deformation showed. The roller and test bar were then placed on the specimen stage of a metallurgical microscope allowing to take metallographic images continuously during the process.

For the test A (see Figure 3.3 - Fig 7 of [89], page 48), the author observed that the configuration of lines begun to appear at points B and G in Figure 3.3(a). As rolling continued the deformation area grew but the signs of deformations appeared in four deformation zones as showed in Figure 3.3(b). Almost no deformation was observed inside the four zones but the deformation concentrated only on the slip lines (limits between the areas) resembling the letter X.

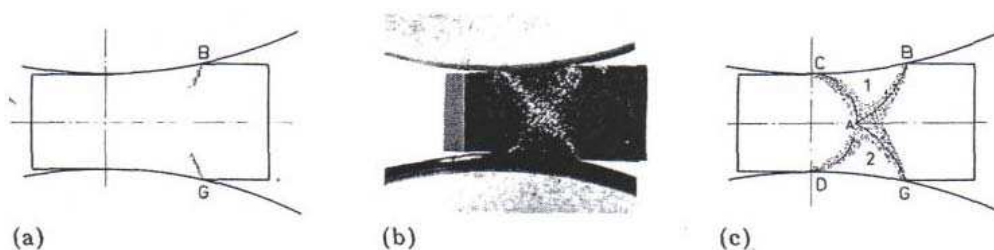


Figure 3.3: Test A, $R = 10mm$, $2h_e = 2.5mm$, $2h_s = 2.08mm$, contact length is estimated $L = \sqrt{R(2h_e - 2h_s)} = 2.05mm$. The test bar was recrystallized annealed 0.15% C mild steel.

Test	A	B	C	D	E	F	G
$R(\text{mm})$	10.0	23.84	23.84	10.34	24.0	24.0	100
$2h_e(\text{mm})$	2.50	3.374	3.440	1.800	3.43	3.00	4.86
$2h_s(\text{mm})$	2.08	3.330	3.330	1.380	3.00	2.80	4.22
$L(\text{mm})$	2.05	1.020	1.619	2.084	3.21	2.19	8.00

Table 3.1: Series of experiments performed by Piispanen [89].

Other rolling parameters showed in Table 3.1 were also experimented. Except the test D where two bars were put one on the other and rolled at the same time, the concentration of deformation on the slip lines was confirmed for all the tests B, C, E (see Figure 3.4 for the result of the test C). The same result was observed for the test F which is a second rolling pass using the rolled bar after the test E.

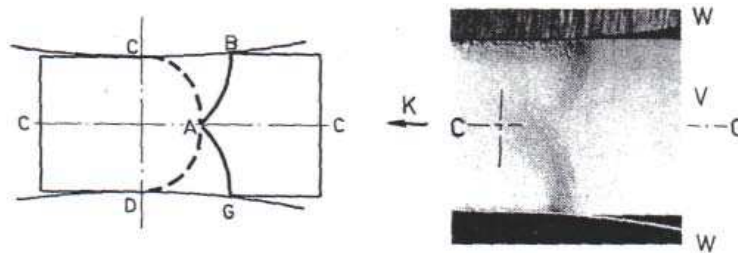


Figure 3.4: Test C, $R = 23.84\text{mm}$, $2h_e = 3.44\text{mm}$, $2h_s = 3.33\text{mm}$, $L = 1.62\text{mm}$. The test bar was a recrystallization annealed 1% Cr, 1% Si steel.

Since these interesting results, the author proposed a upper bound model considering that the deformation is concentrated on the shear slip lines, that is called later unitriangular velocity field. The details of this model will be presented in a following section 3.2.3

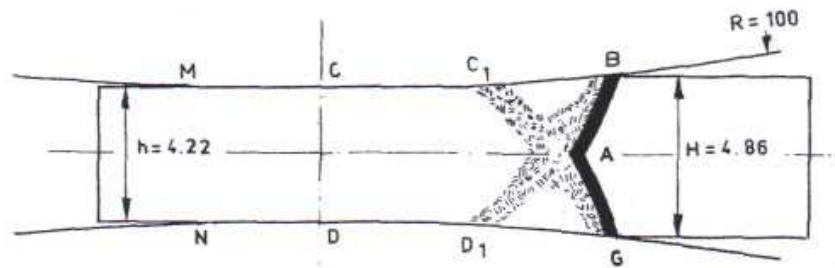


Figure 3.5: Test G, $R = 100\text{mm}$, $2h_e = 4.86\text{mm}$, $2h_s = 4.22\text{mm}$, $L = 8.00\text{mm}$. The test bar was an annealed 0.15% C mild steel.

The test G is quite different where the contact length is twice higher than the strip thickness and Figure 3.5 showed a clear deformation in the zone BAG at the entry side. The first letter X of deformation concentration occurs only a half of the contact length and we may expect another one between C1D1CD. However, the deformation observed was not clear. This difference is not random. We will see later that it is better to apply multitriangular velocity field in this case. Furthermore, in the next chapter a new UBM model with continuous velocity field with shear concentration on certain slip zones allows also to explain why when the contact length is twice the strip thickness we expect to have two letter X.

3.2.2 Concept for analysis of linear and rotational velocity fields

Avitzur and Pachla [10] investigates an upper bound approach to plan strain deformation of a rigid - perfectly plastic material where the deformation region is divided into a finite number of rigid triangular bodies that slide with respect to one another. By consequence, there is no continuous plastic deformation power and all the plastic deformation power concentrates on the surfaces of velocity discontinuity or in other words the first term of the equation 3.27 is equal to zero and the second one represents the total plastic power. The authors give the concept and specific equation for the three general cases of neighboring rigid body zones where the zones are both in rotational motion (case 1), one in linear, the other in rotational motion (case 2) and both in linear motion (case 3). The shape of the surface of velocity discontinuity and the shear power losses are clearly presented. As a result of this article, when one of the rigid bodies exhibit rotational motion, the surface of velocity discontinuity is found to be cylindrical (circular in the plan strain study) and it is planar in the case with both bodies in linear motion. The velocity discontinuity is found to be constant along the entire surface of velocity discontinuity.

Even though Avitzur and Pachla [10] are not the first who study rolling process by rigid bodies *UBM*, but their study synthesized the concept and gave powerful tool to develop more complex rigid bodies *UBM* models for metal forming processes at that time. The concept is applicable to strip drawing, extrusion, forging, rolling, leveling and machining. The same authors presents then the applications of this concept to drawing, cutting and rolling processes in [11].

Remark: It is assumed that in order to get higher accuracy an attempt should be made to have the assumed velocity field resemble to the actual one as closely as possible. However, even when the assumed velocity is inaccurate, the power consumption calculated based on that field will can approximate the actual power. This family of rigid bodies velocities allows only to have an estimation of power but not velocity field.

3.2.3 Unitriangular velocity field

Johnson and Mellor [51] analyzed strip rolling by the unitriangular velocity field based on the curvilinear triangle, opening a new avenue of approach, the *UBM* in rolling. As can be seen in Figure 3.6, the strip is divided into three zones. Two zones before and after the roll-bite are in linear motion with a velocity V_e and V_s . And the triangular zone under the roll-bite is in rotational motion around the work-roll center O_c with a rotational velocity w . Applying the concept of Avitzur and Pachla [10], the surfaces of velocity discontinuity \overline{AP} and \overline{PB} are circular corresponding to the center O_1 on the axes Oz at vertical position z_1 and radius r_1 and O_2 on the axes Oz at vertical position z_2 and radius r_2 .

Geometrical parameters: We will see here below that all geometrical parameters z_1 , r_1 , z_2 and r_2 can be expressed by the only one x_p (that we chose arbitrarily). Indeed, the fact that the points A and P belong to the arc (O_1, r_1) implies

$$\overline{AO_1}^2 = (x_1 - x_A)^2 + (z_1 - z_A)^2 \Leftrightarrow r_1^2 = L^2 + (z_1 - h_e)^2 \quad (3.28)$$

$$\overline{PO_1}^2 = (x_1 - x_P)^2 + (z_1 - z_P)^2 \Leftrightarrow r_1^2 = x_P^2 + z_1^2. \quad (3.29)$$

Comparing the right side of these two equations we obtain

$$z_1(x_P) = \frac{L^2 + h_e^2 - x_P^2}{2h_e}. \quad (3.30)$$

Thus, the position of O_1 and the radius r_1 are expressed as functions of x_P thanks to 3.30 and 3.29. Similarly for the arc \overline{PB} we obtain

$$r_2(x_P) = \frac{h_s^2 + x_P^2}{2h_s} \quad (3.31)$$

$$z_2(x_P) = h_s - r_2(x_P) \quad (3.32)$$

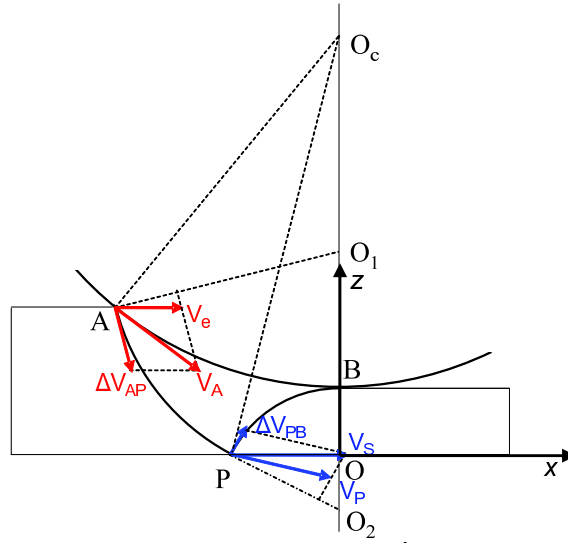


Figure 3.6: Strip rolling - The unitriangular velocity field.

And by consequence the length of the arcs \widehat{AP} and \widehat{PB} are completely determined as a functions of x_p

$$\begin{cases} \widehat{AP} = 2r_1 \arcsin \frac{\overline{AP}}{2r_1} = 2r_1 \arcsin \frac{\sqrt{(L+x_p)^2 + h_c^2}}{2r_1} \\ \widehat{PB} = 2r_2 \arcsin \frac{\overline{PB}}{2r_2} = 2r_2 \arcsin \frac{\sqrt{x_p^2 + z_2^2}}{2r_2}. \end{cases} \quad (3.33)$$

Velocity discontinuities As stated Avitzur and Pachla [10], the velocity discontinuities are constant all along these arcs. They will be obtained as a function of geometrical parameter x_p and the rotational velocity ω of the triangular rigid body. Noting that $V_A = \omega AO_c$, since the uniformity of the triangles $AV_A\Delta V_{AP}$ and AO_1O_c (see Figure 3.6) we can obtain the entry velocity and the velocity discontinuity over AP as follows

$$\begin{cases} V_e = V_A \frac{O_1O_c}{AO_c} = [z_c - z_1(x_p)] \omega \\ \Delta V_{AP} = V_A \frac{AO_1}{AO_c} = r_1(x_p)\omega. \end{cases} \quad (3.34)$$

Of course, with similar analysis the exit velocity and the velocity discontinuity over PB are

$$\begin{cases} V_e = [z_c - z_2(x_p)] \omega \\ \Delta V_{PB} = r_2(x_p)\omega. \end{cases} \quad (3.35)$$

Calculations of powers: By definition of the velocity field, it is obvious that the continuous plastic deformation power $J_{\dot{\epsilon}}$ is equal to 0. All plastic power is concentrated on the surfaces of velocity discontinuity. Using the second equations of 3.34 and 3.35, this power can be obtained as

$$J_{\Delta u} = \frac{\sigma_0}{\sqrt{3}} [\widehat{AP} \cdot \Delta V_{AP} + \widehat{PB} \cdot \Delta V_{PB}] = \frac{\sigma_0}{\sqrt{3}} \omega [\widehat{AP}(x_p)r_1(x_p) + \widehat{PB}(x_p)r_2(x_p)]. \quad (3.36)$$

If we note

$$P_{\Delta u}(x_p) = \frac{\sigma_0}{\sqrt{3}} \omega [\widehat{AP}(x_p)r_1(x_p) + \widehat{PB}(x_p)r_2(x_p)] \quad (3.37)$$

the power of velocity discontinuity can be expressed by

$$J_{\Delta u}(\omega, x_p) = P_{\Delta u}(x_p)\omega. \quad (3.38)$$

The friction power is given by

$$\begin{cases} J_{fric}(\omega, x_p) = P_{fric}|\omega - \omega_c| \\ \text{where } P_{fric} = m \frac{\sigma_0}{\sqrt{3}} \widehat{AB}. \end{cases} \quad (3.39)$$

And using the first equations of 3.34 and 3.35 the power supplied by entry and exit tensions can be written by

$$\begin{cases} J_{ten}(\omega, x_p) = -T_e h_e V_e + T_s h_s V_e = P_{ten}\omega \\ \text{where } P_{ten} = -T_e h_e [z_c - z_1(x_p)] + T_s h_s [z_c - z_2(x_p)]. \end{cases} \quad (3.40)$$

Finally the power function defined by the equation 3.27 is, thus obtained

$$J(\omega, x_p) = P_{\Delta u}(x_p)\omega + P_{fric}|\omega - \omega_c| - P_{ten}(x_p)\omega \quad (3.41)$$

or

$$J(\omega, x_p) = \begin{cases} [P_{\Delta u}(x_p) - P_{ten}(x_p) - P_{fric}] \omega - P_{fric}\omega_c & \text{if } \omega < \omega_c \\ [P_{\Delta u}(x_p) - P_{ten}(x_p) + P_{fric}] \omega + P_{fric}\omega_c & \text{if } \omega > \omega_c \end{cases} \quad (3.42)$$

Optimum power: The power function $J(\omega, x_p)$ given by 3.42 is a function of two independent parameters x_p and ω . With respect to ω this function is linear and has a minimum at the point $\omega = \omega_c$ if and only if the slope is negative before and positive after this point. In other words, $J(\omega, x_p)$ has a minimum with respect to ω if and only if

$$-P_{fric} < P_{\Delta u}(x_p) - P_{ten}(x_p) < P_{fric} \quad (3.43)$$

and the minimum is obtained when the rigid body rotates with a same velocity as that of the work-roll. In this case, the power function becomes 1-variable function

$$J_1(x_p) = J(\omega_c, x_p) = [P_{\Delta u}(x_p) - P_{ten}(x_p)] \omega_c \quad (3.44)$$

where $P_{\Delta u}(x_p)$ and $P_{ten}(x_p)$ are given by 3.37 3.40.

Optimization of this 1-variable function gives an minimum upper bound approach of the supplied power. The results of this model will be compared to the slabs velocity field in the section 4.5.

Approach of roll force: On the shear arcs AP and PB the shear stress amplitude is equal to the material yield shear stress k as showed in Figure 3.7. Let consider first the arc \widehat{AP} and consider that the shear stress k is constant along this arc. It is obvious that the total tangential force \vec{F}_t integral of shear stress along \widehat{AP} is a vector parallel to \vec{PA} or

$$\vec{F}_t = \int_{\widehat{PA}} \underline{k} dl = k \vec{PA}. \quad (3.45)$$

Similarly, the normal force \vec{F}_n which is the integral of normal stress is perpendicular to \vec{F}_t .

If now, we consider that the force exerted by the roll on the strip is vertical (because the resulting force along x is, in a real rolling condition, much smaller than the one in z direction), this force must satisfy the condition as showed by three green vectors in Figure 3.7. By uniformity of triangles forming by the three green force vectors and the $AA'P$ (A' is the projection of A on Ox , we can write following relation

$$\frac{F_{AP}}{AP} = \frac{F_t}{h_e}. \quad (3.46)$$

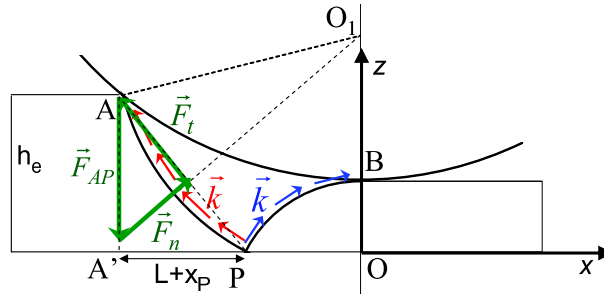


Figure 3.7: Calculating of roll force for unitriangular velocity field approach.

Using 3.45 and $\overline{AP}^2 = h_e^2 + (L + x_p)^2$ the equation 3.46 implies

$$F_{AP} = \frac{k \cdot \overline{AP}^2}{h_e} = k \left[h_e + \frac{(L + x_p)^2}{h_e} \right]. \tag{3.47}$$

The force F_{PB} can be derived in a same way

$$F_{PB} = k \left[h_s + \frac{x_p^2}{h_s} \right]. \tag{3.48}$$

And the total force is obtained

$$F = F_{AP} + F_{PB}. \tag{3.49}$$

3.2.4 Multitriangular velocity field

For cold rolling, the contact length is generally several times higher than the strip thickness, the unitriangular approach is less realistic. Camurri and Lavanchy [22] in 1984 applied the upper bound method with slip line velocity field to cold strip rolling by introducing multitriangles slip lines. This model has been reanalyzed by Avitzur, Talbert and Gordon [12] by using the concept presented in [10].

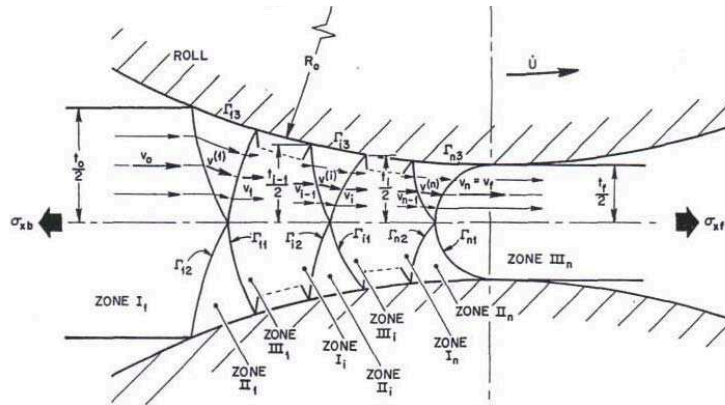


Figure 3.8: The multitriangular velocity field for strip rolling.

Figure 3.8 shows the application of the multitriangular velocity field to the process of strip rolling. Within the curvilinear triangles with apexes P_i on the plane of symmetry, a rotational velocity field prevails. Other triangles with their bases on the plane of symmetry and apexes on the surface of the roll, bound the regions of linear motion

parallel to the plane of symmetry. According to the analysis of Avitzur and Pachla [10], the axes of symmetry of all the cylindrical surfaces of velocity discontinuity are situated along the z -axis. Each of the curvilinear triangles can be treated separately as a unitriangular problem. When the upper bounds for each triangle are computed and added together, the total power is obtained.

There are several ways to optimize such a system. Avitzur, Talbert and Gordon [12] propose to choose at the beginning arbitrarily the points A_i and B_i then the positions of P_i is optimized for each triangle separately as for the unitriangular case. For each single triangle, the power function is only optimized with respect to x_{P_i} but not to ω_i because ω_i needs satisfying flow rate conservation condition and so fixed when treating each separated triangle. The powers of each triangle are then added together to obtain the total power. Next, the positions of A_i and B_i are selected along the roll surface and now positions of P_i corresponding to the separated triangle optimum are found and upper bound approach is finally evaluated.

In this case of multitriangular velocity field, the meaning of the neutral region becomes evident. To fulfill the volume constancy requirement, the angular velocities ω_i increase as the material moves forwards the exit. When the global optimum occurs, among the treated rigid body triangular regions there is one that rotates with the same rotational velocity as the work-roll. The segment between the point A_i and B_i of this triangle represents the neutral zone.

3.3 2D continuous velocity fields

3.3.1 Continuous eccentric velocity field

Velocity field

Avitzur [5, 6, 7] performed several analyses with including *UBM* to cold strip rolling. The author proposed, for the first time, a continuous velocity field that let us call "eccentric" velocity field. This field is described as: Cylindrical symmetry exists along each arc connecting any two symmetrical points on the opposing rolls. The arcs are eccentric and each one meets the roll surfaces at right angles. The radius of these arcs increases as the material point advances further toward the exit (see Figure 3.9). The velocity of each material point on an arc is on the direction of the radius of the arc (passing through the arc center). On the entry arc (surface of velocity discontinuity), the condition of continuity of normal velocity through the entry arc implies

$$u(\theta_e, \vartheta) = V_e \cos \vartheta. \quad (3.50)$$

This velocity decreases when ϑ increases from 0 to θ_e . In the same analogy, the velocity at any other material point is given by

$$u(\theta, \vartheta) = A(\theta) \cos \vartheta.$$

As the velocity is, by construction, tangential to the work-roll surface, the only condition so that the velocity field is kinematically admissible is the incompressibility or the flow rate constancy written as

$$C_{vol} = \int_0^{\theta} A(\theta) \cos \vartheta \cdot r(\theta) d\vartheta = A(\theta)r(\theta) \sin \theta = A(\theta) \cdot h(\theta) \quad (3.51)$$

where r is the radius of the arc and θ is the angle of the arc length (equal to the angular position of the point P , intersection of the arc with the work-roll). We deduce then

$$A(\theta) = \frac{C_{vol}}{h(\theta)} \quad (3.52)$$

and therefore

$$u(\theta, \vartheta) = \frac{C_{vol}}{h(\theta)} \cos \vartheta. \quad (3.53)$$

Calculating of power functions

Based on the hypotheses of small angle, the author simplified the velocity as follows: each material point on a same arc has identical speed and forward all to the center of the arc. And here following are the power function obtained.

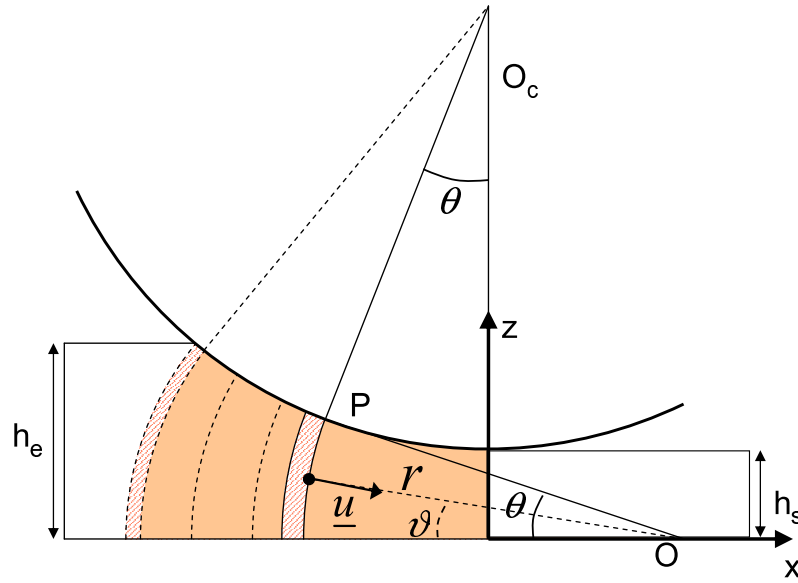


Figure 3.9: Continuous eccentric velocity field.

Power of continuous plastic deformation: After some mathematical developments the author obtain

$$J_{\dot{\epsilon}} = \frac{2}{\sqrt{3}} \sigma_0 C_{vol} \ln \frac{h_e}{h_s}. \quad (3.54)$$

In fact, as can be seen in Figure 3.9, an arc at the entry of plastic zone will stay an arc. Only its size (height) becomes smaller when the material point moves forward the exit. The plastic power obtained can be understood as the power to deform the material from h_e to h_s under plane strain condition without shear deformations.

Power of velocity discontinuity at entry: The velocity discontinuity at the entry arc is equal to $V_e \sin \vartheta$, using the hypothesis of small angle the power of velocity discontinuity can be computed as

$$J_{\Delta u} = \frac{\sigma_0}{\sqrt{3}} \int_0^{\theta_e} V_e \sin \vartheta r_e d\vartheta = \frac{\sigma_0}{\sqrt{3}} V_e r_e (1 - \cos \theta_e). \quad (3.55)$$

where r_e is the radius of the entry arc defined by $r_e \theta_e = h_e$. Thus,

$$J_{\Delta u} = \frac{\sigma_0}{\sqrt{3}} V_e r_e \left(\frac{1}{2} \theta_e^2 \right) = \frac{\sigma_0}{2\sqrt{3}} C_{vol} \theta_e \quad (3.56)$$

with $\theta_e \simeq \sqrt{\frac{2(h_e - h_s)}{R}}$.

Power of friction: The difference of velocity between the strip and the roll on the contact surface is

$$\Delta \underline{u} = u - V_c = \frac{C_{vol}}{h_s + \frac{R}{2} \theta^2} - V_c$$

Therefore, the friction power is

$$\begin{aligned}
 J_{fric} &= \int_0^{\theta_e} \frac{m\sigma_0}{\sqrt{3}} \left| \frac{C_{vol}}{h_s + \frac{R}{2}\theta^2} - V_c \right| R d\theta \\
 &= \frac{m\sigma_0}{\sqrt{3}} \left[\int_0^{\theta_n} \left(\frac{C_{vol}}{h_s + \frac{R}{2}\theta^2} - V_c \right) R d\theta + \int_{\theta_n}^{\theta_e} \left(V_c - \frac{C_{vol}}{h_s + \frac{R}{2}\theta^2} \right) R d\theta \right] \\
 &= \frac{m\sigma_0}{\sqrt{3}} \left[V_c R (\theta_e - 2\theta_n) + \int_0^{\theta_n} \frac{C_{vol}}{h_s + \frac{R}{2}\theta^2} R d\theta - \int_{\theta_n}^{\theta_e} \frac{C_{vol}}{h_s + \frac{R}{2}\theta^2} R d\theta \right] \\
 &= \frac{m\sigma_0}{\sqrt{3}} \left[V_c R (\theta_e - 2\theta_n) - C_{vol} \sqrt{\frac{2R}{h_s}} \left\{ \arctan \left(\sqrt{\frac{R}{2h_s}} \theta_e \right) - 2 \arctan \left(\sqrt{\frac{R}{2h_s}} \theta_n \right) \right\} \right]
 \end{aligned} \tag{3.57}$$

By noting that

$$h_e = h_s + \frac{R}{2}\theta_e^2$$

it can be deduced that

$$\sqrt{\frac{R}{2h_s}} \theta_e = \sqrt{\frac{h_e}{h_s} - 1}$$

Power of the tensions: The following formula is valid for all 2D velocity fields

$$J_{ten} = (T_s - T_e) C_{vol}. \tag{3.58}$$

Optimization of total power functions: By writing the equality of strip and work-roll velocity at the neutral point θ_n , the flow rate can be given by

$$C_{vol} = V_c h_n = V_c h_s \left(1 + \frac{R\theta_n^2}{2h_s} \right). \tag{3.59}$$

The total power becomes a function of unique parameter θ_n and the optimum solution is analytically obtained as follows

$$\boxed{\sqrt{\frac{R}{2h_s}} \theta_n = \frac{1}{3} \left\{ \arctan \sqrt{\frac{h_e}{h_s} - 1} - m \sqrt{\frac{2h_s}{R}} \left[\ln \frac{h_e}{h_s} + \frac{1}{4} \sqrt{\frac{2h_s}{R}} \sqrt{\frac{h_e}{h_s} - 1} - \frac{T_s - T_e}{\frac{2}{\sqrt{3}}\sigma_0} \right] \right\}}. \tag{3.60}$$

3.3.2 Continuous simple velocity field

Bouharaoua and al [18] study a symmetric rolling of flat and thin sheets. The authors based on a hypothesis that a material vertical cross section will stay vertical all along the roll-bite. This hypothesis is equivalent to the one of the slab method. The difference is that the *UBM* approaches by velocity field and the slab method bases on the stress field. The hypothesis of homogenous deformation implies obviously that the longitudinal velocity u_x is constant across the thickness direction and depends only on x . Then, the incompressibility of the material deduces that the vertical velocity u_z is linear in z . The authors obtain a velocity field as follows

$$\begin{cases} u_x = \frac{C_{vol}}{h(x)} \\ u_z = \frac{h'(x)C_{vol}}{h^2(x)} \cdot z \end{cases} \tag{3.61}$$

where C_{vol} denotes the flow rate of the rolled material through an across section. The flow rate must be constant and equal to $C_{vol} = V_e h_e = V_s h_s$. It is unique parameter to determine. The thickness function $h(x)$ in the case of circular work-roll is defined as

$$h(x) = R + h_s - \sqrt{R^2 - x^2} \quad (3.62)$$

and its derivative is obtained

$$h'(x) = \frac{-x}{\sqrt{R^2 - x^2}} \quad (3.63)$$

This field is called "simple" because it is deduced quite directly from the hypothesis of homogeneity of longitudinal deformation across the thickness direction and the incompressibility of the material. Nevertheless, we will see later that this field is the same as the elliptical flow lines introduced in 3.3.5.

Since in independence of u_x in z , the surfaces of velocity discontinuity at entry and exit, Γ_e and Γ_s are both vertical. Moreover, at the exit $x = 0$, as $h'(0) = 0$ the vertical velocity is equal to zero. In other words, the velocity discontinuity does not really occurs on Γ_s even if Γ_s is always the limits between plastic and elastic zones. This velocity field is illustrated in Figure 3.10.

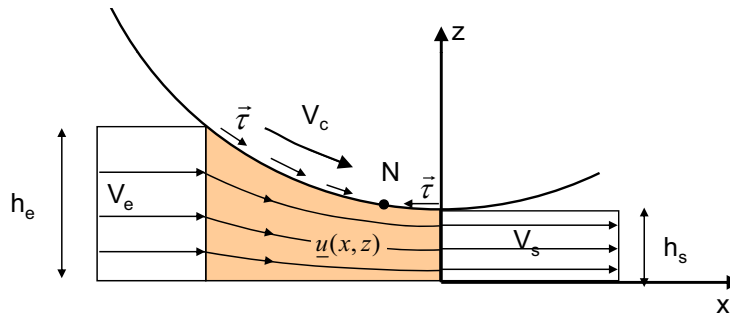


Figure 3.10: Continuous simple velocity field with homogenous deformation across the thickness. As $h'(0) = 0$ the velocity is continuous at the exit.

Calculating of power functions

Bouharaoua and al [18] did developed as far as possible to get analytical expression of all the power functions. However, they obtained the continuous plastic deformation power $J_{\dot{\epsilon}}$ as a double integral with respect to x and z . Here will be presented results of our development to get analytical solution for the integral in z and obtain an expression of $J_{\dot{\epsilon}}$ as a single integral with respect to x .

Power of continuous plastic deformation: After the calculations presented in the appendix B.1, we have:

$$J_{\dot{\epsilon}} = \frac{\sigma_0}{2\sqrt{3}} C_{vol} \int_{-L}^0 \left[I_2 + \frac{4h'^2}{I_1} \text{Ln} \left(\frac{I_1 + I_2}{|2h'|} \right) \right] \frac{dx}{h} \quad (3.64)$$

where

$$\begin{cases} I_1 = |h \cdot h'' - 2h'^2| \\ I_2 = \sqrt{4h'^2 + I_1^2} \end{cases}$$

Power of velocity discontinuity: By remarking that $[[\underline{u}]] = |u_z(x = -L)|$ power of velocity discontinuity can be written as :

$$\begin{aligned} J_{\Delta u} &= \int_0^{h(-L)} \frac{\sigma_0}{\sqrt{3}} [[\underline{u}]] dz = \int_0^{h(-L)} \frac{\sigma_0}{\sqrt{3}} \frac{|h'(-L)| C_{vol}}{h^2(-L)} z dz \\ &= \frac{\sigma_0}{2\sqrt{3}} |h'(-L)| C_{vol}. \end{aligned} \quad (3.65)$$

Power of friction: At the contact surface, the difference of velocity between the strip and the roll is given by

$$[[\underline{u}]] = \left| V_c - \sqrt{u_1^2(z=h) + u_3^2(z=h)} \right| = \left| V_c - \frac{h_e V_e}{h} \sqrt{1+h'^2} \right|.$$

Therefore, the friction power is

$$\begin{aligned} J_{fric} &= \int_{-L}^0 \frac{m\sigma_0}{\sqrt{3}} \left| V_c - \frac{h_e V_e}{h} \sqrt{1+h'^2} \right| \sqrt{1+h'^2} dx \\ &= \frac{m\sigma_0}{\sqrt{3}} \int_{-L}^0 \left| V_c - \frac{\sqrt{1+h'^2}}{h} C_{vol} \right| \sqrt{1+h'^2} dx. \end{aligned} \quad (3.66)$$

Power of the tensions: The following formula is valid for all 2D velocity fields

$$J_{ten} = (T_s - T_e) C_{vol}. \quad (3.67)$$

As can be seen, the power of velocity discontinuity $J_{\Delta u}$, friction power J_{fric} and tensions power J_{ten} are analytically obtained. The plastic $J_{\dot{\epsilon}}$ is 1-variable integral and can be performed numerically without difficulty. The total power is finally a function of unique variable of the problem C_{vol} and the minimization is solved thanks to Newton-Raphson method. The results of this model will be compared to some others in the section 4.5.

Otherwise, it should be noted that in their study, S.Bouharaoua et al [18] do not take into account the power dissipated by the discontinuity of velocity at the entry of the roll bite.

3.3.3 Improved velocity field

When the ratio thickness over work-roll radius increases, the heterogeneity of the deformation across thickness direction increases and can not be neglected. To take into account this dependence, Bouharaoua and al [18] propose to improve their linear form of vertical velocity to a third degree polynomial depending on z and obtain :

$$\begin{cases} u_x = a(x) + f(x)z^2 \\ u_z = -a'(x)z - f'(x)\frac{z^3}{3} \end{cases} \quad (3.68)$$

where $f(x) = \frac{3}{h^3(x)} [k - a(x)h(x)]$. As a result, to describe the velocity field, they need a scalar parameter k and a function, $a(x)$. The calculation becomes very heavy and far to be analytical. By consequence the minimization is no longer simple to compute.

3.3.4 Circular stream lines velocity field

T.Hoang [47] proposes a velocity field by considering that the material stream lines in the roll bite are circular. To simplify the equations, the author introduces two new coordinates s , exit height of the stream line and θ angular position of the considered point (see Figure 3.11). The material is supposed to follow the circular stream lines with the same center as the work roll O_c and a radius defined by

$$R(s) = \frac{Rh_s}{s}. \quad (3.69)$$

These relation between these new coordinates and Cartesian ones are

$$\begin{cases} x = -\frac{Rh_s}{s} \sin \theta \\ z = s + \frac{Rh_s}{s} (1 - \cos \theta) \end{cases} \quad (3.70)$$

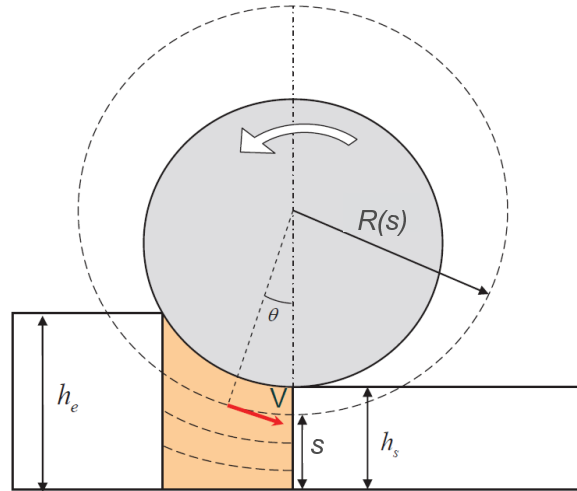


Figure 3.11: Continuous circular velocity field. The velocity is also continuous at the exit. *Figure taken from [47].*

And the circular velocity field is given by

$$\underline{u}(x, z) = \frac{p(s)s^2}{Rh_s + (s^2 - Rh_s) \cos \theta} \begin{bmatrix} \cos \theta \\ -\sin \theta \end{bmatrix} \quad (3.71)$$

where $p(s)$ is the velocity at the roll bite exit as a function of the height s across the thickness direction. For symmetric rolling, this function is constant. And it is taken linear for asymmetric rolling conditions. In this case, this function allows to model the curvature of the strip at the exit of roll bite. This is called *ski* or *longbow defect* (see Figure 2.11).

Unlike Bouharaoua and *al* [18], T.Hoang [47] takes into account the dissipation of the discontinuity of velocity at the entry of roll bite. However, he simplifies the calculation of this dissipation in considering that the discontinuity surface is a vertical straight surface. This is not exact because by construction, the longitudinal velocity in the roll bite u_x depends on z while it is constant and equal to V_e before the roll bite. Although the induced error may be small we can not compare the results of this model to other ones.

3.3.5 Elliptical stream lines velocity field

Method for constructing velocity fields

In 2001 Dogruoglu [31] introduced a rigorous and systematic method for constructing kinematically admissible velocity fields necessary in the analysis of plastic forming processes by *UBM*. The objective of the method is build a family of kinematically admissible velocity fields by pre-assuming a certain form of the flow lines. In his applications, the flow lines are chosen being circular and elliptical.

We can sum up the results of this method as follows. If the flow lines in the plastic deformation zone is represented as a one-parameter family of curves

$$f(x, z) = \xi, \quad 0 \leq \xi \leq 1. \quad (3.72)$$

then the following velocity field

$$\begin{cases} u_x = -\frac{\partial f}{\partial z} F(\xi) \\ u_z = \frac{\partial f}{\partial x} F(\xi) \end{cases} \quad (3.73)$$

verifies automatically the incompressibility condition. So that the velocity field given by 3.73 is kinematically admissible, it is necessary to choose the flow lines that include boundary lines of the problem (for example the work-roll surface in rolling process).

The function $F(\xi)$ is an arbitrary differentiable function which will be determined by the initial conditions of the considered problem. In rolling process, $F(\xi)$ is determined by one of two conditions of the continuity of the velocity components in the direction normal to the boundaries Γ_e and Γ_s of the plastic deformation zone. In other words, the form of Γ_e or Γ_s can be chosen arbitrarily. After, $F(\xi)$ is obtained and the velocity field is determined. The other condition will be used to determine the related boundary of the deformation zone.

Elliptical flow lines

The author applied then this method to determine an elliptical flow lines velocity field. The elliptical flow lines family is defined by

$$f(x, z) = \frac{z}{R + h_s - \sqrt{R^2 - x^2}} = \xi, \quad 0 \leq \xi \leq 1. \tag{3.74}$$

Now if the exit surface of velocity discontinuity is chose as a vertical line defined by

$$x = 0, z = z_2 \quad 0 \leq z_2 \leq h_s. \tag{3.75}$$

Inserting 3.75 into 3.74 we obtain

$$z = z_2(\xi) = h_s \xi. \tag{3.76}$$

Using the definition of velocity field 3.73, the continuity of normal velocity through Γ_s becomes

$$u_x(0, z) = -\frac{\partial f}{\partial z}(0, z)F(\xi) = -\frac{1}{h_s}F(\xi) = V_s.$$

Then,

$$F(\xi) = -h_s V_s = -C_{vol} \tag{3.77}$$

equal to the flow rate (with opposite sign).

Finally, the author obtained following elliptical velocity field

$$\begin{cases} u_x = -\frac{\partial f}{\partial z}F(\xi) = \frac{C_{vol}}{R + h_s - \sqrt{R^2 - x^2}} \\ u_z = \frac{\partial f}{\partial x}F(\xi) = \frac{C_{vol}xz}{\sqrt{R^2 - x^2} [R + h_s - \sqrt{R^2 - x^2}]^2} \end{cases} \tag{3.78}$$

To complete the solution, the entry surface is found to be also a vertical plane defined by

$$x = \sqrt{(2R + h_s - h_e)(h_e - h_s)}, z = z_2 \quad 0 \leq z_2 \leq h_s. \tag{3.79}$$

Remark: Using the expression of thickness function and its derivative given correspondingly by 3.62 and 3.63 to simplify the elliptical flow lines velocity field given by 3.78 we obtain exactly the simple velocity field defined by 3.61. Indeed, these two velocity fields are the same.

Results

Dogruoglu [31] computed the power functions by introducing the neutral point position X_n (x^* according to the authors notation) as the unique parameter instead of C_{vol} . The optimization becomes more simple. The author compared then the obtained minimum power J with the results of the eccentric velocity field model given in a Avitzur’s book [8].

Dogruoglu introduced, then the ideal plastic deformation power

$$J_{def}^I = \frac{2\sigma_0}{\sqrt{3}}C_{vol} \ln \frac{h_e}{h_s} \tag{3.80}$$

which is in fact the plastic deformation if the strip material is deformed under plane strain condition only in longitudinal and thickness directions without shear deformation. And a comparison is based on the relative difference between the obtained plastic deformation power and this ideal one. However, Dogruoglu did not take into account the power of velocity discontinuity in the plastic deformation power. He calculated the relative difference by

$$\text{Relative difference} = \frac{J_{\bar{\epsilon}} - J_{def}^I}{J_{def}^I}. \quad (3.81)$$

In the considered rolling case ($m = 0.6$, $hs/R = 0.002$), the author showed that this relative difference is excellently small, varying from 0.19% down to 0.014% when the reduction increases from 5% to 60%, meaning that the plastic deformation is very closed to the actual one.

Nevertheless, let consider for example a slip lines velocity field such us unitriangular one, there is no continuous deformation power, $J_{\bar{\epsilon}} = 0$. All plastic deformation power is generated by the velocity discontinuity, $J_{\Delta u}$. In this case the relative difference, defined by the formula of Dogruoglu 3.82 is equal to 0 implying that the plastic deformation is lower than the ideal one. This is, of course not true. Indeed, the total plastic deformation power must include both power of continuous plastic deformation and the power of velocity discontinuity. Then, the relative difference should be defined as

$$\text{Relative difference} = \frac{J_{\bar{\epsilon}} + J_{\Delta u} - J_{def}^I}{J_{def}^I}. \quad (3.82)$$

With this correction, for the same considered rolling case, the relative difference varies from 3.73% to 1.07%.

3.4 Discussions

This chapter shows that the *UBM* based on the extremum principle formulated by [91] is largely used in metal rolling process to evaluate especially the supplied power and torque. There were developed many slip lines (rigid body) velocity fields. The unitriangular is suitable to be used in hot rolling conditions where a high friction coefficient occurs and the ratio thickness over contact length is close to 1. For cold rolling, the contact length is usually much higher than strip thickness, the multitriangular is more efficient. An other advantage of this velocity field is that the sliding between the strip and the work-roll out of the neutral zone is allowed which correspond better to the condition of cold rolling.

Nevertheless, the optimization of solution for multitriangular is not simple mainly due to the unknown number of triangles. It is necessary to vary it and the number of parameters will vary at the same time. Some author solve mathematically the optimization problem by consider the number of triangles as a continuous "real" number but not "integer" number, see [57, 87, 9]. This method allowed to obtain lower upper bound in many cases. Withal, the velocity field obtained by non-integer number of triangles seems to be somewhat illusive.

Unlike the slip line or rigid bodies velocity fields the continuous ones give often more interesting information about the velocity field itself. The main difficulty is how to parameterize a good velocity fields. Authors proposed different methods for constructing kinematically admissible velocity field. The most famous one is based on flow functions and flow lines ([31]). Advantage of the method is that you can imagine any flow lines that verify the boundary condition (work-roll surface must be a flow line), the method will give expression of the velocity field. Yet, this advantage is also an disadvantage because the flow lines need to be pre-assumed and sometimes it is not easy to imagines the complicated one. For example, in the next chapter, the flow lines of rolled material as results of *Lam3-Tec3* are complicated. It oscillates somehow around a smooth curve. In the same chapter, we will introduce an other method to build kinematically admissible velocity field that does not pre-assume flow lines but the flow lines will be outputs of the model. There will also be presented a comparison of unitriangular, continuous simple (elliptical) velocity fields with the new oscillating one and *Lam3-Tec3* results.

By giving the flow velocity the continuous velocity fields own an other advantage to approach the flow patterns such as 3D models approaching the width variation of the rolled strip. Some *UBM* models will be presented in the chapter 5.

Chapter 4

Oscillation of mechanical fields in roll bite

The rolling process has been analyzed by various analytical and numerical methods as the slab method, UBM and FEM . The FEM calculation allows having accurate estimation of mechanical solution but computing time is usually long. Beside, the heterogeneity of strain or stress fields across the strip thickness needs understanding and taking into account to explain heterogeneity of metallurgical characteristics and microstructure after rolling or rolled-product apparent defect prediction. This heterogeneity remains very little investigated. Orowan is one of rare authors who take into account the variation of stress field in the thickness. However, the shear stress is imposed linear across the thickness direction. The chapter presents firstly a method for constructing kinematically admissible velocity field for rolling process. This method is not based on pre-assumed flow lines as usual but on the understanding of their physical behavior. Then, a new family called "oscillating" velocity fields allowing to model the non-linear heterogeneity of deformation in the thickness is proposed. And application of UBM results to a final velocity field that corresponds to a lower rolling power in comparison with the unitriangular and the elliptical ones. This obtained velocity field, having characteristics of wave propagation, matches well Lam3-Tec3 results.

Contents

4.1	Introduction	72
4.2	Method for constructing velocity field	72
4.2.1	General admissible conditions of velocity field	72
4.2.2	Applications	75
4.3	An oscillating velocity field proposal	76
4.4	UBM with the oscillating velocity field	79
4.4.1	New strategy for minimization of power function	79
4.4.2	Numerical resolution - programming	81
4.5	Comparison with Lam3-Tec3 and other UBM models	86
4.5.1	Power and neutral point	86
4.5.2	Plastic area - discontinuity surfaces	87
4.5.3	Velocity isovalue surfaces	88
4.5.4	Oscillation of velocity field along the streamlines	89
4.6	Conclusions and perspectives	93
4.6.1	Conclusions	93
4.6.2	Perspectives	94

4.1 Introduction

Although in flat product cold rolling condition, the strip thickness is very small compared to its width and the contact length with the work-roll, the vertical velocity, vertical strain, vertical strain rate fields are not homogenous across the strip thickness. These fields oscillate in both x and z directions. This is an interesting results that may be in contrast to what could be imagined (the thinner the strip, more homogenous the mechanical fields). This chapter introduces a complete application of *UBM* to analyze this heterogeneity of mechanical field and compare to *Lam3-Tec3*.

As a reminder, following the *UBM* introduced in the previous chapter, the actual velocity field in a rolling process is the one that minimizes the power function 3.27. Usually, a family of velocity fields with few parameters is studied of which the velocity field minimizing the power function is the best approximation of the real one. The lower the power, the better the approximation. The rigid body (or slip lines) velocity fields such as unitriangular, multitriangular are obviously heterogenous velocities across the thickness but the changes between the rigid regions are abrupt. The shear stresses are concentrated only on certain slip lines. In the contrary, the typical continuous velocity field like simple (called also elliptical) has longitudinal and vertical deformation rates $\dot{\epsilon}_{xx}$ and $\dot{\epsilon}_{zz}$ which are homogeneous in the thickness. The circular velocity field is not so different from the simple one. This chapter presents new family of velocity fields also in plane strain condition. These velocity fields are contiguous and have certain concentration of shear strain rate somehow similar to slip lines ones.

That family is built as an addition of an "oscillating part" to the "simple" (elliptical) velocity field of which the longitudinal component is constant in the strip thickness (see 3.61). We show that the best field of that family gives a better approximation than the simple one. This study proves there is an oscillating part in the velocity field during the rolling process. A careful observation of the fields obtained by a finite-element method *Lam3-Tec3* shows that the oscillation phenomenon is in fact really present even for thin strip. And the oscillations predicted by the analytical model (*UBM*) match very well the *Lam3-Tec3* results.

4.2 Method for constructing velocity field

4.2.1 General admissible conditions of velocity field

The model is developed under the same assumptions as presented in the part 3.1.2. Let remind that before the roll-bite the velocity is uniform and equal to V_e and it is also uniform and equal to V_s after the roll-bite (see Figure 3.2). The material is deformed plastically in the zone Ω delimited by the two surfaces Γ_e and Γ_s which are also the surfaces of velocity discontinuity because the velocity field in this field is different from \underline{V}_e and \underline{V}_s . Modeling of the velocity in this area is the key point of an *UBM* model. Once the velocity fields in all the three zones are modeled, the Γ_e and Γ_s can be determined.

Using the boundary conditions described for a general elasto-plastic previously (section 2.1.3) and simplify them for rigid perfectly plastic condition (especially the conditions of the symmetry on $z = 0$ given by 2.3), the kinematically admissible conditions of the velocity field in the plastic deformation zone Ω are:

- Incompressibility of rigid plastic material:

$$\operatorname{div} \underline{u}(x, z) = \frac{\partial u_x}{\partial x}(x, z) + \frac{\partial u_z}{\partial z}(x, z) = 0 \quad \forall (x, z) \in \Omega \quad (4.1)$$

- Boundary conditions on the surface of symmetry $z = 0$:

$$u_z(x, 0) = 0 \quad \forall x \in [-L, 0] \quad (4.2)$$

and

$$\frac{\partial u_x}{\partial z}(x, 0) = 0 \quad \forall x \in [-L, 0]. \quad (4.3)$$

- Boundary condition on the contact surface $z = h(x)$:

$$u_z(x, h(x)) - u_x(x, h(x)) \cdot h'(x) = 0 \quad \forall x \in [-L, 0]. \quad (4.4)$$

Concerning the flow rate, if the three conditions 4.1, 4.2 and 4.4 are verified, it can be demonstrated that the volume flow rate through a cross section of the strip is conserved (constant). Indeed, if $C_{vol}(x)$ denotes the flow rate through the cross section at x , it is defined as a function of x

$$C_{vol}(x) = \int_0^{h(x)} u_x(x, z) \cdot dz. \quad (4.5)$$

We consider now its derivative:

$$\frac{dC_{vol}(x)}{dx} = \frac{d}{dx} \int_0^{h(x)} u_x(x, z) \cdot dz = h'(x)u_x(x, h(x)) + \int_0^{h(x)} \frac{\partial u_x}{\partial x}(x, z) \cdot dz.$$

Using the equations 4.1 then 4.2 and 4.4 we obtain:

$$\begin{aligned} \frac{dC_{vol}(x)}{dx} &= h'(x)u_x(x, h(x)) - \int_0^{h(x)} \frac{\partial u_z}{\partial z}(x, z) \cdot dz \\ &= h'(x)u_x(x, h(x)) - u_z(x, h(x)) + u_z(x, 0) \\ &= \left[h'(x)u_x(x, h(x)) - u_z(x, h(x)) \right] + u_z(x, 0) \\ &= 0. \end{aligned}$$

This implies the conservation of the flow rate:

$$C_{vol} = \int_0^{h(x)} u_x(x, z) \cdot dz = \text{const} \quad \forall x \in [-L, 0]. \quad (4.6)$$

Thus, the fourth conditions 4.1, 4.2, 4.3, 4.4 (or 4.6) are all the kinematically admissible conditions of a velocity field defined throughout the plastic deformation zone Ω .

It is easy to verify that the "simple" velocity field given by 3.61 verifies these conditions. This field describes the average behavior of strain in the thickness. We remark that any kinematically admissible velocity field can be written as a sum of the simple velocity field and an addition term as following:

$$\underline{u}(x, z) = C_{vol} \cdot \begin{bmatrix} \frac{1}{h(x)} + f(x, z) \\ \frac{h'(x)}{h^2(x)} \cdot z + g(x, z) \end{bmatrix}$$

The admissible conditions will be rewritten thanks to the 2 functions $f(x, z)$ and $g(x, z)$. The first condition 4.1 implies that:

$$\frac{\partial f}{\partial x}(x, z) + \frac{\partial g}{\partial z}(x, z) = 0 \quad \forall (x, z) \in \Omega \quad (4.7)$$

There exists always a function denoted $F(x, z)$ so that:

$$\begin{cases} f(x, z) = \frac{\partial F(x, z)}{\partial z} \\ g(x, z) = -\frac{\partial F(x, z)}{\partial x} \end{cases}$$

With this expression of $f(x, z)$ and $g(x, z)$, the condition 4.1 is always verified. $F(x, z)$ is flow function for the addition part determined within a constant.

The condition 4.2 is equivalent to $F(x, 0) = \text{const}$. As the value of this constant has no real importance, it can be chosen equal to 0, then

$$F(x, 0) = 0 \quad \forall x \in [-L, 0]. \quad (4.8)$$

The condition 4.3 becomes:

$$\frac{\partial^2 F}{\partial z^2}(x, 0) = 0. \quad (4.9)$$

And the condition 4.6 gives:

$$F(x, h(x)) - F(x, 0) = 0.$$

Finally, any 2D kinematically admissible velocity field can be written as:

$$\underline{u}(x, z) = C_{vol} \cdot \begin{bmatrix} \frac{1}{h(x)} + \frac{\partial F(x, z)}{\partial z} \\ \frac{h'(x)}{h^2(x)} \cdot z - \frac{\partial F(x, z)}{\partial x} \end{bmatrix} \quad (4.10)$$

with kinematically admissible conditions:

$$\begin{cases} F(x, 0) = 0 \quad \forall x \in [-L, 0] \\ F(x, h(x)) = 0 \quad \forall x \in [-L, 0] \\ \frac{\partial^2 F}{\partial z^2}(x, 0) = 0 \quad \forall x \in [-L, 0]. \end{cases} \quad (4.11)$$

The tensors of strain rate: Since 4.10, all the derivatives of the velocity field are calculated as follow:

$$\frac{\partial u_x}{\partial x}(x, z) = C_{vol} \cdot \left[-\frac{h'}{h^2} + \frac{\partial^2 F(x, z)}{\partial x \partial z} \right] \quad (4.12)$$

$$\frac{\partial u_x}{\partial z}(x, z) = C_{vol} \cdot \frac{\partial^2 F(x, z)}{\partial z^2} \quad (4.13)$$

$$\frac{\partial u_z}{\partial x}(x, z) = C_{vol} \cdot \left[\left(\frac{h'}{h^2} \right)' z - \frac{\partial^2 F(x, z)}{\partial x^2} \right] \quad (4.14)$$

$$\frac{\partial u_z}{\partial z}(x, z) = C_{vol} \cdot \left[\frac{h'}{h^2} - \frac{\partial^2 F(x, z)}{\partial x \partial z} \right] \quad (4.15)$$

The components of strain rate tensors $\underline{\dot{\epsilon}}(\underline{u})$ are:

$$\begin{aligned}
 \dot{\epsilon}_{xx}(\underline{u}) &= \frac{\partial u_x}{\partial x}(x, z) = C_{vol} \cdot \left[-\frac{h'}{h^2} + \frac{\partial^2 F(x, z)}{\partial x \partial z} \right] \\
 \dot{\epsilon}_{zz}(\underline{u}) &= \frac{\partial u_z}{\partial z}(x, z) = C_{vol} \cdot \left[\frac{h'}{h^2} - \frac{\partial^2 F(x, z)}{\partial x \partial z} \right] = -\dot{\epsilon}_{xx}(x, z) \\
 \dot{\epsilon}_{xz}(\underline{u}) &= \frac{1}{2} \left[\frac{\partial u_x}{\partial z} + \frac{\partial u_z}{\partial x} \right] = \frac{C_{vol}}{2} \cdot \left[\left(\frac{h'}{h^2} \right)' z + \frac{\partial^2 F(x, z)}{\partial z^2} - \frac{\partial^2 F(x, z)}{\partial x^2} \right] \\
 \dot{\bar{\epsilon}}(\underline{u}) &= \sqrt{\frac{2}{3}} (\dot{\epsilon}_{xx}^2(\underline{u}) + 2\dot{\epsilon}_{xz}^2(\underline{u}) + \dot{\epsilon}_{zz}^2(\underline{u})) = \frac{2}{\sqrt{3}} \sqrt{\dot{\epsilon}_{xx}^2(\underline{u}) + \dot{\epsilon}_{xz}^2(\underline{u})}
 \end{aligned} \tag{4.16}$$

4.2.2 Applications

The expression 4.10 of kinematically admissible velocity is only a different form of flow function method (for example [31]). On the other hand, the kinematically admissible conditions written as 4.11 are relatively simplified and enable to easily propose some family of function $F(x, z)$. For example, any function defined by $t(x)z^n$ with $n = 1$ or $n > 2$ verifies the first and the third equations of 4.11. These arguments lead naturally to following family of functions

$$F(x, z) = g_1(x)z + \sum_{n=3}^{\infty} g_n(x)z^n. \tag{4.17}$$

The only condition so that the velocity defined by equations 4.10 and 4.17 is kinematically admissible is the second equation of 4.11. Of course, n can also be real or integer numbers but they are necessarily greater than 2.

Example of third order polynomial velocity field

If $g_n(x)$ are chosen so that $g_n(x) = 0$ for all $n > 3$, we have

$$F(x, z) = g_1(x)z + g_3(x)z^3. \tag{4.18}$$

The only kinematically admissible condition is (second equation of 4.11)

$$F(x, h(x)) = g_1(x)h(x) + g_3(x)h^3(x) = 0 \quad \forall x \in [-L, 0] \tag{4.19}$$

which implies, then

$$g_1(x) = -g_3(x)h^2(x) = 0 \quad \forall x \in [-L, 0]. \tag{4.20}$$

Substituting 4.20 into 4.18 we have

$$F(x, z) = g_3(x)z(z^2 - h^2(x)). \tag{4.21}$$

Finally, any velocity field given by 4.10 where the function $F(x, z)$ defined by 4.21 and the function $g_3(x)$ is freely chosen, even constant. And the 3-order polynomial velocity field is given by:

$$\underline{u}(x, z) = C_{vol} \cdot \begin{bmatrix} \frac{1}{h(x)} + (3z^2 - h^2) g_3(x) \\ \frac{h'(x)}{h^2(x)} z - (z^3 - h^2 z) g_3'(x) \end{bmatrix} \tag{4.22}$$

We will see in the next section another proposition of the function $F(x, y)$ having a nature of wave propagation that leads to a new velocity field with oscillating characteristics.

4.3 An oscillating velocity field proposal

In order to minimize the rolling power in function of velocity knowing that the space of function $F(x, z)$ is an infinite-dimensional space, we need to parameterize it meaning restrict and transform the space of $F(x, z)$ into a finite-dimensional one. The parameterizing manner is more interesting if there are less number of parameters and when the optimum power is lower. We introduce in this section a particular way to build the function $F(x, z)$ with few parameters.

First, it can be seen that the first equation of 4.11 implies that

$$\frac{\partial^2 F}{\partial x^2}(x, 0) = 0 \quad \forall x \in [-L, 0].$$

Therefore, the third equation of 4.11 can be rewritten as

$$\frac{\partial^2 F}{\partial z^2}(x, 0) - \frac{\partial^2 F}{\partial x^2}(x, 0) = 0 \quad \forall x \in [-L, 0]. \quad (4.23)$$

The kinematically admissible conditions given by equation 4.11 can be rewritten as follows

$$\begin{cases} F(x, 0) = 0 \quad \forall x \in [-L, 0] \\ F(x, h(x)) = 0 \quad \forall x \in [-L, 0] \\ \frac{\partial^2 F}{\partial z^2}(x, 0) - \frac{\partial^2 F}{\partial x^2}(x, 0) = 0 \quad \forall x \in [-L, 0]. \end{cases} \quad (4.24)$$

The third equation is similar to a "wave propagation" one will allows to propose similar "oscillation" solutions.

Indeed, let study now following equations similar to the kinematically admissible conditions 4.11:

$$\begin{cases} F^*(x, 0) = 0 \quad \forall x \in [-L, 0] \\ F^*(x, h(x)) = 0 \quad \forall x \in [-L, 0] \\ \frac{\partial^2 F^*}{\partial z^2}(x, z) - \frac{\partial^2 F^*}{\partial x^2}(x, z) = 0 \quad \forall (x, z) \in \Omega \end{cases} \quad (4.25)$$

The third equation means that the shear strain rate $\dot{\epsilon}_{xz}$ is not only equal to 0 on the surface of symmetry $z = 0$ but every where in the roll-bite (see the second equation). It is similar to the D'Alambert equation for one-dimensional wave problem. The general solution of this equation is: $F^*(x, z) = G^*(x + z) + H^*(x - z)$ with G and H any 1-variable functions, twice differentiable. Hence, the equations 4.25 are strictly equivalent to:

$$\begin{cases} F^*(x, 0) = G^*(x + 0) + H^*(x - 0) = 0 \quad \forall x \in [-L, 0] \\ F^*(x, h(x)) = G^*(x + h(x)) + H^*(x - h(x)) = 0 \quad \forall x \in [-L, 0] \\ F^*(x, z) = G^*(x + z) + H^*(x - z) \quad \forall (x, z) \in \Omega \end{cases}$$

By simplifying, this general solution of 4.25 can be given by:

$$\begin{cases} F^*(x, z) = G^*(x + z) - G^*(x - z) \quad \forall (x, z) \in \Omega \\ G^*(x + h(x)) = G^*(x - h(x)) \quad \forall x \in [-L, 0] \\ \forall G \in C^2(\mathfrak{R}) \end{cases} \quad (4.26)$$

Now, let come back to the admissible conditions 4.24. The difference with respect to the equations 4.25 is that the d'Alambert equation is not verified every where in the roll-bite but only on the surface of symmetry $z = 0$. Of course, all functions verifying 4.25 satisfy also 4.24. Meaning all functions $F(x, z)$ given by 4.26 are also solution of 4.11. However, having no solution to describe the whole admissible space, we propose to study a family of functions verifying the following equation:

$$\boxed{\begin{cases} F(x, z) = A_e [G_e(x + z) - G_e(x - z)] . K_e(x) \quad \forall (x, z) \in \Omega \\ G_e(x + h(x)) = G_e(x - h(x)) \quad \forall x \in [-L, 0] \\ \forall G_e, K_e \in C^2(\mathfrak{R}) \end{cases}} \quad (4.27)$$

where A_e is a parameter that allow to represent the amplitude of $F(x, z)$ and thus the oscillation part in the velocity field. G_e and K_e are two one-variable functions, twice differentiable. When $A_e = 0$ the velocity field is identical to the "simplified" or elliptical one.

It is easy to verify that all functions $F(x, z)$ given by 4.27 verify the kinematically admissible conditions 4.11. Even if this family dose not contain all admissible functions $F(x, z)$, we will see later that the velocity solution (best velocity of the family) carries effectively oscillation characteristics and gives lower power than the simple one.

Periodicity of velocity fields and determination of G_e

Noting that the equation 4.27 is given for every x in the roll-bite, if this function G is known on a segment $[x_0 - h(x_0), x_0 + h(x_0)]$, for any x_0 in the roll-bite, it is entirely defined in the whole roll-bite. It seems to be a quasi periodic function with a period equal to $2h(x)$ - the thickness of the strip - varying along the roll bite.

Therefore, to construct the function G_e all along the roll-bite, it is only necessary to do it on a segment, for example the segment at the entry of the roll-bite $[x_e - h(x_e), x_e + h(x_e)]$. This function is denoted G_0 . To have the continuity of the velocity field, the function G_e and its derivative need to be continuous. Therefore,

$$\begin{cases} G_0(x_e + h(x_e)) = G_0(x_e - h(x_e)) \\ G_0'(x_e + h(x_e)) = \frac{1 - h'(x_e)}{1 + h'(x_e)} G_0'(x_e - h(x_e)) \end{cases} \quad (4.28)$$

Choice of function G_0 : the function G_0 can be chosen as

$$\begin{cases} G_0(x) = \cos(g(x)) \\ g(x) = a_0 + a_1x + a_2x^2. \end{cases} \quad (4.29)$$

With this construction 4.29, it is easy to check that $G_0(x)$ satisfies the two continuity conditions of 4.28 if g verifies following 3 conditions:

$$\begin{cases} g(x_e - h(x_e)) = \pi \\ g(x_e + h(x_e)) = -\pi \\ g'(x_e + h(x_e)) = \frac{1 - h'(x_e)}{1 + h'(x_e)} g'(x_e - h(x_e)) \end{cases} \quad (4.30)$$

The 3 parameters: a_0, a_1, a_2 are then completely determined.

Choice of function K_e

We chose a function with one parameter, as

$$K_e(x) = x^3 \quad (4.31)$$

which models the decrease of the oscillation amplitude from the entry towards the exit of the roll-bite.

Choice of function F

Both functions G_e and K_e are now completely determined. The function $F(x, z)$ given by equations 4.27 contain therefore only one parameter A_e . It can be noted that, the function G_e is somehow similar to the wave propagation from the entry forward the exit of the roll-bite. Now in the analogy we propose to add a similar function representing the wave propagation from the exit towards the entry of the roll bite. Similarly to G_e , G_s is also constructed by using the periodicity equation $G_s(x + h(x)) = G_s(x - h(x)) \forall x \in [-L, 0]$ but based on the its definition on the exit segment $[-h_s, h_s]$ instead of the entry one $[x_e - h_e, x_e + h_e]$. Regarding the function K_s , the analogy is understood as follows. The function K_e is maximum (in absolute value) at the entry and vanishes at the exit. The function K_s is chosen as

$$K_s(x) = (x - x_e)^3 \quad (4.32)$$

so that it is maximum at the exit and vanishes at the entry.

Finally

$$F(x, z) = A_e [G_e(x + z) - G_e(x - z)] K_e(x) + A_s [G_s(x + z) - G_s(x - z)] K_s(x). \quad (4.33)$$

Summary of velocity fields

From the expression of velocity field 4.10 and the choice of the function $F(x, z)$ by 4.33 the velocity is

$$\underline{u}(x, z) = C_{vol} \cdot \underline{v}(A_e, A_s, x, z) \quad (4.34)$$

where $\underline{v}(x, z)$ is *elementary velocity field* of which the components are defined as follows

$$v_x(A_e, A_s, x, z) = \frac{1}{h(x)} + A_e [G'_e(x + z) + G'_e(x - z)] K_e(x) + A_s [G'_s(x + z) + G'_s(x - z)] K_s(x) \quad (4.35)$$

and

$$v_z(A_e, A_s, x, z) = \frac{h'(x)}{h^2(x)} \cdot z - A_e \left[(G'_e(x + z) - G'_e(x - z)) K_e(x) + (G_e(x + z) - G_e(x - z)) K'_e(x) \right] - A_s \left[(G'_s(x + z) - G'_s(x - z)) K_s(x) + (G_s(x + z) - G_s(x - z)) K'_s(x) \right]. \quad (4.36)$$

As being discussed previously, all functions G_e , K_e and G_s , K_s are completely defined. The velocity field contents therefore three parameters A_e , A_s and C_{vol} that need determining by minimizing the power function given by 3.27. Of course, we can chose $A_e = 0$ and $A_s \neq 0$ if we only want to model what the oscillation from the exit and inversely $A_e \neq 0$ and $A_s = 0$ if we are only interested in the oscillation from the entry.

By writing the equality of the strip velocity and work-roll velocity at the neutral point, we have

$$V_c = \sqrt{u_x^2(x_n, h_n) + u_z^2(x_n, h_n)} = C_{vol} v_x(A_e, A_s, x_n, h_n) \sqrt{1 + h'_n} \quad (4.37)$$

where $h_n = h(x_n)$ and $h'_n = h'(x_n)$. We deduce then

$$C_{vol} = \frac{V_c}{v_x(x_n, h_n) \sqrt{1 + h'_n}} \quad (4.38)$$

where $v_x(A_e, A_s, x, z)$ given by 4.35. C_{vol} becomes a function of A_e, A_s and x_n , denoted $C_{vol}(A_e, A_s, x_n)$. Thus, we can rewrite the velocity field as

$$\underline{u}(x, z) = C_{vol}(A_e, A_s, x_n) \cdot \underline{v}(A_e, A_s, x, z). \quad (4.39)$$

Remark: The elementary velocity is the velocity field if the flow rate is equal to an unity ($C_{vol} = 1$). It characterizes the stream lines of material flow. Depending on the value of A_e and A_s that the amplitude of oscillation parts is more or less important and change the stream lines compared to the classic ones corresponding to the classic velocity field. As this elementary velocity does not depend on the neutral point position x_n , the flow patterns defined from this velocity family are independent of x_n . The parameter x_n is only involved in velocity field through the total flow rate $C_{vol}(A_e, A_s, x_n)$.

Discussion: The new family of the velocity fields introduced in this section has an oscillation terms. The periodicity characteristic of this oscillation has particularly been brought out and the function G_e and/or G_s describing this phenomenon is carefully built. Finally, with only three parameters A_e , A_s and x_n this velocity family is able to model the mechanical fields heterogeneity across the strip thickness. In this velocity family, the power function $J(\underline{u})$ depending on the velocity field becomes a function of these three parameters A_e , A_s and x_n , $J(\underline{u}(A_e, A_s, x_n))$. The minimization of this function with respect to the three parameters is then numerically possible. Hereafter, we will present an optimization strategy efficient in terms of computing time.

4.4 UBM with the oscillating velocity field

4.4.1 New strategy for minimization of power function

After introducing this new velocity field family represented by three parameters x_n , A_e and A_s . The power function given by 3.27 becomes a function of these three parameters and the optimization problem can be written as:

$$\begin{cases} \frac{\partial J}{\partial x_n}(A_e, A_s, x_n) = 0 \\ \frac{\partial J}{\partial A_e}(A_e, A_s, x_n) = 0 \\ \frac{\partial J}{\partial A_s}(A_e, A_s, x_n) = 0. \end{cases} \quad (4.40)$$

This section presents a new optimization strategy that allows to obtain the optimum neutral point more easily and to decrease significantly the computation time. This strategy is applicable if the power function is analytically derivable with respect to x_n . And this is true for every kinematically admissible velocity field expressed as 4.39. The method consisting in optimizing analytically the power function with respect to x_n and then numerically with respect to A_e and A_s .

4.4.1.a Calculation of power functions and derivatives

Power of plastic deformation: Indeed, thanks to the expression 4.39 of the velocity field, the power dissipated by plastic deformation in Ω (the first term of the equation 3.27 right side) can be expressed as follow:

$$\begin{aligned} J_{\dot{\epsilon}}(\underline{u})(A_e, A_s, x_n) &= C_{vol}(A_e, A_s, x_n) \cdot J_{\dot{\epsilon}}(\underline{v})(A_e, A_s) \\ \text{where } J_{\dot{\epsilon}}(\underline{v})(A_e, A_s) &= \int_{\Omega} \sigma_0 \cdot \dot{\epsilon}(\underline{v})(A_e, A_s, x, z) \, d\Omega. \end{aligned} \quad (4.41)$$

Power of discontinuity of velocity: Also the power dissipated by velocity discontinuity (the second term of the equation 3.27 right side) becomes:

$$\begin{aligned} J_{\Delta u}(A_e, A_s, x_n) &= C_{vol}(A_e, A_s, x_n) \cdot J_{\Delta \underline{v}}(A_e, A_s) \\ \text{where } J_{\Delta \underline{v}}(A_e, A_s) &= \int_{S_d} \frac{\sigma_0}{\sqrt{3}} \|\Delta \underline{v}(A_e, A_s, x, z)\| \, dS. \end{aligned} \quad (4.42)$$

Power of entry and exit tensions: In the same way, the tensions power (the fourth term of the equation 3.27 right side):

$$\begin{aligned} J_{ten}(\underline{u})(A_e, A_s, x_n) &= C_{vol}(A_e, A_s, x_n) J_{ten}(\underline{v}) \\ \text{where } J_{ten}(\underline{u}) &= \int_{S_{Td}} \underline{T}^d \cdot \underline{v}(A_e, A_s, x, z) \, dS = T_s - T_e. \end{aligned} \quad (4.43)$$

Thus, their derivatives with respect to x_n are nicely represented by:

$$\begin{cases} \frac{\partial J_{\dot{\epsilon}}(\underline{u})}{\partial x_n}(A_e, A_s, x_n) = \frac{\partial C_{vol}(A_e, A_s, x_n)}{\partial x_n} \cdot J_{\dot{\epsilon}}(\underline{v})(A_e, A_s) \\ \frac{\partial J_{\Delta u}(\underline{u})}{\partial x_n}(A_e, A_s, x_n) = \frac{\partial C_{vol}(A_e, A_s, x_n)}{\partial x_n} \cdot J_{\Delta \underline{v}}(A_e, A_s) \\ \frac{\partial J_{ten}(\underline{u})}{\partial x_n}(A_e, A_s, x_n) = \frac{\partial C_{vol}(A_e, A_s, x_n)}{\partial x_n} \cdot (T_s - T_e) \end{cases} \quad (4.44)$$

Power of contact friction: About the friction power (the third term of the equation 3.27 right side), its dependence on x_n is more complicated. However, we will show that its derivative with respect to x_n can be equally obtained analytically. The difference of velocity on the contact surface is defined by:

$$\Delta \underline{u}_c(x) = \|\underline{u}(x, h(x))\| - V_c. \quad (4.45)$$

The friction power is then written as:

$$\begin{aligned} J_{fric}(\underline{u})(A_e, A_s, x_n) &= \int_{S_c} \tau \cdot \|\Delta \underline{u}_c(x, h(x))\| \cdot dS \\ &= \frac{\bar{m} \cdot \sigma_0}{\sqrt{3}} \cdot \left[\int_{x_n}^0 - \int_{-L}^{x_n} \right] (\|\underline{u}(x, h(x))\| - V_c) \cdot \sqrt{1 + h'^2(x)} dx. \end{aligned}$$

By definition of neutral point, $|\Delta \underline{u}_c(x_n, h_n)| = 0$ we can deduce then:

$$\begin{aligned} \frac{\partial J_{fric}(\underline{u})}{\partial x_n}(A_e, A_s, x_n) &= \frac{\bar{m} \cdot \sigma_0}{\sqrt{3}} \left\{ \left[\int_{x_n}^0 - \int_{-L}^{x_n} \right] \frac{\partial \|\underline{u}(A, x, h(x))\|}{\partial x_n} \sqrt{1 + h'^2(x)} dx - 2\Delta \underline{u}_c(x_n, h_n) \sqrt{1 + h_n'^2} \right\} \\ &= \frac{\bar{m} \cdot \sigma_0}{\sqrt{3}} \frac{\partial C_{vol}(A_e, A_s, x_n)}{\partial x_n} \left[\int_{x_n}^0 - \int_{-L}^{x_n} \right] \|\underline{v}(A, x, h(x))\| \cdot \sqrt{1 + h'^2(x)} dx. \end{aligned}$$

Let denote now

$$J_{fric}^{V_c}(x_n) = \frac{\bar{m} \cdot \sigma_0}{\sqrt{3}} \cdot \left[\int_{-L}^{x_n} - \int_{x_n}^0 \right] V_c \cdot \sqrt{1 + h'^2(x)} dx \quad (4.46)$$

and

$$\begin{aligned} J_{fric}^{\underline{v}}(A_e, A_s, x_n) &= \frac{\bar{m} \cdot \sigma_0}{\sqrt{3}} \cdot \left[\int_{x_n}^0 - \int_{-L}^{x_n} \right] \|\underline{v}(A, x, h(x))\| \cdot \sqrt{1 + h'^2(x)} dx \\ &= \frac{\bar{m} \cdot \sigma_0}{\sqrt{3}} \cdot \left[\int_{x_n}^0 - \int_{-L}^{x_n} \right] v_x(A, x, h(x)) \left(1 + h'^2(x)\right) dx. \end{aligned} \quad (4.47)$$

In fact, $-J_{fric}^{V_c}(x_n)$ is the power of the friction stress on the work-roll that rotates at peripheral velocity V_c . It depends only on the neutral position but not on the strip speed. And $-J_{fric}^{\underline{v}}(A_e, A_s, x_n)$ is the power of the friction stress acted on the strip corresponding to the strip elementary velocity $\underline{v}(A_e, A_s, x, z)$. Then we can rewrite both the friction power and its derivative with respect to x_n as:

$$\begin{cases} J_{fric}(\underline{u})(A_e, A_s, x_n) = J_{fric}^{V_c}(x_n) + C_{vol}(A_e, A_s, x_n) \cdot J_{fric}^{\underline{v}}(A_e, A_s, x_n) \\ \frac{\partial J_{fric}}{\partial x_n}(A_e, A_s, x_n) = \frac{\partial C_{vol}(A_e, A_s, x_n)}{\partial x_n} \cdot J_{fric}^{\underline{v}}(A_e, A_s, x_n). \end{cases} \quad (4.48)$$

Total rolling power function: The total power function and its derivative with respect to x_n becomes:

$$\begin{cases} J(A_e, A_s, x_n) = J_{fric}^{V_c}(x_n) + C_{vol}(A_e, A_s, x_n) \left[J_{\dot{\epsilon}}(\underline{v})(A_e, A_s) + J_{\Delta \underline{v}}(\underline{v})(A_e, A_s) + J_{fric}^{\underline{v}}(A_e, A_s, x_n) - T_s + T_e \right] \\ \frac{\partial J}{\partial x_n}(A_e, A_s, x_n) = \frac{\partial C_{vol}(A_e, A_s, x_n)}{\partial x_n} \left[J_{\dot{\epsilon}}(\underline{v})(A_e, A_s) + J_{\Delta \underline{v}}(\underline{v})(A_e, A_s) + J_{fric}^{\underline{v}}(A_e, A_s, x_n) - T_s + T_e \right]. \end{cases} \quad (4.49)$$

4.4.1.b Numerical resolution strategy

Thanks to 4.49, the first equation of 4.40 - the optimization of the power function with respect to x_n - is now rewritten as

$$\frac{\partial J}{\partial x_n}(A_e, A_s, x_n) = 0 \Leftrightarrow \left[J_{\dot{\epsilon}}(\underline{v})(A_e, A_s) + J_{\Delta \underline{v}}(\underline{v})(A_e, A_s) + J_{fric}^{\underline{v}}(A_e, A_s, x_n) - T_s + T_e \right] = 0. \quad (4.50)$$

This is an equation allowing to determine x_n as a function of A_e and A_s . If $x_n^1(A_e, A_s)$ denotes the solution of this equation (4.50) then by substituting 4.50 into the first equation of 4.49 and using 4.46 the minimum power with respect to x_n is obtained as following function of A_e, A_s

$$\begin{aligned} J_1(A_e, A_s) &= J(x_n^1(A_e, A_s), A_e, A_s) = J_{fric}^{V_c}(x_n^1(A_e, A_s)) \\ &= \frac{\bar{m}\sigma_0}{\sqrt{3}} \left[\int_{-L}^{x_n^1(A_e, A_s)} - \int_{x_n^1(A_e, A_s)}^0 \right] V_c \sqrt{1 + h'^2(x)} dx = \frac{\bar{m}\sigma_0}{\sqrt{3}} V_c (\widehat{AN} - \widehat{NB}) \end{aligned} \quad (4.51)$$

We can deduce from this equation that

$$\begin{cases} \frac{\partial J_1}{\partial A_e}(A_e, A_s) = 2 \frac{\bar{m}\sigma_0}{\sqrt{3}} V_c \sqrt{1 + h'^2(x_n^1)} \cdot \frac{\partial x_n^1}{\partial A_e}(A_e, A_s) \\ \frac{\partial J_1}{\partial A_s}(A_e, A_s) = 2 \frac{\bar{m}\sigma_0}{\sqrt{3}} V_c \sqrt{1 + h'^2(x_n^1)} \cdot \frac{\partial x_n^1}{\partial A_s}(A_e, A_s). \end{cases} \quad (4.52)$$

In other words, the optimization of $J_1(A_e, A_s)$ and $x_n^1(A_e, A_s)$ with respect to A_e, A_s are obtained at a same value of A_e, A_s . This analysis of the power function and its derivatives results finally to the following three-step numerical resolution:

1. For given values of A_e, A_s , solve 4.50 by Newton algorithm to obtain $x_n^1(A_e, A_s)$. This step gives us numerically the function $x_n^1(A_e, A_s)$.
2. Minimize of $x_n^1(A_e, A_s)$ issued from the first step by Newton-Raphson algorithm (see section 5.3.5.c). The first and second order derivatives of $x_n^1(A_e, A_s)$ are calculated numerically. We obtain at the end of this step the optimum value of A_e, A_s and minimum value of $x_n = x_n^1(A_e, A_s)$.
3. Compute the minimum rolling power using 4.51

4.4.1.c Application field of this strategy

This new method of minimization is applicable for 2D approaches where the friction power J_{fric} is analytically derivable with respect to x_n . For 3D approach, we will see in the next chapter that the derivative of J_{fric} with respect to x_n is much more complicated and need to be calculated numerically.

It is an application for all velocity fields of which the elementary part does not depend explicitly on x_n . Or, the flow lines are independently of the neutral point (no perturbation of the neutral point as singularity point on the flow lines). This is in fact valid for all velocity fields studied in the literature till our days.

4.4.2 Numerical resolution - programming

The previous section presents a new optimization strategy. In this section the details of numerical calculation of all elementary power functions $J_{\dot{\epsilon}}(\underline{\nu})(A_e, A_s)$, $J_{\Delta\underline{\nu}}(A_e, A_s)$ and $J_{fric}^{\underline{\nu}}(A_e, A_s, x_n)$ given by 4.41, 4.42 and 4.43 will be detailed.

4.4.2.a Surface of velocity discontinuity at roll-bite entry

As a reminder, by construction we propose a differential continuous velocity field in each zone: before, inside and after the roll bite. The second zone (inside the roll-bite) can be understood as the plastic deformation zone. There are two discontinuity surfaces, one at the roll bite entry and one at the roll bite exit, as showed in Figure 4.1. The interesting point is that the form of these discontinuity surfaces is not predefined but is a output of the model. Indeed, during the research of optimum velocity field, the discontinuity surfaces changes as a function of velocity field. Here are presented the details how to determine numerically the discontinuity surfaces as well as how to calculate numerically the elementary dissipation powers $J_{\Delta\underline{\nu}}(A_e, A_s)$.

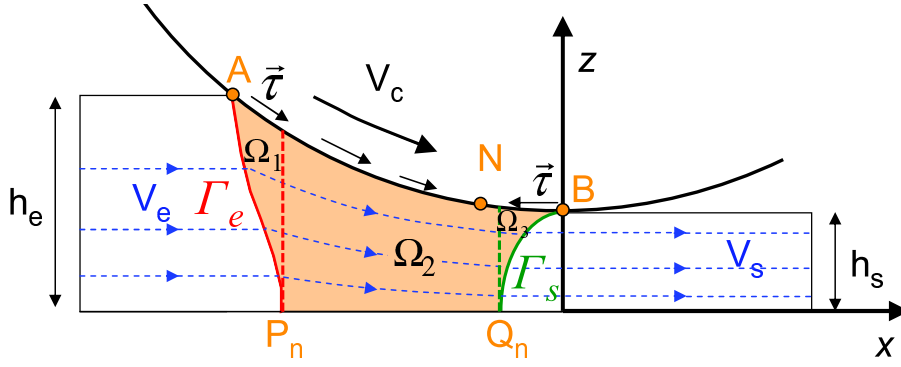


Figure 4.1: The plastic area Ω is limited by the surfaces of velocity discontinuity Γ_e , Γ_s . This plastic deformation zone is divided into three zone Ω_1 , Ω_2 and Ω_3 .

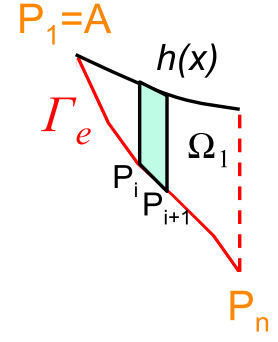


Figure 4.2: Zoom of Ω_1 , entry plastic zone.

We study first the entry one. Reminding that before the plastic deformation zone Ω , the velocity is uniform and equal to V_e , and by definition of the flow rate, we can write:

$$V_e = C_{vol}(A_e, A_s, x_n) \cdot \frac{1}{h_e}.$$

In the analogy of the elementary velocity field definition 4.39, the elementary velocity field before the roll-bite is $v_e = \frac{1}{h_e}$. With the simple velocity (3.61), as the longitudinal velocity is constant across the thickness, the discontinuity surface of velocity field is therefore a cross section.

However, with the oscillating velocity proposed in previous session which is also rewritten as 4.39, the discontinuity surface Γ_e is no longer a cross section because the longitudinal velocity varies in the thickness direction. The difference of elementary velocity between the plastic zone and the entry zone is calculated as:

$$\Delta \underline{v} = \begin{bmatrix} v_x(x, z) - \frac{1}{h_e} \\ v_z(x, z) \end{bmatrix} \quad (4.53)$$

where $v_x(x, z)$ and $v_z(x, z)$ are given by 4.35 and 4.36 respectively. The kinematically admissible condition of velocity on the discontinuity surface is defined as $\Delta \underline{v} \cdot \underline{n} = 0$. In other words, the discontinuity of velocity needs to be tangential to the discontinuity surface at any point of Γ_e :

$$\frac{\Delta \underline{v}}{\|\Delta \underline{v}\|} = \underline{t}. \quad (4.54)$$

Based on this statement, the velocity discontinuity surface is determined starting from a chosen point on this surface. The chosen point is the first point of contact between the work-roll and the strip $P_1(x_{P_1}, z_{P_1}) \equiv A$ with $x_1 = -L$, $z_1 = h(-L)$. P_1 is the beginning point of the velocity discontinuity surface at roll-bite entry, $P_1 \in \Gamma_e$. If $P_2(x_{P_2} = x_{P_1} + dx_1, z_{P_2} = z_{P_1} + dz_1) \in \Gamma_e$ is a neighboring point of P_1 and the distance between them is denoted by $dl = \sqrt{dx_1^2 + dz_1^2}$ then the tangential direction is approximated by:

$$\underline{t} \approx \frac{1}{dl} \begin{bmatrix} dx_1 \\ dz_1 \end{bmatrix}.$$

The admissible condition of velocity discontinuity 4.54 implies that:

$$\begin{bmatrix} dx_1 \\ dz_1 \end{bmatrix} = \begin{bmatrix} \Delta v_x(P_1) \\ \Delta v_z(P_1) \end{bmatrix} \frac{dl}{\|\Delta \underline{v}\|} \quad (4.55)$$

And

$$\Delta v_1 = \sqrt{\left[v_x(P_1) - \frac{1}{h_e} \right]^2 + v_z^2(P_1)} \quad (4.56)$$

In practice, the value of dl is chosen ($= h_e/20$ for example) and the equation 4.55 allows to determine the point P_2 and the dissipation power on this segment P_1P_2 as

$$J_{\Delta v_1} = \frac{\sigma_0}{\sqrt{3}} \|\Delta v_1\| dl. \quad (4.57)$$

Similarly from P_2 , we determine the next point P_3 and the dissipation power on the segment P_2P_3 . By repeating this operation until $P_n(x_{P_n}, z_{P_n})$ with $z_{P_n} = 0$ the discontinuity surface and the corresponding dissipation power is completely determined. This approximation requires that dl is chosen small enough depending on the complexity of the discontinuity surface.

$$\begin{cases} J_{\Delta v}^{\Gamma_e} = \frac{\sigma_0}{\sqrt{3}} \sum_{i=1}^{n-1} \|\Delta v_i\| dl \\ \text{with } \|\Delta v_i\| = \sqrt{\left[v_x(P_i) - \frac{1}{h_e} \right]^2 + v_z^2(P_i)} \end{cases} \quad (4.58)$$

4.4.2.b Surface of velocity discontinuity at roll-bite exit

In a general case, the discontinuity surface at the roll-bite exit can also exist and is different from a cross section. If $Q_1(0, h_s) \equiv B$ denotes the last contact point, it is chosen as the first point of Γ_s . And following the same method used to determine Γ_e , we can determine Γ_s with $Q_n(x_{Q_n}, z_{Q_n})$ denoting the last end of Γ_s , $z_{Q_n} = 0$. All calculations are similar.

4.4.2.c Elementary plastic deformation power

As can be seen in the second equation of 4.41, in order to calculate the deformation power $J_{\dot{\epsilon}}(\underline{v})(A_e, A_s)$, it is necessary to compute the $\ddot{\epsilon}(\underline{v})(A_e, A_s)$. The elementary strain rate tensor $\underline{\dot{\epsilon}}(\underline{v})$ corresponding to the elementary velocity $\underline{v}(A_e, A_s, x, z)$ defined by 4.35 and 4.36 can be obtained as follows:

$$\begin{cases} \dot{\epsilon}_{xx}(\underline{v})(x, z) = -\frac{h'}{h^2} + A_e \left[\left(G_e''(x+z) + G_e''(x-z) \right) K_e(x) + \left(G_e'(x+z) + G_e'(x-z) \right) K_e'(x) \right] \\ \quad + A_s \left[\left(G_s''(x+z) + G_s''(x-z) \right) K_s(x) + \left(G_s'(x+z) + G_s'(x-z) \right) K_s'(x) \right] \\ \dot{\epsilon}_{xz}(\underline{v})(x, z) = \frac{1}{2} \left(\frac{h'}{h^2} \right)' z - \left[G_e'(x+z) - G_e'(x-z) \right] K_e'(x) - \frac{1}{2} \left[G_e(x+z) - G_e(x-z) \right] K_e''(x) \\ \quad - \left[G_s'(x+z) - G_s'(x-z) \right] K_s'(x) - \frac{1}{2} \left[G_s(x+z) - G_s(x-z) \right] K_s''(x) \\ \dot{\epsilon}_{zz}(\underline{v})(x, z) = -\dot{\epsilon}_{xx}(\underline{v})(x, z) \\ \ddot{\epsilon}(\underline{v})(x, z) = \frac{2}{\sqrt{3}} \sqrt{\dot{\epsilon}_{xx}^2(\underline{v}) + \dot{\epsilon}_{xz}^2(\underline{v})} \end{cases} \quad (4.59)$$

Plastic deformation zone

In order to compute numerically the plastic deformation power, it is necessary to divide the plastic deformation zone Ω into three zones. The first one, Ω_1 defined between the three surfaces: Γ_e , $z = h(x)$, $x = x_{P_n}$. The Ω_2 is the area limited by: $z = 0$, $z = h(x)$, $x = x_{P_n}$ and $x = x_{Q_n}$. And the last one, Ω_3 is comprised between $x = x_{Q_n}$, $z = h(x)$ and Γ_s . The integral in the expression of $J_{\dot{\epsilon}}(\underline{v})(A_e, A_s)$ is calculated separately in each area.

Integration in Ω_1

At the same time of the determination of each point $P_i(x_{P_i}, z_{P_i})$ and the dissipation by velocity discontinuity on Γ_e (see section 4.4.2.a) the plastic dissipation power can be also calculated as:

$$J_{\dot{\epsilon}}^{\Omega_1}(\underline{v})(A_e, A_s) = \int_{\Omega_1} \sigma_0 \cdot \dot{\tilde{\epsilon}}(\underline{v})(A_e, A_s, x, z) \cdot d\Omega = \sigma_0 \sum_{i=1}^{n-1} dx_i \cdot J_{\dot{\epsilon}}^i(\underline{v})(A_e, A_s)$$

where $J_{\dot{\epsilon}}^i$ is the elementary plastic deformation power in the zone delimited by: $z \in P_i P_{i+1}$, $z = h(x)$, $x = x_i$, $x = x_{i+1}$ (see Figure 4.2). If the coordinates of the element $P_i P_{i+1}$ are given as

$$\begin{cases} x_i^{ele} = \frac{1}{2}(x_i + x_{i+1}) \\ z_i^{ele} = \frac{1}{2}(z_i + z_{i+1}) \end{cases} \quad (4.60)$$

$J_{\dot{\epsilon}}^i$ can be obtained by

$$J_{\dot{\epsilon}}^i(\underline{v})(A_e, A_s) = \int_{z_i^{ele}}^{h(x_i^{ele})} \dot{\tilde{\epsilon}}(\underline{v})(A, x_i^{ele}, z) dz. \quad (4.61)$$

The integral in this equation is done numerically using Gauss integration method presented in the section A. We can find also in the same section the value of weighting factors ω_k and function arguments ζ_k used in Gauss Quadrature Formulas. Reminding that, in a given segment the N-point Gauss integration gives the exact value for any polynomial of $2N-1$ order. However, for an oscillation function having several periods on the integration segment, this approach is no longer accurate. By construction (see the section 4.3), the velocity field is oscillating with a period equal to $2h(x)$. By consequence, the strain rate field $\dot{\tilde{\epsilon}}(\underline{v})$ has also the same oscillation period. In the thickness direction, only a half the strip thickness is studied. As a half of thickness corresponds to a half of oscillation period, the field $\dot{\tilde{\epsilon}}(\underline{v})$ can be accurately approximated by a 5-order polynomial. So in the thickness direction, only one element is sufficient to integrate. In choosing $N = 3$ we have a good compromise of calculation time and precision.

Hence, using Gauss integration operator $IGauss_{1D}^{N=3}$ given by A.12 to approximate the integral of the equation 4.61 we obtain:

$$J_{\dot{\epsilon}}^i(\underline{v})(A_e, A_s) \approx IGauss_{1D}^{N=3}(f_i, z_i^{ele}, h(x_i^{ele}), 1) \\ \text{with } f_i = z \rightarrow \dot{\tilde{\epsilon}}(\underline{v})(A_e, A_s, x_i^{ele}, z)$$

therefore

$$\boxed{J_{\dot{\epsilon}}^{\Omega_1}(\underline{v})(A_e, A_s) \approx \sigma_0 \sum_{i=1}^{n-1} dx_i \cdot IGauss_{1D}^{N=3}(f_i, z_i^{ele}, h(x_i^{ele}), 1) \\ \text{with } f_i = z \rightarrow \dot{\tilde{\epsilon}}(\underline{v})(A_e, A_s, x_i^{ele}, z)} \quad (4.62)$$

where n is the number of point P_i on Γ_e . x_i^{ele} , z_i^{ele} and dx_i are given by 4.60. $IGauss_{1D}^{N=3}$ is the Gauss-Legendre operator approaching 1D integral defined by A.12. $\dot{\tilde{\epsilon}}(\underline{v})$ is calculated thanks to the equations 4.59.

Integration in Ω_3

This is done similarly as the integration in Ω_1 .

Integration in Ω_2

By developing the 2D integral in Ω_2 of the elementary plastic deformation power into a double integral, we obtain:

$$J_{\dot{\epsilon}}^{\Omega_2}(\underline{v})(A_e, A_s) = \int_{\Omega_2} \sigma_0 \cdot \dot{\tilde{\epsilon}}(\underline{v})(A_e, A_s, x, z) \cdot d\Omega \\ = \sigma_0 \int_{x_{P_n}}^{x_{Q_n}} \int_0^{h(x)} \dot{\tilde{\epsilon}}(\underline{v})(A_e, A_s, x, z) \cdot dz dx. \quad (4.63)$$

These integrals are equally done numerically Gauss-Legendre integration. Similarly as in Ω_1 , for the integral though the thickness, only one element is enough. But in the longitudinal direction, we need to divide the segment $[x_{P_n}, x_{Q_n}]$ into a certain number of elements n_x^{ele} so that the size of each element is less than a half of period, $h(x)$. This number is chosen as $n_x^{ele} = \text{trunc}\left(\frac{L}{h_s}\right)$. The size of each element is then

$$\Delta x = \frac{x_{Q_n} - x_{P_n}}{n_{ele}}$$

The i_{th} is between two nodes $x_{i-1}^{node} = x_{P_n} + (i-1)\Delta x$ and $x_i^{node} = x_{P_n} + i\Delta x$. Thus:

$$\boxed{J_{\check{e}}^{\Omega_2}(\varrho)(A_e, A_s) \approx \sigma_0 \cdot IGauss_{2D}^{N=3}(f_2, x_n^{\Gamma_e}, 0, 0, h(\cdot), n_x^{ele}, 1)} \quad (4.64)$$

with $f_2 := (x, z) \rightarrow \check{e}(\varrho)(A_e, A_s, x, z)$

where $IGauss_{2D}^{N=3}$ is the Gauss-Legendre operator approaching 2D integral defined by A.15 and $\check{e}(\varrho)(A_e, A_s, x, z)$ given by the equations 4.59.

4.4.2.d Elementary friction dissipation power

Both friction power $J_{fric}^{V_c}(x_n)$ given by 4.46 and $J_{fric}^{\varrho}(A_e, A_s, x_n)$ given by 4.47 are necessary to be calculated. With the elementary velocity given by 4.35 and 4.36, the two integrals are already explicit enough. Noting n_{ele}^b and n_{ele}^a are the number of elements before and after the neutral point. Similarly as above we chose:

$$n_{ele}^b = \text{trunc}\left(\frac{x_n + L}{h_s}\right) \quad \text{and} \quad n_{ele}^a = \text{trunc}\left(\frac{-x_n}{h_s}\right)$$

so that the elements are smaller than a half of oscillation period. The sizes of elements before and after the neutral point are then given by:

$$\Delta x^b = \frac{x_n - x_e}{n_{ele}^b} \quad \text{and} \quad \Delta x^a = \frac{-x_n}{n_{ele}^a}$$

Using Gauss-Legendre integration method, we have:

$$\boxed{J_{fric}^{V_c}(x_n) \approx \frac{\overline{m} \cdot \sigma_0}{\sqrt{3}} V_c \left[IGauss_{1D}^{N=3}(f_c, -L, x_n, n_{ele}^b) - IGauss_{1D}^{N=3}(f_c, x_n, 0, n_{ele}^a) \right]} \quad (4.65)$$

with $f_c = x \rightarrow \sqrt{1 + h'^2(x)}$

And similarly:

$$\boxed{J_{fric}^{\varrho}(A_e, A_s, x_n) \approx \frac{\overline{m} \cdot \sigma_0}{\sqrt{3}} \cdot \left[-IGauss_{1D}^{N=3}(f_{v_x}, -L, x_n, n_{ele}^b) + IGauss_{1D}^{N=3}(f_{v_x}, x_n, 0, n_{ele}^a) \right]} \quad (4.66)$$

with $f_{v_x} = x \rightarrow v_x(A_e, A_s, x, h(x)) \left(1 + h'^2(x)\right)$

4.4.2.e Elementary tensions power

The elementary tensions power is explicitly given by the second equation of 4.43.

4.5 Comparison with *Lam3-Tec3* and other *UBM* models

This session is a comparison of *UBM* results obtained with three velocity fields: untriangular one, elliptical (or simple) one and oscillating - the new one and the Finite Elements Method *Lam3-Tec3*. The *Lam3-Tec3* is a software developed by ArcelorMittal Group and several partners. *Lam3-Tec3* is able to give the solution (strain and stress fields) at stationary state and the final mesh gives the material flow lines.

For this comparison, three rolling conditions corresponding to roughing mill, finishing and cold rolling mill are considered (see details in Table 4.1).

Case	Mill	$2h_e$ mm	$2h_s$ mm	red %	$2R$ mm	T_e Mpa	T_s Mpa	σ_0 Mpa	m	V_c m/s
1	Hot roughing	126.4	79.0	37.5	1043.0	0.0	0.0	76.000	0.6000	1.73138
2	Hot finishing 1st stand	36.0	24.0	33.3	680.00	0.0	5.0	150.000	0.3000	1.50000
3	Cold tandem 1st stand	2.8	1.7	40.3	538.65	51.0	150.0	516.619	0.0974	6.45600

Table 4.1: Rolling cases for comparison of *UBM* models and *Lam3-Tec3*.

4.5.1 Power and neutral point

Dependence of x_n^1 and J_1 on A_e and A_s

As discussed previously, the equations 4.52 implies that the optimization of $J_1(A_e, A_s)$ and $x_n^1(A_e, A_s)$ with respect to A_e, A_s are obtained at a same value of A_e, A_s . Indeed, this remark is confirmed for the case of roughing mill (case 1, Table 4.1) by Figure 4.5 showing the dependence of x_n^1 , solution of 4.50 and J_1 given by 4.51 as a functions of A_e when $A_s = 0$. It can be seen also in Figure 4.4 illustrating the variation of x_n^1 and J_1 as a functions of A_s for $A_e = 0$ that the functions are optimum at the same value of A_s . The same conclusion is observed with the finishing condition (Figures 4.5 and 4.6) and cold rolling condition (Figures 4.7 and 4.8).

Furthermore, these graphics show also that the minimum values of x_n^1 and J_1 are reached at A_e and A_s which are different from 0, i.e different from the simple (elliptical) velocity field solution. By comparing the two graphics of each rolling case (the graphics are not at a same scale), it can be seen that the optimum neutral position x_n^1 as well as the optimum power J_1 obtained by varying A_e are lower than that obtained by varying A_s . That means, the oscillation part from the entry side contributes more efficiently to the reduction of power.

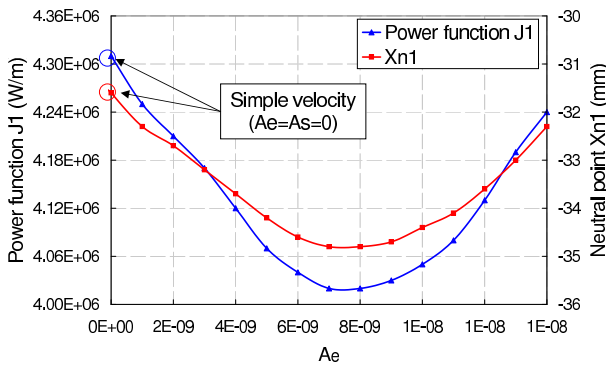


Figure 4.3: Roughing Mill condition (case 1, Table 4.1). The dependence of x_n^1 and J_1 as functions of A_e when $A_s = 0$.

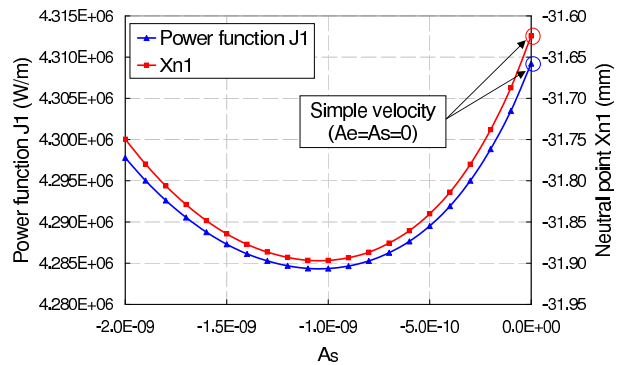


Figure 4.4: Roughing Mill condition (case 1, Table 4.1). The dependence of x_n^1 and J_1 as functions of A_s when $A_e = 0$.

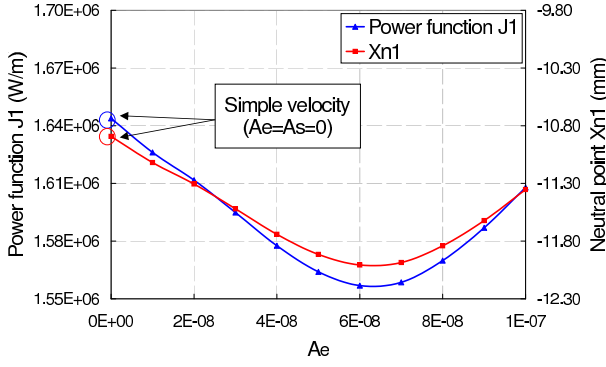


Figure 4.5: Finishing Mill 1st stand condition (case 2, Table 4.1). The dependence of x_n^1 and J_1 as functions of A_e when $A_s = 0$.

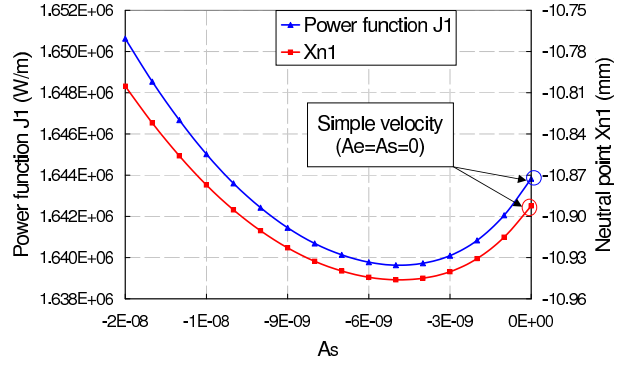


Figure 4.6: Finishing Mill 1st stand condition (case 2, Table 4.1). The dependence of x_n^1 and J_1 as functions of A_s when $A_e = 0$.

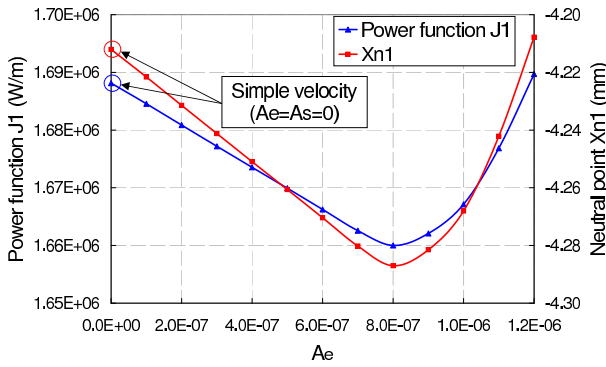


Figure 4.7: Cold Mill 1st stand condition (case 3, Table 4.1). The dependence of x_n^1 and J_1 as functions of A_e when $A_s = 0$.

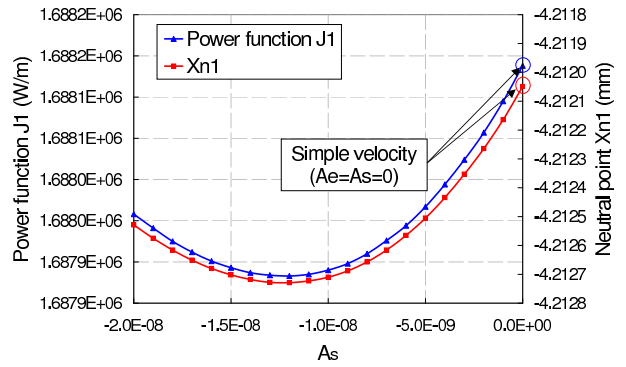


Figure 4.8: Cold Mill 1st stand condition (case 3, Table 4.1). The dependence of x_n^1 and J_1 as functions of A_s when $A_e = 0$.

Comparison of optimum power to other models

The function $J_1(A_e, A_s)$ as well as $x_n^1(A_e, A_s)$ are both convex in both directions (see the graphics above). The optimum values of A_e and A_s are obtained by 2D Newton-Raphson algorithm without difficulty. The obtained results are given in Tables 4.2, 4.3 and 4.4. The roll torque is evaluated by

$$T = \frac{J.R}{V_c} \tag{4.67}$$

About the unitriangular velocity, the optimum power is quit interesting in the case 1 - roughing mill condition. It is lower than the that of simple velocity. But in the case 2 - hot finishing mill and case 3 - cold rolling mill, it is much higher than the power given by the simple and oscillating velocity fields. In these cases, the multitriangular model should give significantly better results.

In all the three cases, the oscillating velocity field gives a lower upper bound estimation of rolling power J , torque T and neutral position x_n than the simple (elliptical) one. These new estimations are much closer to Lam3-Tec3 results. The three results tables shows that the improvement is mainly thanks to a decrease of plastic deformation power J_{def} and secondarily to friction one J_{fric} .

4.5.2 Plastic area - discontinuity surfaces

Unlike the case of simple (elliptical) velocity field, with the oscillating velocity field the entry and exit discontinuity surfaces Γ_e and Γ_s are not prefixed but they are outputs of the UBM model. The obtained results corresponding to the

Case 1 Hot roughing	xn mm	fs %	Torque kNm/m	$J_{\dot{\epsilon}}$ kw/m	$J_{\Delta u}^e$ kw/m	$J_{\Delta u}^s$ kw/m	J_{def} kw/m	J_{ten} kw/m	J_{fric} kw/m	J kw/m	Re-Diff %
Unitriangular		16.68	1229	0	2987	1095	4082	0	0	4082	24.00
Simple	-31.62	2.241	1298	2934	479	0	3413	0	896	4309	18.35
Oscillating											
$A_e=8.172e-9$	-35.10	2.976	1202	2642	562	56	3259	0	733	3992	12.19
$A_s=-8.6e-10$											
<i>Lam3-Tec3</i>		8.429	1168				3494	0	383	3876.5	14.24

Table 4.2: Case 1 - Roughing Mill. Comparison of the obtained powers of *UBM* using different velocity fields: unitriangular, simple (elliptical) and oscillating with *Lam3-Tec3*.

Case 2 Hot finishing	xn mm	fs %	Torque kNm/m	$J_{\dot{\epsilon}}$ kw/m	$J_{\Delta u}^e$ kw/m	$J_{\Delta u}^s$ kw/m	J_{def} kw/m	J_{ten} kw/m	J_{fric} kw/m	J kw/m	Re-Diff %
Unitriangular		14.3	435.0	0.0	1372	645	2022.1	102.9	0.0	1919.2	39.9
Simple	-10.89	1.40	372.6	1295.4	150.5	0.0	1445.9	91.3	289.2	1643.8	12.8
Oscillating											
$A_e=6.320e-8$	-12.07	1.80	351.8	1252.3	114.4	11.6	1378.3	91.6	265.4	1552.1	7.1
$A_s=-4.927e-9$											
<i>Lam3-Tec3</i>	-12.30	4.62	340.3				1378.0	94.2	217.5	1501.3	4.2

Table 4.3: Case 2 - Finishing Mill. Comparison of the obtained powers of *UBM* using different velocity fields: unitriangular, simple (elliptical) and oscillating with *Lam3-Tec3*.

Case 3 Cold rolling	xn mm	fs %	Torque kNm/m	$J_{\dot{\epsilon}}$ kw/m	$J_{\Delta u}^e$ kw/m	$J_{\Delta u}^s$ kw/m	J_{def} kw/m	J_{ten} kw/m	J_{fric} kw/m	J kw/m	Re-Diff %
Unitriangular		17.1	310	0	5163	2898	8061.0	626.1	0.0	7434.9	314.9
Simple	-4.212	3.93	70.4	1726.0	54.2	0.0	1780.3	555.6	463.5	1688.1	3.2
Oscillating											
$A_e=8.06e-7$	-4.287	4.03	69.2	1723.3	31.5	0.4	1755.1	556.2	460.9	1659.9	1.7
$A_s=-8.41e-9$											
<i>Lam3-Tec3</i>	-4.325	4.50	68.2				1745.0	558.7	447.4	1633.7	0.6

Table 4.4: Case 3 - Cold rolling. Comparison of the obtained powers of *UBM* using different velocity fields: unitriangular, simple (elliptical) and oscillating with *Lam3-Tec3*.

three cases of Table 4.1 are given in Figure 4.10, 4.12 and 4.14. We can see that, at the entry side the first contact point A is deformed at first then the plastic deformation advances progressively to the strip center. Inversely at the exit side, the strip center stops being deformed at first and the contact surface (point B) is the last plastically deformed point. The *Lam3-Tec3* results given in Figures 4.9, 4.11 and 4.13 confirm also this remark.

By consequence, the discontinuity surfaces are no longer vertical planes but curved ones resulting to a smaller plastic deformation domain Ω . This, in addition to that fact that the oscillating velocity requires less deformation power in comparison with the simple one on a same integration domain, allows to decrease the plastic deformation power.

4.5.3 Velocity isovalue surfaces

By construction of the *UBM* velocity field, the discontinuity surfaces Γ_e and Γ_s are equally the limits between the non-deformation and plastic deformation zones. As for *Lam3-Tec3*, the velocity discontinuity surfaces do not really exist because the velocity field is continuous. The comparison of discontinuity surface between *UBM* and *Lam3-Tec3* is not simple. However, this velocity field of *Lam3-Tec3* varies strongly through small zones at the entry and exit of the roll-bite. Hence, that should be interesting to compare the isovalue surfaces of the velocity field which are the isovalue



Figure 4.9: Case 1 - Hot roughing mill. Plastic deformation area by *Lam3-Tec3*.

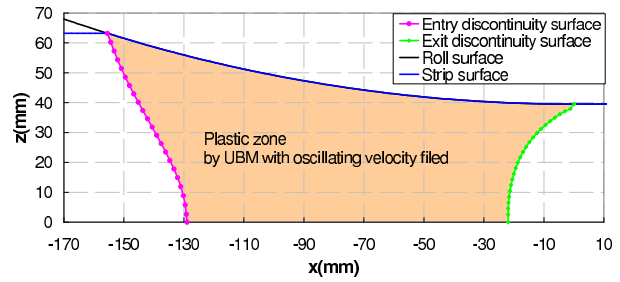


Figure 4.10: Case 1 - Hot roughing mill. Discontinuity surfaces Γ_e and Γ_s obtained by the *UBM* with oscillation velocity field.



Figure 4.11: Case 2 - Hot finishing first stand. Plastic deformation area by *Lam3-Tec3*.

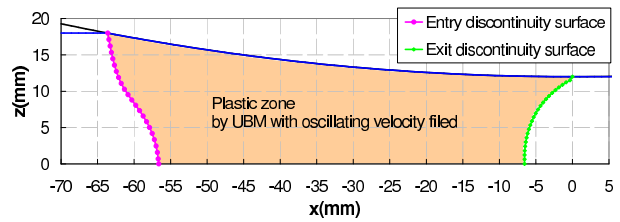


Figure 4.12: Case 2 - Hot finishing first stand. Discontinuity surfaces Γ_e and Γ_s obtained by the *UBM* with oscillation velocity field.



Figure 4.13: Case 3 - Cold rolling first stand. Plastic deformation area by *Lam3-Tec3*.

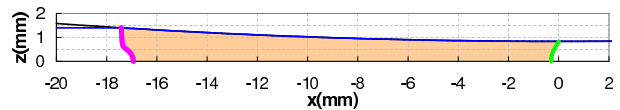


Figure 4.14: Case 3 - Cold rolling first stand. Discontinuity surfaces Γ_e and Γ_s obtained by the *UBM* with oscillation velocity field.

curves in 2D modeling.

To do this comparison, the isovalue cartography is, at first obtained with "GLview" a post-treatment software allowing to visualize the results of *Lam3-Tec3*. Figures 4.15, 4.17 and 4.19 show the *Lam3-Tec3* results of longitudinal velocity u_x for the 3 rolling cases. The limits between two successive zones are the isovalue curves of u_x . Then, using the same value of ratio u_x/V_e we build the isovalue curves of u_x with *UBM* results (Figures 4.16, 4.18 and 4.20).

If the hypothesis "a cross section will stay a cross section" of the simple velocity field is assumed, the isovalue curves of u_x are the straight vertical lines. Nevertheless, the results of *Lam3-Tec3* as well as of *UBM* show that the isocurve are very different from a straight vertical lines. And the *UBM* results are relatively closed results to that of *Lam3-Tec3*.

4.5.4 Oscillation of velocity field along the streamlines

4.5.4.a Streamlines

Existing methods for constructing velocity field as [31]... usually based on a the given stream lines. For example, by assuming that the flow lines are circular or elliptical, that the velocity fields will be determined. By this way, these methods introduce also quite important constraints to the velocity fields because it is very difficult to imagine a very

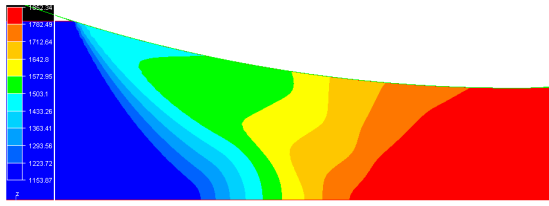


Figure 4.15: Case 1 - Hot roughing mill. From the left to the right hand side, the 9 isovalue curves (limits between 2 successive colors) obtained by *Lam3-Tec3* correspond to the ratio $u_x/V_e =$: 1.0464, 1.1062, 1.1659, 1.2256, 1.2854, 1.3451, 1.4048, 1.4645, 1.5243

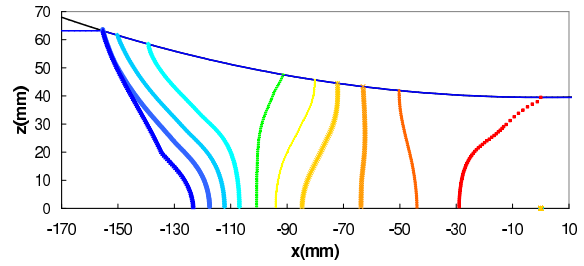


Figure 4.16: Case 1 - Hot roughing mill. From the left to the right hand side, the 9 isovalue curves obtained by *UBM* correspond to the same ratio u_x/V_e and the last curve (in red) correspond to $u_x = 1.5840V_e = 0.9967V_s$.

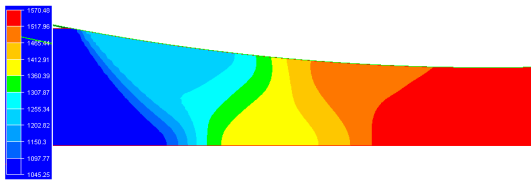


Figure 4.17: Case 2 - Hot finishing first stand. From the left to the right hand side, the 9 isovalue curves obtained by *Lam3-Tec3* correspond to the ratio $u_x/V_e =$: 1.0507, 1.1010, 1.1513, 1.2015, 1.2518, 1.3021, 1.3523, 1.4026, 1.4529

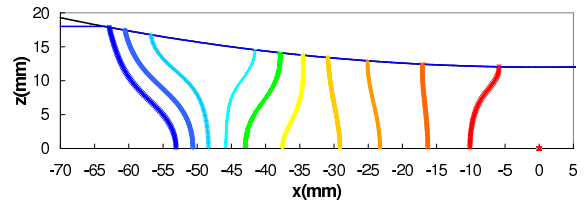


Figure 4.18: Case 2 - Hot finishing first stand. From the left to the right hand side, the 9 isovalue curves obtained by *UBM* correspond to the same ratio u_x/V_e . In addition, the last curve corresponds to $u_x = 1.4874V_e = 0.99V_s$.

good and complete flow lines. For this reason, until today, except circular and elliptical flow lines, there does not exist any other imagined flow lines pattern to approach rolling process.

The method that we introduce in this chapter discards this constrain. Contrarily to previous methods, the form of the flow lines are not pre-assumed but complete results of the model. In order to simplify the comparison with *Lam3-Tec3* where the number of elements in the half thickness is equal to 19, the *UBM* results will be analyzed at the equivalent streamlines meaning 20 streamlines from the symmetry line ($z = 0$) to the strip surface ($z = h(x)$).

Figure 4.21 shows the streamlines obtained by the *UBM* with the velocity corresponding to the optimum value of x_n and A_e, A_s for the case 3 - cold rolling first stand. The streamlines are named from 1 (the symmetry line $z = 0$) to 20 (the strip surface $z = h(x)$). Before the roll-bite, these streamlines line are equidistant with a distance of $h_e/19$. It can be seen the streamlines oscillate slightly throughout the plastic deformation zone, especially at the beginning of the roll-bite while before and after the roll-bite they are straight and equidistant. Figure 4.22 illustrates that the streamlines obtained by *UBM* and *Lam3-Tec3* are very closed.

For the case 1 (roughing mill) and 2 (finishing mil), the streamlines are not showed here but the numeration of the streamlines is the same as showed in Figure 4.21 for the case 3. In this session, we will study the behavior of the velocity field along each streamline.

4.5.4.b Oscillation of longitudinal velocity

It should be reminded that the new velocity field is the sum of the classic part (simple velocity) and the oscillating part (see the expression of velocity field given by 4.10). Figures 4.23, 4.25 and 4.27 show the optimum velocity field obtained by *UBM* along the stream lines 1, 5, 10, 15 and 20 for the three rolling cases. In all the cases, at the entry of the roll-bite, the stream line 20 (in contact surface) is the first that starts to increase its velocity, meaning it is deformed



Figure 4.19: Case 3 - Cold rolling first stand. From the left to the right hand side, the 9 isovalue curves obtained by *Lam3-Tec3* correspond to the ratio $u_x/V_e =$: 1.0983, 1.1679, 1.2375, 1.3070, 1.3766, 1.4462, 1.5157, 1.5853, 1.6549.

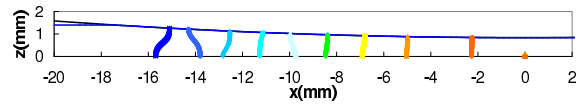


Figure 4.20: Case 3 - Cold rolling first stand. From the left to the right hand side, the 9 isovalue curves obtained by *UBM* correspond to the same ratio u_x/V_e .

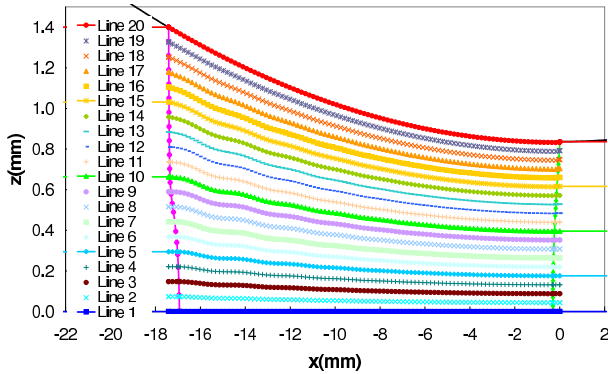


Figure 4.21: Case 3 - Cold rolling first stand. Streamlines obtained by the *UBM* with oscillating velocity.

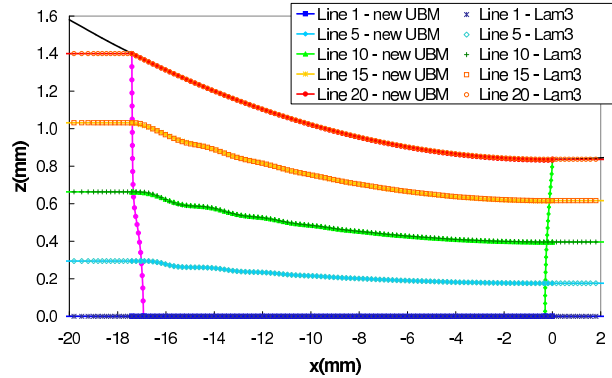


Figure 4.22: Case 3 - Cold rolling first stand. Comparison of streamlines between *UBM* and *Lam3-Tec3*.

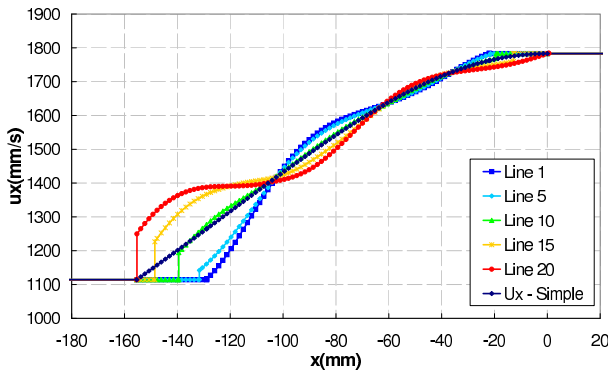


Figure 4.23: Case 1 - Hot roughing mill. Longitudinal velocity obtained by *UBM*.

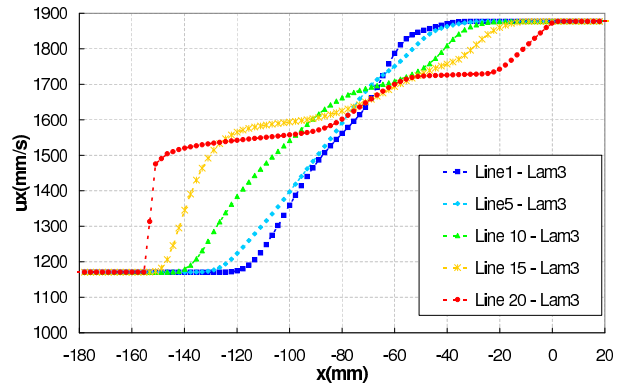


Figure 4.24: Case 1 - Hot roughing mill. Longitudinal velocity obtained by *Lam3-Tec3*.

first, and progressively the line 15, 10 ... and the line 1 at the center of the strip is deformed last. In this area the velocity of line 1 increases more and more slowly while the longitudinal velocity of other lines increases more and more quickly. And after about a half entry thickness the tendency is inverted, the line 1 is the fastest and the line 20 is the slowest. This longitudinal velocity field along a stream line oscillates around the classic part which is the same for all stream lines. The period is similar to the thickness which varies from h_e at the entry to h_s at the exit of the roll bite. The amplitude of this oscillation decreases along the roll bite.

Figures 4.24, 4.26 and 4.28 show the longitudinal velocity obtained by *Lam3-Tec3*. While in the case 3, *Lam3-Tec3* and *UBM* give a very similar forward slip (see Table 4.4), the forward slip obtained by *Lam3-Tec3* in the case 1 and 2 is higher than that obtained by *UBM* (see Tables 4.2 and 4.3). That means the entry and exit velocities are also higher which can be seen by comparing Figure 4.23 to 4.24 and 4.25 to 4.26. Nevertheless, it can be seen in these figures that the velocity fields obtained by *Lam3-Tec3* oscillate with a same periodicity as those obtained by *UBM*. Even though

4. Oscillation of mechanical fields in roll bite

4.5 Comparison with Lam3-Tec3 and other UBM models

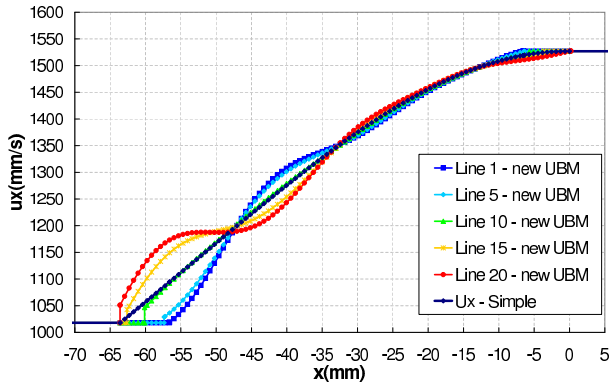


Figure 4.25: Case 2 - Hot finishing first stand. Longitudinal velocity obtained by UBM .

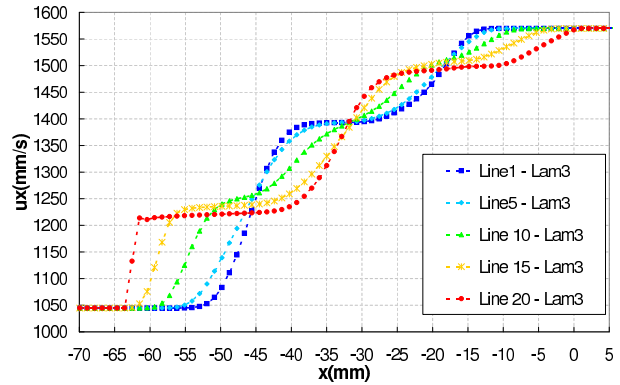


Figure 4.26: Case 2 - Hot finishing first stand. Longitudinal velocity obtained with Lam3-Tec3 .

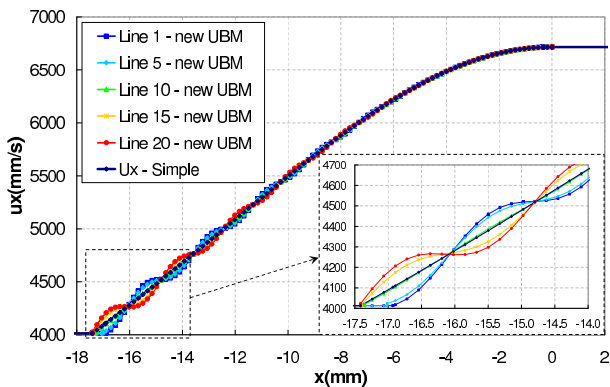


Figure 4.27: Case 3 - Cold rolling first stand. Longitudinal velocity obtained by UBM .

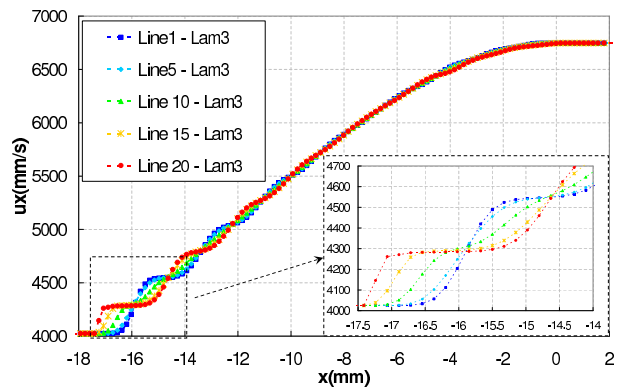


Figure 4.28: Case 3 - Cold rolling first stand. Longitudinal velocity obtained by Lam3-Tec3 .

the amplitude of oscillation by Lam3-Tec3 is higher but the order of velocity value of the streamlines is the same (from the fastest one to the slowest one).

4.5.4.c Oscillation of vertical velocity

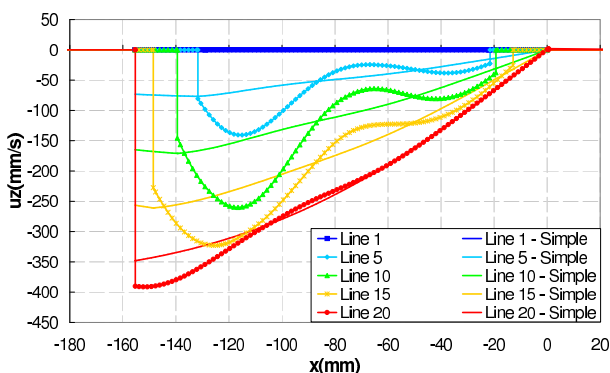


Figure 4.29: Case 1 - Hot roughing mill. Vertical velocity obtained by UBM and its simple part.

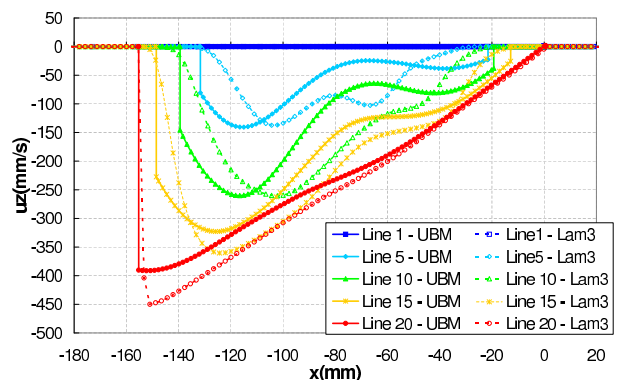


Figure 4.30: Case 1 - Hot roughing mill. Comparison of vertical velocity between UBM and Lam3-Tec3 .

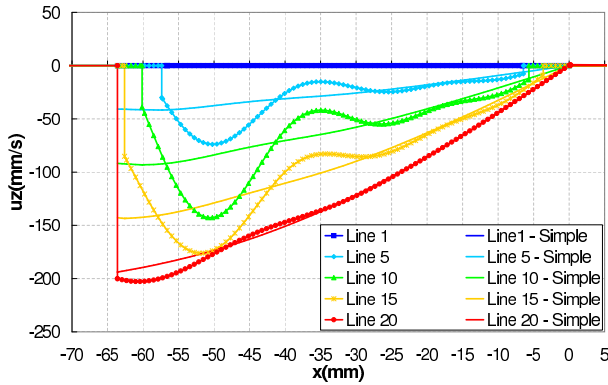


Figure 4.31: Case 2 - Hot finishing first stand. Vertical velocity obtained by *UBM* and its simple part.

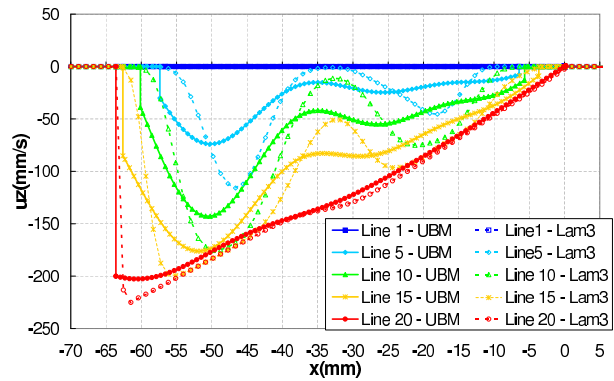


Figure 4.32: Case 2 - Hot finishing first stand. Comparison of vertical velocity between *UBM* and *Lam3-Tec3*.

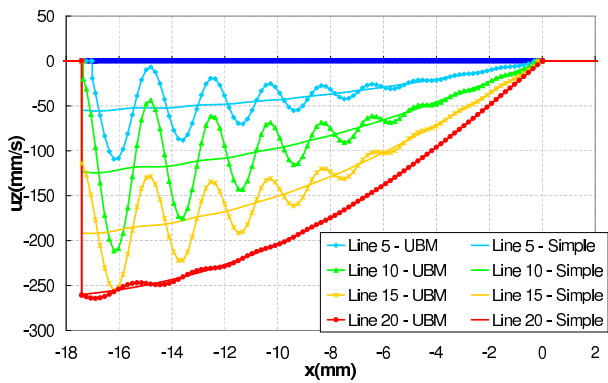


Figure 4.33: Case 3 - Cold rolling first stand. Vertical velocity obtained by *UBM* and its simple part.

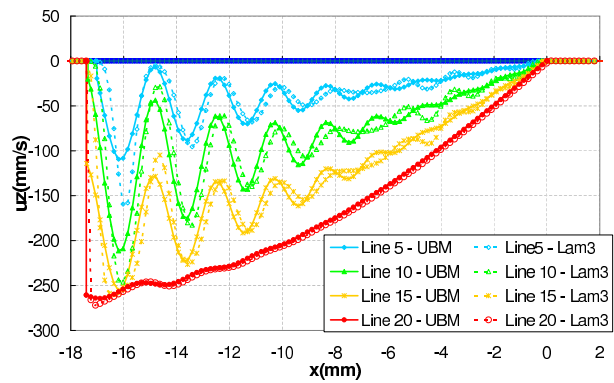


Figure 4.34: Case 3 - Cold rolling first stand. Comparison of vertical velocity between *UBM* and *Lam3-Tec3*.

Figures 4.29, 4.31 and 4.33 show the vertical velocity field as well as its simple part obtained by *UBM* along the stream lines 1, 5, 10, 15 and 20 for the three studied rolling cases. Obviously, along the center, line 1 the vertical velocity is equal to 0 and there is no oscillation of vertical velocity. As for the contact surface, line 20, the oscillation is relatively small. Merely along the other streamlines the vertical velocity field oscillate around the simple part and the oscillation can be very important. These oscillations have same period equal to the strip thickness $2h(x)$ as that of the longitudinal velocity and their amplitude decreases also from the entry to the exit.

It can be seen in Figures 4.30, 4.32 and 4.34 that like the longitudinal velocity, the *UBM* vertical velocity field is quite closed even if the oscillation amplitude is less important than the *Lam3-Tec3* result.

4.6 Conclusions and perspectives

4.6.1 Conclusions

The present chapter introduces a new approach of the velocity fields in the roll-bite and gives a high understanding about a particular phenomenon: the velocity oscillates spatially in both thickness and longitudinal directions. We presented a new optimization strategy that consists in obtaining an equation determining the optimum neutral point. This result allows to improve the numerical algorithm as well as the calculation time. The *UBM* using the new proposed velocity family results to an optimum velocity that oscillates spatially throughout the roll-bite with a pseudo-period equal

to the local strip thickness $h(x)$. This obtained oscillating velocity field matches very well the *Lam3-Tec3* results and improves the upper bound of rolling power and torque in comparison with the simple (elliptical) velocity field. This velocity field has characteristics of both elliptical (continuous) and multitriangular (rigid movements) velocity fields.

4.6.2 Perspectives

Polynomial velocity family

As explained previously, the oscillation velocity allows to reduce mainly the deformation power. Consider now the family $F(x, z) = \sum g_i(x) \cdot z^i \forall i \neq 2$ that is introduced in the section 4.2.2. This family would allow to model the heterogeneity of mechanical fields across the thickness. But unlike the oscillating one, it allows especially to have higher strip speed on the contact before the neutral point and lower strip speed on the contact after and this fact would help to reduce the differential velocity between the strip and the work-roll and reduce therefore the friction power. The numerical calculation presented in this chapter enables the study by *UBM* with this polynomial velocity field family.

As can be remarked from the results showed in Table 4.2, 4.3 and 4.4, the oscillating velocity field gives very closed deformation power to *Lam3-Tec3* one while the friction power is significantly higher. Hence, studying this polynomial velocity field may be interesting.

Perturbation of velocity field around the neutral point

By definition, the neutral point is the point where the contact shear stress (friction stress) is discontinuous (positive before and negative after). This discontinuity of friction creates a discontinuity of the shear stress σ_{xz} meaning that for the material with Mises's behavior without viscosity effect (given by 3.13), the $\dot{\epsilon}_{xz}$ is also discontinuous. All the previous continuous velocity fields (eccentric, simple-elliptical and oscillating) are not able to take into account this phenomenon. In order to model that, it is necessary to separate the roll-bite into two areas with a discontinuity surface at the neutral point. Furthermore, as the neutral point is not known and needs determining, it is necessary to build a velocity field depending explicitly on the neutral point. Meaning that the neutral point is not only involved in the velocity field via the flow rate as 4.39 but the elementary velocity field depends also on the x_n .

Moreover, we can observe that the *UBM* under-estimates the forward slip in comparison with *Lam3-Tec3* for all the three rolling cases while neutral point obtained by *UBM* is quite closed to *Lam3-Tec3*. Inversely, the unitriangular over-estimate it. This fact is not a random and can be explained by the existing of a neutral zone - sticking area (but not a point). With much more freedom degree the velocity of *Lam3-Tec3* can approach the actual one even around the neutral point and is able to model well the neutral zone. The rigid motion model such as multitriangular one is able to model the neutral zone. The triangular that corresponds to the neutral zone rotates around the work-roll center with the same angular velocity. For this reason, the longitudinal velocity increases from the surface contact $z = h(x_n)$ to the strip center $z = 0$. While continuous velocity fields studied until our days (eccentricity, simple-elliptical, circular or oscillating ones) have flow patterns (elementary part) that do not depend on the neutral point. Meaning that, at the neutral point, the distribution of longitudinal velocity across the strip thickness can be different from that described above for neutral zone. That is why these models under-estimate very often the flow rate through the cross section at the neutral point.

The oscillating velocity with advantage of low deformation power and the multitriangular with advantage of neutral zone modeling can be combined together to create the new one. The idea is to model the neutral zone as a rigid curvilinear triangular with a base denoted N_1N_2 on the surface of the roll and with an apex P on the plane of symmetry as shown in Figure 4.35. This triangular rotates around the work-roll center with a same angular velocity. Before this neutral zone the velocity is the oscillating one given by 4.10 with

$$F(x, z) = A_e [G_e(x + z) - G_e(x - z)] K_e(x).$$

And after the neutral zone with

$$F(x, z) = A_s [G_s(x + z) - G_s(x - z)] K_s(x).$$

Finally, this model needs equally only three parameters A_e, A_s and x_P position of the neutral triangular apex. The curves PN_1 and PN_2 are two surfaces of velocity discontinuity that could be determined by the same method for determination of entry and exit discontinuity surfaces Γ_e and Γ_s (see 4.4.2.a).

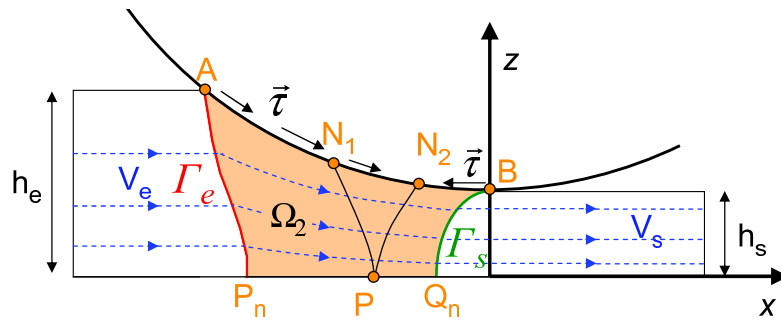


Figure 4.35: Proposition of combining model: oscillating velocity with neutral rigid triangular.

Chapter 5

Rigid-plastic *UBM* model for width spread

The first two sections of this chapter show a relatively wide study of existing models for width spread. Important effort began in the area of the 1960's in developing empirical formula to predict the spread. The most popular ones are [115, 104, 43, 14]. Later, several 3D analyses using FEM for flat and shape rolling [77, 78, 54] where the shape and the spread are predicted. Montmitonnet [76] gives even a complete thermomechanical solution. However, as the FEM is well-known to be high time-consuming, the UBM is more commonly used thanks to its simplicity and rapidity. Some typical UBM models [59, 99] with interesting velocity fields are then presented. The third section is an analysis of 3D kinematically admissible velocity fields suitable to the flat thin strip rolling that is followed by an UBM analysis. A parametric study brings out the impact of rolling parameters on the width spread of the strip. And the UBM results show a very good agreement in comparison with the experiments performed at ArcelorMittal (AM).

Contents

5.1 Statistical models for width spread	98
5.1.1 Typical empirical formulae	98
5.1.2 Domain of validity - unsuitable for cold rolling	99
5.2 3D rigid-plastic UBM for width variation analysis	99
5.2.1 Advantage of UBM in comparison to FEM and empirical models	99
5.2.2 Difference between 2D and 3D UBM	100
5.2.3 UBM with 3D "simple" velocity field [83]	100
5.2.4 UBM with combination of basic velocity fields by Komori [59]	101
5.2.5 UBM with 3D polynomial velocity field [99]	103
5.3 Chosen rigid-plastic model of width variation in rolling	105
5.3.1 UBM is chosen	105
5.3.2 Assumptions of the model	105
5.3.3 Choice of velocity	107
5.3.4 Computation of power function	109
5.3.5 Numerical resolution	111
5.3.6 Comparison with ArcelorMittal trials on the pilot rolling mill	114
5.3.7 Parametric study for using UBM model	114
5.4 Conclusions and perspectives	117

5.1 Statistical models for width spread

5.1.1 Typical empirical formulae

Although many studies on rolling problem allowing to estimate roll force and torque have been carried out, the width variation problem had remained for a very long time rebellious. Considerable effort began in the area of the 1960's. During that period emphasis was placed on developing empirical formula to predict the net spread. The most popular authors of these formulae are Wusatowski [115], Hill, Sparling [104] and Helmi & Alexander [43] and Beese [14].

Table 5.1 gives some typical empirical formulae giving the width spread factor S defined by

$$S = \frac{\ln\left(\frac{w_s}{w_e}\right)}{\ln\left(\frac{h_e}{h_s}\right)} \tag{5.1}$$

as a function of geometrical parameters ratios determining the rolling conditions.

Authors	Using $\frac{w_e}{L}, \frac{w_e}{h_e}, r$	Using $\frac{w_e}{R}, \frac{w_e}{h_e}, r$
Siebel [101]	$-0.35 \left(\frac{2w_e}{L}\right)^{-1} \frac{r}{\ln(1-r)}$	$-0.35 \left(\frac{w_e}{h_e}\right)^{-1} \left(\frac{2h_e}{R}\right)^{-0.5} \frac{r^{1.5}}{\ln(1-r)}$
Hill ¹ (1950)	$\frac{1}{2} \exp\left[-\frac{1}{2\sqrt{2}} \frac{2w_e}{L}\right]$	$\frac{1}{2} \exp\left[-\frac{1}{2\sqrt{2}} \left(\frac{w_e}{h_e}\right) \left(\frac{2h_e}{R}\right)^{0.5} r^{-0.5}\right]$
Wusatowski [115]	$\exp\left[-1.9872 \left(\frac{2w_e}{L}\right)^{-1.12} \left(\frac{w_e}{h_e}\right)^{0.12} r^{0.56}\right]$	$\exp\left[-1.9872 \left(\frac{w_e}{h_e}\right) \left(\frac{2h_e}{R}\right)^{0.56}\right]$
Sparling [104]	$0.981 \exp\left[-1.615 \left(\frac{2w_e}{L}\right)^{1.1} \left(\frac{w_e}{h_e}\right)^{-0.2} r^{0.3}\right]$	$0.981 \exp\left[-1.615 \left(\frac{w_e}{h_e}\right)^{0.9} \left(\frac{2h_e}{R}\right)^{0.55} r^{-0.25}\right]$
Helmi[43]	$0.95 \left(\frac{w_e}{h_e}\right)^{-1.1} \exp\left[-\frac{1}{\sqrt{2}} \left(\frac{2w_e}{L}\right) \left(\frac{w_e}{h_e}\right)^{-0.971}\right]$	$0.95 \left(\frac{w_e}{h_e}\right)^{-1.1} \exp\left[-\frac{1}{\sqrt{2}} \left(\frac{w_e}{h_e}\right)^{0.029} \left(\frac{2h_e}{R}\right)^{0.5} r^{-0.5}\right]$
Beese [14]	$0.61 \left(\frac{w_e}{h_e}\right)^{-1.27} \exp\left(-0.38 \frac{2h_e}{L}\right)$	$0.61 \left(\frac{w_e}{h_e}\right)^{-1.27} \exp\left[-0.38 \left(\frac{2h_e}{R}\right)^{0.5} r^{-0.5}\right]$

Table 5.1: Some typical empirical formulas giving the width variation factor S . *It is important to note that the authors use, in their original formulae, total initial width w_1 , total initial thickness h_1 while in the present thesis we use half of initial width w_e and half of initial thickness h_e . That is why these formulae seem to be different from the original ones.*

Effect of the thickness reduction ratio An increase of the thickness reduction ratio r (in keeping a constant entry thickness h_e) leads to a longer contact length. Therefore the resistance to elongation in the longitudinal direction will be increased and the metal will be forced to spread more effectively in the lateral direction. This tendency is well confirmed by Siebel formula, Sparling formula, Hill formula, Helmi & Alexander formula and Beese formula. As can be deduced directly from the formulae shown in Table 5.1, they predict a strong, much more than linear, dependence of width spread coefficient on the reduction. The exception to this trend is the Wusatowski formula that predicts a constant width spread coefficient when the relative reduction r increases.

The absolute spread can be deduced from 5.1 as

$$\Delta w = w_e \left[\left(\frac{h_e}{h_s}\right)^S - 1 \right]. \tag{5.2}$$

This equation implies that the absolute spread Δw depends in a similar manner as the spread coefficient S on the thickness reduction ratio.

Effect of slab initial width All empirical models predict a steep decrease of the width spread coefficient with an increase in the slab initial width. This means that the ratio of the transverse elongation to longitudinal one becomes smaller when the initial width increases. It is worth to note that the absolute width spread also decreases with an increase in the initial thickness although not at the same rate as the width spread coefficient.

Effect of slab initial thickness The width spread coefficient S generally increases with an increase in the initial slab thickness if the relative reduction r is kept constant. The exception to this trend is the formula derived by Helmi & Alexander. This model predicts that when the initial thickness increase, width change increases then decreases after reaching a maximum at a certain initial slab thickness.

Effect of slab roll diameter Similar to an increase in the reduction ratio, an increase in the work roll diameter produces a longer contact zone between the roll and the slab. This would increase resistance to the longitudinal elongation thus causing an increase in the metal flow in the lateral direction. The qualitative evaluation of this phenomenon is analytically confirmed by all empirical models presented in this section.

5.1.2 Domain of validity - unsuitable for cold rolling

The empirical approaches introduced in this section are not based on the resolution of equations but on the analysis of experimental results. The experimental results were either extracted from industrial production or issued from laboratory experiments specifically performed to measure and study the strip width variation. In these experiments, the strip are sometimes made of steel but sometimes of simulation materials such as lead or even plasticine. That is a reason using these models for quantitative evaluation of width variation in steels rolling may be degraded due to the fact that the elastic deformation (of plasticine) as well as thermal deformation are negligible. For the same reason, extrapolation of these formulas to the rolling conditions which are different from the experiments ones, the results can be hazardous.

Parameter	Unit	Siebel	Wusatowski	Sparling	Helmi & Alexander
Year of publication		1932	1955	1968	1968
Environment		Laboratory	Divers industrial data	Laboratory	Laboratory
Material		Low carbon steel	Carbon steel	Carbon steel	0.18%C steel
Temperature	°C	700-1200		1000-1200	1000
Velocity	m/s		$0.4 \leq V_c \leq 17$	$V_c \leq 0.6$	$V_c \leq 0.15$
Reduction	%	$10 \leq r \leq 50$	$10 \leq r \leq 90$	$10 \leq r \leq 30$	$10 \leq r \leq 30$
Work-roll radius	mm	$90 \leq R \leq 215$	$210 \leq R \leq 600$	125	47.5
Initial width	mm	$6 \leq w_e \leq 200$	$5 \leq w_e \leq 180$	$33 \leq w_e \leq 250$	$5 \leq w_e \leq 80$
Initial thickness	mm	$3.3 \leq h_e \leq 61$	$2 \leq h_e \leq 90$	$12.7 \leq h_e \leq 25.4$	$4.7 \leq h_e \leq 12.7$

Table 5.2: Rolling conditions of trials allowing to tune the empirical models.

Table 5.2 shows the rolling experimental conditions of the trials that allow to elaborate the empirical models mentioned above. It can be seen from this table that, these domain of validity of these empirical models correspond to billets (long product) rolling or flat hot rolling. It is therefore not recommended to extrapolate these formulae to the cold rolling domain where the width over thickness ratio varies from 400 to over 2000 for automotive product rolling and up to 5000 for packaging product rolling.

5.2 3D rigid-plastic *UBM* for width variation analysis

5.2.1 Advantage of *UBM* in comparison to *FEM* and empirical models

In the literature, there are many analyses using *FEM* for flat and shape rolling such as [77, 78, 54] where the shape and the spread are predicted and [76] where a complete thermomechanical solution is even found. Some efforts have been made in order to reduce the computing capacity and time. Certain authors, based on the *UBM*, use numerical methods for integration which are similar to *FEM*, [58, 1]. Nevertheless, the *FEM* stays generally at high time-consuming level. That is the reason why the *UBM* is commonly used thanks to its simplicity and rapidity. On the other hand, unlike the empirical models presented above, the *UBM* is physical and fully predictive. It is, hence applicable for any range of geometrical parameter ratio including cold rolling conditions with high width-thickness ratio. In the present thesis, we are interested in the *UBM* 3D rolling analyses.

As a reminder, the principle of *UBM* is based on *theorem 2* (3.17) stating that among all kinematically admissible velocity fields the actual one minimizes the rolling power function 3.27. Applying this principle to rolling process require that the work-roll shape is given, the strip material is rigid-plastic and the friction shear stress is known - Tresca friction for example (see more detail in 3.1.2). Thus, to model the width variation problem by *UBM*, the main point is to build kinematically admissible velocity fields for 3D rolling problem.

Before introducing the typical existing *UBM* -based models for width spread analyses, it is worth to note a difference between 2D and 3D boundary conditions that may influence the velocity constructing method as well as the resolution of *UBM*.

5.2.2 Difference between 2D and 3D *UBM*

Lateral free surface: In a 2D model, there are boundary conditions imposed on the velocity field at all the four boundary surfaces of the roll bite : entry, exit, the contact surface and the surface of symmetry $z = 0$. However, in a 3D model, there is a free surface, the later surface defined by $y = w(x)$ on which the boundary condition is not imposed on the velocity field but on the stress field ($\sigma_{ij} = 0$). The difficulty is that the **actual** velocity field needs to be, in a steady state, tangential to the free surface but a kinematically admissible one does not necessarily verify this condition.

How can we, thus introduce a family of such kinematically admissible velocity fields?

A solution for this difficulty is: imagine a *virtual boundary* for the velocity field noted $\varphi(x)$ which can be different from $w(x)$ so that the velocity is tangential to this *virtual boundary*. Thus, we can easily represent the kinematically admissible velocity field thanks to this virtual boundary function.

Change in resolution strategy: As already mentioned in the paragraph 2.1.1.a, the principal difficulty of the stationary models is that the geometry of the strip during and after deformation is an additional unknown of the problem. In our problem, the function $w(x)$ is the unknown that we are interested to search.

To find the function $w(x)$ at the equilibrium state, let first initialize it as $w(x) = w_e$ for example. Then using the principle of the *UBM*, search for the velocity field represented by the virtual boundary $\varphi(x)$ that minimizes the rolling power. If the virtual boundary is equal within a certain precision to the function $w(x)$, we have a velocity field that is tangential to the real free surface and that is the stable solution. Otherwise, if $\varphi(x) \neq w(x)$ within a certain precision, the velocity is not tangential to the real free surface, the material has tendency to flow to have a new boundary that is $\varphi(x)$. Therefore, take $w(x) = \varphi(x)$ and repeat the operations. In general, after few iterations the convergent geometry is obtained. That is the main change in comparison with 2D *UBM* models.

5.2.3 *UBM* with 3D "simple" velocity field [83]

5.2.3.a Model description

Oh et Kobayashi [83] are one of the pioneers who applied the *UBM* to 3D analysis of rolling process. The authors supposed a velocity field as follows

$$\begin{cases} u_x(x, y) = C_{vol} \frac{1}{h(x)\varphi(x)} \\ u_y(x, y) = C_{vol} \frac{\varphi'(x)y}{h(x)\varphi^2(x)} \\ u_z(x, z) = C_{vol} \frac{h'(x)z}{h^2(x)\varphi(x)}. \end{cases} \quad (5.3)$$

where $\varphi(x)$ is the velocity virtual boundary which coincides to the width function for the actual velocity at stationary regime. Let call this velocity field "3D simple velocity field" because like the 2D simple one (see 3.3.2), this 3D velocity field states also that a cross section remains a cross section under the deformation along the roll bite.

In order to compute and minimize the power function given by 3.27, the authors parameterize the free surface function $\varphi(x)$, that represents the width evolution, as a third-order polynomial in x . The function is chosen so that

$$\begin{cases} w(-L) = w_e \\ w'(0) = 0 \end{cases} \tag{5.4}$$

With these two equations, the width function can be represented by a third order polynomial of x as follows

$$\varphi(x) = w_e + \alpha + \left(\frac{\beta}{L} - \frac{3\alpha}{L^2}\right)x^2 + \left(\frac{\beta}{L^2} - \frac{2\alpha}{L^3}\right)x^3. \tag{5.5}$$

with two unknown parameters that are α - the total width variation and $\beta = w'(-L)$ - sloop of width function at roll bite entry.

In addition of these two unknowns, there is an other parameter, the flow rate C_{vol} which can be expressed as a function of the neutral line position (neutral point in 2D model) x_n . The three parameters are obtained by minimizing the rolling power function. *This model is studied in detail in the following section 5.3 of the present chapter. It results are compared to pilot (laboratory) rolling experiments and show a good agreement. The question on the rapidity (computing time) is also investigated.*

5.2.3.b Parametric study - application to Hot Finishing Mill

D.Pirus [90] reproduced successfully this model in *fortran* and validated it by comparing with the results published by Oh et Kobayashi [83]. Pirus used Newton-Raphson method for the minimization resolution of rolling power. He carried out, then a sensibility study of the width variation for finishing mill conditions. This study led to a conclusion that the width variation is always positive, meaning the strip always spreads out under rolling process. And the spread increases with an increase in the reduction, strip entry thickness, work-roll diameter or strip yield stress. Inversely, it decreases with an increase in strip width, entry and exit tensions, friction coefficient and work-roll Young modulus.

5.2.4 *UBM* with combination of basic velocity fields by Komori [59]

5.2.4.a Velocity field

In 2002, K. Komori [59] introduced a new *UBM* to analyze the 3D deformation for rolling. He proposes to represent the velocity field as a linear combination of predefined fundamental velocity fields \underline{u}_i as

$$\underline{u} = a_i \underline{u}_i. \tag{5.6}$$

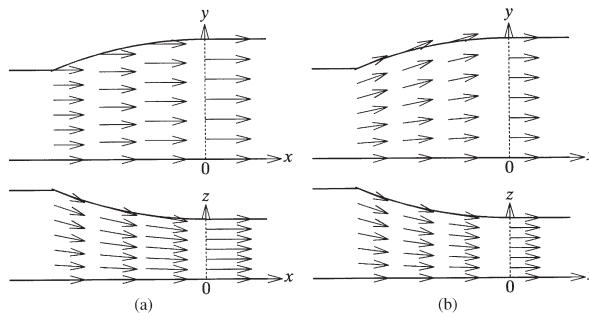


Figure 5.1: Illustrated fundamental kinematically admissible velocity fields: (a) \underline{u}_1 and (b) \underline{u}_2 (Fig.4 in [59]).

In the article, two fundamental fields are mentioned. The first one \underline{u}_1 is similar to the 2D simple velocity field 3.61, called equally "elliptical velocity field" (3.3.5) representing the deformation in thickness direction (plane strain deformation)

$$\begin{cases} u_{1x} = V_c \frac{h_e}{h} \\ u_{1y} = 0 \\ u_{1z} = V_c \frac{h_e}{h} \frac{zh'}{h}. \end{cases} \quad (5.7)$$

The second fundamental velocity field \underline{u}_2 representing the deformation in width direction is given by

$$\begin{cases} u_{2x} = V_c \\ u_{2y} = -V_c \frac{yh'}{h} \\ u_{2z} = V_c \frac{zh'}{h}. \end{cases} \quad (5.8)$$

5.2.4.b Calculation and minimization of power function

Using the velocity given by 5.6, the power function defined by 3.27 becomes a function of a_i . And the integrations are obtained using similar method as finite-element analysis. The first and second order derivatives of the power function with respect to a_i are also derived analytically before being integrated numerically. Then, the minimization of the rolling power is performed with respect to two parameters a_1 and a_2 by the Newton-Raphson method.

5.2.4.c Discussions

Komori's combination method advantages: It is worth to highlight that, with the proposed combination method for constructing velocity field, the structure of the computer program is quite independent to the choice of fundamental velocity fields. It seems, therefore relatively simple to enrich the velocity field and quality of the analysis by assuming more kinematically admissible velocity fields.

Regarding unknown integration domain: However, unlike the resolution proposed in the paragraph 5.2.2, only one iteration is performed by considering that the domain of integration (strip geometry) is the initial configuration without width spread. Then, the optimum velocity gives a new geometry for the strip which is considered as the final geometry of the strip in stable regime. While according to us, it would be necessary to repeat the operations by integrating the power over the new geometry and find the new velocity field, then repeat again until the velocity field is tangential to the free surface.

Surface of velocity discontinuity is assumed vertical: In the paper, the author considers that the entry surface of velocity discontinuity is a cross section. That is true by coincidence for the chosen velocity based on two fundamental ones 5.7 and 5.8. However, when other fundamental velocities are chosen or added, the surface of velocity discontinuity may be different from a cross section and need to be determined based on the velocity field. See 4.4.2.a, an example of method for numerical determination of surface of velocity discontinuity for a 2D velocity field.

The "3D simple velocity fields" family includes Komori's one: In his paper, the author only presented two velocity fields given by 5.7 and 5.8. It is not difficult to demonstrate that the combination of these velocities following 5.6 is a specific case of the "3D simple velocity" given by 5.3. Indeed, if we chose the virtual boundary function $\varphi(x)$ and C_{vol} as follows

$$\begin{cases} C_{vol} = (a_1 + a_2) V_c h_e w_e \\ \frac{1}{\varphi(x)} = \frac{1}{w_e} + \frac{a_2 V_c}{C_{vol}} (h(x) - h_e) \end{cases} \quad (5.9)$$

then the "3D simple velocity field" can be expressed by

$$\underline{u}_{simple} = a_1 \underline{u}_1 + a_2 \underline{u}_2 \tag{5.10}$$

equal to Komori's velocity. In other words, the "3D simple velocity fields" family includes and becomes Komori's for a specific choice of function $\varphi(x)$ given by 5.9.

5.2.5 *UBM* with 3D polynomial velocity field [99]

5.2.5.a velocity field using dual stream functions

Serek [99] proposed, in 2008 a model for plate rolling in hot and cold condition using *UBM*. The velocity fields are constructed by means of Dual Stream Functions and the rigid-plastic boundary at the entrance of the roll bite is assumed to be a quadratic form instead of a plane and normal to rolling direction. By using Dual Stream Functions as partly given in [117], the unknown three velocity components can be reduced to two and the incompressibility condition is satisfied. By defining $\psi(x, y, z)$ and $\chi(x, y, z)$ stream functions, the velocity components u_x, u_y, u_z in three dimensional non-compressible flow are written as follows:

$$\begin{cases} u_x = \frac{\partial \psi}{\partial y} \frac{\partial \chi}{\partial z} - \frac{\partial \psi}{\partial z} \frac{\partial \chi}{\partial y} \\ u_y = \frac{\partial \psi}{\partial z} \frac{\partial \chi}{\partial x} - \frac{\partial \psi}{\partial x} \frac{\partial \chi}{\partial z} \\ u_z = \frac{\partial \psi}{\partial x} \frac{\partial \chi}{\partial y} - \frac{\partial \psi}{\partial y} \frac{\partial \chi}{\partial x} \end{cases} \tag{5.11}$$

The volume flow rate at any cross section in three dimensional coordinates is written as

$$Q = (\psi_2 - \psi_1) (\chi_2 - \chi_1). \tag{5.12}$$

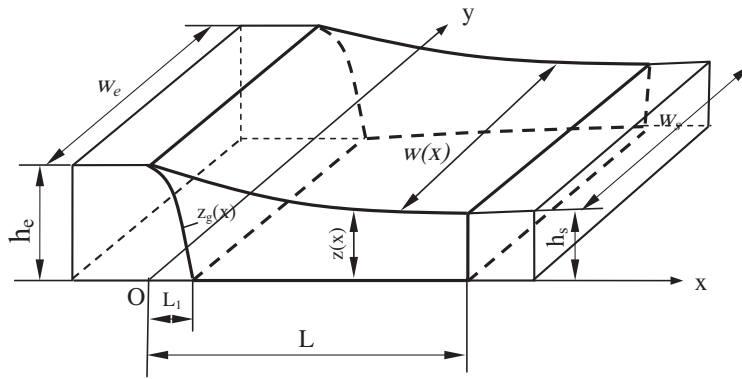


Figure 5.2: Illustration of deformation zone corresponding to Serek's polynomial velocity field (Fig. 1 in [99]).

Based on previous studies [13, 71], Serek [99] chooses a stream function for metal flow in $x - z$ plane defined in the roll bite, as follows

$$\psi = C_{vol} \left\{ \frac{z}{h} + f(x)z [z - h] \right\} \tag{5.13}$$

where $f(x)$ is a gradient of velocity distribution in horizontal direction. Some mistakes are observed the formulae of ψ given by equations 5 and 11 in in [99] but the velocities deduced from the stream functions are correct.

Metal flow in $y - z$ plane of the roll bite presented by the stream function as follows

$$\chi = -\frac{y}{w} \tag{5.14}$$

where w is the width profile at the free surface. This function is chosen as a third order polynomial so that its derivative is equal to zero at entry $x = -L$ and exit $x = 0$ (our point of reference is different from [99]) of the roll bite, then

$$w = w_e + \Delta w \left[1 - \frac{2x^3}{L^3} - \frac{3x^2}{L^2} \right]. \quad (5.15)$$

The rigid-plastic boundary (surface of velocity discontinuity) at the roll bite entry can be determined by equality of flow rate before and inside the roll bite

$$\psi = C_{vol} \left\{ \frac{z_e(x)}{h} + f(x)z [z_e(x) - h] \right\} = C_{vol} \frac{z_e(x)}{h_e} \quad (5.16)$$

then

$$z_e(x) = h + \frac{\frac{1}{h_e} - \frac{1}{h}}{f(x)}. \quad (5.17)$$

By assuming that this entry surface is quadratic and the exit one is vertical, the function $f(x)$ can be deduced as

$$f(x) = ax^2. \quad (5.18)$$

If L_1 denotes the x -distance between the starting and finishing points of the entry surface Γ_e we have

$$0 = z_e(L_1 - L) = h(L_1 - L) + \frac{\frac{1}{h_e} - \frac{1}{h(L_1 - L)}}{a(L_1 - L)^2} \Rightarrow a = \frac{\frac{1}{h(L_1 - L)} - \frac{1}{h_e}}{(L_1 - L)^2 h(L_1 - L)}. \quad (5.19)$$

L_1 is an output of the model which is determined by the optimization of the power function. The velocity is finally obtained as

$$\begin{cases} u_x = C_{vol} \left[\frac{1}{h} + f(x)(2z - h) \right] \frac{1}{w} \\ u_y = C_{vol} \left[\frac{1}{h} + f(x)(2z - h) \right] \frac{w' y}{w^2} \\ u_z = C_{vol} \left[\frac{h' z}{h^2} + f'(x)z(z - h) - f(x)zh' \right] \frac{1}{w}. \end{cases} \quad (5.20)$$

This velocity field verifies all kinematically admissible conditions. Figure 5.2 illustrates the deformation area as well as the parameters of Serek's velocity field.

5.2.5.b Calculation and optimization of power function

The calculation and optimization of the power function is performed numerically in *Matlab*. We remark however that, according to the paper nomenclature, m denotes "Coulomb" friction but the author does not explain in detail how the friction power can be calculated. The m seems to be actually "Tresca" friction coefficient.

5.2.5.c Discussions

The velocity field given in this paper is interesting. It allows to model a non-vertical surface of velocity discontinuity at the roll bite entry and more general than the 3D simple one (for a same choice of w).

Non-null shear strain rates on surface of symmetry $z = 0$: It is noted that the shear strain rates $\dot{\epsilon}_{xz}$ and $\dot{\epsilon}_{yz}$ deduced from the velocity field 5.20 are not equal to zero when $z \rightarrow 0$. Meaning that the shear strain ϵ_{xz} and ϵ_{yz} are different from 0 closed to the surface of symmetry, $z \rightarrow 0$. This fact seems unrealistic. However, the condition of nullity of strain rates $\dot{\epsilon}_{xz}$ and $\dot{\epsilon}_{yz}$ when $z \rightarrow 0$ (two first equations of 2.3) are not strictly necessary conditions for any kinematically admissible velocity field although the actual velocity field, being continuous and continuously derivable, itself verifies these conditions.

Integration domain: The paper does not precise how and what is the geometry of the strip over which the power function is integrated. If the geometry of the strip is considered as the initial one, this is the same mistake as Koromi's model. If the strip geometry is defined by the width function w given by 5.15 that is also used in the velocity expression, the results should not be corrects because in this manner, both geometry of strip and velocity vary during optimization. The correct way is to fixe the strip geometry and to vary only the velocity. That is why, it is necessary to introduce a virtual boundary φ and an iteration method as explained in the paragraph 5.2.2 and in Figure 2.2.

Results and comparison to experiments The rolling experiments were performed using the work rolls of the mill, having a diameter of 200 mm and a length 150 mm, driven by a 35 kW constant torque, dc motor. The roll speed is kept constant at 20 rpm, giving a roll surface velocity of 209 mm/s. Following Serek's *UBM* model, the rolling force and elongations in horizontal and vertical directions were computed for a bar of rectangular plate with dimensions of 10 x 50 x 150 mm. The optimum velocity field was attained after optimization of the power function and the analysis was carried out with the optimum velocity field.

Nevertheless, there is no detail about the method for approaching the rolling pressure and the rolling force but the results of these parameters were presented. On the other hand, the graphic 4 and 5 show that the rolling force reaches minimum for an optimum value of total spread. This can lead to a misunderstanding "why the rolling force but not the power or torque as expected?". In addition, the results show that a total spread equal to 25 mm, i.e 50% of width spread that is a very high spread ratio. Moreover, the width spread is quite constant as a function of reduction. It is almost equal to 25 mm for all levels of reduction from 10% to 50%. These results of the width spread behavior are quite unexpected and in the contrary in comparison to other models.

5.3 Chosen rigid-plastic model of width variation in rolling

5.3.1 *UBM* is chosen

As already mentioned above, the statistical models are too simple to be representative all the varying rolling condition in rolling. The *FEM* models require inversely high computing time while recent studies showed relatively high-quality developments of the *UBM* for width variation analysis. There were advancements in terms of both velocity fields approaches and numerical methods giving advantage of simplicity and rapidity. We propose, hence to use the *UBM* of which the principle is studied in the previous chapters.

We propose to use the resolution regarding the free surface $y = w(x)$ given in the paragraph 5.2.2 thanks to a virtual boundary of the velocity field $\varphi(x)$. And the resolution is solved by iteration method until the virtual and the real boundary are identical within a chosen precision, $\varphi(x) \simeq w(x)$. In each iteration, the minimization of rolling power is calculated by the Newton-Raphson method.

Concerning the numerical method for integration of power function and its derivatives, the effort is made in order to go as far as possible analytically before using numerical method. That is important point allowing to reduce significantly the number of elements required and therefore the computing time.

5.3.2 Assumptions of the model

This section presents general assumptions that define the conditions cold rolling process, denoted as **GA** (General Assumptions). Although, some of them have been already mentioned in previous chapters or sections, let list them all together.

5.3.2.a GA1-Symmetry

Only symmetric rolling is considered, i.e the rolling stand is top-bottom and left-right (operator-motor sides) symmetric. This hypothesis is already discussed in the paragraph 2.1.1.b. As a consequence, it is sufficient to study a quarter of total geometry of rolling mill.

5.3.2.b GA2 - Work roll shape

The roll is considered to have no initial bending meaning a straight profile across the width direction. On the other hand, it can be flattened and its radius is determined by Hitchcock's model. In other words, the roll is considered cylindrical without bending having the deformed radius. Therefore, the product thickness is constant in along the width direction, denoted $h(x)$.

5.3.2.c GA3 - Tresca friction law

As discussed in the section 3.1.2, the friction between the strip and the roll is an internal force and Tresca friction law 2.13 is assumed because the friction stress is known as a function of the material yield stress.

5.3.2.d GA4 - Strip rigid-plastic behavior

The strip mechanical behavior is considered rigid-plastic satisfying Von-Mises criterion. As a consequence, the material is incompressible under deformation

$$\text{div} \underline{u} = \frac{\partial u_x}{\partial x} + \frac{\partial u_y}{\partial y} + \frac{\partial u_z}{\partial z} = 0 \quad (5.21)$$

and the velocity field is homogenous and unidirectional before and after the roll bite.

The three assumptions **GA2**, **GA3** and **GA4** are necessary and enable to apply the *UBM*. They are already mentioned in one of previous chapter (see section 3.1.2).

5.3.2.e GA5 - Average behavior across thickness direction

GA5: In automotive rolling process, the product thickness is much smaller than its width and the contact length. This reality induces to an assumption (**GA5**) as follows: the vertical deformation rate is constant across thickness direction, meaning the component $\dot{\epsilon}_{zz}(x, y, z) = \dot{\epsilon}_{zz}(x, y)$. That implies therefore a linear vertical velocity u_z as a function of z

$$u_z(x, y, z) = z \cdot \dot{\epsilon}_{zz}(x, y). \quad (5.22)$$

Further, issued from the equations 5.21 and 5.22 we assume also that u_x and u_y do not neither depend on z . The fact that transversal velocity u_y does not depend on z implies that the strip width profile is independent of z and therefore becomes a function of x , denoted $w(x)$.

Validity: A deep analysis of 2D velocity field by *Lam3-Tec3* and *UBM* is done in the chapter 4. As a result of this analysis, Figure 4.34 shows that even for thin strip cold rolling condition ($h_e = 1.4\text{mm}$, $L_c = 17\text{mm}$) the velocity field oscillates significantly around its average behavior represented by the 2D simple velocity. The assumption *GA5* seems therefore unrealistic.

However, the real question is "what is the impact of the velocity oscillations on the width variation". To answer to this question, let compare several *Lam3-Tec3* simulations using 5 elements (fine mesh) and 1 element in the strip half thickness. Figure 5.3 shows results in terms of width spread for different meshing. The fine mesh has 5 elements in the half thickness and the others has only 1 element in the half thickness. It can be see that the results with different meshes are practically the same. Moreover, by remarking that with 1 element in the thickness, *Lam3-Tec3* considers a homogenous deformation in the thickness.

The hypothesis GA5 is finally confirmed in the case of narrow strip rolling. We may understand the GA5 as follows: in terms of width variation, it is enough to consider the average behavior of the velocity field in the thickness direction.

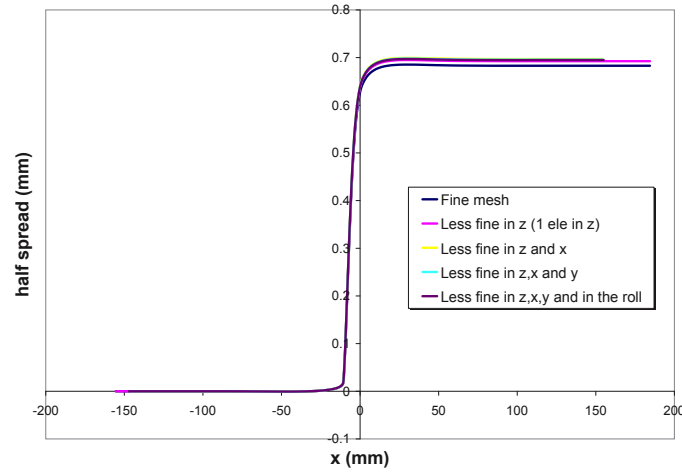


Figure 5.3: Comparison of width spread between different meshes with $2R = 298.3\text{mm}$, $2h_e = 1.31\text{mm}$, $2w_e = 70\text{mm}$, $2h_s = 0.872\text{mm}$, Coulomb friction $\mu = 0.0744$.

5.3.3 Choice of velocity

5.3.3.a General velocity field

By using Dual Stream Functions, a 3D velocity of an incompressible material in the plastic deformation zone Ω can be given by 5.11. And the boundary conditions of this velocity field are:

- Boundary conditions on the surface of symmetry $z = 0$:

$$\psi(x, y, 0) = \text{const} \quad \forall (x, y) \in [-L, 0] \times [0, \varphi] \quad (5.23)$$

- Boundary condition on the contact surface $z = h(x)$:

$$\psi(x, y, h) = \text{const} \quad \forall (x, y) \in [-L, 0] \times [0, \varphi] \quad (5.24)$$

- Boundary conditions on the surface of symmetry $y = 0$:

$$\chi(x, 0, z) = \text{const} \quad \forall (x, z) \in [-L, 0] \times [0, h] \quad (5.25)$$

- Boundary conditions on the virtual free surface $y = \varphi$:

$$\chi(x, \varphi, z) = \text{const} \quad \forall (x, z) \in [-L, 0] \times [0, h] \quad (5.26)$$

5.3.3.b Choice of stream functions

The assumption **GA5** implies that the $x - z$ plane stream function ψ is linear as a function of z . Thus, thanks to two boundary conditions on $z = 0$ (5.23) and $z = h$ (5.24), we can choose the $x - z$ plane stream function ψ as follows

$$\psi = C_{vol} \frac{z}{h}. \quad (5.27)$$

The same assumption **GA5** stating further that u_x and u_y do not depend on z , implies thus a $x - y$ plane stream

function χ independent of z . It is easy to verify that the following function

$$\chi = -\frac{y}{\varphi} \quad (5.28)$$

is a solution by verifying both boundary conditions on $y = 0$ (5.25) and on $y = \varphi$ (5.26). This solution describes a constant strain rate $\dot{\epsilon}_{yy}$ across the width direction. We remark that any other $x - y$ stream function verifying the assumption **GA5** can be written as a sum of this simple solution and an addition term depending on x and y as follows

$$\chi = -\left[\frac{y}{\varphi} + g(x, y)\right]. \quad (5.29)$$

Now, the boundary conditions 5.25 and 5.26 becomes

$$\begin{cases} g(x, 0) = 0 \\ g(x, \varphi) = 0. \end{cases} \quad (5.30)$$

Since the equation 5.27, we deduce that the plastic deformation boundary surfaces (surface of velocity discontinuity) at the roll bite entry and exit are vertical. By writing the equality of the stream flow at these surfaces to the uniforms and homogenous flow before and after the roll bite we have

$$\begin{cases} -\psi(-L, y, z)\chi(-L, y, z) = C_{vol} \frac{yz}{\varphi_e h_e} \\ -\psi(0, y, z)\chi(0, y, z) = C_{vol} \frac{yz}{\varphi_s h_s}. \end{cases} \quad (5.31)$$

The equations imply quite directly that

$$\begin{cases} g(-L, y) = 0 \\ g(0, y) = 0. \end{cases} \quad (5.32)$$

Finally, by substituting 5.27 and 5.29 into 5.11 we obtain a solution for 3D velocity field as follows

$$\begin{cases} u_x(x, y) = C_{vol} \frac{1}{h} \left[\frac{1}{\varphi} + \frac{\partial g}{\partial y} \right] \\ u_y(x, y) = C_{vol} \frac{1}{h} \left[\frac{y\varphi'}{\varphi^2} - \frac{\partial g}{\partial x} \right] \\ u_z(x, z) = C_{vol} \frac{zh'}{h^2} \left[\frac{1}{\varphi} + \frac{\partial g}{\partial y} \right] \end{cases} \quad (5.33)$$

with kinematically admissible conditions given by

$$\begin{cases} g(x, 0) = 0 \\ g(x, \varphi) = 0 \\ g(-L, y) = 0 \\ g(0, y) = 0. \end{cases} \quad (5.34)$$

5.3.3.c Discussions

Boundary effect at the edge and function g

When the function $g(x, y) = 0$, the component u_x depends only on x and the component u_y is linear in y and so in y . To verify the velocity field, we show in Figure 5.4 the dependence of u_x and u_y in y calculated by *Lam3-Tec3* for a case of rigid roll. For different abscissas, in the central part (from $y = 0$ to $y = 495mm$) the longitudinal velocity is constant and the lateral velocity u_y is linear in y . That means, $g(x, y)$ is mostly equal to zero in this part and increases exponentially at the edge of the strip. It represents therefore the bound effect.

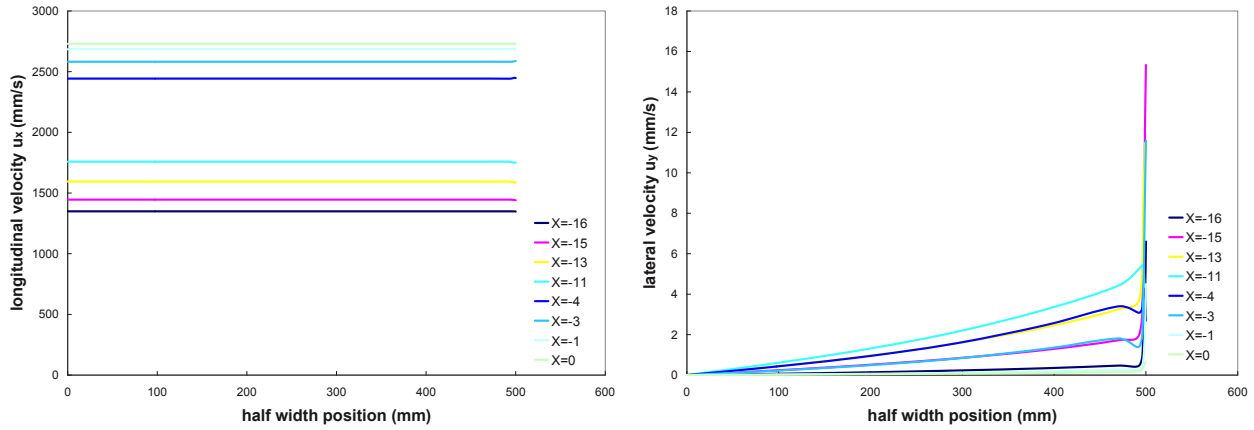


Figure 5.4: Longitudinal and lateral velocities distribution across the width direction. Result *Lam3-Tec3* for $2R = 298.3mm$, $2h_e = 1.31mm$, $2w_e = 70mm$, $2h_s = 0.872mm$, Coulomb friction $\mu = 0.0744$.

Two natures of the width spread

Then, the width spread is composed of two contributions. The first is associated to the central part where the velocity u_y is linear in y and the second is associated to the bound effect represented by the function $g(x, y)$. The size of the bound effect area is strongly related to the strip's thickness.

In the following, before presenting the *UBM* for the lateral spread, we perform a 2D study on the rolling stability which allows to understand the rolling conditions in industry and to validate the *UBM* for a 2D velocity field compared to a classic method for rolling, the slab method.

5.3.3.d Final choice of velocity field

In this thesis, we propose to study at first the phenomenon corresponding to the spread of the central part without bound effect *i.e* $g(x, y) = 0$. The 3D velocity field written by 5.33 becomes the "3D simple velocity" given by 5.3. If necessary, deeper understanding of the function g should be studied to go further.

5.3.4 Computation of power function

In order to reduce the computing time, the power functions are mostly calculated analytically. The integrations are as much as possible done analytically before using the numerical method. These calculations are long and are, thus presented in the appendix B.2. The power consumed by the discontinuity of velocity $J_{\Delta u}$ and the power of external forces J_{ten} are completely analytical. However, the two other powers consumed by plastic deformation $J_{\dot{\epsilon}}$ and by friction J_{fric} are developed analytically in y and z and have form of an unidimensional integral in function of x . We note that these calculations are independent of the width function form *i.e* the parametrization of this function.

Power of plastic deformation

$$J_{\dot{\epsilon}} = \frac{\sigma_0}{\sqrt{6}} C_{vol} \int_{-L}^0 P_x(x) dx \tag{5.35}$$

where

$$P_x(x) = \frac{2}{3} \sqrt{Q^2 + f^2 + g^2} + \frac{Q^2 + \frac{1}{3}f^2}{g} \text{Ln} \left(\frac{g + \sqrt{Q^2 + f^2 + g^2}}{\sqrt{Q^2 + f^2}} \right) + \frac{Q^2 + \frac{1}{3}g^2}{f} \text{Ln} \left(\frac{f + \sqrt{Q^2 + f^2 + g^2}}{\sqrt{Q^2 + g^2}} \right) + \frac{4Q^3}{3fg} \left[\arctan \left(\frac{Qg}{(\sqrt{Q^2 + f^2} + f)(\sqrt{Q^2 + f^2 + g^2} + \sqrt{Q^2 + f^2})} \right) - \arctan \left(\frac{g}{\sqrt{Q^2 + g^2} + Q} \right) \right]$$

with the three functions reducing the expression of the power $J_{\dot{\epsilon}}$ given by

$$\begin{aligned} Q &= \sqrt{2\frac{h'^2}{h^2} + 2\frac{\varphi'^2}{\varphi^2} + 2\frac{h'\varphi'}{h\varphi}} \\ f &= \frac{1}{\sqrt{2}} \left| \varphi'' - \frac{h'\varphi'}{h} - 2\frac{\varphi'^2}{\varphi} \right| \frac{b}{\varphi} \\ g &= \frac{1}{\sqrt{2}} \left| h'' - \frac{h'\varphi'}{\varphi} - 2\frac{h'^2}{h} \right|. \end{aligned}$$

Power of the discontinuity of velocity

$$J_{\Delta u} = \frac{\sigma_0}{\sqrt{3}} C_{vol} \left[\frac{\sqrt{\varphi_e'^2 + h_e'^2}}{3} + \frac{h_e'^2}{6|\varphi_e'|} \text{Ln} \left(\frac{|\varphi_e'| + \sqrt{\varphi_e'^2 + h_e'^2}}{|h_e'|} \right) + \frac{\varphi_e'^2}{6|h_e'|} \text{Ln} \left(\frac{|h_e'| + \sqrt{\varphi_e'^2 + h_e'^2}}{|\varphi_e'|} \right) \right] \quad (5.36)$$

where the 2 notations h_e' and φ_e' are defined as

$$\begin{cases} h_e' = h'(-L) \\ \varphi_e' = \varphi'(-L). \end{cases}$$

Power of friction

$$J_{fric} = \frac{m\sigma_0 C_{vol}}{2\sqrt{3}} \int_{-L}^0 \frac{b}{\varphi} \frac{\sqrt{1+h'^2}}{h} \left[\sqrt{\varphi'^2 + I^2} + \frac{I^2}{|\varphi'|} \text{Ln} \left(\frac{|\varphi'| + \sqrt{\varphi'^2 + I^2}}{I} \right) \right] dx. \quad (5.37)$$

with

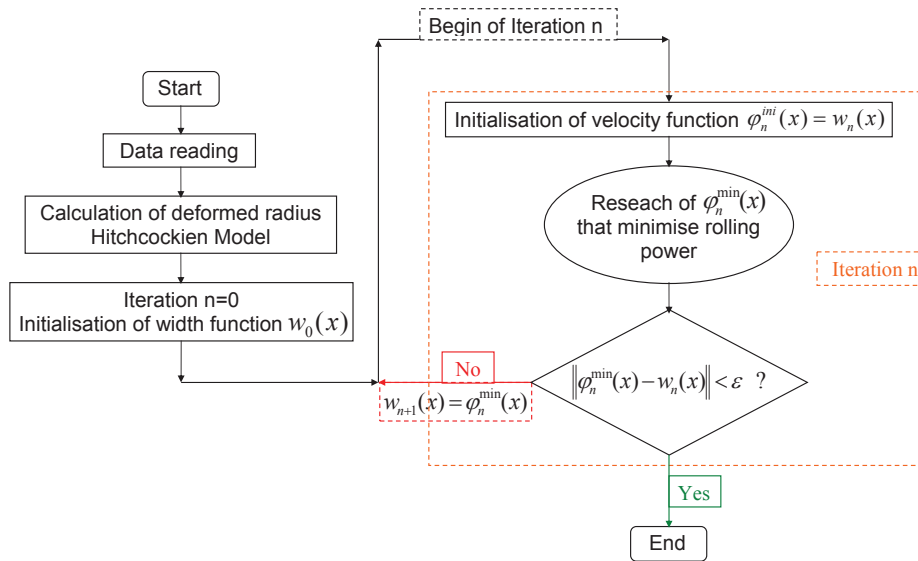
$$I = \left| \sqrt{1+h'^2} - \frac{h\varphi V_c}{C_{vol}} \right|.$$

Power of entry and exit tensions

$$J_{ten} = \left(-T_e + T_s \frac{b}{\varphi} \right) C_{vol}. \quad (5.38)$$

Total rolling power

$$J = J_{\dot{\epsilon}} + J_{\Delta u} + J_{fric} - J_{ten}. \quad (5.39)$$

Figure 5.5: General numerical resolution algorithm for 3D rigid-plastic *UBM* .

5.3.5 Numerical resolution

5.3.5.a Algorithm

The algorithm of the resolution is shown in Figure 5.5 that can be divided into 5 steps as following:

1. First, the programme reads the data file that contents all the necessary parameters concerning the rolling process.
2. Then, if the option of roll's deformation is active, it calculates the deformed radius by the **Hitchcock's model**.
3. Next, by using an empirical model - **Beese's model** [14] (see Table 5.1) that gives an approximate width spread of the strip, we initialize our width function for the first iteration. **Beese's model** is simple, direct and therefore very fast. Nevertheless, in some cases such as crowned strip rolling it is really not accurate and then the program needs more iterations to converge (see chapter 6).
4. For each iteration, the width function is given at the end of the previous iteration or by the initiation mentioned above for the first iteration. And here, the most important work of the *UBM* begins. For example, in *iteration n*, we calculate the rolling power composed of the powers consumed by plastic deformation, discontinuity of velocity, friction and external forces, depending on the width function $w_n(x)$ (given by the previous iteration) and equally on function of the velocity field that is represented by the function $\varphi_n(x)$. Then, in minimizing this rolling power we obtain a solution for velocity function noted $\varphi_n^{min}(x)$.

However, noting that space of functions is of infinite dimensions, we need to parameterize the velocity function $\varphi_n(x)$ by a limited number of parameters. In the section 5.3.5.b we present two parameterizations, a classical and a new. In many cases, we need only two parameters to well describe the function but three parameters are necessary for more complicated cases like crowned sheet rolling (see chapter 6).

In this space of finite dimensions, the minimization is carried out by the Newton-Raphson method that is presented in section 5.3.5.c.

5. At the end of each iteration, we test if the difference between the solution of velocity function $\varphi_n^{min}(x)$ and the function $w_n(x)$ is smaller than a given precision ϵ related to the precision of the width spread. Until this test is true, we continue next iteration $n+1$, by taking the width function for this iteration like $w_{n+1}(x) = \varphi_n^{min}(x)$.

Remark regarding unknown geometry of the strip (see 5.2.2): It is worth to note from the algorithm showed in Figure 5.5 that for some iteration n , the strip geometry is given $w_n(x)$, we search for the optimum velocity field presented by it virtual boundary $\varphi_n^{min}(x)$ by minimizing the rolling power. Next, we consider that the material flows following this solution velocity field and has a new geometry which is $w_{n+1}(x) = \varphi_n^{min}(x)$. In this new geometry, the strip has tendency to flow with an other optimum velocity $\varphi_{n+1}^{min}(x)$ and will have a new geometry. That continues until that the geometries of two successive iterations are identical within a chosen precision. Numerically, the identity of two functions is expressed by $\|\varphi_{n+1}^{min}(x) - w_n(x)\| < \epsilon$. The strip geometry no longer changes and gives a stable configuration. This is the solution of the stabilized state of the rolling.

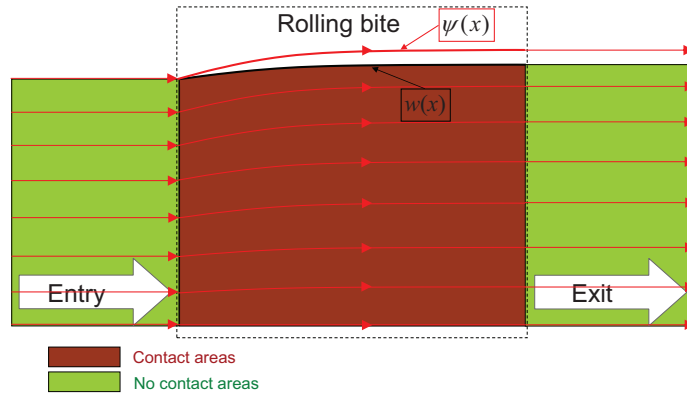


Figure 5.6: Optimal velocity field associated to a virtual bound $\varphi(x)$ for a given geometry represented by a width function $w(x)$ at an iteration of the resolution.

5.3.5.b Choice of width profile function

First of all, the numerical resolution mentioned above requires a same parameterizing of both real and virtual width functions ² because at a stabilized solution these two functions will be numerically identical. These functions are both equal to w_e at the roll bite entry and at the exit their derivative is equal to zero. In addition, in order to keep the advantage of the UBM in term of computing time, the number of parameters is essentially limited. There are presented here following two forms of the width function using two parameters. In these two cases, the first parameter α is the width spread and the second β is a parameter related to the tangency of the width at the entry of roll gap.

Form 1 : Polynomial in x

The classical form is a polynomial in x . With 2 conditions at the entry and exit, the width function can be expressed by a polynomial of degree 3 as a function of x and 2 parameters α and β :

$$w = w_e + \alpha + \beta x^2 + \left(\frac{\alpha}{L^3} + \frac{\beta}{L} \right) x^3. \tag{5.40}$$

Remark :

This form is useful and practical. Yet, it does not represent the direct relation between the reduction in thickness and the width spread of the strip in rolling. The greater the reduction, the greater the width variation. Consequently, we propose another form which expresses the function $w(x)$ as a function of $h(x)$ instead of x in the form 1.

Form 2 : Polynomial in $h(x)$

$$w = w_e + \frac{h_e - h}{h_e - h_s} \left[\alpha + \beta \left(1 - \frac{h}{h_s} \right) \right]. \tag{5.41}$$

²virtual width function is called also the velocity function because our velocity field will be expressed in this function

And finally, the velocity function $\varphi(x)$ is parameterized in the same way of the width function but with the parameters noted α_1 and β_1 .

$$\varphi(x, \alpha_1, \beta_1) = w(x, \alpha = \alpha_1, \beta = \beta_1). \quad (5.42)$$

With these parameterizations, for a given strip geometry (α and β are given) the power function J is a function of three parameters. The first one is V_e in the expression of C_{vol} ($C_{vol} = h_e w_e V_e$). Two others are α_1 and β_1 in the velocity function $\varphi(x)$. The minimization of the power function is performed by the Newton-Raphson method presented in the following section.

5.3.5.c Newton-Raphson method for minimization

Let present here Newton-Raphson method for the minimization problem of a n -variable real function $P : \mathbb{R}^n \rightarrow \mathbb{R}$ so that $(x_1, x_2, \dots, x_n) \rightarrow P(x_1, x_2, \dots, x_n)$. The minimization problem is represented by :

$$\begin{cases} \frac{\partial P}{\partial x_1} = 0 \\ \frac{\partial P}{\partial x_2} = 0 \\ \dots \\ \frac{\partial P}{\partial x_n} = 0. \end{cases} \quad (5.43)$$

The method consists in solving iteratively. In a given iteration where the equation 5.43 is not yet satisfied, the step of change of the variables between two successive iteration is determined as follows

$$\begin{pmatrix} P_{11} & P_{12} & \dots & P_{1n} \\ P_{21} & P_{22} & \dots & P_{2n} \\ \dots & \dots & \dots & \dots \\ P_{n1} & P_{n2} & \dots & P_{nn} \end{pmatrix} \begin{pmatrix} dx_1 \\ dx_2 \\ \dots \\ dx_n \end{pmatrix} = - \begin{pmatrix} P_1 \\ P_2 \\ \dots \\ P_n \end{pmatrix} \quad (5.44)$$

where $P_i = \frac{\partial P}{\partial x_i}$ et $P_{ij} = \frac{\partial^2 P}{\partial x_i \partial x_j}$. In our program the derivatives are calculated numerically using:

$$\begin{cases} P_i = \frac{P(x_i + \delta x_i) - P(x_i - \delta x_i)}{2\delta x_i} \\ P_{ii} = \frac{P(x_i + \delta x_i) + P(x_i - \delta x_i) - 2P(x_i)}{\delta x_i^2} \\ P_{ij} = \frac{P(x_i + \delta x_i, x_j + \delta x_j) + P(x_i - \delta x_i, x_j - \delta x_j) - P(x_i - \delta x_i, x_j + \delta x_j) - P(x_i + \delta x_i, x_j - \delta x_j)}{4\delta x_i \delta x_j} \end{cases} \quad (5.45)$$

with δx_i is chosen numerical parameters which are small enough. And the convergence criterion is choose as follows:

$$P(x_1, x_2, \dots, x_n) < P(x_1, x_2, \dots, x_i \pm \epsilon_i, \dots, x_n) \quad \forall i = 1..n \quad (5.46)$$

with ϵ_i is the predefined precision related to the parameter x_i .

5.3.5.d Computing time

The program is performed in C++ as the main part of a combined model. The computing time of the whole model varies from 0.01s to 0.05s (CPU: Intel Core I5-4200M, 250GHz) that enables online applications (see more details in the section 8.1).

5.3.6 Comparison with ArcelorMittal trials on the pilot rolling mill

This section presents a comparison between the results obtained with the *UBM* using 3D simple velocity field and the experiments performed on ArcelorMittal pilot rolling mill with narrow strips (about 65 – 70mm of width). These experiments were carried out on two types of steel, soft - **DWI** $\sigma_0 = 280\text{Mpa}$ and hard - **soldur** $\sigma_0 = 933\text{Mpa}$. The rolling parameters of the trials corresponding to these types of steel are presented in Tables C.1 and C.2 of Appendix C. The *Lam3-Tec3* calculations for these experiments are also presented in the same appendix. In this modeling, the friction is modeled by Coulomb’s law. This friction is, furthermore anisotropic with an anisotropy defined by the ratio between the transversal friction on the longitudinal friction. And we observe that this anisotropy has a significant impact on the exit profile of the strip. Therefore, in comparing the exit profile of the strip calculated by *Lam3-Tec3* with the measure, we obtain the good value of friction anisotropy coefficient. On the other hand, in *UBM* model the friction is modeled as an isotropic Tresca’s law. The friction coefficient value is obtained by seeking the good forward slip defined by the difference in % of strip exit velocity and the roll velocity which are both measured during the experiments.

The models results are equally given in Tables C.1 and C.2. And Figure 5.7 shows two histograms comparing the width variations obtained in the experiments, with *UBM* model and with *Lam3-Tec3* model for the two types of steel: **DWI** and **Soldur**. It can be seen that the *UBM* gives very coherent results in comparison with the measurement as well as with *Lam3-Tec3*, especially for **DWI** steel trials. These results are also presented in Figure 5.8 which shows that for soft steel (**DWI**), the model matches really well the measurements. It matches, however slightly less for hard steel (**Soldur**). For this steel, the *UBM* model underestimates the width spread for most of the cases. This may be explained by the fact that for very hard steel, the edge drop phenomenon due to the local deformation of the work-roll at the edge of the strip is more important leading to a greater width spread. Whilst this phenomenon is not taken into account by the *UBM* model.

We conclude then, the *UBM* predicts well the width spread of the pilot experiments with narrow strips. Improving the work-roll deformation model could help to improve the model accuracy especially for hard and very hard material.

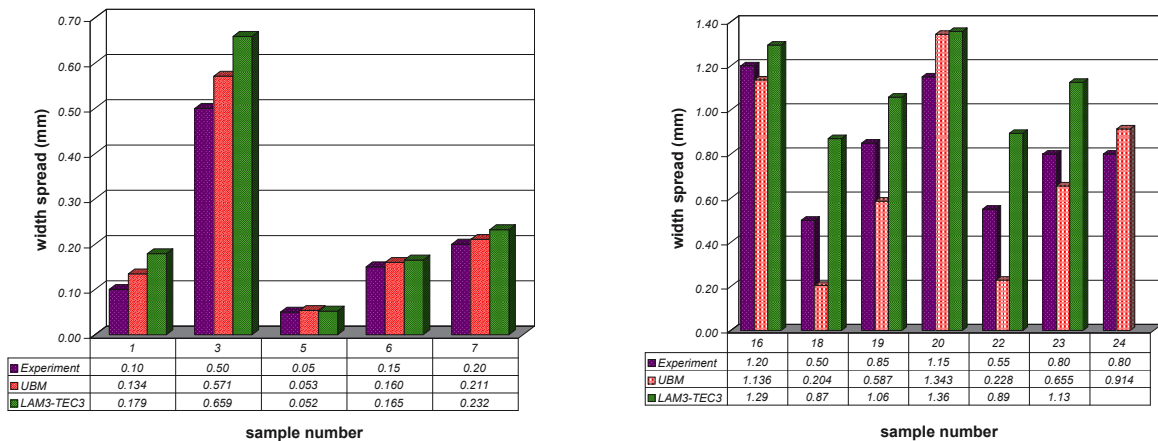
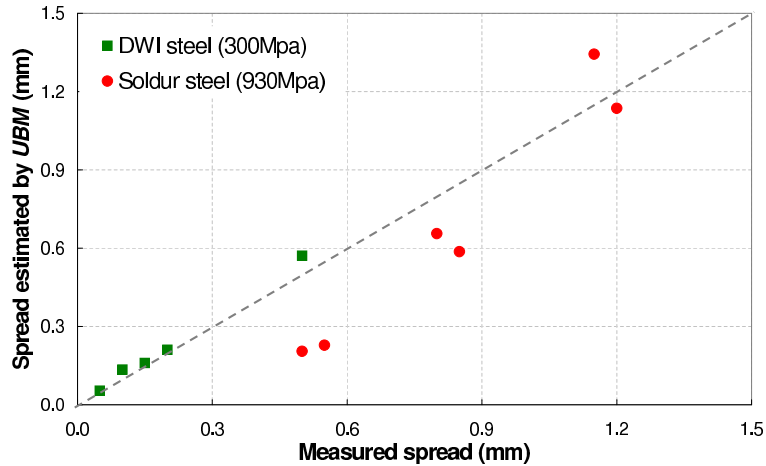


Figure 5.7: Comparison of width spread obtained by *UBM* and *Lam3-Tec3* with experiments results for **DWI** (left) and **Soldur** (right) steels.

5.3.7 Parametric study for using *UBM* model

In this section, the effect of rolling parameters on the width spread is studied in a theoretical rolling condition defined in Table 5.3. The parameters will be changed one by one to study their effect on the width spread and the rolling power.

Figure 5.8: *UBM* width spread measurements for **DWI** and **Soldur** steels.

Parameters	Notation	Value	Unit
Half entry thickness	h_e	2.5	mm
Half entry width	w_e	25	mm
Reduction in thickness	r	30	%
Yield stress of the strip	σ_0	600	Mpa
Roll's radius	R	250	mm
Roll's velocity	V_c	1000	mm/s
Entry and exit tensions	T_e, T_s	150	Mpa
Tresca's friction coefficient	m	0.4	

Table 5.3: The rolling parameters of the referent point for the parametric study.

5.3.7.a Influence of rolling parameters on width spread

The dependence of the width spread on the rolling parameters is demonstrated in Figure 5.9. It is observed that the width spread

- increases as a function of: the reduction r , the roll radius R , the friction coefficient m and the entry thickness h_e
- is independent of the roll velocity V_c
- decreases with an increase in: the entry width w_e as well as the entry and exit tensions T_e, T_s .

In the first order, the width spread increases rapidly with the thickness reduction and falls down exponentially with an increase in the strip entry width. This is a very common result observed by many works in the literature (see previous sections 5.1 and 5.2). In the second order, it grows almost linearly as a function of the roll radius because of the increase of the contact length and linearly decreases with the entry and exit tensions. The dependence of the width spread on the entry tension is slightly more important than the exit tension. This could be due to the fact that the entry section is larger than the exit one. Finally, in the third order, the entry thickness and the friction coefficient make the width spread increase but more slightly. In some other cases, the friction coefficient may have negative influence on the width spread.

In addition, two extremity phenomena can be observed also in Figure 5.9. First, for an extremely narrow strip *i.e.* $w_e < 8\text{mm}$, the width spread increases with the entry width w_e which is in contrary to the general case. Indeed, the smaller the w_e , the less material to spread out therefore the smaller the width spread. Secondly, for a very thin strip *i.e.* h_e is very small, we observe an inverse impact of the entry thickness on the width spread. Anyway, these phenomena are two really special cases that are hardly met in flat rolling.

5.3.7.b Influence of rolling parameters on rolling power

Rolling power and rolling torque

As a reminder, the minimum of the *rolling power* function gives an upper bound estimation of the real one provided by the motor on the work-roll. The associated roll torque can be evaluated from the power by equation 4.67. Figure 5.10 points out that the rolling power J increases strongly with the reduction r and depends almost linearly in the other parameters. It increases also as a function of the roll radius R , the friction coefficient m , the strip entry thickness h_e , the strip entry width w_e , the entry tension T_e except only the exit tension T_s . As the exit tension makes the strip move in rolling direction, the necessary rolling power is smaller when this tension increases. Or it can be seen from the equation 5.38 that the dependence of the rolling power on T_e and T_s is related to the term of power of external forces J_{ten} . At stable state, $w = \varphi$, we have $J_{ten} = (T_s - T_e)C_{vol}$. That is why the rolling power J increases with T_e and decreases with T_s with almost the same sensitivity.

Comparison between two parameterizations of the width function

Moreover, it should be interesting to compare the efficiency of the two forms of the width function presented in the paragraph 5.3.5.b in order to choose the best one. As a reminder, the best form is the one which gives the lowest rolling power.

Let firstly choose the *form 1*, polynomial in x as the reference and study the difference in terms of rolling power of the *form 2*, polynomial in $h(x)$ in comparison with the first one. Figure 5.11 shows that this difference is negative for $r \leq 45\%$. That means if the reduction $r \leq 45\%$, the polynomial in $h(x)$ form is better. But inversely the *form 1* is better for very high reduction. In addition, Figures 5.9 and 5.10 show that the width spread as well as the rolling power are almost identical. Therefore, for us the two forms of width function can be considered equivalent. The *form 1* is slightly advantageous in terms of computing time.

Volume specific rolling energy

Let now introduce a quantity called *specific rolling energy* that represents the energy provided by the motor to roll an unity volume of material. It is defined as

$$E_{vol} = \frac{J}{C_{vol}}. \quad (5.47)$$

This parameter may help to study how it is possible to save rolling energy by well choosing values of the rolling parameters. It can be seen in Figure 5.12 that this quantity increases as a function of the thickness reduction. Moreover, unlike the rolling power which linearly grows up as a function of the entry width, the specific rolling energy is practically constant except for very narrow strip - $w_e < 20mm$. Indeed, the higher the strip width, the higher the sliding velocity in y direction and thus the higher the friction power which contributes to an increase of the specific rolling energy as a function of the strip width. However, the width spread tends to zero very rapidly when the strip width increases, the lateral velocity field is asymptotic to zero. That explains why the specific rolling energy becomes a constant as a function of the width for large strip.

Beside, it can be noted that the deformation dissipation energy per volume unit increases with the reduction r but is almost independent on the strip thickness h_e if r is constant. And the tensions power per volume unit (deduced from the equation 5.38) is strictly independent of h_e . On the other hand, the friction power is proportional to the contact length L which is proportional to $\sqrt{Rh_e r}$ while the volume flow rate C_{vol} is proportional to h_e . Therefore, the friction energy per volume unit is proportional to $1/\sqrt{h_e}$. Thus, the friction energy per volume unit decreases as a function of entry thickness. That is why the specific energy decreases when entry thickness increases as it can be seen in the graphic $E_{vol} - r$ of Figure 5.12.

When h_e , w_e and r are constant, the specific rolling energy depends similarly as the rolling power on the other rolling parameters. Actually, Figure 5.12 shows that E_{vol} decreases when: T_s or h_e increase and when r , m , R , T_e or σ_0 decrease.

However, in a rolling process, the strip initial geometry, the desired reduction and the product characteristics are the given constraints, meaning w_e , h_e , r and σ_0 are fixed. The only three parameters which allow to optimize the specific rolling energy are m , R and $T_s - T_e$. But an increase in $T_s - T_e$ will require equally a certain energy. Thus,

increase $T_s - T_e$ to decrease E_{vol} is a solution that just allows to transfer the energy consumed by the rolling motor to other machines but does not save the total consumed energy. It is possible to save energy by using small rolls and by lubricating the contact surface to reduce to friction coefficient between the roll and the strip.

Nevertheless, it is complicated in developing more in this subject because there are a lot of constraints concerning the roll and the lubrication system. For example, the roll must not be too small to assure a certain rigidity in flexion. The friction coefficient needs to be enough to keep the rolling stability. The choice of roll radius and the lubricant is an optimization problem which is not studied further in this thesis.

5.4 Conclusions and perspectives

In this chapter, we study a velocity field family which explains the width variation of a rigid-plastic strip. This width variation can be composed of two parts: the homogenous lateral flow in the central part of the strip as well as the apparition of the boundary effect near to the strip edge. This complex effect is modeled by a function g . However, in a first order approach, let neglect this phenomenon and consider therefore that $g = 0$. As a result, the velocity field becomes the "3D simple one" as given by [83]. It is demonstrated also in this chapter that the 3D simple velocity is, for a specific choice of width function (see the last paragraph of section 5.2.4.c) equivalent to the one proposed by [59] based on a combination of some fundamental velocity fields.

It is worth to highlight, in particular that using *UBM* the free surface $y = w(x)$ is an additional unknown of the problem (see section 5.2.2). A solution for this difficulty is employed. The idea is to fix the strip geometry and search for the optimum velocity, update the strip geometry so that the new width is tangential to that optimum velocity field and repeat these operations until the geometry and the optimum velocity are unchanged and coincided. However, [59] only uses one iteration and [99] does not precise how he deals with this issue.

With the chosen velocity field (3D simple one), the *UBM* gives a good coherence in terms of the width spread in comparison with experiments performed on ArcelorMittal pilot mill. In addition, the *UBM* analysis allows studying effect of rolling parameters on the strip width spread. The results show that width spread increases strongly with an increase in the reduction and falls down exponentially with an increase in the strip entry width. It grows almost linearly as the roll radius increases and decreases with an increase in the entry or exit tensions. The entry thickness and the friction coefficient have less important impact on the width spread. These are very common results observed by previous works in the literature (see previous sections 5.1 and 5.2).

The results obtained in this chapter raise up a further *UBM* analysis for a crowned strip rolling. The lateral boundary function ($\varphi(x)$ and $w(x)$) is parameterized differently but the method principle is essentially unchanged. This study is presented in the chapter 6 as an attempt to study the relation between strip spread and strip thickness profile or flatness.

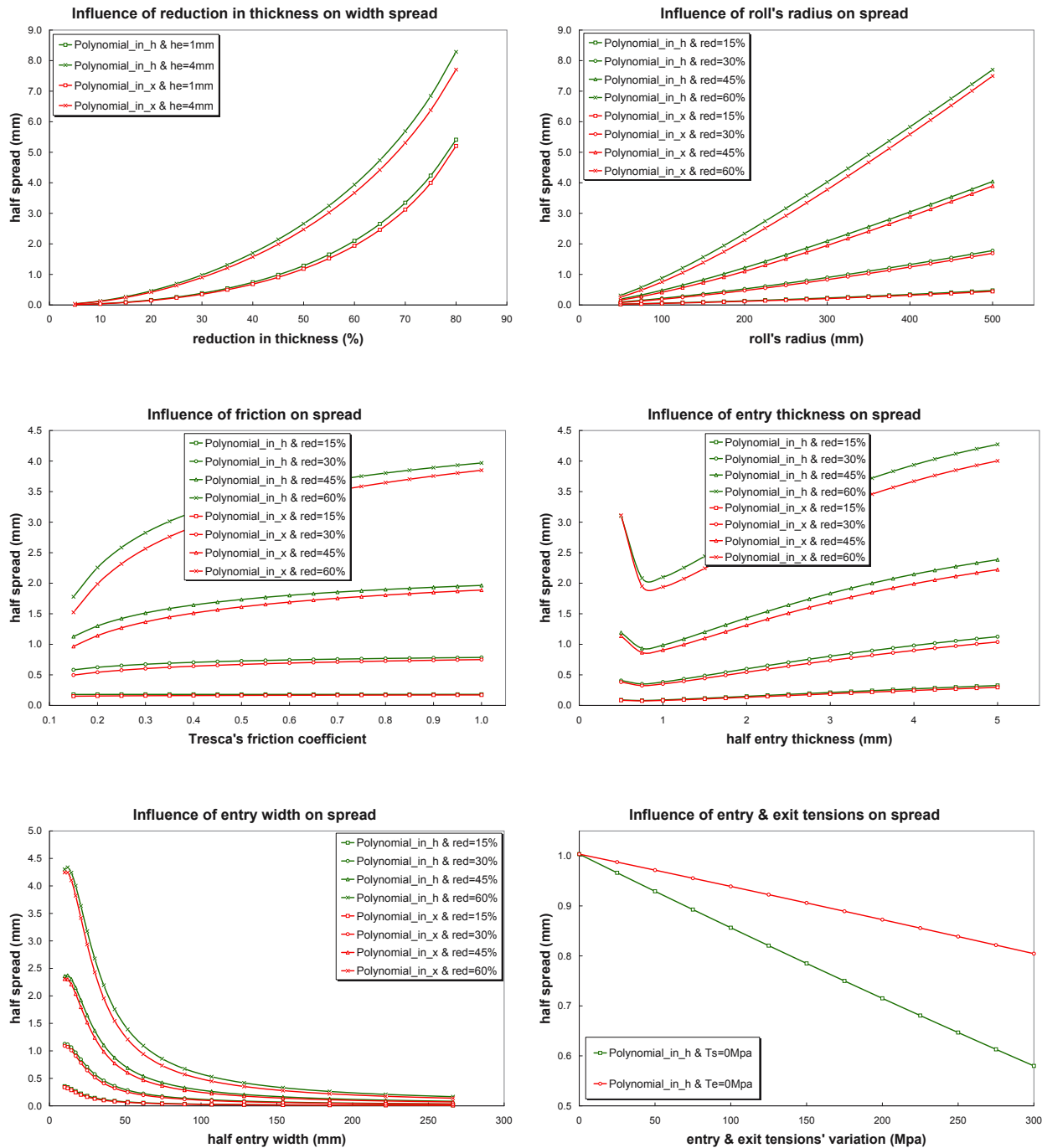


Figure 5.9: Influence of rolling parameters on width spread.

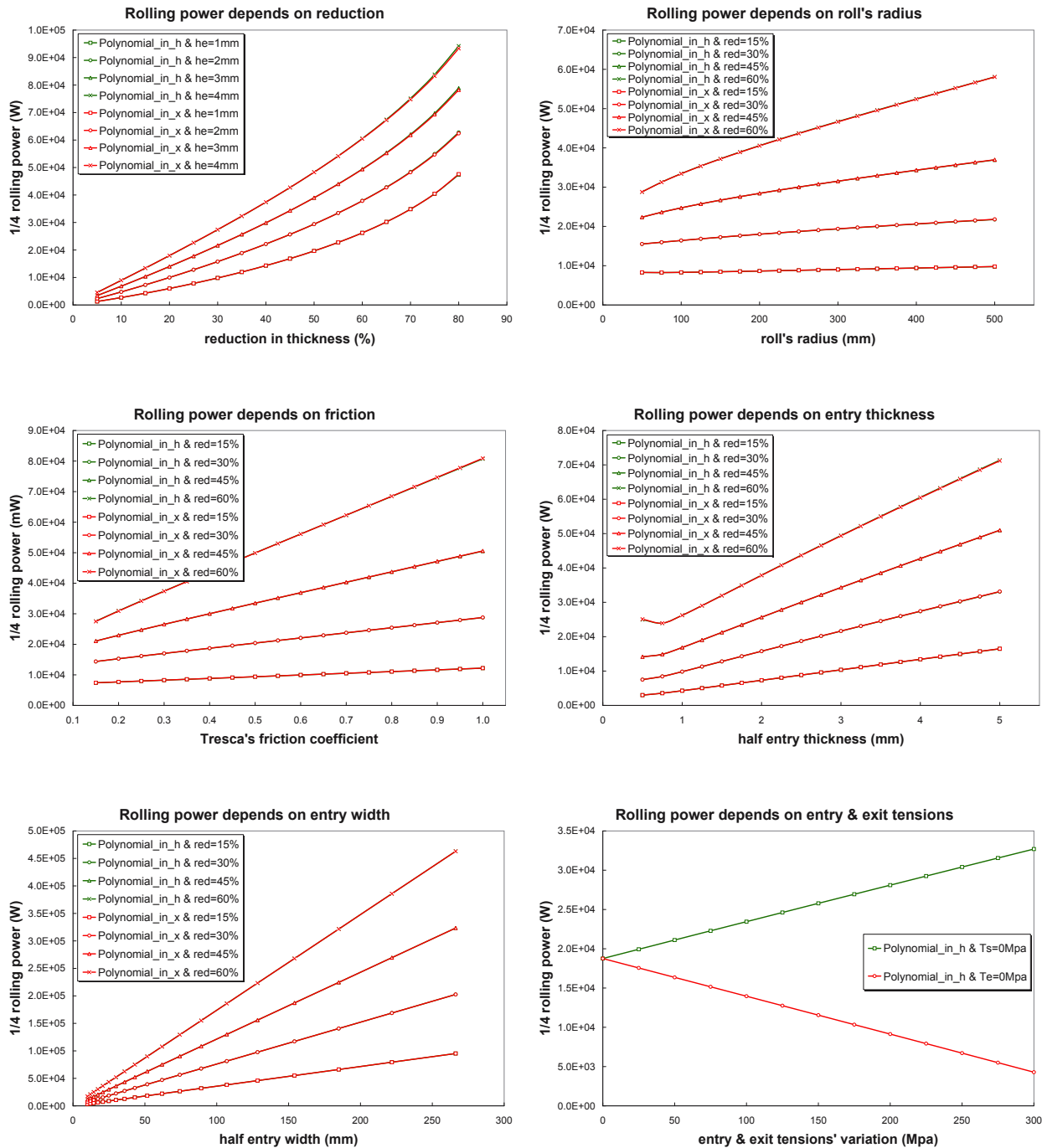


Figure 5.10: Influence of rolling parameters on rolling power.

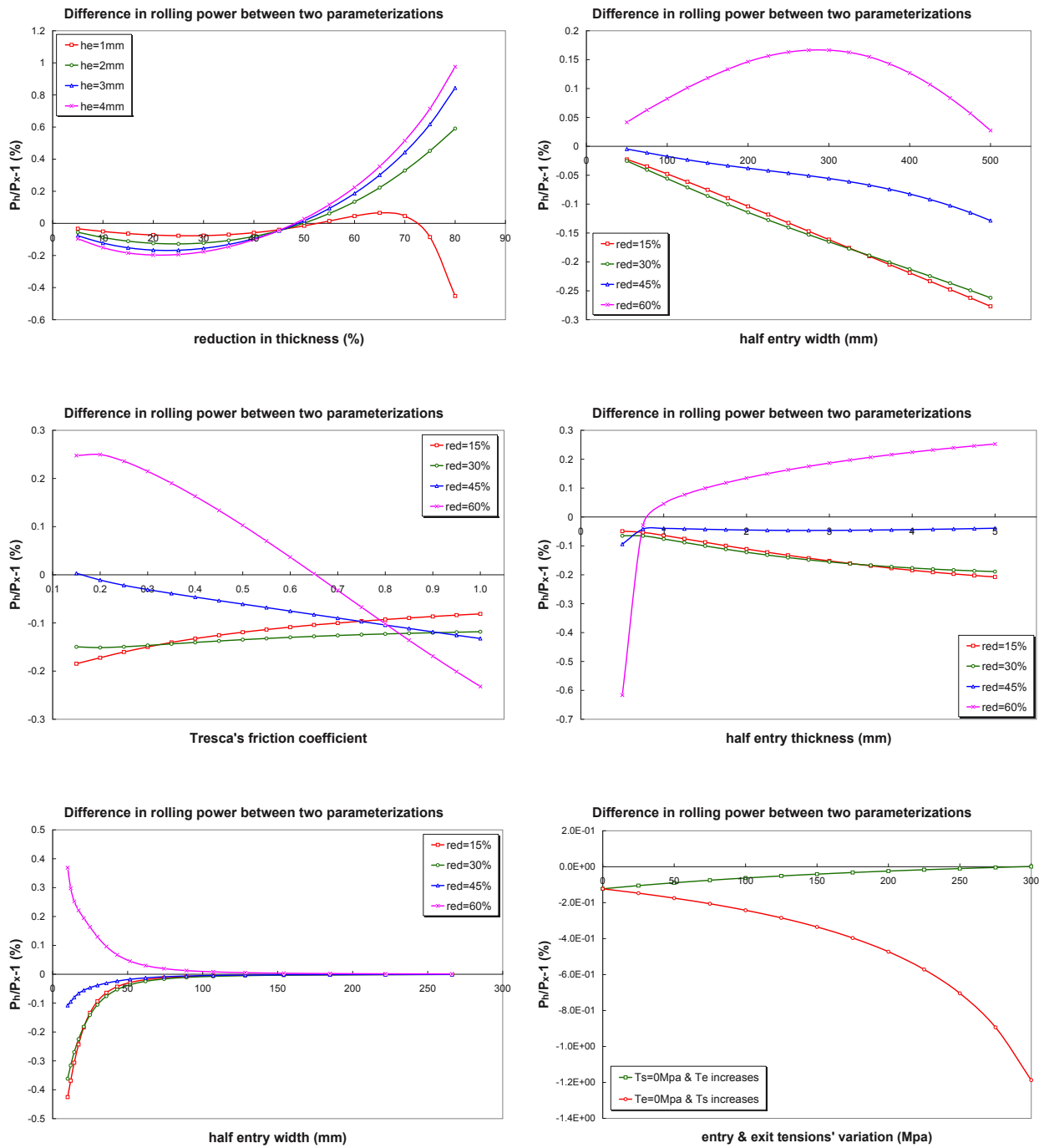


Figure 5.11: The difference in rolling power obtained with (%) of *form 2* in comparison with that obtained with *form 1*.

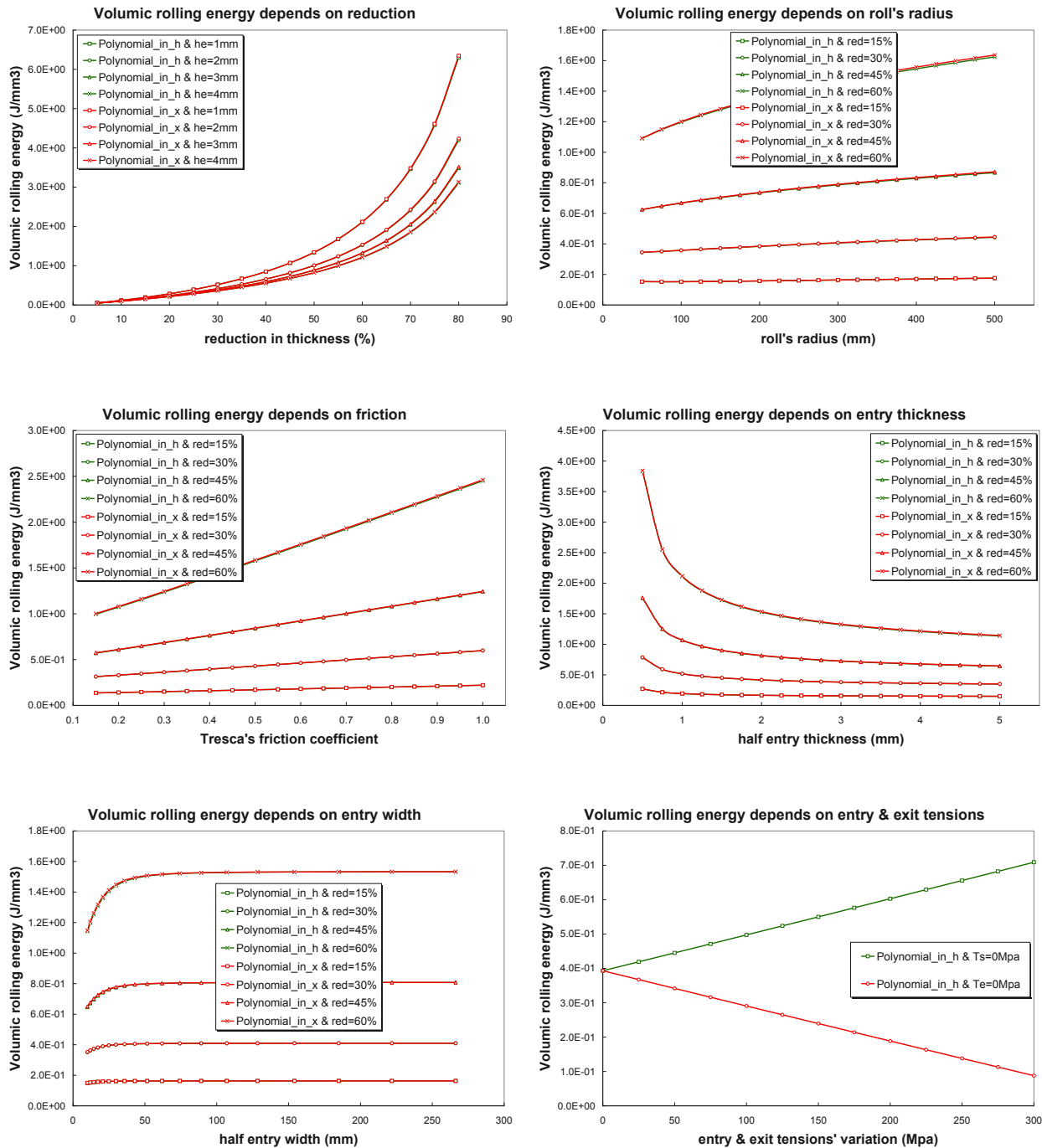


Figure 5.12: Influence of rolling parameters on specific rolling energy.

Chapter 6

UBM for crowned strip rolling

Contents

6.1	Velocity field proposition	124
6.1.1	Assumptions	124
6.1.2	Kinematically admissible conditions and velocity field in area II	125
6.1.3	Velocity field in area I	127
6.1.4	Velocity field in area III	127
6.2	Calculation of the powers	129
6.2.1	Power of plastic deformation	129
6.2.2	Power of discontinuity of velocity	130
6.2.3	Power of friction	131
6.2.4	Power of entry and exit tensions	131
6.3	Numerical resolution	131
6.3.1	Width function parameterizing	131
6.3.2	Minimization	132
6.4	Comparison between <i>UBM</i> and <i>Lam3-Tec3</i>	132
6.5	Conclusion	133

Introduction

The previous chapter (5) shows the typical models in the literature, from statistical to *FEM* and *UBM* ones predicting the width spread for flat strip rolling. These models consider a rectangular form of the strip. On the other hand, for certain long and shape rolling processes, an important number of 3D models were developed to predict the shape variation including the width spread. Some are based on *FEM* [78, 79, 55], others on *UBM* [96, 1].

For flat automotive product rolling, some efforts were made in the subject of the strip shape (thickness profile). Such studies aim at analyzing the flatness and roll force distribution across the width direction. The width spread is also analyzed and the results show out that the downstream shape influences closely the lateral spread. This mechanism has been modelled by various authors using a mixture of analytical and numerical methods [109, 73, 3, 30, 29]. These analyses also point out that for thin strip rolling there is a very small lateral spread, with the exception near the edge where the lateral stress is small allowing the material to spread, rather than being compressive (in the lateral direction) as is the case for plane strain rolling conditions. This is the width spread caused by "edge drop phenomenon".

In this chapter, a new *UBM* approach is developed for cold rolling of strip with an initial thickness crown that might be created by the earlier rolling process (hot rolling or previous stand). The model allows to understand how the strip spread depends on the change of the strip thickness profile in rolling. First, an analysis is proposed to study

kinematically admissible velocity fields by supposing some simplifying hypothesis. As the geometry of the strip is more complex than the case of flat strip rolling, the roll bite is divided into three areas and the velocity field is different throughout each of them. Then, the rolling power are calculated correspondingly to the three zones. All the powers calculations are more complicated and need being approximated numerically. The Gauss's method is used and the computing time is well improved. On the other hand, the numerical resolution is the same as in the previous chapter. The only change is that there are more parameters in the rolling power function to minimize because the real and virtual width functions are parameterized using three parameters instead of two in the case of flat rectangular strip. The same method, Newton-Raphson is used for optimization problem.

6.1 Velocity field proposition

6.1.1 Assumptions

Firstly, the general assumptions presented in the previous chapter (see subsection 5.3.2) are also assumed. In addition, some specific assumptions (denoted SA) which are associated only to a crowned strip rolling will be necessary to simplify the velocity field construction.

6.1.1.a SA1:

The first SA mentions that in the upstream, the strip has a positive crown, *i.e* the strip thickness is maximum at the center and decreases along the width direction. In other words, the strip entry thickness $h_e(y)$ is a mono-decreasing function. In industry, this type of crown is observed almost all the time. Hence, the center of the strip is in the contact with the roll before the edges. The roll-bite is divided into two parts: partial and total rolled parts. It is possible, thus to distinguish three areas associated with these two parts as shown in Figure 6.1. In each area, the velocity field is different and will be studied one by one in the next section by considering the kinematically admissible conditions.

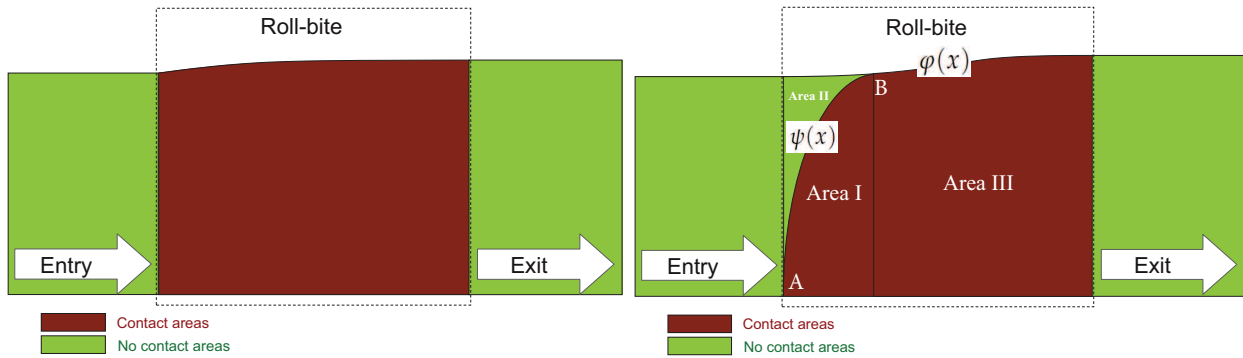


Figure 6.1: Comparison of the roll-bite geometry between a flat (left) and a crowned (right) strip rolling.

This assumption allows determining the function $\psi(x)$ representing the interface between the areas **I** and **II**. To begin with, let imagine that the strip has no lateral spread in the way that lateral velocity is equal to zero everywhere in the strip. To simplify the reading of the thesis, this no-spread configuration is conventionally called **imaginary configuration**. The interface between the areas **I** and **II** is presented by a function $\psi_0(x)$ that satisfies the following equation:

$$h_e(\psi_0(x)) = h(x) \Leftrightarrow \psi_0(x) = h_e^{-1}(h(x)) \quad (6.1)$$

where $h(x)$ is the thickness imposed by the work-roll profile. As a reminder, $h(x) = R + h_s - \sqrt{R^2 - x^2}$ for a circular work-roll. To determine the function $\psi(x)$, let return to the **real configuration** in which the strip spreads and the lateral velocity may be different from zero anywhere. To simplify further, an additional hypothesis is assumed as follows.

6.1.1.b SA2:

The displacement of material elements in the area **II** in comparison with the imaginary configuration is just a translation in horizontal plane. In other words, this area is not affected by the roll but only by the lateral spread of the area **I**. Thus,

$$\begin{cases} u_x^{II} = V_e \\ u_y^{II} \text{ is independent on } y \\ u_z^{II} = 0. \end{cases} \quad (6.2)$$

In consequence, the fact that $u_y^{II} = \text{constant}$ allows to determine the function $\psi(x)$ in the real configuration as:

$$\psi(x) = \psi_0(x) + \varphi(x) - w_e \quad (6.3)$$

and the fact that $u_z^{II} = 0$ implies that

$$h(x, y) = h_e(y - \varphi(x) + w_e) \quad (6.4)$$

everywhere in the area **II**.

6.1.2 Kinematically admissible conditions and velocity field in area **II**

6.1.2.a Boundary conditions

On contact surface $z = h(x)$: the velocity must be tangential to the surface. Then :

$$u_z^{I,III}(x, y, z = h(x)) = u_x^{I,III}(x, y)h'(x). \quad (6.5)$$

From equations 5.22 and 6.5 we have:

$$u_z^{I,III}(x, y, z = h(x)) = \frac{h'(x)}{h(x)} u_x^{I,III}(x, y)z. \quad (6.6)$$

On the virtual lateral surface $y = \varphi(x)$: the velocity is tangential to the virtual lateral surface represented by the function $\varphi(x)$ that may be different from real lateral surface $w(x)$ in a current iteration of numerical resolution. That means

$$u_y^{I,III}(x, \varphi(x)) = \varphi'(x)u_x^{I,III}(x, \varphi(x)). \quad (6.7)$$

In this state, the velocity in the area **II** is completely known

$$\boxed{\begin{aligned} u_x^{II} &= V_e \\ u_y^{II} &= V_e \varphi' \\ u_z^{II} &= 0. \end{aligned}} \quad (6.8)$$

On plan of symmetry $y = 0$: the condition of symmetry of lateral velocity is written as

$$u_y(x, y = 0) = 0. \quad (6.9)$$

6.1.2.b Volume flow rate conservation

The volume flow rate is calculated easily in the upstream part by :

$$C_{vol} = V_e S_e = V_e \int_0^{w_e} h_e(y_0) dy_0. \quad (6.10)$$

In area I and II: In this part, the volume flow rate is composed of two terms corresponding to the two areas **I** and **II** :

$$C_{vol}^I = h \int_0^\psi u_x^I dy \quad (6.11)$$

and

$$C_{vol}^{II} = V_e \int_\psi^\varphi h(x, y) dy \quad (6.12)$$

In using equations 6.27, 6.4 and in changing of variable $y_0 = y - \varphi + w_e$, we obtain

$$C_{vol}^{II} = V_e \int_{\psi_0}^{w_e} h_e(y_0) dy_0 \quad (6.13)$$

Thus, the flow rate conservation can be expressed by :

$$\begin{aligned} C_{vol} &= C_{vol}^I + C_{vol}^{II} \\ \Rightarrow C_{vol}^I &= h \int_0^\psi u_x^I dy = V_e \int_0^{\psi_0} h_e(y_0) dy_0. \end{aligned} \quad (6.14)$$

In area III: the flow rate conservation condition is given by

$$C_{vol} = h \int_0^\varphi u_x^{III} dy = V_e \int_0^{w_e} h_e(y_0) dy_0 \quad (6.15)$$

6.1.2.c Conditions of incompressibility

In continuous velocity field areas

As can be seen previously, the material is considered incompressible, *i.e* the velocity must satisfy the equation 5.21 everywhere. In the area **II**, the velocity given by the equation 6.8 is automatically verified this condition. Let consider this equation for area **I** and **III** :

$$\nabla \underline{u}^{I,III} = \frac{\partial u_x^{I,III}}{\partial x} + \frac{\partial u_y^{I,III}}{\partial y} + \frac{\partial u_z^{I,III}}{\partial z} = 0. \quad (6.16)$$

On the surfaces of velocity discontinuity

The same as the case of flat strip rolling, on the exit surface, there is no discontinuity of velocity. On the other hand, a crowned strip rolling geometry is more complicated and may have plural surfaces of velocity discontinuity instead of one. At the entry between upstream part and area **II**, there is no discontinuity. This will be a condition concerning the width function $w(x)$. The first surface of discontinuity of velocity is the interface between the areas **I** and **II**, and the second is between the areas **I** and **III**. In general, the condition of pertinence of a velocity field on a surface of discontinuity is that the normal velocity through this surface is to be continuous. Study now this condition for these two surfaces of velocity discontinuity.

Surface of velocity discontinuity between the areas I and II :

$$\begin{aligned} (\underline{u}^{II} - \underline{u}^I) \underline{n}^{I-II} &= 0 \\ \Leftrightarrow u_y^{II}(x) - u_y^I(x, \psi(x)) &= \psi' \left[u_x^{II}(x) - u_x^I(x, \psi(x)) \right]. \end{aligned} \quad (6.17)$$

Surface of velocity discontinuity between the areas I and III:

$$u_x^{III}(-L, y) = u_x^I(-L, y) \quad \text{for } \forall y \in [0, \varphi]. \quad (6.18)$$

6.1.3 Velocity field in area I

In the previous section, a kinetically admissible velocity field in the area **II** was proposed as given in equation 6.8. In this section, we search for a kinetically admissible velocity field in area **I**. The equation 6.14 can be rewritten as :

$$\int_0^\psi u_x^I dy = \frac{V_e}{h} \int_0^{\psi_0} h_e(y_0) dy_0.$$

By using a simple change of integration variable $y_0 = \frac{\psi_0}{\psi} y$ we have :

$$\begin{aligned} \int_0^\psi u_x^I dy &= \frac{V_e}{h} \int_0^\psi h_e\left(\frac{\psi_0}{\psi} y\right) \frac{\psi_0}{\psi} dy \\ \Leftrightarrow \int_0^\psi \left(u_x^I - \frac{V_e}{h} h_e\left(\frac{\psi_0}{\psi} y\right) \frac{\psi_0}{\psi} \right) dy &= 0. \end{aligned}$$

We propose thus

$$u_x^I = \frac{V_e}{h} h_e\left(\frac{\psi_0}{\psi} y\right) \frac{\psi_0}{\psi}. \quad (6.19)$$

The component u_z^I is easily determined by the equation 6.6. In addition, the equation 6.16 becomes :

$$\begin{aligned} \frac{\partial u_y^I}{\partial y} &= -\frac{\partial u_x^I}{\partial x} - \frac{\partial u_z^I}{\partial z} \\ \text{or } \frac{\partial u_y^I}{\partial y} &= -\frac{V_e}{h} \left[h_e'\left(\frac{\psi_0}{\psi} y\right) \left(\frac{\psi_0}{\psi}\right)' \frac{\psi_0}{\psi} y + h_e\left(\frac{\psi_0}{\psi} y\right) \left(\frac{\psi_0}{\psi}\right)' \right] \end{aligned}$$

Furthermore, in using the condition of symmetry with respect to the plan $y = 0$, equation 6.9, we obtain :

$$u_y^I = -\frac{V_e}{h} h_e\left(\frac{\psi_0}{\psi} y\right) \left(\frac{\psi_0}{\psi}\right)' y. \quad (6.20)$$

Hence, the velocity field in this area is completely determined while the condition on the surface of discontinuity between area **I** and **II** has not been used yet. We will demonstrate that this condition is satisfied by the velocity field proposed. In substituting the equations 6.19 and 6.20 into the equation 6.17, we have :

$$\begin{aligned} V_e \varphi' + V_e \left(\frac{\psi_0}{\psi}\right)' \varphi &= \psi' \left(V_e - V_e \frac{\psi_0}{\psi} \right) \\ \Leftrightarrow \varphi' + \varphi_0' &= \psi'. \end{aligned}$$

Indeed, this equation is implied by the equation 6.27. The velocity field in area **I** is finally kinematically admissible and given by:

$$\boxed{\begin{aligned} u_x^I &= \frac{V_e}{h} h_e\left(\frac{\psi_0}{\psi} y\right) \frac{\psi_0}{\psi} \\ u_y^I &= -\frac{V_e}{h} h_e\left(\frac{\psi_0}{\psi} y\right) \left(\frac{\psi_0}{\psi}\right)' y \\ u_z^I &= u_x^I \frac{h'}{h}. \end{aligned}} \quad (6.21)$$

6.1.4 Velocity field in area III

A velocity field similar to the one of the area **I** in which ψ is replaced by φ and ψ_0 by w_e , is a possible solution for the area **III**. However, in this way, at the roll bite exit, the longitudinal velocity depends always in y while it is observed

not. *Lam3-Tec3* gives a solution that is homogenous in lateral direction at the exit, see Figure 6.2. For this reason in our model, the velocity is homogenized by a function noted $\zeta(x)$ depending only on x . This function is equal to 1 at the begin and 0 at the end of the area **III**. This function is freely modeled and in this study, it is chosen as

$$\zeta = \left(\frac{x}{L^{III}} \right)^2 \quad (6.22)$$

where L^{III} is the contact length of the totally laminated part (area **III**). We propose finally:

$$u_x^{III} = \frac{V_e}{h} h_e \left(\frac{w_e}{\varphi} y \right) \frac{w_e}{\varphi} \zeta(x) + \bar{\zeta}(x).$$

The function $\bar{\zeta}(x)$ is added to ensure the volume flow rate conservation. Thus, it is identified by the equation 6.15 as

$$\bar{\zeta} = \frac{V_e}{h} \frac{S_e}{\varphi} (1 - \zeta)$$

where $S_e = \int_0^{w_e} h_e(y) dy$ denotes the entry across section of the strip.

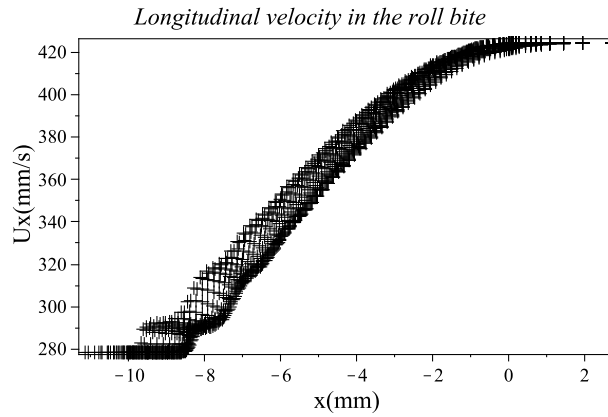


Figure 6.2: Illustration with *Lam3-Tec3* result for E16 rolling conditions - Table C.2 - with a 0.06mm-crown over strip half thickness. The longitudinal velocity is non-homogenous along the roll-bite but is homogenous at the roll bite exit.

Moreover, the condition on the contact surface (equation 6.6) gives directly u_z^{III} . And u_y^{III} is determined by the condition of incompressibility (equation 6.16). Finally, a solution of velocity filed in the area **III** can be:

$$\begin{cases} u_x^{III} = \frac{V_e}{h\varphi} \left[w_e h_e \left(\frac{w_e}{\varphi} y \right) \zeta + S_e (1 - \zeta) \right] \\ u_y^{III} = u_x^{III} \frac{\varphi'}{\varphi} y + \frac{V_e}{h\varphi} \zeta' \left[y S_e - \varphi \int_0^{\frac{w_e}{\varphi} y} h_e(y_0) dy_0 \right] \\ u_z^{III} = u_x^{III} \frac{h'}{h} z. \end{cases} \quad (6.23)$$

with $\zeta(x)$ is given by equation 6.22.

6.2 Calculation of the powers

6.2.1 Power of plastic deformation

6.2.1.a Areas I and III

In these areas, the velocity fields are similar. It is thus possible to generalize the calculation by studying a velocity field as follows

$$\begin{cases} u_x(x, y) \\ u_y(x, y) \\ u_z(x, y, z) = d_{33}(x, y)z \end{cases} \quad (6.24)$$

in a given domain Ω . This is a general form for the two velocity fields presented previously corresponding to the two areas. For the area **I**, the domain is $\Omega_I = [x = (-L, -L^{III}), y = (0, b^I(x))]$ and $\Omega_{III} = [x = (-L^{III}, 0), y = (0, w(x))]$ for the area **III**.

The plastic deformation power is computed by

$$\begin{aligned} J_{\dot{\epsilon}} &= \int_{\Omega} \sigma_0 \sqrt{\frac{2}{3} \underline{d} : \underline{d}} d\Omega \\ &= \int_{\Omega} \sigma_0 \sqrt{\frac{2}{3} (d_{xx}^2 + d_{yy}^2 + d_{zz}^2 + 2d_{xy}^2 + 2d_{xz}^2 + 2d_{yz}^2)} d\Omega \\ &= \int_{\Omega_{2D}} dx dy \int_0^h \sqrt{\frac{2}{3}} \sigma_0 \sqrt{Q^2 + g^2 \left(\frac{z}{h}\right)^2} dz \\ &= \frac{\sigma_0}{\sqrt{6}} \int_{\Omega_{2D}} dx dy \int_0^1 2\sqrt{Q^2 + g^2 z^2} h dz^* . \end{aligned}$$

with Ω_{2D} is the projection of Ω on the xy plan. Then, by using the formula B.1, we obtain

$$J_{\dot{\epsilon}} = \frac{\sigma_0}{\sqrt{6}} \int_{\Omega_{2D}} h \left[\sqrt{Q^2 + g^2} + \frac{Q^2}{g} \ln \frac{g + \sqrt{Q^2 + g^2}}{Q} \right] dx dy . \quad (6.25)$$

where

$$\begin{aligned} Q(x, y) &= \sqrt{d_{xx}^2 + d_{yy}^2 + d_{zz}^2 + 2d_{xy}^2} = \sqrt{\frac{\partial u_x^2}{\partial x} + \frac{\partial u_y^2}{\partial y} + d_{zz}^2 + \frac{1}{2} \left(\frac{\partial u_x}{\partial y} + \frac{\partial u_y}{\partial x} \right)^2} \\ g(x, y) &= \frac{1}{h} \sqrt{\frac{1}{2} \frac{\partial d_{zz}^2}{\partial x} + \frac{1}{2} \frac{\partial d_{zz}^2}{\partial y}} . \end{aligned}$$

6.2.1.b Area II

In this area, the velocity field is much more simple. The only component that is different from zero is :

$$d_{xy}^{II} = d_{yx}^{II} = \frac{1}{2} V_e \varphi'' . \quad (6.26)$$

Therefore, the plastic deformation power is easily calculated :

$$J_{\dot{\epsilon}}^{II} = \frac{\sigma_0}{\sqrt{3}} V_e \int_{-L}^{-L^{III}} \int_{w^I(x)}^{w(x)} \varphi'' h^{II}(y) dx dy$$

where $w^I(x)$ is the width of the area **I**. This function can be determined by the following equation

$$w^I(x) = \psi_0(x) + w(x) - w_e \quad (6.27)$$

which is in the same analogy as the equation 6.27. By changing the variable $y_0 = y - w^I(x) + \psi_0(x) = y - w(x) + w_e$, we obtain finally

$$J_{\dot{\epsilon}}^{II} = \frac{\sigma_0}{\sqrt{3}} V_e \int_{-L}^{-L^{III}} \varphi'' dx \int_{\psi_0}^{w_e} h_e(y_0) dy_0 \quad (6.28)$$

6.2.2 Power of discontinuity of velocity

6.2.2.a Between the areas **I** and **II**

The discontinuity of velocity is previously proved tangential to the surface. It is given by :

$$\Delta \underline{V}^{I-II} = \begin{bmatrix} \Delta u_x^{I-II} \\ \Delta u_y^{I-II} \\ \Delta u_z^{I-II} \end{bmatrix} = \begin{bmatrix} u_x^{II}(x, \psi) - u_x^I(x, \psi) \\ u_y^{II}(x, \psi) - u_y^I(x, \psi) \\ 0 - u_x^I(x, \psi) h' \frac{z}{h} \end{bmatrix}$$

Then,

$$\begin{aligned} J_{\Delta u}^{I-II} &= \frac{\sigma_0}{\sqrt{3}} \int_{S_{dis}^{I-II}} \|\Delta \underline{V}\|^{I-II} ds \\ &= \frac{\sigma_0}{\sqrt{3}} \int_A^B \int_0^h \sqrt{\Delta u_x^{I-II^2} + \Delta u_y^{I-II^2} + u_x^{I^2} h'^2 \frac{z^2}{h}} dz dl \\ &= \frac{\sigma_0}{\sqrt{3}} \int_A^B \int_0^1 h \sqrt{Q^{I-II^2} + g^{I-II^2} z^{*2}} dz^* dl \end{aligned}$$

Using again the formula B.1, we have

$$J_{\Delta u}^{I-II} = \frac{\sigma_0}{\sqrt{3}} \int_{-L}^{-L^{III}} h \left[\sqrt{Q^{I-II^2} + g^{I-II^2}} + \frac{Q^{I-II^2}}{g^{I-II}} \ln \frac{g^{I-II} + \sqrt{Q^{I-II^2} + g^{I-II^2}}}{Q^{I-II}} \right] \sqrt{1 + \psi'^2} dx \quad (6.29)$$

where

$$\begin{aligned} Q^{I-II}(x) &= \sqrt{\Delta u_x^{I-II^2} + \Delta u_y^{I-II^2}}(x, \psi(x)) \\ g^{I-II}(x) &= u_x^{I^2} h'^2(x, \psi(x)). \end{aligned}$$

6.2.2.b Between the areas **I** and **III**

The discontinuity of velocity between area **I** and **III** is more simple because it has an unique component different from zero which is given by $\Delta u_y^{I-III} = (u_y^{III} - u_y^I)(x = -L^{III}, y)$. The power consumed by this discontinuity of velocity is:

$$J_{\Delta u}^{I-III} = \frac{\sigma_0}{\sqrt{3}} h(-L^{III}) \int_0^{w(-L^{III})} \|\Delta u_y^{I-III}\| dy \quad (6.30)$$

6.2.3 Power of friction

As explained before, the velocity fields in areas **I** and **III** are similar and we can use the form 6.24 to present both of them. We will find a formula which is applicable to calculate the friction power on the contact surface with the roll of these two areas. The area studied is noted $S_{contact} = [X_1, X_2] \times [0, Y_2(x)]$. For the area **I**, $X_1 = -L$, $X_2 = -L^{III}$, $Y_2(x) = w^I(x)$ and for the area **III**, $X_1 = -L^{III}$, $X_2 = 0$, $Y_2(x) = w(x)$.

The difference of velocity between the roll and the strip on these contact surfaces is:

$$\Delta \underline{V} = \sqrt{\left(u_x \sqrt{1+h'^2} - V_c\right)^2 + u_y^2}.$$

Thus,

$$\begin{aligned} J_{fric} &= \frac{m\sigma_0}{\sqrt{3}} \int_{S_{contact}} \|\Delta \underline{V}\| dS \\ &= \frac{m\sigma_0}{\sqrt{3}} \int_{X_1}^{X_2} dx \int_0^{Y_2(x)} \sqrt{\left(u_x \sqrt{1+h'^2} - V_c\right)^2 + u_y^2} \sqrt{1+h'^2} dy \end{aligned} \quad (6.31)$$

6.2.4 Power of entry and exit tensions

The power of the entry and exit tensions is given by :

$$J_{ten} = - \int_{S_e} T_e u_x^I(-L, y, z) dS + \int_{S_s} T_s u_x^{III}(0, y, z) dS.$$

In using the expressions of velocity fields studied before, we obtain :

$$J_{ten} = V_e S_e \left[-T_e + T_s \frac{b}{\varphi}(x=0) \right]. \quad (6.32)$$

6.3 Numerical resolution

Numerical integral: The integrations in expressions of all these powers are performed using the Gauss's method (see Appendix A.2). This attractive method of integration helps to reduce significantly the computing time of the program.

Algorithm of resolution: As a reminder, the UBM principle for the crowned strip rolling is the same as for the flat strip rolling presented in the previous chapter. Therefore, the numerical resolution is also the same, shown in Figure 5.5.

6.3.1 Width function parameterizing

In the previous chapter, there were presented two parameterizing forms for width function $w(x)$ (and virtual width function $\varphi(x)$). The first is a 3rd-order polynomial of x and the second one is a polynomial of $h(x)$. We, then, demonstrated that the second form relating directly the width function to the reduction in thickness via the function $h(x)$ is better than the first form for a reduction $r < 45\%$ in giving smaller rolling power, see section 5.3.7.b.

By consequence, in this case of crowned strip rolling, let study only the second form. However, in this case, the width function must have a null derivative at the first point of contact at $x = -L$ because the width of the laminated area (area **I**) tends to zero at this point. This condition is represented in the following form of the width function by a new parameter k :

$$w(x) = w_e + \left(\frac{h - h_e^{centre}}{h_s - h_e^{centre}} \right)^k [\alpha + \beta(h - h_s)]. \quad (6.33)$$

for $k > 1$.

6.3.2 Minimization

The minimization of the power function to find the optimal velocity field for each iteration is also performed by Newton-Raphson method presented in the subsection 5.3.5.c. Nevertheless, there are 4 parameters instead of 3 with the new parameter k in addition. The calculation time increases certainly but the method is unchanged.

Remark: The optimization program for 4 parameters has not been built yet while it is possible to fix the parameter k , $k = 2$ for example, and minimize the rolling power in 3 parameters by using the 3-parameter optimization program already done in previous chapter. Therefore, by varying the value of k and by observing the variation of the corresponding minimum rolling power we can choose the best value of k that gives the minimum rolling power.

6.4 Comparison between UBM and Lam3-Tec3

This section presents the width spread calculated by the UBM model for a crowned strip rolling, in comparison with Lam3-Tec3. The strip is narrow enough so that all elastic deformations are negligible. The rolling parameters correspond to the trial E16 of the experiments with hard steel presented in Table C.2. Nevertheless, the entry thickness is modified so that the average entry thickness is the same and the strip crown is a polynomial of degree 2 or 4, two typical forms of strip crown.

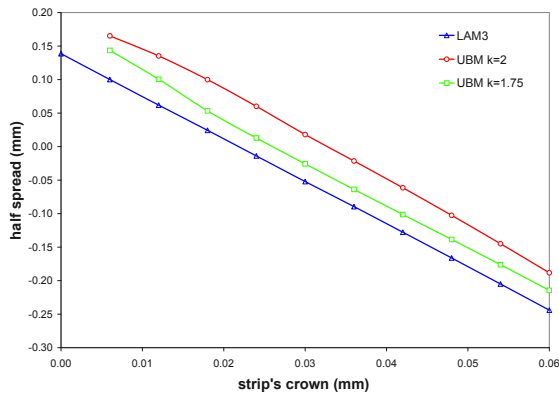


Figure 6.3: Crown of degree 2. Comparison of width spread between UBM and Lam3-Tec3.

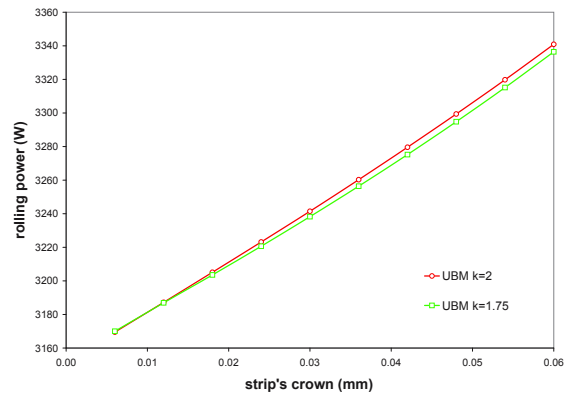


Figure 6.4: Crown of degree 2. Comparison of rolling power calculated by UBM with different values of k .

Figure 6.3 shows the width spread calculated by Lam3-Tec3 and by the UBM model with $k = 2$ and $k = 1.75$ for a crown of polynomial of degree 2. It is observed that the three curves have a same negative slope, implying the width spread decreases almost linearly as a function of strip crown and that the UBM results match very well those of Lam3-Tec3 independently on the value of k in terms of the tendency. In absolute value, with $k = 1.75$ the UBM curve is closer to the Lam3-Tec3 curve than with $k = 2$. In addition, Figure 6.4 shows that the minimum rolling power corresponding to $k = 1.75$ is lower than that with $k = 2$. Knowing that the smaller the rolling power, the better width spread calculated by the UBM.

Similarly, for a crown of polynomial of degree 4, it can be seen in Figure 6.5 that the width spread decreases also linearly with an increase in the strip entry crown but more slightly. The UBM and Lam3-Tec3 have a good coherence in terms of tangency of this decrease. And in comparing the minimum rolling power calculated by the UBM for $k = 2$, $k = 1.75$ and $k = 1.5$ (see Figure 6.6) we conclude, an other time, that the more minimized the rolling power, the better width spread the UBM gives. Therefore, we need in a near future a 4-parameter to give better results.

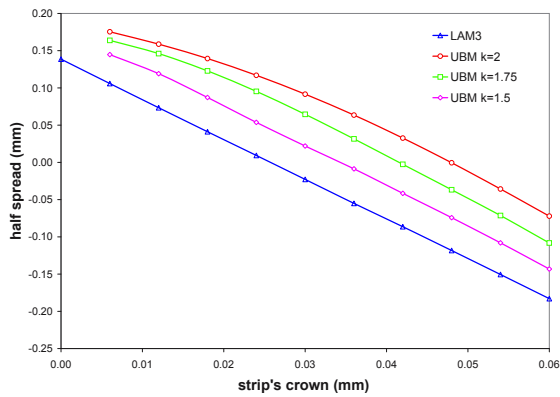


Figure 6.5: Crown of degree 4. Comparison of width spread between *UBM* and *Lam3-Tec3* .

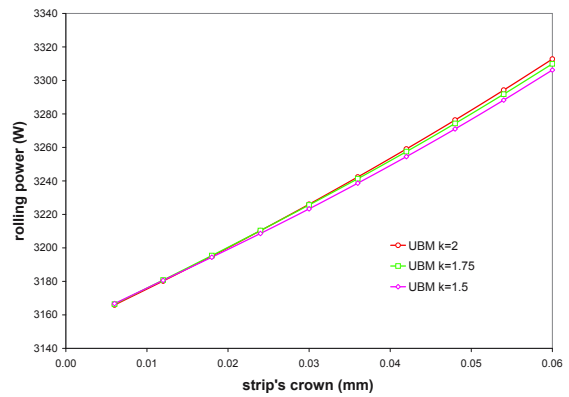


Figure 6.6: Crown of degree 4. Comparison of rolling power calculated by *UBM* with different values of *k*.

6.5 Conclusion

The previous chapter (5) presented existing models from statistical to *FEM* and *UBM* ones predicting the width spread for flat strip rolling. These models consider a rectangular cross section of the strip at the entry. For long and shape product rolling processes, an important number of 3D models were developed to predict the shape variation including the width spread. In this chapter, a new *UBM* approach is developed for cold rolling of a strip with initial thickness crown while work-roll is considered straight and perfectly cylindrical. The model allows to understand how the strip spread depends on the initial thickness profile. As the geometry of the strip is more complex than the case of flat strip rolling, the roll bite is divided into three areas in which the velocity field is different. The optimization of rolling power is performed by using Newton-Raphson algorithm. As a result, the model shows that the width variation decreases with an increase in the strip initial crown and the *UBM* results match very well those obtained with *Lam3-Tec3* .

This model development showed that the *UBM* is applicable even when the geometry seems to be complicated. Furthermore, similarly to this *UBM* model, it is possible to develop another one for a rectangular strip and crown work-rolls. When the work-roll crown is positive, *i.e* the center diameter is more important than the work-roll ends, the strip center is also in contact with the work-roll before the strip edges. The geometry problem would be treated in a resembling way. This is an interesting perspective of this chapter.

Chapter 7

A thermal-elastic-plastic width model

*The previous chapters present the UBM -based models for width variation of flat and crowned strip in rolling process. The results match well to the experiments on pilot mill using narrow strips. However, it is important to note that the UBM assumes a rigid-plastic behavior of the strip that is justified for a narrow strip because the elastic width variation are negligible. On the opposite, in industrial rolling the strip is large and the elastic width variation which is proportional to the strip width is no longer negligible. This elastic deformation is reversible but it has important impact on the plastic one. In addition, friction and plastic deformation powers may heat the strip about 50-100°C up. The material is, thus dilated in the width direction but it can not because of the contact friction with the roll. That creates compression plastic deformation - called thermal contraction. **In this chapter, after a bibliography review a new width variation model for online applications is developed taking into account effects of elastic and thermal deformations in addition to the width variation of UBM model proposed in the previous chapters.***

Contents

7.1 Bibliographic review on width variation in industrial cold rolling	136
7.1.1 Main phenomena involved in width variation	136
7.1.2 Effect of rolling parameters on width variation	137
7.1.3 Existing models for industrial rolling width variation	141
7.2 Analytical thermal-elastic-plastic width variation model	143
7.2.1 Why develop new model?	143
7.2.2 Assumptions - analysis of width variation using <i>Lam3-Tec3</i>	143
7.2.3 Proposal of thermo-elasto-plastic width variation model	148
7.2.4 Development of simplified model	151
7.3 A simplified entry elasto-plastic compression model	151
7.4 A simplified elastic spring back model - elastic slab method	153
7.4.1 Assumptions	155
7.4.2 Basic equations	155
7.4.3 Resolution algorithm	157
7.5 A simplified model for roll-bite	158
7.5.1 Total width variation in roll-bite - rigid-plastic <i>UBM</i>	158
7.5.2 Elastic deformation - Stress approach	158
7.5.3 Thermal dilatation - temperature variation model	159
7.6 Summary	160

Introduction

In the first section, an analysis based on *Lam3-Tec3* results allow to bring out the contribution of elastic deformation in the total plastic width spread in a large strip rolling case. Following, a new assumption is proposed to build a new model taking into account elastic deformation effect. In this model, as the elastic deformation is important, it is necessary to determine stress fields in the strip. In the roll-bite, the material is plasticized in a almost-plane strain deformation condition, the slab method (see section 2.3.1.a) gives a good prediction of average values over thickness direction of the stress fields. Then, two following sections present simplified methods to model two phenomena: elasto-plastic compression at the entry and elastic spring back at the exit of roll bite. Finally, in the last section, comparisons of width spread with *Lam3-Tec3* as well as with industrial rolling observations are presented to validate the new model.

7.1 Bibliographic review on width variation in industrial cold rolling

7.1.1 Main phenomena involved in width variation

Based on some studies existing perviously in literature, N.Legrand *et al* [64] give a global view about phenomena involved in the width variation of the strip in flat automotive rolling. According to the authors, the width spread in rolling is a thermo-mechanic problem. They bring out three main physical phenomena contributing to the width variation as follows.

7.1.1.a Edge drop

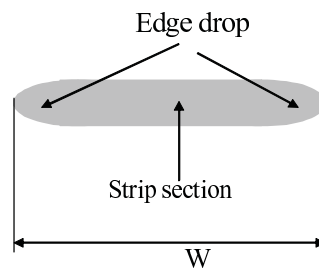


Figure 7.1: Strip cross section after rolling.

This phenomenon is due to a 3D plastic flow near strip edges (approximately 20 to 30 mm from strip edges). Especially, at the strip edges the roll is significantly deformed elastically (see Figures 1.8 and 2.12) decreasing locally the strip thickness. By consequence, after rolling the strip thickness is lower at the edges than at the center (Figure 7.1). This phenomenon promotes an increase of the strip width. The problem of strip edge drop in cold rolling has been extensively investigated [56, 74, 21, 42] and certain number of other works.

7.1.1.b Elastic spring back

According to Legrand *et al* [64] the strip "elastic spring back" at the roll-bite exit contributes to strip width increase in cold rolling. In roll bite, the transverse stress is negative, *i.e* the material is compressed in width direction. And the elastic recovery mainly corresponds to transverse stress σ_{yy} relaxation just at the roll-bite exit. The authors give an estimation of this transverse stress based on *Lam3-Tec3* FE ([40]) simulations. They point out that the contribution of transverse stress relaxation to width broadening depends on steel strip work hardening which can be significant in cold rolling. Due to this work hardening, strip elastic recovery at the roll bite exit (relaxation of transverse stress σ_{yy}) is greater than strip elastic compression that takes place at the roll bite entry, thus strip width increases.

In this chapter (section 7.2.2.f), a further study of width variation phenomena shows that the elastic stress evolution in the roll-bite influences and changes the plastic transversal deformation. Therefore, its contribution in width variation

depends not only on material work hardening but also strongly on entry and exit tensions values as well as friction coefficients...

7.1.1.c Thermal contraction

Edwards [33] explains that successive strip thermal contraction in each inter-stand (due to cooling) combined with no possibility of strip thermal expansion in each roll bite (due to friction) is one possible cause of strip width decrease in cold rolling. During cold rolling, strip temperature increases in the roll bite due to plastic strain and friction. However, it is assumed that this temperature increase occurs without any possibility of thermal expansion due to roll-strip friction forces in the roll bite. Then outside the roll-bite, strip is cooled down by coolant spray and natural cooling with a free thermal contraction. As a consequence, the thermal irreversible expansion/contraction tends to decrease strip width continuously through the successive stands.

Indeed according to us, more precisely the thermal deformation itself is reversible but in the roll-bite due to the contact constrain the thermal dilatation generates a negative plastic deformation across the width that is irreversible and contributes to the width necking of the strip. More details will be pointed out in the section 7.2.2.f.

7.1.2 Effect of rolling parameters on width variation

Width variation is mostly negative in industrial rolling

Lafontaine [60] investigated on strip width variation in cold rolling using a database from Arcelor Florange's 5-stand tin-plate and 4-stand sheet cold tandem mills. He observed that strip width variation is usually negative (necking) and this width necking is statistically higher on tin plate than on sheet product. He showed that the wider the strip, the higher the width necking and that width contraction is statistically higher with IF (soft) steels than with harder ones.

Using width measurement device existing on the industrial plants combined with a new width measurement device developed by ArcelorMittal research, Legrand and Ngo [65] analyse database of several cold rolling mills. They observe equally that the width variation in both tin plate and sheet cold rolling mills is usually negative. They perform also specific trials to analyse width variation problem using ArcelorMittal research Maizières pilot mill and some ArcelorMittal industrial rolling mills. The results of this work as well as those of a few other articles are presented hereafter to point out the effect of rolling parameters on the width variation.

7.1.2.a Anisotropic friction effect

On a study of edge drop phenomenon, Legrand *et al* [64] perform cold rolling trials on ArcelorMittal Research Maizières pilot mill with a 50m/min rolling speed and strip width varying from 60 to 70 mm, initial thickness from 1.5 to 3.0 mm, work-roll diameter of 400 mm. They measure the entry and exit profile in order to bring out the edge drop phenomenon. In addition, the authors use *Lam3-Tec3* ([40]) to simulate these trials to get better understanding of- the phenomena. By comparing the measured strip exit thickness profiles and that obtained by *Lam3-Tec3* simulation, the authors bring out the anisotropy of friction coefficient: friction coefficient in the transverse direction (across the strip width) μ_y is higher than that in the rolling direction μ_x . Figure 7.2 show an example of the trial named E16 where the anisotropic factor is equal to 2. They obtain anisotropy facto varying from 2 to 4 depending on the trials conditions.

According to the authors, such an anisotropic friction can be explained by the work-roll circumferential striations due to grinding process which generates an anisotropy of the work-roll roughness as showed by Figure 7.3.

By comparing width variations obtained from pilot mill trials and from numerical simulations, they show that the FE model *Lam3-Tec3* is able to predict strip width with an accuracy of +/-0.25 mm if anisotropic friction is taken into account (see Figure 7.4). They conclude that transverse friction has a significant influence on strip width: a variation of transverse friction μ_y by a factor of 2 to 4 makes a strip width modification by 0.5 to 1.2 mm. Therefore, transverse friction appears as a possible actuator for strip width control.

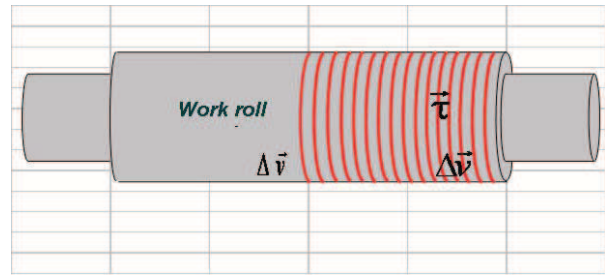
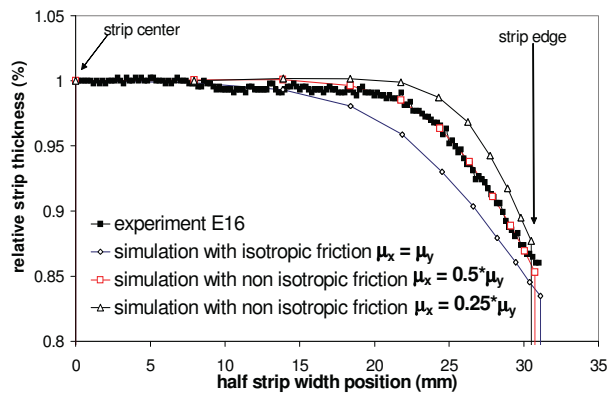


Figure 7.2: Comparison calculated/measured strip thickness profile: evidence of an anisotropic roll-bite friction ($\mu_x = 0.0496$, $\mu_y = 2*\mu_x$).

Figure 7.3: Illustration of grinding striations inducing anisotropic friction in cold rolling.

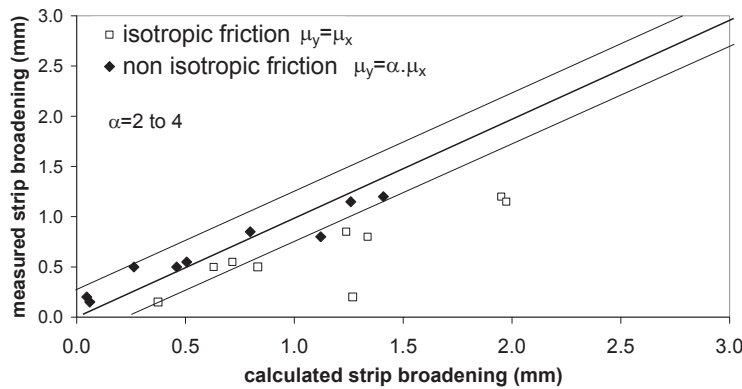


Figure 7.4: Comparison calculated/measured strip width variations. Lam3-Tec3 simulations with isotropic and non-isotropic roll-bite friction coefficients for both steel grades.

7.1.2.b Effect of bending is indeed effect of strip flatness

Schwarz [98] analyzed strip width variation on Biache’s cold tandem mill (France) where a strip width sensor was implemented at the tandem exit. He showed that roll bending, strip tension, rolling pressure and thermal effects have a significant influence on strip width. However no model was used or developed. The results presented were essentially statistical and not predictive.

By doing similar simulations using Lam3-Tec3 ([40]) as [64] (described above) Legrand and Ngo [65] analyse the effect of bending on width variation on stand 1 and 5 of a tin plate rolling mill. They show that the higher the bending the lower the edge drop and by consequence the smaller the width variation (or more necking if the width variation is negative).

An increase of bending gives long center tendency in strip flatness by distancing the heads of top and bottom work-rolls and lightening the reduction at the strip edges. Indeed, the strip width variations and flatness are determined by the work-rolls in-charged profile whatever this profile is a results of a bending or a designed inimical profile. In other words, the strip width variation depends on its flatness and the change in flatness during rolling. The bending is a parameter influencing the strip flatness like many others such as the work-roll initial profile, thermal crown (related to a non-homogeneous distribution temperature along the rolls)...

7.1.2.c Effect of tensions

In addition, Legrand and Ngo [65] performed trials on Florange 4-stand automotive rolling mill by rolling 2 coils with same rolling conditions except inter-stand tensions. The rolling parameters are given in Table (7.1). Both coils thickness is reduced from 2.8mm to 0.66mm thanks to the 4 stands. T_1 and T_5 are the entry and exit tensions of the tandem mill and T_{ij} is the interstand tension between stands i and j . It can be seen that the coil "37870-07" is rolled with higher tensions and gets 2mm more necking than the coil "37870-01". The authors conclude hence that the strip tensions have important influence on the width variation and can be a potential width actuator.

Coil ID Unit	$2w_e$ mm	$2h_e$ mm	$2h_s$ mm	T_1 Mpa	T_{12} Mpa	T_{23} Mpa	T_{34} Mpa	T_4 Mpa	Δw mm
37870-01	1170	2.8	0.66	54.5	150.2	156.2	199.1	39.0	-2.91
37870-07	1169	2.8	0.66	65.7	176.5	228.4	246.7	39.3	-4.89

Table 7.1: Industrial trials to analyse tensions effect on width variation: thicknesses, tensions and width variations of the 2 tested coils (negative width variation means width decrease).

7.1.2.d Effect of reduction

Figure 7.5 shows strip width variation produced by Florange 5-stands cold tin plate mill for two different levels of strip reduction (86.5%: D&I food and 92.0%: D&I drink), for the same steel grade D&I. Each point of the graphic corresponds to one coil. It can be seen that an increase of strip thickness reduction by from 86.5% to 92.0% decreases strip width from 5mm to 10mm. Thus, the higher the total reduction the higher the strip width decrease possibly due to a stronger thermal effect (higher heating in the bite) that promotes a width decrease.

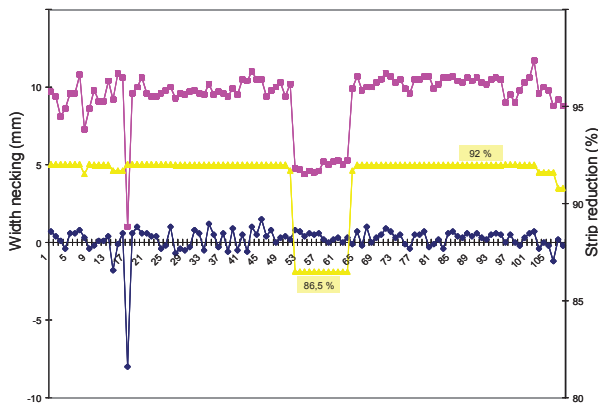


Figure 7.5: Important effect of reduction on width variation is showed by a comparison of two series of coils rolled at two reduction levels at Florange 5-stand tin plate mill.

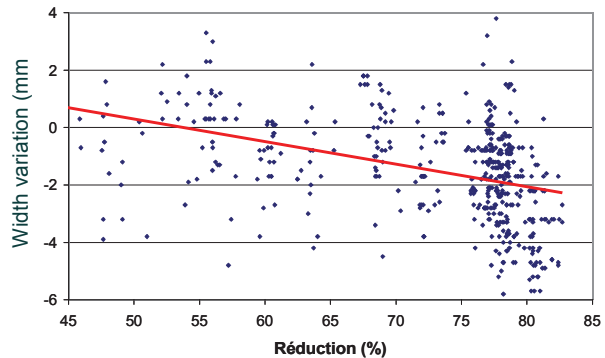


Figure 7.6: Effect of reduction on width variation observed statistically on database of Mardyck 5-stand sheet tandem mill.

7.1.2.e Effect of nominal strip width

As a reminder Lafontaine [60] has already concluded in his study that the higher the strip width the more important the width necking. Legrand and Ngo [65] confirmed this tendency based on a database analysis of width variation at Mardyck 5-stand and Florange 4-stand sheet cold rolling mills - see Figures 7.7 and 7.8. They explained the tendency by the fact that the higher the strip width the higher the thermal contraction contribution as it is proportional to the strip nominal width. It can be seen more in detail from Figure 7.7 that, indeed the strip width variation amplitude

increases with an increase in strip nominal width meaning that if the width variation is negative (necking) it becomes more negative and inversely if it is positive (spread) it gets more positive.

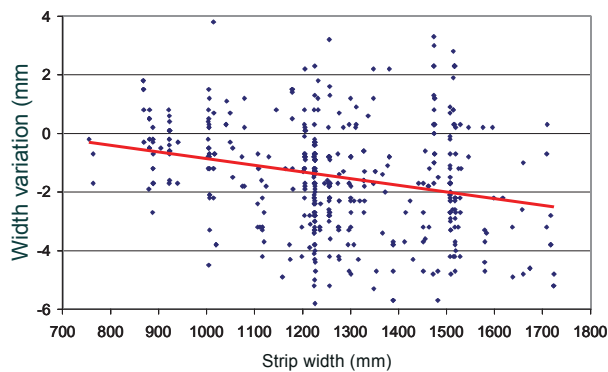


Figure 7.7: Effect of strip nominal width on width variation observed statistically on database of Mardyck 5-stand sheet tandem mill.

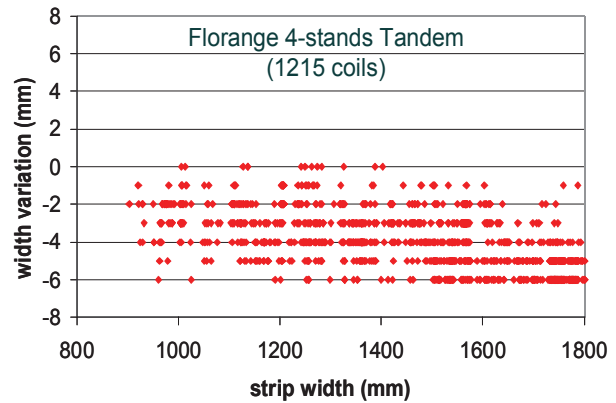


Figure 7.8: Same observation on Florange 4-stand sheet tandem mill.

7.1.2.f Effect of strip entry thickness and strip yield stress

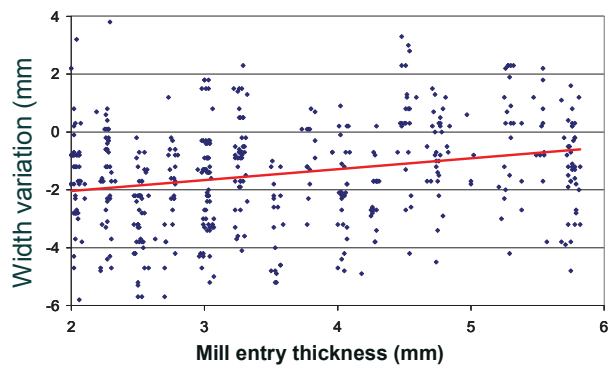


Figure 7.9: Effect of strip entry thickness on width variation observed statistically on database of Mardyck 5-stand sheet tandem mill.

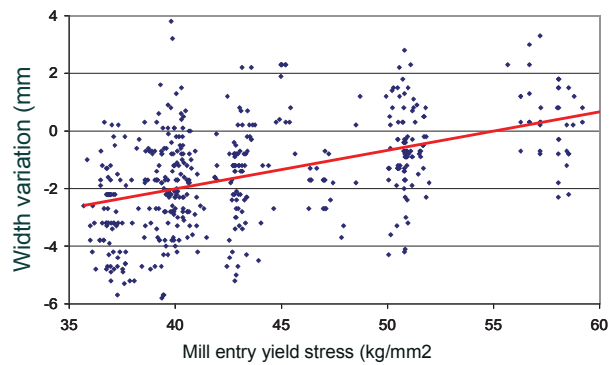


Figure 7.10: Effect of strip yield stress on width variation observed statistically on database of Mardyck 5-stand sheet tandem mill.

It can be seen in Figure 7.9 that the strip width increases with an increase in strip entry thickness but the effect is relatively weak. On the other hand, Figure 7.10 shows that on the Mardyck 5-stand sheet tandem mill the harder the strip the higher the strip width which is possibly due to a higher elastic broadening. However, it is worth to note that, in industrial rolling the harder the steel the lower total reduction. That means the graphic 7.10 does not shows the only effect of strip yield stress and the tendency could be that of the total reduction. Indeed, for soft steel as the total reduction is higher there is more width necking due to reduction effect.

7.1.2.g Summary of rolling parameters effect on strip width variation

Table 7.2 shows a recapitulation of the experiment trials and the industrial database analyses existing in the literature about the impact of rolling parameter on strip width variation. Only in some cases, the corresponding authors give

explanations (or share their point of view about possible explanations) because the phenomena remains. These results will be used to validate the simplified model which is developed afterward.

$\Delta w_{Total} = \Delta w_{EdgeDrop} + \Delta w_{SpringBack} - \Delta w_{Thermal}$						
Parameter	Nomenclature	Edge drop Δw	Spring back Δw	Thermal Δw	Total Δw	Impact level
Nominal width	w ↗	?	↗	↗	$ \Delta w $ ↗	high
Reduction	red ↗	?	?	↗	↘	high
Entry thickness	h_e ↗	?	?	?	↗	low
Strip yield stress	σ_0 ↗	↗	↗	↗	↗	?(*)
Entry & exit tensions	T_e, T_s ↗	?	?	?	↘	average
Work-roll radius	R ↗	↗	?	?	↗	low
Bending	B ↗	↘	?	?	↘	average
Friction anisotropy	α_μ ↗	↘	?	?	↘	average

Table 7.2: Summary of bibliographic review about how rolling parameters influence the strip width variation with explanations if existing. (*) means that the effect of strip yield stress is not clear due to the correlation between strip yield stress and the total reduction in industrial database.

7.1.3 Existing models for industrial rolling width variation

7.1.3.a Streamlines finite difference method - [23]

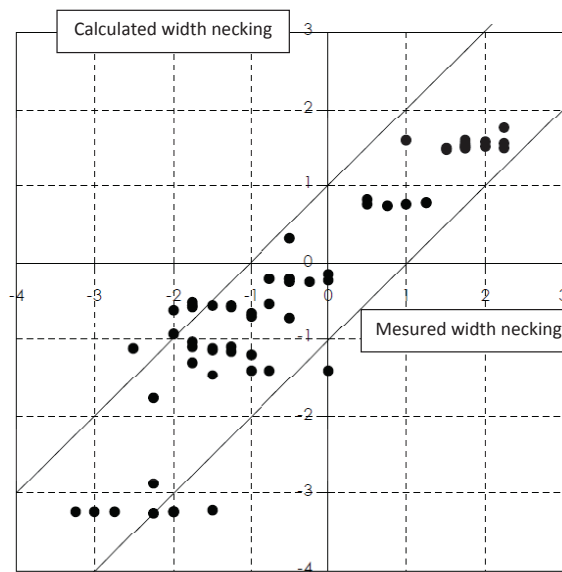


Figure 7.11: Comparison of predicted width necking to the measurements done at Feblatil 4-stand tandem mill.

Counhaye [23] developed a multidimensional model based on finite differences numerical resolution, called "Streamlines" model. This method allows to simulate stationary problem formed by equilibrium equations combined with elasto-plastic behavior. The model is coupled to a tool deformation model based on influence functions method and a Coulomb friction model with possibility to take into account friction anisotropy. The principle of the method is to integrate the elasto-plastic laws and equilibrium equations along material streamlines. The streamlines are adjusted iteratively at the same time with shear stresses. This resolution gives stationary solution very similar to that obtained by finite elements methods. The streamlines approach is an alternative solution to *FEM*.

Using the "Streamlines" model, Counhay [23] was the first to quantitatively predict strip width variation in flat automotive cold rolling conditions. The author interpret width variation mechanism by three phenomena given perviously in the section 7.1.1. The strip width variations predicted by the model is in correct agreement with measured widths (accuracy +/- 1mm) - see Figure 7.11

7.1.3.b Lam3-Tec3 - [40, 64]

As already mentioned above, Legrand *et al* [64] developed a model for width variation in large strip industrial rolling conditions and pointed out the three phenomena involved in the strip width variation as can be seen previously (section 7.1.1) and state that the total width is given by:

$$\Delta w = \Delta w_{EdgeDrop} + \Delta w_{SpringBack} - \Delta w_{Thermal} \quad (7.1)$$

where $\Delta w_{EdgeDrop}$, $\Delta w_{SpringBack}$ and $\Delta w_{Thermal}$ are respectively the width variation parts due to edge drop, spring back and thermal contraction phenomena. The first two terms $\Delta w_{EdgeDrop}$ and $\Delta w_{SpringBack}$ are obtained by mechanical simulation using *Lam3-Tec3*. As for the thermal term, it is given by:

$$\Delta w_{thermal} = \alpha \Delta T \quad (7.2)$$

where ΔT is the variation of strip temperature from entry to exit of the roll-bite. The authors use a thermal model developed by Dusser *et al* [32].

Important contribution of elastic and thermal deformation

The authors applied this model to simulate the trials that they performed on ArcelorMittal Maizières Research pilot mill to interpret these trials and bring out the anisotropy of friction (see 7.1.2.a). They also applied the model to analyse the contribution of each of the three terms in sheet and tin plate mills. The results are given in Tables 7.3 and 7.4. It can be seen that the three terms are in a same order in both tandem mill configurations. The thermal contraction in the case of tin plate mill is even very important because of very high reduction. The width variation due to elastic spring back is also important. It is twice greater the edge drop term in the case of sheet tandem mill and equivalent to edge drop in the case of tin plate.

	Stand 1	Stand 2	Stand 3	Stand 4	Stand 5	Total
$\Delta w_{EdgeDrop}$ (mm)	0.26	0.31	0.16	0.11	0.01	0.85
$\Delta w_{SpringBack}$ (mm)	0.16	0.24	0.30	0.26	1.00	1.96
ΔT (°C)	34.8	16.1	30.6	23.7	6.4	111.6
$\Delta w_{Thermal}$ (mm)	0.6	0.28	0.53	0.41	0.11	1.92
Δw_{Total} (mm)	-0.18	0.27	-0.07	-0.04	0.9	0.89

Table 7.3: Results of contribution of width variation phenomenon using *Lam3-Tec3* and a thermal model [32] on Mardyck tandem mill for a nominal width $w = 1232mm$, $h_e = 5.54mm$ and $h_s = 2.54mm$, $red = 54\%$ (see [64] for more details).

	Stand 1	Stand 2	Stand 3	Stand 4	Stand 5	Total
$\Delta w_{EdgeDrop}$ (mm)	0.14	0.09	0.38	0.30	0.79	1.70
$\Delta w_{SpringBack}$ (mm)	0.24	0.17	0.14	0.26	0.61	1.40
ΔT (°C)	32.2	24.0	50.2	52.3	82.4	241.1
$\Delta w_{Thermal}$ (mm)	0.41	0.31	0.64	0.67	1.05	3.07
Δw_{Total} (mm)	-0.03	-0.05	-0.12	-0.11	0.35	0.03

Table 7.4: Results of contribution of width variation phenomenon using *Lam3-Tec3* and a thermal model [32] on Cockerill tin plate mill for a nominal width $w = 910mm$, $h_e = 2.50mm$ and $h_s = 0.087mm$, $red = 84.5\%$ (see [64] for more details).

7.2 Analytical thermal-elastic-plastic width variation model

7.2.1 Why develop new model?

Importance of elastic and thermal deformation: According to the studies presented above for industrial rolling process of flat and large product, there are three mechanisms contributing to strip width variation: edge drop, elastic spring-back (relaxation of transversal stress at exit of the stand) and thermal contraction. Edge drop and elastic spring-back promotes an increase of strip width while the thermal contraction makes it decrease which explains why in industrial database the width variation can be positive and negative. Furthermore, to quantify the part of each mechanism, [64, 65, 23] developed models based on FEM (*Lam3-Tec3*) and FDM ("Streamlines method") and illustrated that the width variation due to elastic spring-back and the thermal contraction is important in general flat cold rolling condition. And they can be greater than the width variation due to edge drop in tin-plate mill condition with high reduction level.

In the chapter 5, some statistical models (see 5.1) as well as *UBM*-based models (5.2) for width variation analysis are presented. The width variation predicted by these models is always positive while the industrial observations in automotive cold rolling mills show that the width variation is mostly negative - called necking. These models assuming a rigid-plastic behavior of the strip are not able to model the spring back phenomena.

No existing model is fast enough for online applications In addition, there exist very few attempts to develop width variation models for flat automotive cold rolling. In our knowledge, only FEM (*Lam3-Tec3*, *Abaqus*) and Streamlines Finite Difference (see [64, 65, 23]) are able to describe width variation problem but the computing time is too high (several hours) to be used for preset and online control applications.

Conclusion: Those are the reason why we aim at developing a rapid model able to predict the width variation in industrial flat large strip cold rolling. The approach is to use *Lam3-Tec3* to analyse and understand in details width variation phenomena in order to adopt suitable hypotheses allowing to develop this simplified model in keeping the key phenomena and influence parameters.

7.2.2 Assumptions - analysis of width variation using *Lam3-Tec3*

Three general assumptions

Firstly, here are the assumptions that are not based the analysis of *Lam3-Tec3* results. They are, nevertheless necessary to fixe the working domain of the model to develop.

7.2.2.a Symmetry:

The considered rolling process is both top-bottom and operator-motor side symmetric. Therefore, only one quarter of the geometry needs to be studied (see 2.1.1.b).

7.2.2.b Coulomb friction model:

As we are interested in elastic deformation, especially in the elastic spring back area where the strip is deformed elastically under contact with the work-roll at the exit of the roll-bite, Coulomb's law seem to be more realistic to model the friction. As a reminder, the Tresca's friction depending on the material yield stress is not suitable for elastic deformation areas where the yield stress does not involves in the problem.

7.2.2.c Work roll deformation:

The work-roll shape is considered circular and straight meaning that only the flattening can be taken into account by Hitchcock's model (see 2.4.2.a) and the deflection deformation is not considered. The edge drop is therefore not modelled by this model. The reader of this thesis will see later that a *UBM* -based model is one part of the width variation global model that we develop in this chapter. And the *UBM* -based model is the one presented in the section 5.3 which considers a circular and straight work-roll. By the way, as the chapter 6 presents an *UBM* -based model of width variation for a crowned strip, it is possible to develop an *UBM* -based model for a non-straight work-roll shape. This potential development is one of perspectives of this work.

Three specific assumptions - *Lam3-Tec3* simulations

Secondly, follows are the assumptions which are issued from the understanding of physical phenomena involved in width variation in cold rolling by analyzing *Lam3-Tec3* results. Let study the *Lam3-Tec3* simulation results for a industrial rolling conditions given in Table 7.5.

Stand	$2w_e(\text{mm})$	$2h_e(\text{mm})$	$2h_s(\text{mm})$	red(%)	$2R(\text{mm})$	$\bar{\sigma}_0(\text{Mpa})$	μ	$T_e(\text{Mpa})$	$T_s(\text{Mpa})$
1	1170.0	2.800	1.677	40.11	538.65	516.619	0.036412	51.0	150.0
2		1.677	1.007	39.95	517.24	555.480	0.038186	150.0	156.0
3		1.007	0.663	34.16	601.48	620.368	0.022206	156.0	199.2
4		0.663	0.652	1.66	550.81	640.000	0.110	199.2	39.0

Table 7.5: Typical industrial rolling conditions of flat automotive product - ArcelorMittal Florange 4-stand cold rolling mill.

***Lam3-Tec3* simulations:** For each stand, several *Lam3-Tec3* simulations are done taking into account different hypotheses as follows:

- elasto-plastic strip with 10 elements in the half thickness
- elasto-plastic strip with 1 element in the half thickness
- rigid-plastic strip with 1 element in the half thickness (indeed this calculation is performed using a elasto-plastic strip with Young modulus multiplied by 1000)
- thermo-elasto-plastic strip with 1 elements in the half thickness with heat exchange between WR and strip
- thermo-elasto-plastic strip with 1 elements in the half thickness without heat exchange between WR and strip
- thermo-elasto-plastic strip with 10 elements in the half thickness without heat exchange between WR and strip

As mentioned above, the strip flatness influences also the width variation. In order to compare these simulations, they are performed so that the strip flatness is the same. In fact, the thermal-elasto-plastic simulation give a same flatness as elasto-plastic one but the rigid-plastic does not. Thus, we choose work-roll initial profile (crown) to get a similar flatness as that of elasto-plastic.

7.2.2.d Average behavior across strip thickness - Slab method

The graphics in Figure 7.12 illustrate the profile of strip width variation from upstream to downstream of each of the four stands. It can be seen that the width spread is almost the same with 1 or 10 elements in half thickness of the strip. The only exception is the first stand but we do not have explanation for this exception. Hence, to model the width variation it is enough to model an average behavior (stress, strain, strain rate...) across strip thickness. This observation leads us to an assumption which is similar to that of slab method: ***To model the width variation, we can assume an homogeneous deformation across the thickness (as slab method - see 2.3.1.a).***

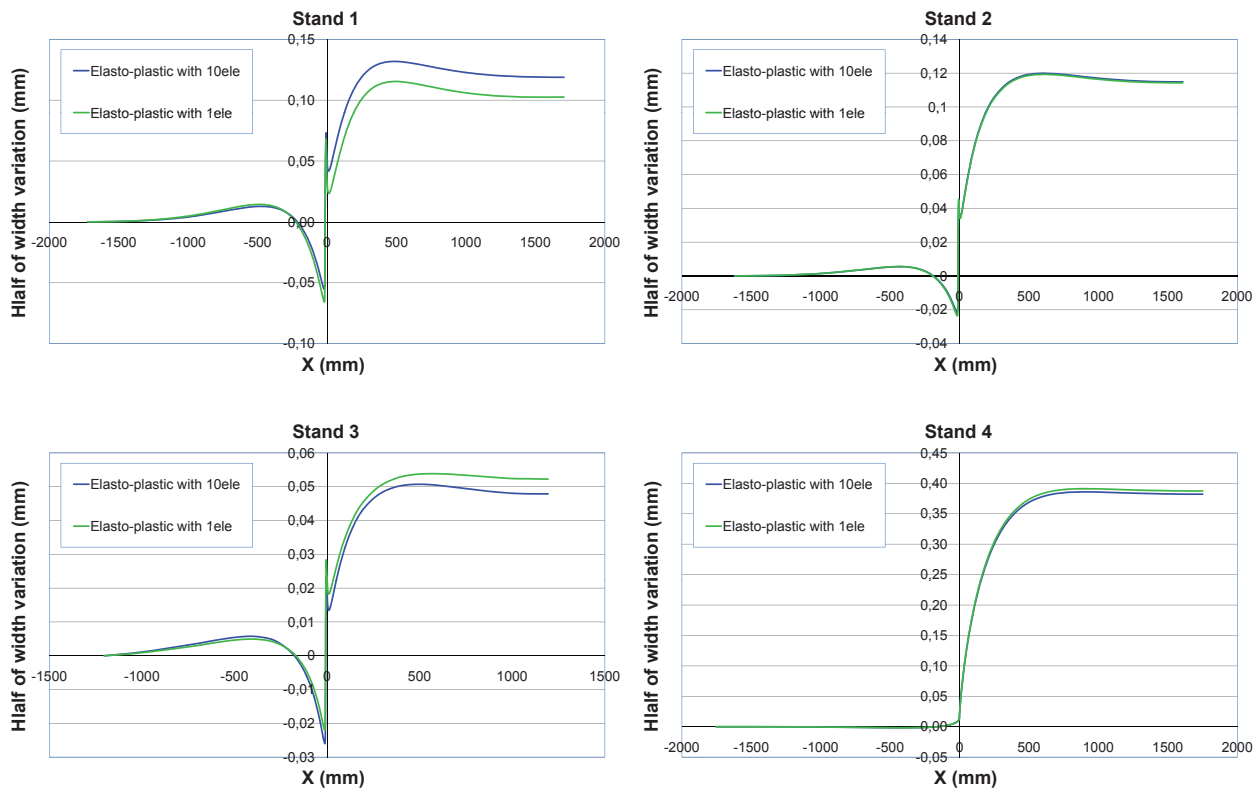


Figure 7.12: Comparison of width variation of *Lam3-Tec3* simulations using 10 and 1 element in strip half thickness for each of Florange cold rolling mill stands.

This assumption allows to simplify drastically our analysis and model development. From now on, the analysis will be based on *Lam3-Tec3* simulations with 1 element in the strip half thickness.

7.2.2.e The strip is deformed plastically before contact with the work-roll

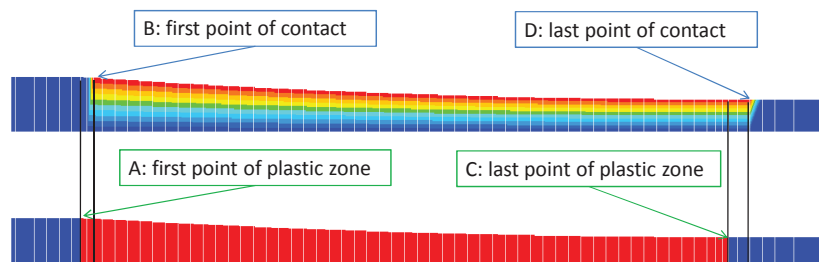


Figure 7.13: Stand 2: Comparison of contact and yield fields.

As a reminder, the existing models in the literature such as [17] and [27] (see sections 2.3.1.e and 2.3.1.f correspondingly) consider that there is a zone where the strip is already under contact with the strip and is deformed elastically before being deformed plastically. This zone is called elastic entry zone. However, in the contrary to this assumption, it can be seen in Figure 7.13 showing a comparison of contact and yield fields obtained with *Lam3-Tec3* for the stand 2 of ArcelorMittal Florange mill, that the strip is deformed before being in contact with the work-roll.

On the other hand, at the roll-bite exit *Lam3-Tec3* results shows, in a good agreement with existing models, an elastic recovery zone at the roll-bite exit where the strip is deformed elastically under contact with the work-roll.

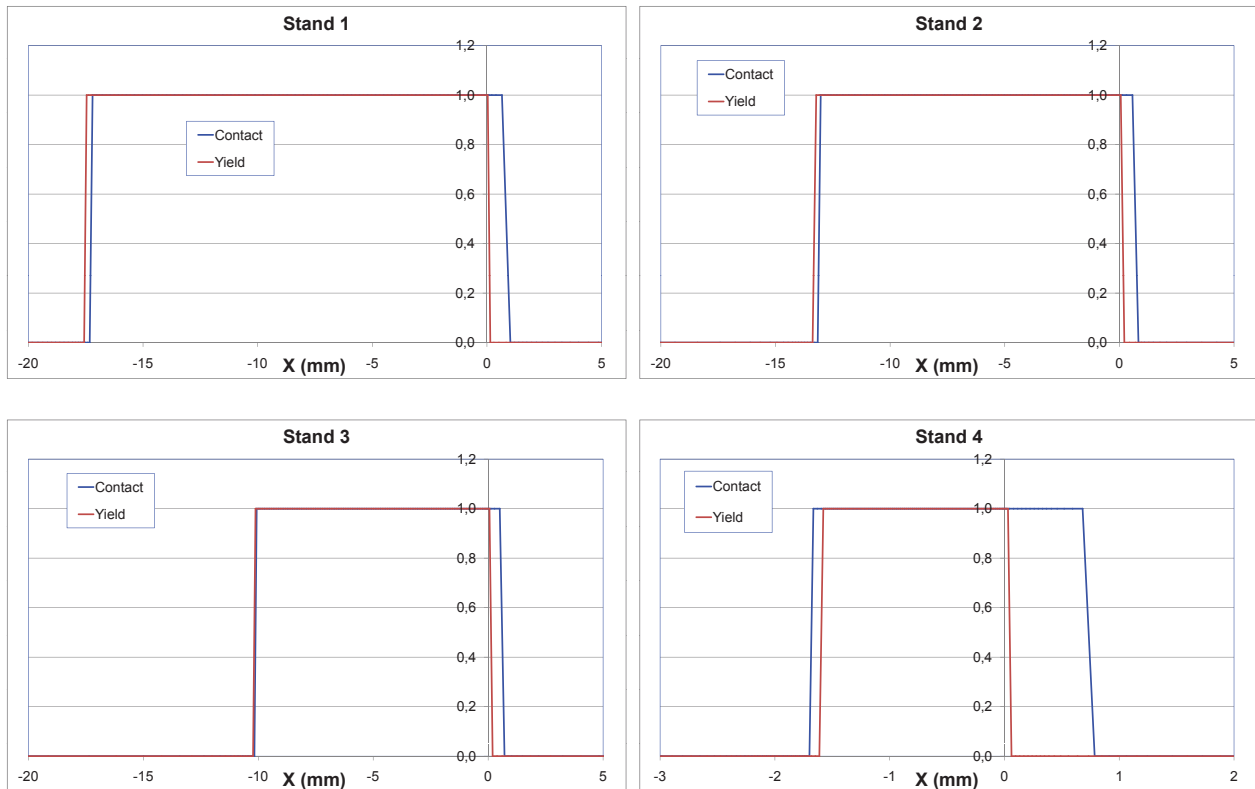


Figure 7.14: The contact and yield fields obtained with *Lam3-Tec3* for the four stands of ArcelorMittal Florange mill. Except the stand 4 where the reduction is very small $red = 1.66\%$, the strip is deformed plastically before contact.

Figure 7.14 shows *Lam3-Tec3* results about the contact and yield area for the four stands. It can be seen that for the first three stands 1, 2 and 3 the strip is deformed plastically before being in contact with the roll. But for the stand 4 with small reduction ($red=1.66\%$), the entry compression is purely elastic as supposed by [17] and [27]. The "Simplified entry compression model" presented in the section 7.3 is not good for the last stand. However, the assumption stating that the last point of plastic deformation is the lowest point of the roll C is quit verified. On the other hand this figure shows existence of an elastic contact area at the exit that is in a good agreement with the simplified model.

Finally, we consider that the strip deformation can be divided into three zones given in Figure 7.15 as follows:

1. **Elasto-plastic compression before contact:** The strip is deformed elastically and then plastically just before its contact with the roll.
2. **Roll-bite:** The roll-bite is defined as the zone from the first point of contact B to the last point of plastic deformation C. It is different to both the plastic zone as well as the contact zone.
3. **Exit elastic spring back:** This zone starts at the last plastic deformation point C and is divided itself into two zones, one under contact (CD) and the other is after last contact point D where the strip is free.

7.2.2.f Assumption of material flow in strip width direction

Impact of elastic deformation: Figures 7.16 show comparison of width variation profiles obtained with elasto-plastic and rigid-plastic strip behavior correspondingly to the four stands. The simulations with rigid-plastic behavior

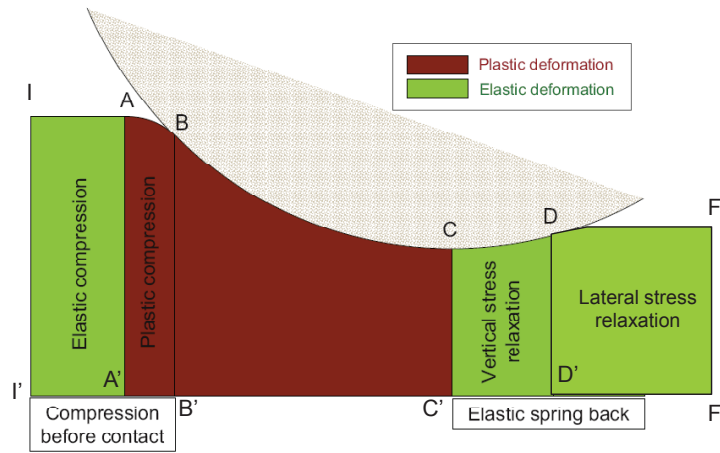


Figure 7.15: Roll-bite of an elasto-plastic strip in typical rolling conditions.

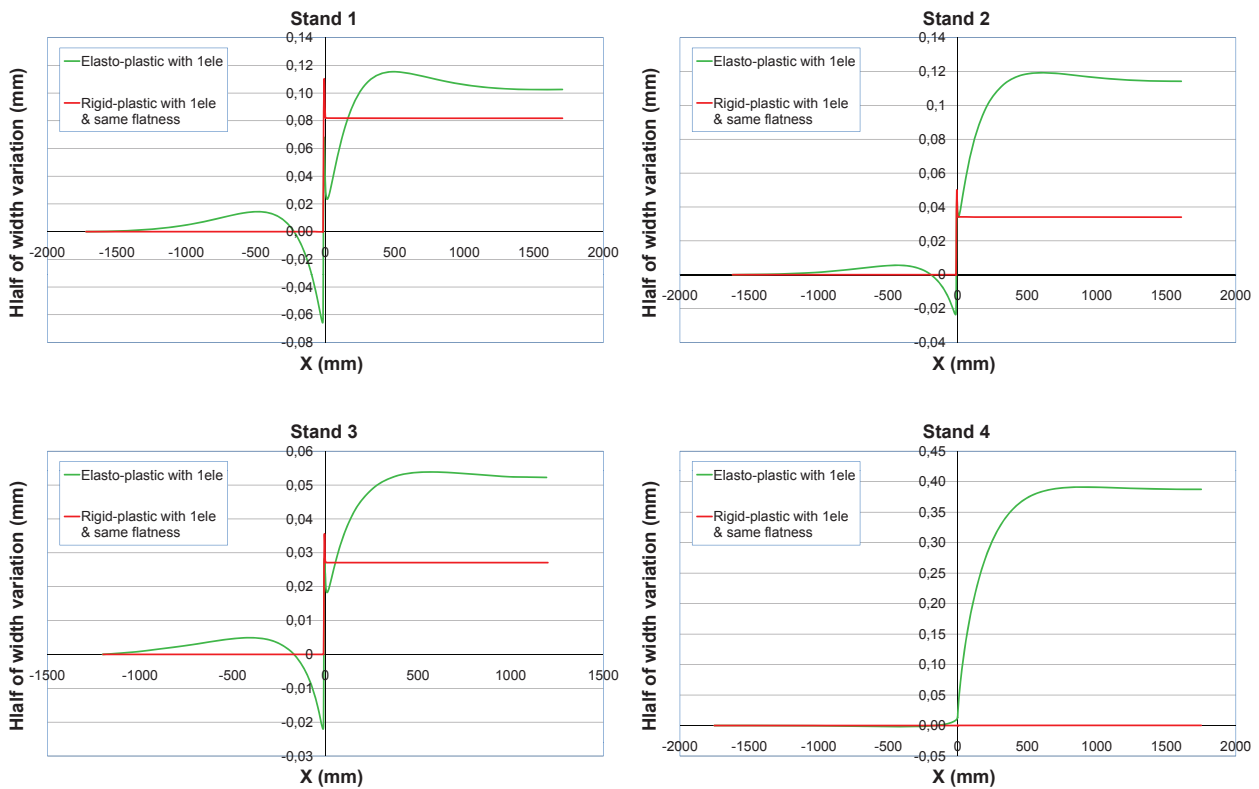


Figure 7.16: Comparison of width variation of *Lam3-Tec3* simulations using elasto-plastic and rigid-plastic strip behavior laws for ArcelorMittal Florange cold rolling mill stands.

give width variations much lower than those given by the elasto-plastic ones. This comparison illustrates that the elastic deformation has an important influence on the plastic one and need taking into account to well estimate the width variation of strip in industrial rolling.

Figures 7.17 show a zoom in the roll bite of Figure 7.16. In the roll-bite, the plastic and elastic spreads have an opposite sign and almost the same absolute value, implying that by action of friction the elastic spread is transformed to plastic spread to keep the same flow as the case of rigid-plastic behavior. In addition, observing that the two curves,

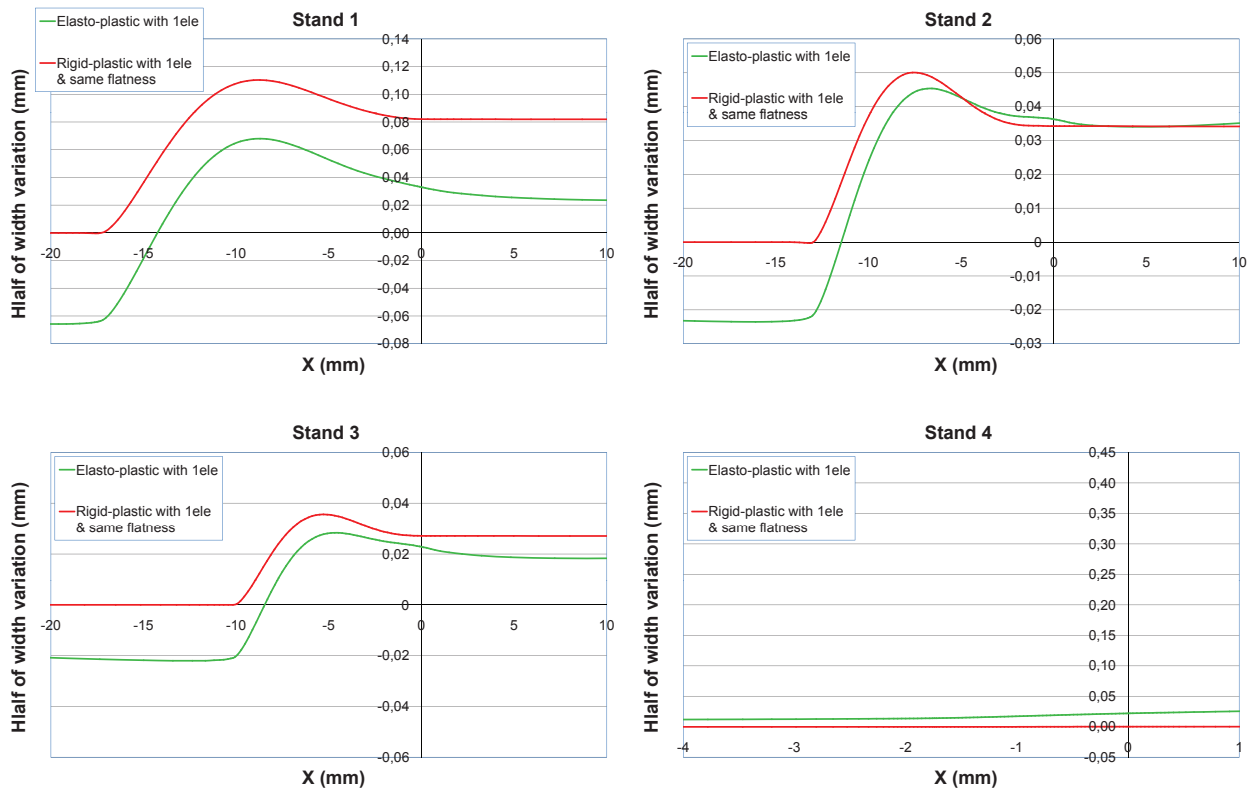


Figure 7.17: Comparison of width variation of *Lam3-Tec3* simulations using elasto-plastic and rigid-plastic strip behavior laws for ArcelorMittal Florange cold rolling mill stands.

elasto-plastic and rigid-plastic width variation profiles are not very different one from the other we propose therefore a new hypothesis to simplify impact of elastic deformation in the plastic width variation as follows:

Independent lateral flow assumption 1 - elasticity influence: In the roll bite the total elasto-plastic width variation profile is same as the rigid-plastic one. It means that the elastic deformation in the roll bite is completely transformed into plastic deformation or in other words, the total material flow in width direction is almost the same in the two cases: elasto-plastic and rigid-plastic simulations.

Impact of thermal deformation - Thermal contraction: Similarly to the study of the impact of elastic deformation, thermal-elasto-plastic simulations with *Lam3-Tec3* are performed considering that 100% of plastic deformation and friction dissipations are transformed into heat. The friction dissipation is shared 50%-50% between the roll and the strip. The heat exchange coefficient between strip and roll is $htc = 2.10^4 \frac{w}{m^2K}$. As can be seen in Figure 7.18 that the total strip width variation of thermo-mechanical simulations is the same as that of mechanical ones. The assumption of independent lateral flow (announced above) is also verified. Like the elastic deformation the thermal width dilatation in the roll bite is also completely transformed into plastic one.

Independent lateral flow assumption 2 - thermal dilation influence: The total strip width variation profile of thermo-mechanical simulations is the same as that of mechanical one.

7.2.3 Proposal of thermo-elasto-plastic width variation model

7.2.3.a Formula of total width variation

According to these assumptions, in this section we present a new family of models of width variation in automotive flat products rolling. The principle is based on the *Independent lateral flow assumptions 1 - elasticity influence* and *2*

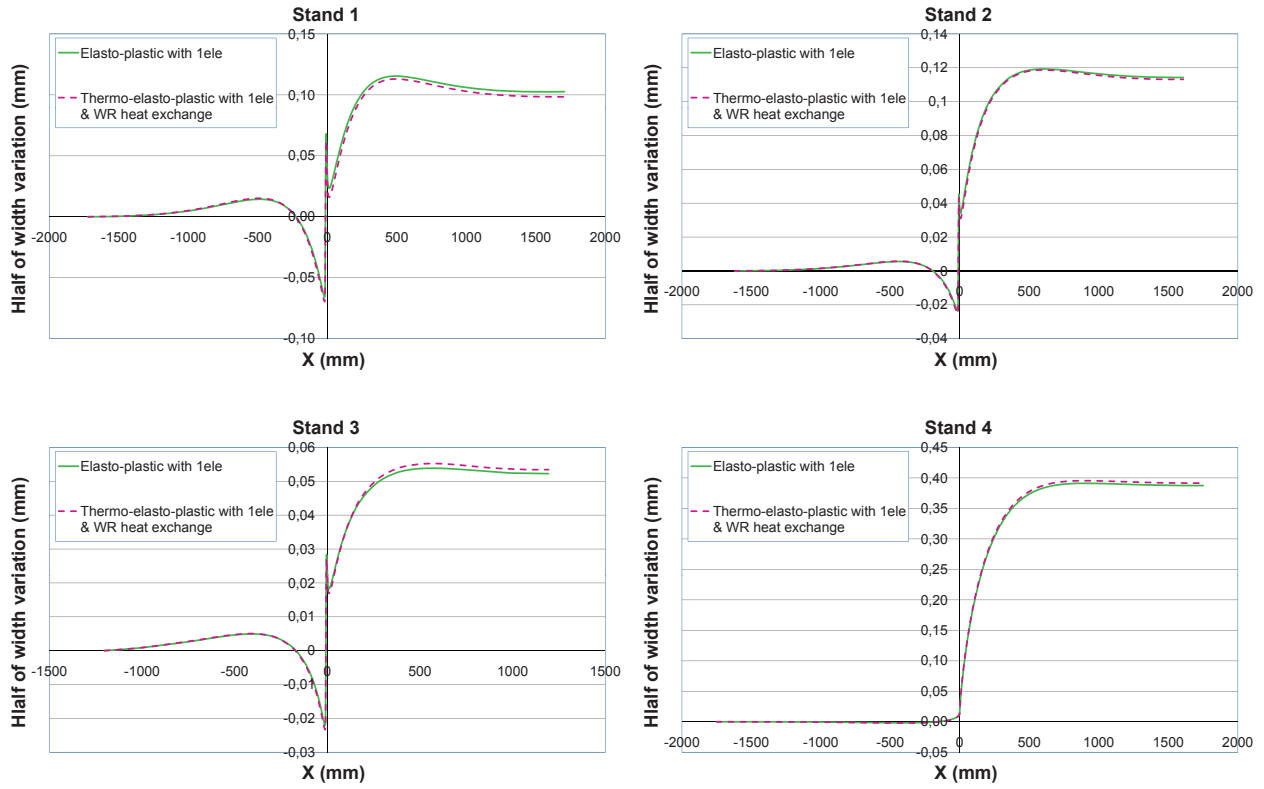


Figure 7.18: Comparison of width variation of *Lam3-Tec3* mechanical and thermo-mechanical simulations using 1 element in strip half thickness - ArcelorMittal Florange cold rolling mill.

- **thermal dilation influence** presented in the subsection 7.2.2.f. Concretely, the independent lateral flow assumption 2 implies that

$$\Delta w_{total}^{thermo-elasto-plastic} = \Delta w_{total}^{elasto-plastic} = \Delta w_{entry}^{elasto-plastic} + \Delta w_{roll-bite}^{elasto-plastic} + \Delta w_{exit}^{elasto-plastic} \quad (7.3)$$

and the independent lateral flow assumption 1 allows to approximate the width variation in the roll-bite by

$$\Delta w_{roll-bite}^{elasto-plastic} = \Delta w^{rigid-plastic} \quad (7.4)$$

In addition, at the exit, the strip is only deformed elastically *i.e.* $\Delta w_{exit}^{elasto-plastic} = \Delta w_{exit}^{elastic}$, we obtain finally:

$$\Delta w_{total}^{thermo-elasto-plastic} = \Delta w_{entry}^{elasto-plastic} + \Delta w^{rigid-plastic} + \Delta w_{exit}^{elastic} \quad (7.5)$$

where

- $\Delta w_{total}^{thermo-elasto-plastic}$ is the total width variation of the strip that is modeled as thermal-elasto-plastic material.
- $\Delta w_{entry}^{elasto-plastic}$ is the width variation before entry of roll-bite of elasto-plastic strip (before point **B** - Figure 7.15).
- $\Delta w_{roll-bite}^{elasto-plastic}$ is the strip width variation in the roll-bite.
- $\Delta w^{rigid-plastic}$ is the strip width variation for a rigid-plastic behavior - This variation only occurs inside the roll-bite because there is no elastic deformation outside the roll-bite.
- $\Delta w_{exit}^{elasto-plastic}$ is the elastic width variation after exit of roll bite for an elasto-plastic strip. This term is purely elastic and is indeed the elastic spring back term $\Delta w_{exit}^{elastic}$ already mentioned above.

7.2.3.b Formula of plastic width variation

The formula 7.5 give us a zone-by-zone breakdown of the thermo-elasto-plastic strip width variation from entry zone through the roll-bite to the exit zone. The impact of elastic and thermal deformations are implicit. In order to better point out these phenomena, let study the "final" strip width variation which corresponds to the plastic one given by:

$$\Delta w_{total}^{plastic} = \Delta w_{total}^{thermo-elasto-plastic} - \Delta w_{total}^{elastic} - \Delta w_{total}^{thermal} \quad (7.6)$$

where

- $\Delta w_{total}^{plastic}$ is the total plastic-deformation part of the strip width variation. This is the final permanent width variation after being cooled down to initial temperature (equal to entry temperature) and relaxed of stress.
- $\Delta w_{total}^{elastic}$ is the total elastic-deformation part of the strip width variation. This term is determined by the difference between the entry and exit the stress tensors. Far from the roll-bite, the stress tensor contents only longitudinal component that is equal to entry and exit tensions. Therefore,

$$\Delta w_{total}^{elastic} = \nu \left(\frac{T_e}{\sigma_0^e} - \frac{T_s}{\sigma_0^s} \right). \quad (7.7)$$

- $\Delta w_{total}^{thermal}$ is the total thermal-deformation part of the strip width variation. This term only depends on the variation of strip temperature given by:

$$\Delta w_{total}^{thermal} = w \alpha_{th} \Delta T \quad (7.8)$$

where α_{th} is strip material dilatation coefficient.

By substituting 7.5 into 7.6 we obtain:

$$\Delta w_{total}^{plastic} = \Delta w_{entry}^{elasto-plastic} + \Delta w^{rigid-plastic} + \Delta w_{exit}^{elasto-plastic} - \Delta w_{total}^{elastic} - \Delta w_{total}^{thermal} \quad (7.9)$$

This formula explicitly shows how the plastic spread in the case of a thermo-elasto-plastic strip is different from that of a rigid-plastic while the formula 7.5 does not. By substituting the total elastic term $\Delta w_{total}^{elastic}$ by the sum of the three elastic terms $\Delta w_{entry}^{elastic}$, $\Delta w_{roll-bite}^{elastic}$ and $\Delta w_{exit}^{elastic}$ we obtain

$$\Delta w_{total}^{plastic} = \left[\Delta w_{entry}^{elasto-plastic} - \Delta w_{entry}^{elastic} \right] + \left[\Delta w^{rigid-plastic} - \Delta w_{roll-bite}^{elastic} - \Delta w_{total}^{thermal} \right] + \left[\Delta w_{exit}^{elasto-plastic} - \Delta w_{exit}^{elastic} \right]. \quad (7.10)$$

And by noting that at the exit there is no plastic deformation, this formula becomes

$$\begin{aligned} \Delta w_{total}^{plastic} &= \left[\Delta w_{entry}^{elasto-plastic} - \Delta w_{entry}^{elastic} \right] + \left[\Delta w^{rigid-plastic} - \Delta w_{roll-bite}^{elastic} - \Delta w_{total}^{thermal} \right] + 0 \\ &= \Delta w_{entry}^{plastic} + \Delta w_{roll-bite}^{plastic} \end{aligned} \quad (7.11)$$

meaning that the total plastic deformation is only caused by the entry and the roll-bite areas.

7.2.3.c Discussions

More complete and clearer formula compared to previous studies [23, 64]

Since the equation 7.9, it seems obvious that first two terms $\Delta w_{entry}^{elasto-plastic}$, $\Delta w^{rigid-plastic}$ are not mentioned by Counhay [23] and Legrand *et al* [64]. That means, the new model consider in addition to the phenomena studied by [23, 64] (see 7.1.1) two other phenomena:

1. **Lateral flow of the roll-bite** $\Delta w^{rigid-plastic}$: The material flow in roll-bite of the strip is not mentioned in [23] and [64], **implicitly** it is neglected. In the industrial rolling condition, the strip is very large and the this part is negligible but it can be very important for a narrow strip (see more in the previous chapters).

2. **Entry compression:** Conversely to the way of the exit elastic spring back, at the roll-bite entry, the strip is compressed and has a variation of its width. The article does not mention this phenomenon but in many cases, it has an important distribution to the total width spread. At the entry, in typical automotive cold rolling conditions the strip is generally deformed plastically before being in contact with the work-roll (see Figure 7.13). In the section 7.3, a new model for the entry compression is proposed in order to estimate the width variation due to the plastic deformation before the contact.

Edge drop is not taken into account

It is also important to highlight that in this thesis, the *edge drop* is not studied because such a study requires a model for roll deformation. This study can be carried out at the same time with the influence of strip flatness on width variation - considered as a perspective of this thesis. In this case, the "edge drop" is indeed a part of lateral flow term $\Delta w^{rigid-plastic}$ which needs to take into account the work-roll in-charged profile especially near to the strip edge (see Figure 2.12 for explanation of this phenomenon).

7.2.4 Development of simplified model

According to the new model 7.9 the stress field needs to be determined. As the strip is large, the 3D mechanical problem may be modeled as 2D - in other words the strip variation is a small perturbation and does not make changes on the global stress field. Therefore, we are interested in a typical 2D model for stress solution such as the slab method. In a simple model considering the behavior of the strip as rigid-plastic, this method is easy to program and gives a good stress field in the roll bite. However, for an elasto-plastic behavior strip, it holds some difficulties particularly at the entry and exit of roll bite.

To solve the whole problem, it is necessary to consider all elasto-plastic equations in three areas: before, inside and after the roll-bite and the two limit conditions on the stress given by entry and exit tensions. These equations are coupled and have to be solved together. The program is heavy and calculation time becomes considerable (see more [27] or 2.3.1.f and [106]). [17] (see 2.3.1.e) propose an alternative simplified resolution allowing to get faster calculation. However, all authors assume that at the entry of roll-bite, the strip is plasticized after being in contact with the roll. Then there is an elastic compression under contact at the entry of which the equations are written similarly to the spring back at the exit. This is in contrary to what we observed with *Lam3-Tec3* simulations (see subsection 7.2.2.e and Figure 7.15).

These are two reasons why we develop here a simplified model based on "slab" hypothesis stating that it is enough to consider homogeneous behavior in the strip thickness to well model the strip width variation (see 7.2.2.d). **Three following sections present respectively simplified models for entry compression, the exit spring back and roll-bite thermal heating.**

7.3 A simplified entry elasto-plastic compression model

Shear stress assumption

At the first point of contact with the work roll, the strip deformed, more exactly sheared in xz plane. This entry area is modelled as a slipping surface (a discontinuity surface of strip material velocity) by the numerous upper bound methods existing in literature. For example, the upper bound method with rigid bodies motions velocity field [10] - see 3.2.3 or continuous eccentric velocity field [5, 6, 7] - see 3.3.1 or continuous simple or elliptical velocity field [18] and [31] - see 3.3.2 and 3.3.5 or circular velocity field [47] - see 3.3.4.

Moreover, as a reminder of the subsection 7.2.2.e, for the typical rolling conditions of Florange 4-stand mill, we observe a plastic deformation area just before contact. This is illustrated in Figure 7.13 for the stand 2. This is true for a case where the thickness reduction is quite high (stands 1, 2 and 3) and not true for the stand 4 where the reduction is only 1.66% (see Figure 7.14). Therefore, let consider the following assumption.

Shear stress assumption: The strip material is deformed plastically just before the contact (point **A** - Figure 7.15) due to an apparition of an enough important xz plane shear stress component σ_{xz}^A . We assume moreover that the other shear stress components are equal to zero $\sigma_{xy}^A = \sigma_{yz}^A = 0$ and there is always no stress in the lateral vertical directions

$$\sigma_{yy}^A = \sigma_{zz}^A = 0.$$

Homogeneous stress in thickness assumption

The analysis of *Lam3-Tec3* calculations resulted to the assumption that: To model the width variation, we can assume an homogeneous deformation across the thickness (see 7.2.2.d).

Now, by writing the equation of equilibrium in longitudinal direction of the strip part before the first point of plastic deformation **IAA'I'** we deduce that

$$\sigma_{xx}^A = T_e.$$

Therefore, the stresses tensor at **AA'** is:

$$\underline{\underline{\sigma}}^A = \begin{bmatrix} T_e & 0 & \sigma_{xz}^A \\ 0 & 0 & 0 \\ \sigma_{xz}^A & 0 & 0 \end{bmatrix} \quad (7.12)$$

The deviatoric stresses tensor is:

$$\underline{\underline{S}}^A = \begin{bmatrix} \frac{2}{3}T_e & 0 & \sigma_{xz}^A \\ 0 & -\frac{1}{3}T_e & 0 \\ \sigma_{xz}^A & 0 & -\frac{1}{3}T_e \end{bmatrix} \quad (7.13)$$

As **A** is the first point of plasticization, the Von Mises criteria is verified:

$$\sqrt{\frac{3}{2} \underline{\underline{S}}^A : \underline{\underline{S}}^A} = \sqrt{\frac{3}{2} \left[\frac{4}{9}T_e^2 + \frac{1}{9}T_e^2 + \frac{1}{9}T_e^2 + 2\sigma_{xz}^A \right]} = \sigma_0$$

Then:

$$\sigma_{xz}^A = -\sqrt{\frac{\sigma_0^2 - T_e^2}{3}} \quad (7.14)$$

Then the stresses at the point **A** is:

$$\underline{\underline{\sigma}}^A = \begin{bmatrix} T_e & 0 & -\sqrt{\frac{\sigma_0^2 - T_e^2}{3}} \\ 0 & 0 & 0 \\ -\sqrt{\frac{\sigma_0^2 - T_e^2}{3}} & 0 & 0 \end{bmatrix} \quad (7.15)$$

Plane strain deformation assumption under contact

Plane strain deformation assumption: Once the strip is under contact with the work-roll, we assume that it is in plane strain deformation. This assumptions means that we consider the strip width variation is a very small perturbation and negligible in terms of stress approaches. Moreover, we assume that at the first point of contact **B**, the shear stresses are equal to zero. By consequence, at **B** all hypotheses if slab method are verified and therefore the stress tensor at this point can be given by the equation 2.24. In addition, similarly to the point **A**, the equilibrium in longitudinal direction implies that:

$$\sigma_{xx}^B = T_e.$$

Finally, we have:

$$\underline{\underline{\sigma}}^B = \begin{bmatrix} T_e & 0 & 0 \\ 0 & T_e - \frac{\sigma_0}{\sqrt{3}} & 0 \\ 0 & 0 & T_e - \frac{\sigma_0}{\sqrt{3}} \end{bmatrix} \quad (7.16)$$

Plane strain deformation between A and B

AB plane strain assumption: We assume that the point A is so closed to the point B that the total width of the strip does no changes between these two points.

This assumption induces that on AB:

$$\Delta\epsilon_{yy}^{elastic} + \Delta\epsilon_{yy}^{plastic} = 0$$

or

$$\Delta\epsilon_{yy}^{plastic} = -\Delta\epsilon_{yy}^{elastic} = \frac{\sigma_{yy}^A - \sigma_{yy}^B - \nu(\sigma_{xx}^A - \sigma_{xx}^B + \sigma_{zz}^A - \sigma_{zz}^B)}{E} \quad (7.17)$$

By substituting the equations 7.16 and 7.16 in to 7.17, we obtain:

$$\Delta\epsilon_{yy}^{plastic} = \frac{(1 - 2\nu)\frac{\sigma_0}{\sqrt{3}} - (1 - \nu)T_e}{E} \quad (7.18)$$

To sum up, at the entry part IAB the strip width variations are given as follows

$$\begin{cases} \Delta w_{entry}^{elasto-plastic} = 0 \\ \Delta w_{entry}^{plastic} = -\Delta w_{AB}^{elastic} = \left[\frac{(1 - 2\nu)\frac{\sigma_0}{\sqrt{3}} - (1 - \nu)T_e}{E} \right] w \end{cases} \quad (7.19)$$

By consequence, the total plastic width variation formula 7.11 can be rewritten as follows where $\Delta w_{roll-bite}^{elastic} = \Delta w_{BC}^{elastic}$:

$$\Delta w_{total}^{plastic} = -\Delta w_{AB}^{elastic} + \Delta w^{rigid-plastic} - \Delta w_{BC}^{elastic} - \Delta w_{total}^{thermal} \quad (7.20)$$

and finally

$$\Delta w_{total}^{plastic} = \Delta w^{rigid-plastic} - \Delta w_{AC}^{elastic} - \Delta w_{total}^{thermal}. \quad (7.21)$$

illustrating that the plastic width variation is only impacted by the elastic and thermal deformation between A and C (the first and last point of plastic deformation). This formula is valid when the following assumptions are verified: *Independent lateral flow assumptions 1 & 2* (see 7.2.2.f and *Plane strain deformation between A and B* presented previously).

7.4 A simplified elastic spring back model - elastic slab method

As mentioned previously, the exit spring back is the width variation of the strip at the roll-bite exit due to a relaxation of strip stresses. Actually, the spring back is realized in two steps (see Figure 7.19 for illustration). The first step is the relaxation of the vertical stress σ_{zz} between the lowest point of the roll C and the last point of contact D. And in the second step, the lateral stress is released within a longer part of the strip. In general, the length of convergence of lateral stress relaxation is approximately equal to the strip width.

The second step appears after contact and the problem is much more simple than the first one because the strip is free. The only unknown for this step is the stress at D. Therefore, the first relaxation step is the principal one of the exit spring back problem. For a 2D problem, the spring back problem is considered to be the first step ([17, 27]) - relaxation of the compression in thickness within the area CD. In this area, the relaxation of vertical stress drives to a variation of the stress in all other directions. Moreover, unlike the entry area AB the tangency of the roll surface at the exit of roll bite is near to zero and therefore the size of the spring back area CD is considerable. It can be about 10% (even much more in the case of small reduction rolling) of contact length. Its great influence on roll force and torque is observed.

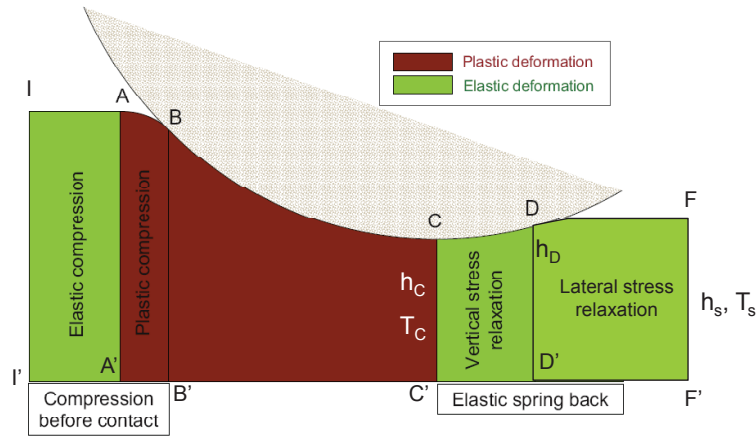


Figure 7.19: At the exit, the exit thickness h_s and tension T_s are known but the thickness h_C and tension T_C at **C** as well as the position x_D and strip thickness h_D at **D** are unknown.

Inputs of model

Exit thickness and tension: At the exit far from the roll bite **F**, the strip thickness is equal to h_s and the stress is given by the exit tension T_s as follows

$$\underline{\underline{\sigma}}^s = \begin{bmatrix} T_s & 0 & 0 \\ 0 & 0 & 0 \\ 0 & 0 & 0 \end{bmatrix}$$

and the elastic strain associated to this stress can be obtained by the linear Hooke law (7.27) as follows

$$\epsilon_{yy}^s \simeq -\nu \frac{T_s}{E}. \tag{7.22}$$

$$\underline{\underline{\epsilon}}^s = \frac{1}{E} \begin{bmatrix} T_s & 0 & 0 \\ 0 & -\nu T_s & 0 \\ 0 & 0 & -\nu T_s \end{bmatrix}. \tag{7.23}$$

If h_s^{relax} denotes the exit strip half thickness after release the stress, the equation 7.23 implies that

$$h_s^{relax} \simeq \left(1 + \nu \frac{T_s}{E}\right) h_s. \tag{7.24}$$

Work-roll shape: The roll shape is an input of the problem that gives the strip thickness function $h(x)$. Even though the resolution of spring back problem does not depend on the form of this function, the roll is modeled to be circle with a deformed radius R_{def} calculated by Hitchcock’s model. Then, the strip thickness within contact area **CD** is given by the work-roll shape and h_C strip thickness at **C** representing the minimum thickness of the strip:

$$h(h_C, x) = h_C + R_{def} - \sqrt{R_{def}^2 - x^2}. \tag{7.25}$$

Outputs of model

The thickness and tension at the exit for from the roll-bite **F** are known but the strip thicknesses h_C at the lowest point **C** and x_D position of the last point of contact **D** are unknowns of the problem. They are the outputs of the problem. The strain and stress as well as the strip width variation through out **CDF** are equally the outputs.

7.4.1 Assumptions

7.4.1.a Homogeneous stress in thickness assumption - slab method:

As a reminder of the *Lam3-Tec3* calculations analysis (see 7.2.2.d), to model the width variation, it is enough to consider a homogeneous deformation across the strip thickness. Hence, we develop in this section a simplified *slab method* to approach the exit spring back problem. Some assumptions are the same as those of rigid-plastic slab method already presented in 2.3.1.a except the hypothesis on rigid-plastic behavior. Two of them stating that *deformations are homogeneous across the thickness* and *shear stresses are negligible* imply that the stress tensor only depends on x but not on y and z , $\underline{\underline{\sigma}}(x)$. By consequence, the elastic deformation strain tensor is also a function of x only. As in this spring back area the plastic strain is unchanged, let use ϵ_{**} **to denote the elastic strain** (which normally denote the total strain). This notation is of course only valid in this section of the thesis.

As the strip thickness is given by 7.25 as a function of h_C and x , the elastic deformation in thickness direction is also a function of h_C and x :

$$\epsilon_{zz}(h_C, x) = \frac{h(h_C, x)}{h_s^{relax}} - 1 \quad (7.26)$$

where h_s^{relax} is the exit strip haft thickness after release the stress T_s given by 7.24.

7.4.1.b Assumption of plane strain deformation

Elastic plane strain deformation within CD: As the first step of spring back is always under contact and the length of this area **CD** is much smaller than the length of the second step, we can suppose that there is no width variation in the first step. This assumption implies that along this vertical stress spring back area, the lateral deformation is unchanged and equal to $\epsilon_{yy}(x) = \text{const} = \epsilon_{yy}$.

Plastic plane strain deformation at C: We suppose firstly that the last point of plastic deformation is **C**, the lowest point of the roll surface. It is considered in addition that the deformation of the strip is also plane at this point.

7.4.1.c Assumption of total relaxation of vertical stress

This assumption states that after the first step, *i.e* at **D**, the stress *i.e* σ_{zz} is totally released.

7.4.2 Basic equations

7.4.2.a Equations of elastic behavior

In elastic domain, the mechanical behavior is modeled by the Hooke law. As the shear stress and strain components are neglected and the other components are functions of x only, the Hooke law is written as follows

$$\begin{cases} \sigma_{xx}(x) = \frac{E}{(1+\nu)(1-2\nu)} [(1-\nu)\epsilon_{xx}(x) + \nu\epsilon_{yy} + \nu\epsilon_{zz}(h_C, x)] \\ \sigma_{yy}(x) = \frac{E}{(1+\nu)(1-2\nu)} [\nu\epsilon_{xx}(x) + (1-\nu)\epsilon_{yy} + \nu\epsilon_{zz}(h_C, x)] \\ \sigma_{zz}(x) = \frac{E}{(1+\nu)(1-2\nu)} [\nu\epsilon_{xx}(x) + \nu\epsilon_{yy} + (1-\nu)\epsilon_{zz}(h_C, x)] \end{cases} \quad (7.27)$$

where E_s and ν are the Young modulus and Poisson coefficient of strip material and ϵ are the elastic strain within **CD**.

By subtracting the second to the third equation of 7.27, we obtain

$$\sigma_{yy}(x) - \sigma_{zz}(x) = \frac{E}{1+\nu} [\epsilon_{yy}(x) + \nu\epsilon_{zz}(x)]. \quad (7.28)$$

And by eliminating ϵ_{xx} from the first and third equation of 7.27 we deduce that

$$\sigma_{zz}(x) = \frac{\nu}{1+\nu}\sigma_{xx}(x) + \frac{E}{1-\nu^2} [\nu\epsilon_{yy}(x) + \epsilon_{zz}(x)]. \quad (7.29)$$

7.4.2.b Boundary conditions at C

As the stress at **C** satisfies at the same time condition of plastic plane strain deformation as well as Von-Mises criterium like the rigid-plastic slab method, it can be given by 2.24, meaning:

$$\underline{\underline{\sigma}}^C = \begin{bmatrix} T_C & 0 & 0 \\ 0 & T_C - \frac{\sigma_0^C}{\sqrt{3}} & 0 \\ 0 & 0 & T_C - \frac{2\sigma_0^C}{\sqrt{3}} \end{bmatrix}. \quad (7.30)$$

where T_C denotes the longitudinal stress at **C**, i.e. $\sigma_{xx}^C = T_C$. We deduce from 7.30 that

$$\sigma_{yy}^C = T_C - \frac{\sigma_0^C}{\sqrt{3}} \quad (7.31)$$

$$\sigma_{zz}^C = T_C - 2\frac{\sigma_0^C}{\sqrt{3}}. \quad (7.32)$$

As **C** is the limit between the plastic and elastic deformation areas, the stress at **C** satisfies also the elastic behavior equations, in particular 7.28 and 7.29. By substituting 7.31 and 7.32 into 7.28 we obtain:

$$\epsilon_{yy} = \epsilon_{zz}^C(h_C) + \frac{1+\nu}{\sqrt{3}} \frac{\sigma_0^C}{E} \quad (7.33)$$

allowing to determine ϵ_{yy} as a function of h_C and only h_C : $\epsilon_{yy}(h_C)$.

Similarly, by substituting 7.31 into 7.29 we can calculate T_C as a function of h_C as follows

$$T_C(h_C) = \frac{E}{(1+\nu)(1-2\nu)} \left(\epsilon_{yy}(h_C) + \nu\epsilon_{zz}^C(h_C) \right) + \frac{1-\nu}{1-2\nu} \frac{\sigma_0^C}{E}. \quad (7.34)$$

7.4.2.c Equilibrium equations within CD - Slab method

The equilibrium equations of a slab in x and z directions are respectively given by 2.27 and 2.28 (see details in subsection 2.3.1.a). To make it easier for the readers, these equations are rewritten here as

- In x direction :

$$\frac{d}{dx} (h(x)\sigma_{xx}(x)) = -\sigma_n(x)h'(x) - \tau(x). \quad (7.35)$$

- In z direction :

$$\sigma_{zz}(x) = -\sigma_n(x) + \tau(x)h'(x). \quad (7.36)$$

In this spring back area the strip is elastically deformed and the friction is modeled by Coulomb model. It is important to note that the longitudinal velocity of the strip is usually greater than the roll velocity in this area. The exceptions cases are those where the neutral point is very closed to the point **C**. In these cases there are two neutral points, one within BC and the other within CD . In this thesis, these exceptions are not studied because of several reasons. Firstly, these cases are not frequent in industrial rolling because they are closed to the stability limit - neutral point is at **C** or does not exist. Secondly, these cases can be treated in a similar way as the case without neutral point in CD which will be studied hereafter because the position of the neutral points can be determined by the flow conservation equation.

We assume therefore, that there is no neutral point in the spring back area and the strip velocity is higher than that of the roll. The friction acted on the strip is, by consequence given by 2.30 with negative sign:

$$\tau = -\mu\sigma_n. \quad (7.37)$$

By eliminating $\tau(x)$ and $\sigma_n(x)$ from three equations 7.35, 7.36 and 7.37 we obtain :

$$\frac{d}{dx}\sigma_{xx}(x) = \frac{1}{h(x)} \left[\frac{h'(x) - \mu}{1 + h'(x)\mu} \sigma_{zz}(x) - h'(x)\sigma_{xx}(x) \right]. \quad (7.38)$$

Finally, by combining the equilibrium equation 7.38 with 7.29, we obtain a differential equation allowing to determine the evolution of σ_{xx} as a function of x :

$$\boxed{\frac{d}{dx}\sigma_{xx}(x) + A(x)\sigma_{xx}(x) = B(h_C, x)}. \quad (7.39)$$

with

$$A(x) = \frac{1}{h} \left[\frac{-v}{1-v} \frac{h' - \mu}{1 + h'\mu} + h' \right] \quad (7.40)$$

$$B(h_C, x) = \frac{1}{h} \frac{h' - \mu}{1 + h'\mu} \frac{E}{1 - v^2} [v\epsilon_{yy}(h_C) + \epsilon_{zz}(h_C, x)].$$

7.4.2.d Boundary conditions at D

Thanks to the assumption of total relaxation of vertical stress, the vertical stress at **D** is equal to zero (see 7.41)

$$\sigma_{zz}^D = 0. \quad (7.41)$$

Moreover, the equilibrium equation of the strip exit part **DD'F'F** in x direction induces that

$$\boxed{\sigma_{xx}^D = T_s}. \quad (7.42)$$

Obviously, the stress at **D** follows the elastic behavior equations. Thus, by substituting 7.41 and 7.42 into 7.29 we obtain

$$\boxed{v\epsilon_{yy}(h_C) + \epsilon_{zz}^D(h_C, x_D) = -\frac{v(1+v)}{E} T_s} \quad (7.43)$$

where the deformation $\epsilon_{zz}^D(h_C, x_D)$ is given by 7.26 for $x = x_D$.

7.4.3 Resolution algorithm

7.4.3.a Determination of h_C

Since the equations above, let introduce a function as follows: For a given h_c

1. calculate $\epsilon_{zz}^C(h_C)$ using 7.26 for $x = 0$
2. calculate $\epsilon_{yy}(h_C)$ using 7.33
3. calculate T_C using 7.34
4. determine x_D so that equation 7.43 is verified

5. using finite difference method to determine $\sigma_{xx}(x = x_D)$ (x_D is obtained in the previous step) from the differential equation 7.38 where $A(x)$ and $B(h_C, x)$ are given by 7.40. The initial condition is at **C** where $x = 0$ and $\sigma_{xx}(x = 0) = T_C$ determined in the step 3.
6. calculate the difference between $\sigma_{xx}(h_C, x = x_D)$ and T_s

Indeed, the difference between $\sigma_{xx}(h_C, x = x_D)$ and T_s determined by this way is an 1-variable function of h_C . We choose, therefore Newton algorithm to determine h_C so that this difference between $\sigma_{xx}(h_C, x = x_D)$ and T_s is equal to 0. The initial value of h_C can be chosen as that of Bland & Ford model (given in the subsection 2.3.1.e).

7.4.3.b Determination of width variation

Once h_C is obtained, repeat the first two operations mentioned above to determine $\epsilon_{yy}(h_C)$. The width variations in spring back areas are then calculated by:

$$\begin{cases} \Delta w^{CD} = 0 \\ \Delta w_{exit}^{thermo-elasto-plastic} = \Delta w^{DF} = [\epsilon_{yy}^s - \epsilon_{yy}(h_C)] w \end{cases} \quad (7.44)$$

where ϵ_{yy}^s is yy component of the strain tensor given by 7.23.

7.5 A simplified model for roll-bite

7.5.1 Total width variation in roll-bite - rigid-plastic UBM

It should be recalled that thanks to two assumptions *Independent lateral flow assumption 1 and 2 for elastic deformation and thermal dilation influences* (presented in the section 7.2.2.f, the total material flow in the roll-bite (between **B** and **C**) of a thermal-elasto-plastic simulation is relatively similar to that of a rigid-plastic model. Moreover, keeping in mind that the edge drop phenomena is not considered in this thesis. In addition, we highlight once more that the strip flatness variation has important impact on the width variation. Our study is limited for the case where strip is flat is at both the entry and exit of the roll-bite (no flatness defect). The strip is thus deformed quite homogeneously across the width direction *i.e* the strip thickness reduction is homogeneous across the strip width. In other words, we can consider a rectangular strip at the entry and a straight under-charge profile of the roll (without deflexion).

In this condition, the rigid-plastic material flow is completely predicted by the model introduced in the section 5.3 using the simple or elliptical 3D velocity field. In this section, the comparison of *UBM* results obtained using two form of the width function (polynomial in x and polynomial in $h(x)$) shows that the results are very similar so we choose the polynomial in x for its simplicity. See all details of the model in 5.3.

In summary, the total width variation in the roll-bite is finally appreciated by

$$\Delta w_{roll-bite}^{thermo-elasto-plastic} \simeq \Delta w_{roll-bite}^{rigid-plastic} = \alpha \quad (7.45)$$

where α is the rigid-plastic width variation that one of two parameters of the width function 5.40 determined by rigid-plastic *UBM* model.

7.5.2 Elastic deformation - Stress approach

According to the assumption *Independent lateral flow assumption 1 - influence of elastic deformation*, the elastic deformation in the roll-bite induces a plastic deformation of a same amplitude but with an opposite sign. Indeed, it is the elastic strain variation between **B** and **C** that need to be determined. As a result of the *entry compression model* (see 7.3), the stress tensor is completely determined at **B**. It is given by 7.16. On the other hand, the stress tensor at **C** is

entirely determined thanks to the *elastic spring back model* (see 7.4). This tensor is given by 7.30 with T_C is an output of *elastic spring back model* calculated in the step 3 of 7.4.3.a. Using the Hooke's law 7.27, the elastic width variation in the roll-bite can be determined by

$$\Delta w_{roll-bite}^{elastic} = w \Delta \epsilon_{yy}^{BC} = w \frac{\Delta \sigma_{yy}^{BC} - \nu (\Delta \sigma_{yy}^{BC} + \Delta \sigma_{yy}^{BC})}{E} \quad (7.46)$$

Finally, by substituting 7.16 and 7.30 into 7.46 we obtain

$$\Delta w_{roll-bite}^{elastic} = w \frac{1-2\nu}{E} \left[(T_C - T_e) - \frac{1}{\sqrt{3}} (\sigma_0^C - \sigma_0^B) \right]. \quad (7.47)$$

In the particular case where the material behavior is modelled without work-hardening effect

$$\Delta w_{roll-bite}^{elastic} = w \frac{(1-2\nu)(T_C - T_e)}{E}. \quad (7.48)$$

7.5.3 Thermal dilatation - temperature variation model

7.5.3.a Assumptions

Assumption of heat generation

Generally in cold rolling, strip is heated in the roll-bite due to the energy dissipated by plastic deformation and friction between the work-roll and the strip. We assume that these energies are completely transformed into heat and at the contact the heat generated by friction is shared equally to the roll and the strip.

Adiabatic thermal process in roll-bite

As a reminder, the assumption *Independent lateral flow assumption 2 - thermal dilatation influence* (see 7.2.2.f) states that the thermal dilatation of the strip in the roll-bite induces plastic deformation of a same amplitude but with an opposite sign. That means it is the strip temperature variation inside the roll-bite that is important but not outside the roll-bite. On the other hand, inside the roll-bite the only heat exchange is due to the contact with the roll. The heat transfer coefficient between the strip and the roll in cold rolling condition (with lubrication) is approximated of about $htc = 2.10^4 w / (m^2 K)$. However, as the rolling speed is quite high (>6000 mm/s) while the contact length is relatively small (<20 mm), let assume that the exchanged heat is negligible in comparison to that generated by plastic deformation and friction.

In order to verify this assumption, consider now the *Lam3-Tec3* simulations with and without heat exchange between the strip and the roll. The simulations are performed for the same rolling conditions given in Table 7.5. Table 7.6 shows the strip temperature variation from the roll-bite entry to the exit. The results obtained with or without heat exchange with the work-roll are very closed for all the four stands conditions. The adiabatic assumption leads to an error on ΔT lower than $1^\circ K$ which corresponds to a relative error lower than 1% for stand 1, 2 and 4. For stand 4, as the temperature variation is quite low because of a small reduction in thickness. These simulations conclude, hence in typical automotive products cold rolling conditions, the adiabatic assumption is valid.

Remark: Unlike cold rolling, in hot rolling conditions (roughing and finishing mills) the strip should be considered in isotherm condition. Indeed, the strip temperature ($\sim 1000^\circ C$ in roughing mill and about $\sim 900^\circ C$ for finishing mill) is much higher than the that of the roll ($\sim 80^\circ C$), the strip-to-roll transferred heat is important and usually equivalent to the heat generated by plastic deformation and friction dissipation.

Stand	Entry T(°K)	With heat exchange		Without heat exchange		Error	
		Exit T(°K)	$\Delta T(^{\circ}\text{K})$	Exit T(°K)	$\Delta T(^{\circ}\text{K})$	°K	%
1	300.0	400.27	100.27	400.82	100.82	0.55	0.55
2	333.0	439.96	106.96	440.96	107.96	1.00	0.94
3	353.0	447.65	94.65	448.49	95.49	0.84	0.89
4	373.0	375.95	2.95	376.06	3.06	0.11	3.63

Table 7.6: Results of thermo-mechanical *Lam3-Tec3* simulations with and without heat exchange between the strip and the roll for typical industrial cold rolling conditions in Table 7.5.

7.5.3.b Simplified thermal model

The rigid-plastic model (5.3) used to estimate the width variation in the roll-bite is, as a reminder based consists in searching for the optimum velocity field by minimizing the rolling power. It does not only give an estimation of width variation along the roll-bite thanks to the velocity field but also a very good approach of plastic deformation, friction and tensions powers. Therefore, the strip temperature variation in the roll-bite can be determined based on powers given by the rigid-plastic *UBM* by considering the assumptions described above:

$$\Delta T = \gamma \frac{J_{def} + c_{share} J_{fric}}{C_{vol} \rho C_p} \quad (7.49)$$

where J_{def} is the plastic deformation power. J_{fric} is the friction power which is shared at a proportion c_{share} to the strip and $1 - c_{share}$ to the roll. C_{vol} is the volumic flow rate which is equally given by the rigid-plastic model, ρ is density and C_p is the masse specific heat capacity of the strip. *It is worth to remind that the plastic deformation power J_{def} is actually the sum of two terms, volumetric continuous deformation power $J_{\dot{\epsilon}}$ and discontinuity of velocity one $J_{\Delta u}$. The first term $J_{\dot{\epsilon}}$ corresponds to the plastic deformation dissipation through the roll-bite area (between **B** and **C**) and the second one $J_{\Delta u}$ refers to the plastic shearing deformation at the entry of the roll-bite (area between **A** and **B**). And γ is a coefficient that we introduce to model the thermal conditions. Typically $\gamma = 1$ for automotive cold rolling condition where we consider that 100% of dissipation transformed into heat and the strip thermal condition is adiabatic. $\gamma \simeq 0$ for hot rolling where the strip is considered in isotherm condition.*

Finally, the thermal width dilatation in the roll-bite can be determined thanks to 7.8 with ΔT given by 7.49. And the plastic width variation in the roll-bite - between **B** and **C** is

$$\Delta w_{roll-bite}^{plastic} = \Delta w_{rigid-plastic} - \Delta w_{roll-bite}^{elastic} - \Delta w_{roll-bite}^{thermal} \quad (7.50)$$

Remark: The friction in elastic spring back area (between **C** and **D**) contributes actually to the strip temperature variation. However, as the the spring back contact length (**BC**) is relatively small in comparison to the total contact length and as the contact pressure decreases down to 0 at **D**, the average friction stress is also lower. Furthermore, the difference of velocity between the strip and the roll is much smaller than that inside the roll-bite. The friction dissipation in spring back area is eventually negligible in comparison to that inside the roll-bite and especially to the plastic deformation dissipation.

7.6 Summary

Bibliography: In the first part of the chapter, a bibliographic study shows that in industrial automotive rolling (flat and large strip) the elastic and thermal deformations have important impact on the final width variation. However, there exist very few width variation models that are applicable for this kind of rolling process. Legrand [64] and Counhaye [23] are the only two existing model in our knowledge. One is based on *Lam3-Tec3* and the other on "streamline" finite difference method. Both requires high computing time. Moreover, these models state both that the total width variation is given by the combination of three terms: edge drop, thermal contraction and elastic spring back (equation 7.1). The two studies give important base for the studies of width variation in automotive cold rolling process. However, the

explanations are quite general. Indeed, the total width variation term is not explicitly defined. It may be understood as the total elasto-plastic width variation for a thermo-elasto-plastic model without the thermal term? It may be referred as the plastic one but in this case the total elastic width variation needs to be extracted or not? Moreover, this formula seems to implicitly suppose that at the entry of the roll-bite? The width variation due to the lateral flow in the roll-bite seems to be neglected equally?

New width variation formula: These are the motivations to go more in details. This chapter presents, thus the new model (see section 7.2) based on some assumptions adequately chosen thanks to an analysis of *Lam3-Tec3* simulations. The most important are two assumptions on lateral flow: **Independent lateral flow assumptions 1 - elasticity influence** and **2 - thermal dilation influence** (see 7.2.2.f). These assumptions lead to two basic formula 7.11 for the plastic width variation which is the permanent width change.

Simplified model for the roll-bite entry: By assuming a homogeneous stress in thickness and by writing the Von Mises plastic criteria at **A**, the stress tensor at this point is entirely determined and given by 7.15. Further, the *plane strain deformation between A and B assumption* leads to rewrite the plastic width variation formula 7.11 by another 8.2.2 that states that the plastic width variation is only impacted by the elastic and thermal deformation between **A** and **C**.

Simplified model for the roll-bite exit: is developed based on a slab method, the four assumptions: plane strain deformation within **CD**, the friction is negative on this segment, the last point of plastic deformation **C** coincides to the lowest point of the work-roll and the vertical stress is totally relaxed at the last point of contact **D**. This model allows to approach the stress at **C** by 7.30 with T_C determined at the same time as h_C by an iterative algorithm 7.4.3. Using 7.15 and 7.30 the elastic width variation within **AC** - the second term of the right hand side of 8.2.2 is obtained by

$$\Delta w_{AC}^{elastic} = \left[\epsilon_{yy}^{elastic-C} - \epsilon_{yy}^{elastic-A} \right] w = \left[\frac{1-2\nu}{E} (T_C - k_C) + \frac{\nu}{E} T_e \right] w. \quad (7.51)$$

Simplified model for the roll-bite: As a reminder, the first term of the right hand side of the equation 8.2.2, $\Delta w^{rigid-plastic}$ represents indeed the total width variation of the thermo-elasto-plastic strip between **B** and **C** that is approximately estimated by the width variation of a rigid-plastic one. This term can be, thus determined by the rigid-plastic *UBM* developed in the section 5.3. The boundary conditions (stress tensor) at **B** and **C** are given by the roll-bite entry and exit models instead of entry and exit tensions initially imposed. In other words, the roll-bite entry and exit model do not only allow to estimate the elastic term by 7.51 but also boundary conditions for the roll-bite model.

Moreover, it should be recalled that the *UBM* is based on an optimization of the rolling power, the plastic deformation and friction dissipation powers are also determined by this model. In addition, for cold rolling processes, as the contact time is small it is usually reasonable to assume that the rolled strip is in adiabatic condition under the roll-bite. This assumption allows to evaluate the increase of strip temperature and therefore the thermal width variation term $\Delta w_{total}^{thermal}$ of the equation 8.2.2. The width variation model is hence completed.

Let call this simplified thermo-elasto-plastic width variation model the **UBM-Slab combined model**.

Chapter 8

The UBM-Slab combined model validation

*The previous chapter presents the new width variation model for a thermal-elasto-plastic strip in rolling process which is called **UBM-Slab combined** model. The programming of this model is detailed in the first section of the present chapter. The results show a very interesting computing time - less than 0.05s enabling online applications including dynamic control. In the second section, a comparison of the width variation obtained by the UBM-Slab combined model with those obtained by Lam3-Tec3 for the four stands of Florange cold rolling mill. It is observed a good agreement between the two models. The total plastic width variations obtained with the two models are very closed. Finally, a parametric study using the UBM-Slab combined model is done and shows clearly how the width variation depends on the rolling. It is important to highlight that these dependencies are very different for narrow and large strips. And once more, the results match really well the tendencies observed in industrial data presented by some studies existing in literature.*

Contents

8.1	Simplified model algorithm and programming	164
8.1.1	Algorithm	164
8.1.2	C++ programming and fast computing time	164
8.2	Validation by comparison with Lam3-Tec3	165
8.2.1	Very good prediction of final plastic width variation	165
8.2.2	The simplified model can be improved?	165
8.3	Validation by comparison with industrial observations	168
8.3.1	Parametric study for a large strip rolling - Stand 1	168
8.3.2	Parametric study for a narrow strip rolling - E16 trial	169
8.3.3	Summary of parametric studies	170
8.4	Conclusions	171

8.1 Simplified model algorithm and programming

8.1.1 Algorithm

As can be noted from the previous sections, the entry compression as well as the exit elastic spring back models are completely independent from each other and from the roll-bite one. They are calculated first. In contrast, the roll-bite model, between **B** and **C**, has actually limits conditions which are outputs of the two other models. Indeed, following the simplified entry model the longitudinal stress at **B** is always equal to the entry tension T_e thanks to the fact that the strip is deformed before the contact. Otherwise, this stress can be different from T_e . And at the exit, the tension at **C**, an output of the exit elastic spring back model T_C is an input for both roll-bite total width variation model (rigid-plastic *UBM*) and roll-bite elastic width variation one. The algorithm of the whole model is therefore illustrated in Figure 8.1 as follows:

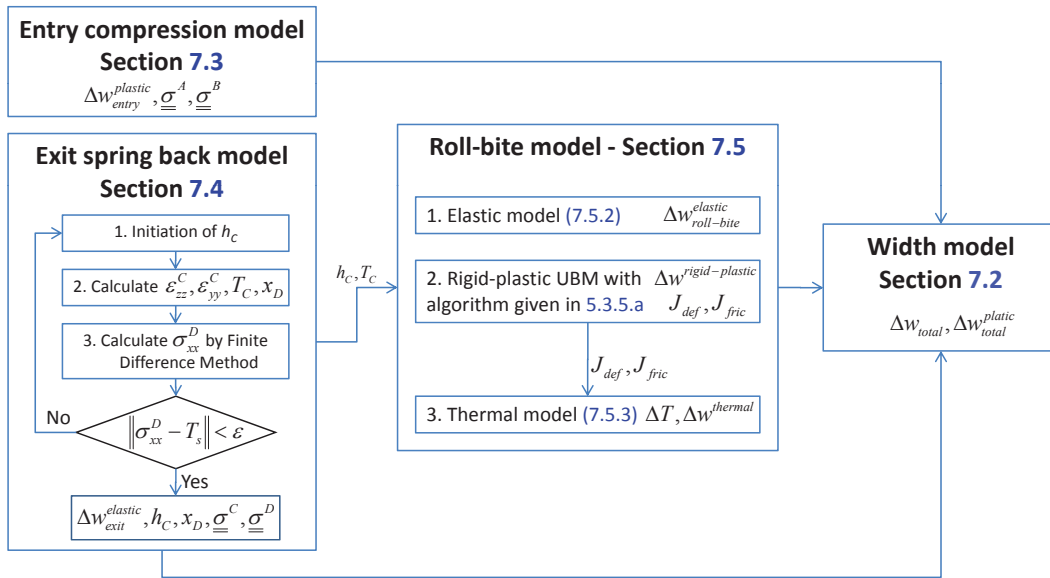


Figure 8.1: Algorithm of the simplified model for width variation of a thermal-elasto-plastic strip in cold rolling.

The entry model is simple and the plastic width variation $\Delta w_{entry}^{plastic}$ is calculated directly using 7.19. Concerning the elastic spring back model, the algorithm is described in the section 7.4.3. The determination of h_C is done by Newton method where the target function is the difference between the longitudinal stress at **D** and the exit tension $\sigma_{xx}^D - T_s = 0$. We obtain finally $h_C, T_C, \Delta w_{exit}^{elastic}$ and evolution of stress fields throughout **CD**. As for the roll-bite, the elastic model is simple. The roll-bite elastic width variation $\Delta w_{roll-bite}^{elastic}$ is resulted from $\underline{\sigma}_B$ and $\underline{\sigma}_C$ outputs of the entry compression and elastic spring back models respectively. The rigid-plastic *UBM* for the total width variation in the roll-bite is feed by h_C and T_C given by elastic spring back model as inputs instead of h_S and T_s . Some outputs of *UBM* model, J_{def} and J_{fric} are used by the thermal model to determine the temperature variation ΔT and the thermal width variation $\Delta w_{roll-bite}^{thermal}$. Finally, all the width variation terms in entry, roll-bite and exit obtained by these models becomes inputs of the width model presented in the section 7.2 to determine the total and plastic width variations Δw_{total} and $\Delta w_{total}^{plastic}$.

8.1.2 C++ programming and fast computing time

The model is entirely programmed in C++. Most of the models described above such as entry compression, roll-bite elastic, thermal models are analytical and require, hence almost no calculation time. The exit elastic spring back contain iterative calculation but the convergence is obtained generally after 2 or 3 iterations. It is also very fast, less

than 1.10^{-3} s. The roll-bite *UBM* require obviously a computing time the most important due to the calculation of powers and iterative calculation to minimize the rolling power. Indeed, thanks to the fact that the calculation of all power functions are obtained analytically (see section 5.3.4). In addition, using Gauss's method to approximate some integrals as the 2D integral of deformation power and the 1D integral of friction power, help to reduce effectively the number of points where the integrated functions need to be calculated. Moreover, the rolling power optimization by Newton-Raphson algorithm requires few iterations, generally 2 for very large strip (as the width variation is small and easy to be found) and 3 or 4 for narrow one. The computing time is finally very fast. The total computing time for Florange 4-stand mill conditions varies from 0.01s to 0.05s (CPU: Intel Core I5-4200M, 250GHz). Table 8.1 shows in details the results obtained by the UBM-Slab combined simplified model for the 4 stands of Florange cold rolling mill conditions given in Table 7.5.

Parameter	Unit	Stand 1	Stand 2	Stand 3	Stand 4	E16
$J_{def} + c_{share}J_{fric}$	w	1115370	1190020	1058860	37426	6594
ΔT	°C	102.1	109.3	96.9	3.6	144.8
X_n	mm	-2.2081	-0.4738	-0.3350	-0.1320	-1.6076
h_C	mm	0.83488	0.50244	0.33075	0.32502	0.43414
T_C	Mpa	138.29	137.95	184.32	-35.53	-21.20
x_D	mm	0.9408	0.7480	0.6740	0.7602	0.8828
L	mm	17.438	13.180	10.192	1.889	9.376
$\Delta w_{entry}^{plastic}$	mm	0.2329	0.0649	0.0949	0.0233	0.0260
$\Delta w_{BC}^{elastic}$	mm	0.0973	-0.0134	0.0316	-0.2616	-0.0034
$\Delta w_{exit}^{thermo-elasto-plastic} = \Delta w^{DF}$	mm	0.0529	0.0733	0.0272	0.4187	0.0294
Δw_{total}	mm	0.0675	0.0782	0.0296	0.4191	0.1410
$\Delta w_{rigid-plastic}$	mm	0.0146	0.0049	0.0024	0.0004	0.1116
$\Delta w_{AC}^{elastic}$	mm	-0.1356	-0.0783	-0.0633	-0.2848	-0.0294
$\Delta w_{total}^{thermal}$	mm	0.7171	0.7676	0.6799	0.0254	0.0523
$\Delta w_{total}^{plastic}$	mm	-0.5668	-0.6844	-0.6142	0.2598	0.0887
Computing Time	ms	30	20	20	10	30

Table 8.1: Results obtained by the simplified model - ArcelorMittal Florange 4-stand cold rolling mill.

8.2 Validation by comparison with *Lam3-Tec3*

8.2.1 Very good prediction of final plastic width variation

Figure 8.2 gives the profile of elastic, thermal, plastic and total width variation obtained with *Lam3-Tec3* for the four stands. For first three stands the total (thermo-elasto-plastic) width variation is relatively small while the thermal one is important. That leads finally to a large negative plastic width variation (width necking). The stand 4 with particular working conditions (very low reduction) is an exception. The plastic deformation is positive meaning a width spread. All these width variations due to elastic, thermal, plastic and total deformations are summed up in Table 8.2 in comparison with those obtained by the simplified model. It can be seen very good agreement between *Lam3-Tec3* and the simplified model regarding all these width variations terms. As the plastic one is the real final width variation of the strip, let take a look on a comparison of this term between *Lam3-Tec3* and the simplified model through graphic 8.3. The four points of the graphic corresponding to four stands are almost perfectly on the bisector line.

8.2.2 The simplified model can be improved?

Let remind the formula allowing to estimate the plastic width variation as

$$\Delta w_{total}^{plastic} = \Delta w_{rigid-plastic} - \Delta w_{AC}^{elastic} - \Delta w_{total}^{thermal}$$

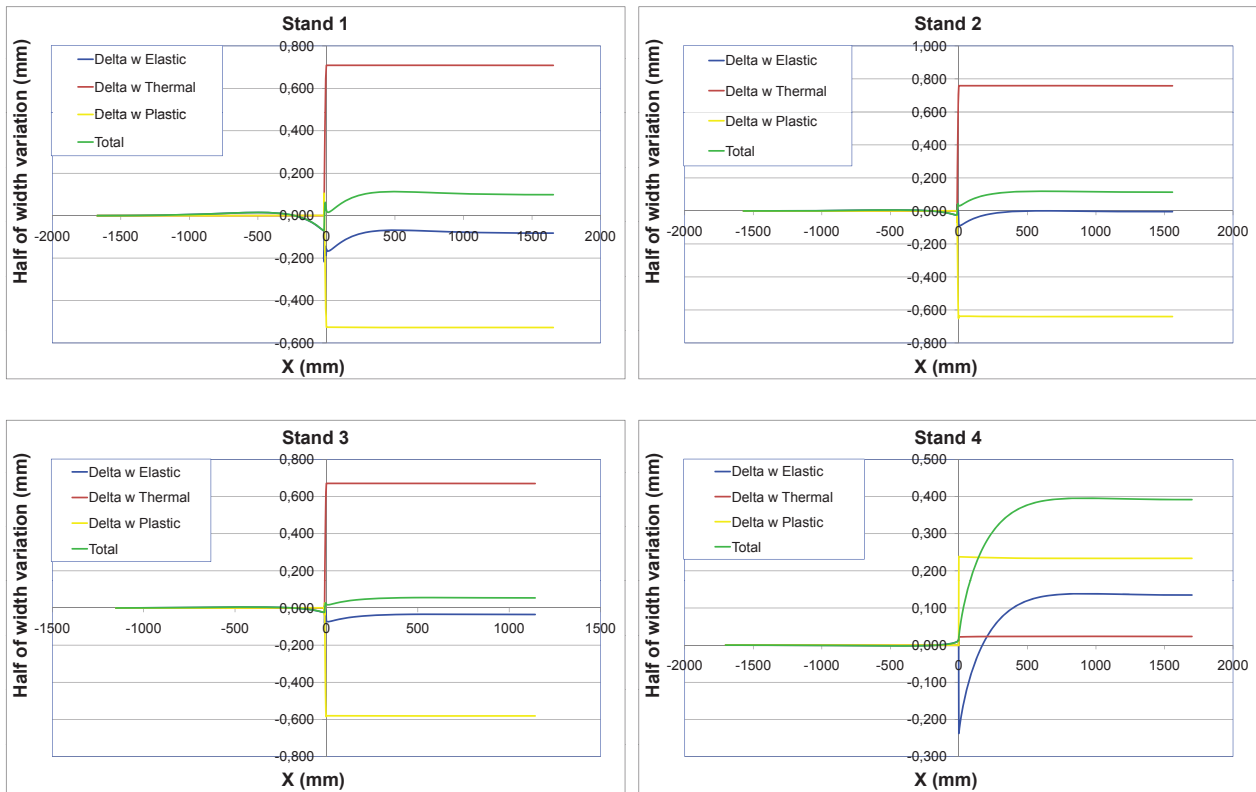


Figure 8.2: Width variations profiles due to elastic, thermal, plastic and total deformations obtained by *Lam3-Tec3* for the four stands of ArcelorMittal Florange mill.

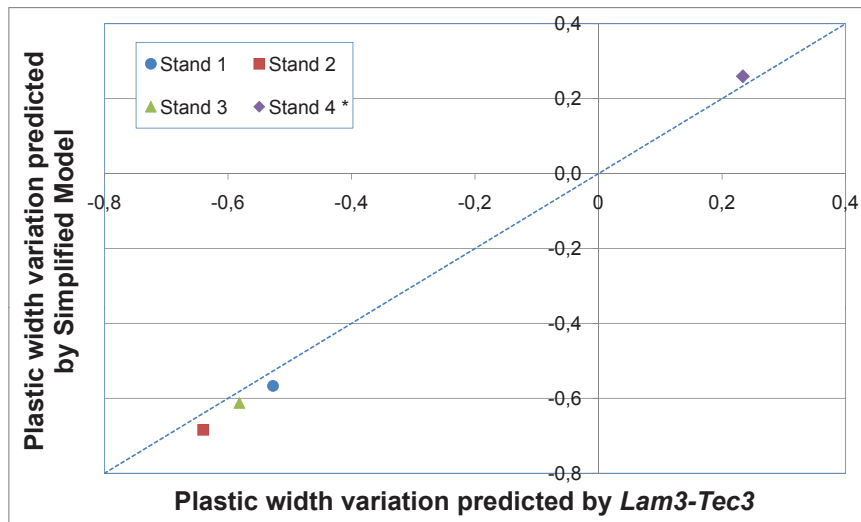


Figure 8.3: Width variation predicted by simplified model as a function of that predicted by *Lam3-Tec3* for the 4 stands of Florange cold rolling mill (see data in Table 7.5).

which is valid when the assumptions *Independent lateral flow assumptions 1 & 2* (see 7.2.2.f) and *Plane strain deformation between A and B* are verified. In this formula, the three terms $\Delta w^{rigid-plastic}$, $\Delta w_{AC}^{elastic}$ and $\Delta w_{total}^{thermal}$ are,

	Elastic		Thermal		Plastic		Total	
	Lam3	New Model	Lam3	New Model	Lam3	New Model	Lam3	New Model
Stand 1	-0.0820	-0.0827	0.7083	0.7171	-0.5271	-0.5668	0.0989	0.0675
Stand 2	-0.0040	-0.0050	0.7585	0.7676	-0.6402	-0.6844	0.1140	0.0782
Stand 3	-0.0350	-0.0361	0.6706	0.6799	-0.5815	-0.6142	0.0542	0.0296
Stand 4	0.1349	0.1339	0.0233	0.0254	0.2337	0.2598	0.3919	0.4191

Table 8.2: Comparison of elastic, thermal, plastic and total width variations obtained by *Lam3-Tec3* and the simplified model - ArcelorMittal Florange 4-stand cold rolling mill.

indeed estimations of the total, elastic and thermal width variations of the strip between **A** and **C**, respectively.

It can be, nevertheless rewritten as

$$\Delta w_{total}^{plastic} = \Delta w^{rigid-plastic} + \Delta w_{IA}^{elastic} - \Delta w_{IC}^{elastic} - \Delta w_{total}^{thermal}$$

which shows that there are four sources of error in the calculation of plastic width variation of the simplified model:

1. the total width variation between AC estimated by rigid-plastic one $\Delta w^{rigid-plastic}$
2. the elastic width variation at **A** (compared to the initial width at **I**)
3. the elastic width variation at **C** (compared to the initial width at **I**)
4. the thermal width variation $\Delta w_{total}^{thermal}$ (indeed depends on the accuracy of plastic and friction powers).

	Δw_{AC}^{total}			$\Delta w_{IA}^{elastic}$			$\Delta w_{IC}^{elastic}$			$\Delta w_{total}^{thermal}$		
	Lam3	Model	Err	Lam3	Model	Err	Lam3	Model	Err	Lam3	Model	Err
Stand 1	0.095	0.015	-0.080	-0.069	0.000	0.069	-0.158	-0.136	0.022	0.708	0.717	0.009
Stand 2	0.058	0.005	-0.053	-0.025	0.000	0.025	-0.088	-0.078	0.010	0.759	0.768	0.009
Stand 3	0.044	0.002	-0.041	-0.023	0.000	0.023	-0.070	-0.063	0.006	0.671	0.680	0.009
Stand 4	0.009	0.000	-0.008	0.015	0.000	-0.015	-0.238	-0.285	-0.047	0.023	0.025	0.002

Table 8.3: Comparison of elastic, thermal and total width variations between **AC** obtained by *Lam3-Tec3* and the simplified model - ArcelorMittal Florange 4-stand cold rolling mill.

Table 8.3 shows a comparison of the four mentioned terms between the simplified model and *Lam3-Tec3*. It can be observed that the thermal width variation is quit well estimated by the new model meaning that the rigid-plastic *UBM* is good enough to approximate the plastic and friction dissipation powers. The width at **C** (or $\Delta w_{IC}^{elastic}$) estimated by the new model is generally similar to *Lam3-Tec3* except for the stand 4 because with very small reduction level the slab assumption is not well verified. The elastic spring back model is, hence relatively accurate when the reduction is important enough (as stands 1, 2 and 3 for example). The most important error comes from the total width variation between **AC**, estimated by rigid-plastic *UBM* model. This model gives always underestimated value in comparison with *Lam3-Tec3*.

As conclusion although the strip plastic width variation predicted by the simplified model is in a very good agreement with *Lam3-Tec3* there exist some further potential improvements. The entry compression model can be improved by better estimating the stress at **C**. The elastic spring back model is good when the reduction level is high enough. The rigid-plastic model provides an accurate prediction of dissipation powers and therefore of thermal width variation. But it underestimates the total width variation in the roll-bite.

8.3 Validation by comparison with industrial observations

8.3.1 Parametric study for a large strip rolling - Stand 1

In this section the new model will be used to evaluate effect of each rolling parameter on the width variation for an industrial rolling condition in order to compare to the observations already presented in literature (see the section 7.1.2). These previous studies are done on the total width variation from the entry to exit of tandem mill, meaning through 4 or 5 stands. The reason is that nowadays to install in a good industrial condition the strip width measurement device between the stands is impossible. Therefore, our analysis consisting in studying how width variation depends on each rolling parameter will be only interpreted relatively but the absolute value of width is an objective.

We choose to study the stand 1 conditions (given in Table 7.5) because the stands 2 and 3 are with very low friction (the forward slip is already close to 0 and the neutral point is closed to the lowest point C). By consequence, when one of some other inputs varies the neutral point can go out of the roll-bite and there is no equilibrium solution. The model does not converge.

8.3.1.a Effect of tensions

Figures 8.4 and 8.5 show that the width variation predicted by the simplified model decreases when one of both entry and exit tensions goes up. *This tendency matches well the observation on industrial data presented in 7.1.2.c.*

Discussions: At first, that seems obvious that the entry and exit tensions do not impact significantly the dissipation power which depends essentially on the strip yield stress and the reduction. That is why the thermal width variation is almost unchanged with a variation of tensions. Moreover, as the rigid-plastic *UBM* width variation is negligible (~ 0) because the strip is very large, it is almost independent on all input parameters (except the strip width). According to the formula of the plastic width variation 8.2.2 the only term that changes as a function of entry and exit tensions is $\Delta w_{AC}^{elastic}$. The equation 7.51 implies that when T_e increases the $\Delta w_{AC}^{elastic}$ increases and leads to a decrease of plastic width variation. When T_s increases, T_C grows and therefore the $w_{AC}^{elastic}$ increases equally and the plastic width variation drops down. As $1 - 2\nu > \nu$, the exit tension seems to have more important impact on the width than the entry one.

8.3.1.b Effect of reduction

It can be seen from the 8.6 that the effect of reduction (for a same entry thickness) on the width variation is very important: the more reduction the more necking. The rigid-plastic width variation (representing total width variation in the roll-bite) is always null approximately and the elastic width variation between A and C is quite constant that can be explained by the equation 7.51. And it is the thermal width variation that changes sharply with an increase in reduction because the plastic deformation as well as the friction powers increase as a function of the reduction.

8.3.1.c Effect of nominal strip width

Unlike the others graphic, the 8.7 shows that the rigid-plastic width variation term changes when the nominal width varies. This term $\Delta w_{roll-bite}^{rigid-plastic}$ is important and even dominant against thermal and elastic terms $\Delta w_{total}^{thermal}$ and $\Delta w_{AC}^{elastic}$ when the width is small ($w_e < 50\text{mm}$ or the total width $2w_e < 100\text{mm}$). This term decreases drastically and becomes negligible as the half width is higher than about 300mm . That is why for the width of $w_e = 585\text{mm}$ of the Stand 1, this term is always almost nullified.

For automotive industrial rolling, the strip width varies from about 800mm to over 2000mm , meaning $w_e > 400\text{mm}$. For this range of width, the rigid-plastic term is closed to 0 and the thermal term increases while the elastic term decreases as linear functions of the width. In this case, as the thermal increases faster than the elastic term decreases the plastic width decreases meaning more necking. Nevertheless, in another case (small reduction for example) it is possible that the thermal term is smaller than the elastic one in absolute value, the plastic width variation is then positive and it would increase with an increase in the nominal width. This tendency is perfectly coherent with the industrial observations presented in the section 7.1.2.e.

8.3.1.d Effect of strip yield stress and friction coefficient

According to the equation 7.51, when the yield stress increases the elastic term $\Delta w_{AC}^{elastic}$ decreases linearly. That is also showed in Figure 8.8. In addition, as both plastic and friction dissipation powers are proportional to the strip yield stress the thermal width variation term grows also linearly as a function of the yield stress. In the stand 1 rolling condition, as the rigid-plastic width variation is negligible and the thermal term is more important than the elastic one, the plastic width variation is negative and decreases (more necking) for harder material. This dependence of the width variation on the yield stress is, however opposite to the industrial data observation presented in the section 7.1.2.f.

As can be seen from the 8.9 that the friction has similar but less important influence on all the width variations terms as the yield stress. Firstly, the thermal terms increases because the friction power increases almost linearly in the friction coefficient. However as the plastic dissipation is unchanged unlike the case when the yield stress varies, the impact of friction coefficient on the thermal term is thus weaker. Secondly, it is important to mention that the simulations are done by varying not only the Tresca friction coefficient m_b in the roll-bite but also the Coulomb friction in the elastic spring back area μ which is changed proportionally to the Tresca one. As the difference of longitudinal stress between **C** and **D** is proportional to the contact friction stress on this segment, *i.e* $T_s - T_C$ increases with an increases in μ . By consequence, the tension T_C decreases a function of friction coefficient and that leads, following 7.51, to a decrease of the elastic width variation term. Once more, as showed in Figure 8.9 the increase of the thermal term is more important than the decrease of the elastic one, the plastic width variation decreases in incurring more necking.

8.3.1.e Effect of strip thickness and work-roll diameter

Figures 8.10 and 8.11 shows that the entry and work-roll diameter have very small impact on the width variation. For classic automotive rolling mills, the work-roll diameter can vary between about 400mm to 600mm. In this range of variation, the work-roll diameter has negligible influence on the width variation.

Similarly for the strip thickness, for automotive rolling condition the strip entry thickness of one stand can vary from about 0.4mm (at last or before last stands) to 6mm (at first stand), meaning h_e varies from 0.2mm to 3mm. The impact of entry thickness is also negligible. This conclusion matches well what was observed by industrial data analyses (see section 7.1.2.f). However, it can be seen in Figure 8.10 there is an increase of the width necking when the strip thickness decreases down to 0.2mm. This range of strip thickness correspond to that of packaging rolling mills last stands where the half strip thickness can be down to less than 0.09mm. In this condition, the lower the strip thickness, the more and more important the ratio contact area over roll-bite volume. By consequence the friction dissipation power may become more and more important in comparison to the plastic one and may lead to an increase in thermal width variation. The strip necking could be significantly more for thin and very thin strips.

8.3.2 Parametric study for a narrow strip rolling - E16 trial

This subsection presents a similar parametric study of the width variation using the simplified model but a narrow strip. The rolling conditions are those of the trial E16 done on ArcelorMittal pilot mill with a strip of 60.2mm wide (see all parameters in Table C.2). The results of the UBM-Slab combined model for this case are presented in Table 8.1. Unlike the industrial strip rolling, for E16 pilot rolling trial the rigid-plastic width variation $\Delta w^{rigid-plastic} = 0.1116mm$ is not negligible and even more important than the elastic and thermal terms $\Delta w_{AC}^{elastic} = -0.0294mm$ and $\Delta w_{total}^{thermal} = 0.0523mm$. The final plastic width variation is, in this case positive $\Delta w_{total}^{plastic} = 0.0887mm$, *i.e* the strip is widened.

8.3.2.a Effect of different parameters on width variation - narrow strip

Figures numbered from 8.12 to 8.19 present effect of different parameters on the plastic width variation for this pilot trial rolling condition. The results are summed up in comparison to those for industrial rolling conditions as follows:

- **Similar tensions effect** meaning the the width variation decreases with an increases in entry or exit tensions. In this case of narrow strip, in addition to the fact that the elastic term $\Delta w_{ACelastic}$ increases, the rigid-plastic one $\Delta w_{rigid-plastic}$ decreases as a function of tensions amplifying the decrease of the plastic width variation.
- Figure 8.14 shows that, like for Stand 1 condition, the thermal width variation term increases rapidly as the reduction grows while elastic term is remained constant. However, for a narrow strip the rigid-plastic term is no longer negligible and increases even more shapely as a function of reduction leading to an increase of the plastic width variation. **The effect of reduction is therefore opposite** (*i.e* width variation grows up while it decreases in the case of large strip). As the width variation is positive for narrow strip and negative for large strip, the reduction **amplify the width variation value in both cases**.
- **Same nominal width effect**. Despite of the difference in reduction, thickness, tensions... the effect of nominal width on the plastic width variation in the case of E16 (Figure 8.15) is very similar to the case of Stand 1 (Figure 8.7).
- Same as the case of large strip, an increase in yield stress or in friction coefficient make grow up the thermal width variation term (because of an increase in dissipation power) and diminish the elastic one (see equation 7.51). But as the increase of thermal term is equivalent to the decrease of the elastic one and the rigid-plastic term is not sensible as a function of yield stress and friction coefficient, **the plastic width variation is almost unchanged as a function of yield stress or friction**. Whilst for large strip, the thermal term is more important than the elastic one, the plastic width variation decreases with an increase in yield stress or friction coefficient.
- **More important effect of strip thickness and roll diameter**. Indeed, similar to the case of large strip both thermal and elastic width variation terms are almost constant when the strip thickness (for a same reduction level) or roll-diameter vary. But contrary to the case of large strip where the rigid-plastic term is not negligible any more and increases as a function of strip thickness and roll-diameter. That lead to an increase of the plastic width variation as a function of these two parameters.

8.3.3 Summary of parametric studies

Parameter	Nomenclature	Industrial observation [64]		UBM-Slab model			
		Large strip		Large strip (stand 1)		Narrow strip (E16)	
		Tendency	Impact	Tendency	Impact	Tendency	Impact
Nominal width	w	$ \Delta w \nearrow$	high	\searrow	high	\searrow	high
Reduction	red	\searrow	high	\searrow	high	\nearrow	high
Entry thickness	h_e	\nearrow	low	\rightarrow	negligible	\nearrow	high
Strip yield stress	σ_0	\nearrow		\searrow	average	\nearrow	low
Entry & exit tensions	T_e, T_s	\searrow	average	\searrow	average	\searrow	low
Work-roll radius	R	\nearrow	low	\rightarrow	negligible	\nearrow	high
Friction coefficient	μ & m			\searrow	low	\searrow	low
Bending	B	\searrow	average				
Friction anisotropy	α_μ	\searrow	average				

Table 8.4: Comparison of parametric studies using the UBM-Slab combined model and bibliographic review on the influence of rolling parameters on strip width variation in two cases: large and narrow strips.

Table 8.4 sums up the existing industrial experiments and statistical observations about effect of rolling parameters on the width variation (see more details in the previous chapter, 7.1.2) as well as the results of parametric studies using the new simplified model for two rolling cases with a large and a narrow strip. The dependence of width variation on rolling parameters obtained by the UBM-Slab combined model is in a very good agreement with that observed statistically on industrial data. For narrow strip, the plastic width variation is positive (widening) and the effects of rolling parameters on the plastic width variation are relatively different. Therefore, the influence of rolling parameters on the width variation

8.4 Conclusions

Fast computing time enables online applications: As the model for roll-bite entry is completely analytical and the exit one is quasi-analytical requiring only one computation loop when searching h_C (see the algorithm in section 7.4.3.a) the computing time of these models are very small (less than a millisecond programmed in C++ code). The main time consuming factor is related to the roll-bite model which is indeed the rigid-plastic *UBM*. Nevertheless, as the powers computation is developed analytically as far as it can be (see section 5.3.4) and the integrals in powers function are computed numerically using Gauss's method, the final computing time (in C++) is less than 0.05s. That enables online applications such as preset and dynamic control of the width.

Good prediction of plastic width variation: The comparison of the plastic width variation obtained by the UBM-Slab combined model with that obtained by *Lam3-Tec3* for the four stands of Florange cold rolling mill shows a good agreement between the two models. The difference of plastic width variations between the two models is less than 6% of for stands 1, 2 and 3 about 10% for the last stand (which only makes very small reduction in strip thickness).

Good prediction of influence of rolling parameter on width variation: Parametric study is done using the UBM-Slab combined model for two rolling conditions, one with large strip (stand 1 condition) and the other with narrow strip (pilot trial E16 condition). The model is able to predict clearly how the width variation depends on the rolling in each case. In the case of industrial condition (stand 1) with large strip, except the yield stress effect, the results match really well the tendencies observed in industrial data presented by some studies existing in literature. It is interesting to highlight that these dependencies are very different for narrow and large strips.

Moreover, as the UBM-Slab combined model is able to explain the contribution of each phenomena involved into the plastic width variation (see formula 8.2.2): the total width variation in the roll-bite, the elastic width variation between the first and last points of plastic deformation **A** and **C**. It allows to understand how and how much each of these three terms varies as function of each rolling parameter.

Key improvement of the model is to take into account influence of flatness: The limit of the UBM-Slab combined model is that it considers only a straight (non-deflexion) work-roll. The flatness of the strip is by consequence not considered. Whilst, the literature highlighted that the flatness (strip thickness profile) has important influence on the strip width variation. This is also confirmed by the study of a crown strip by *UBM* in the chapter 6. It is necessary to remind that the UBM-Slab combined model is valid when the rolling condition allows to obtain good strip flatness. In industrial reality, this condition that is desired but not always obtained. Hence, taking into account this phenomenon is a future improvement of the model open a very high potential opening largely the application domain of the model.

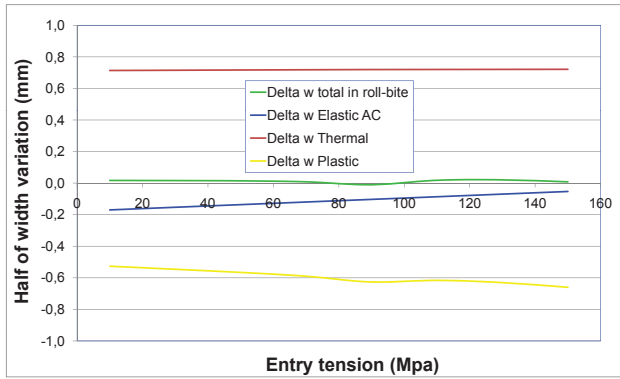


Figure 8.4: Effect of T_e on Δw - Stand 1 condition.

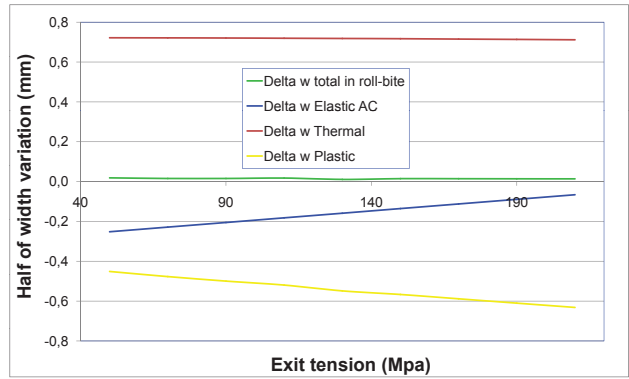


Figure 8.5: Effect of T_s on Δw - Stand 1 condition.

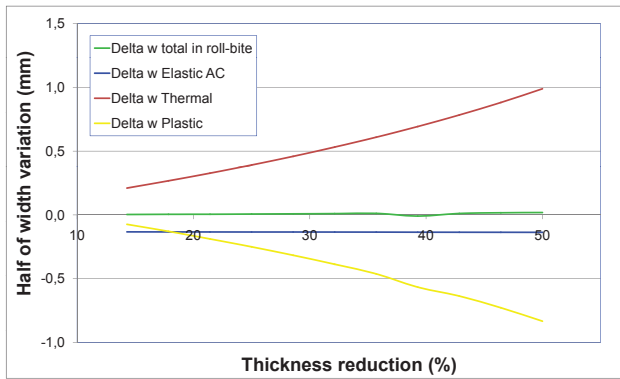


Figure 8.6: Effect of red on Δw - Stand 1 condition.

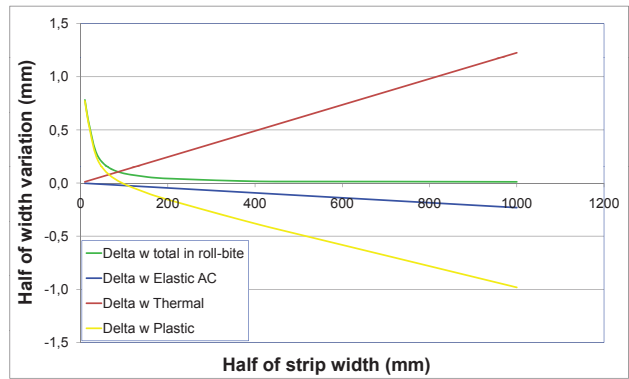


Figure 8.7: Effect of w_e on Δw - Stand 1 condition.

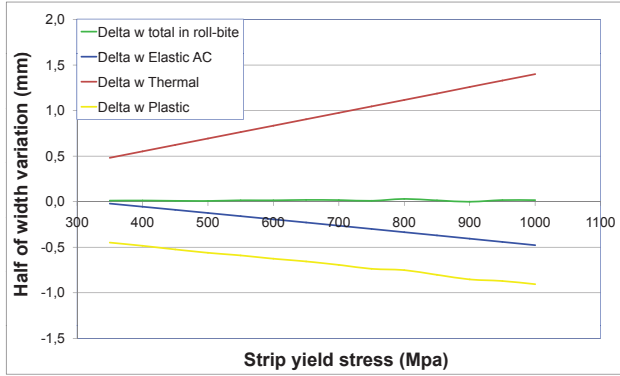


Figure 8.8: Effect of σ_0 on Δw - Stand 1 condition.

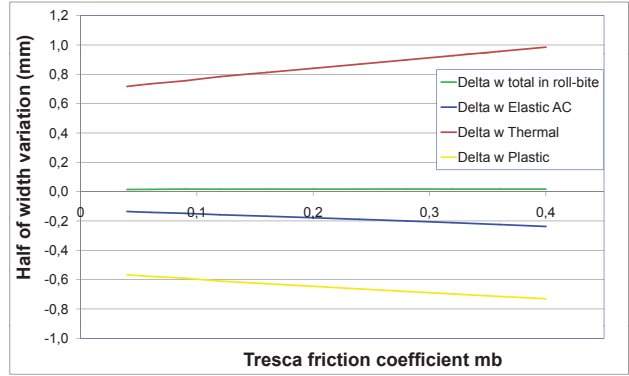


Figure 8.9: Effect of m on Δw - Stand 1 condition.

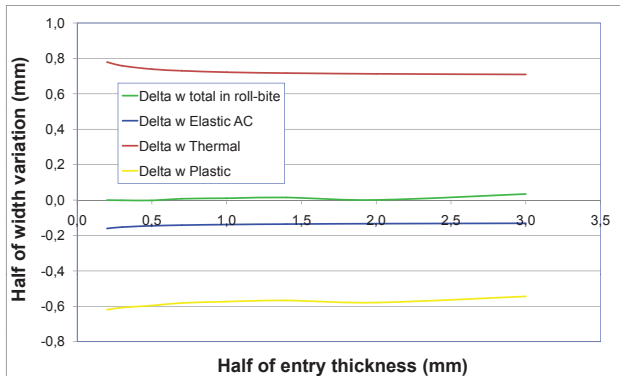


Figure 8.10: Effect of h_e on Δw - Stand 1 condition.

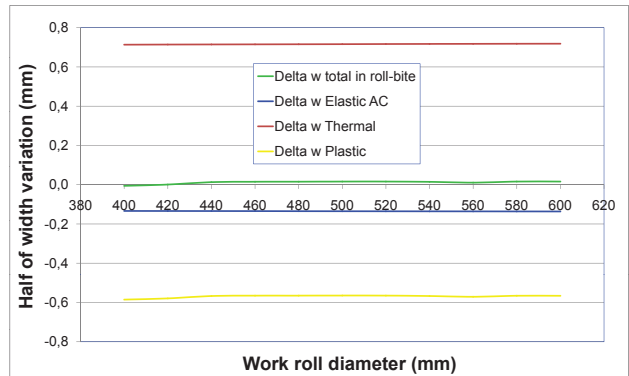


Figure 8.11: Effect of $2R$ on Δw - Stand 1 condition.

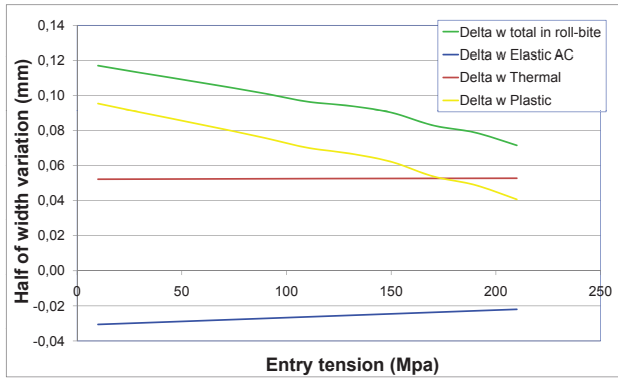


Figure 8.12: Effect of T_e on Δw - narrow strip (E16).

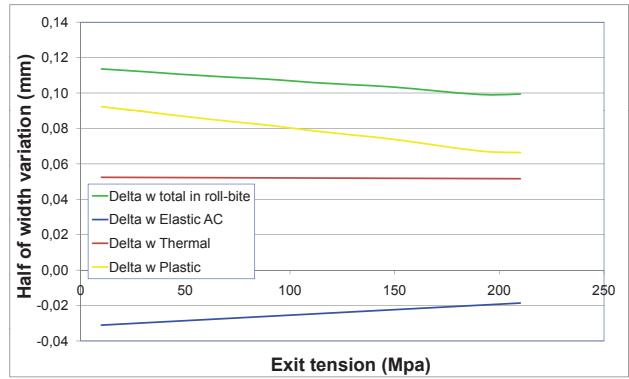


Figure 8.13: Effect of T_s on Δw for a narrow strip.

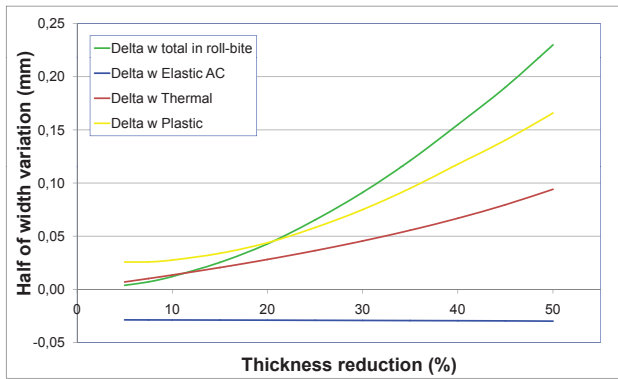


Figure 8.14: Effect of red on Δw - narrow strip (E16).

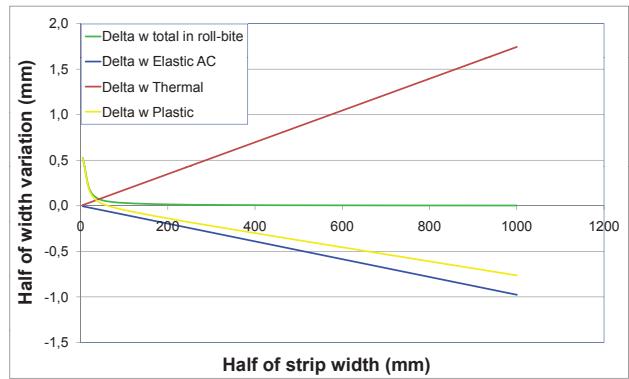


Figure 8.15: Effect of w_e on Δw - narrow strip (E16).

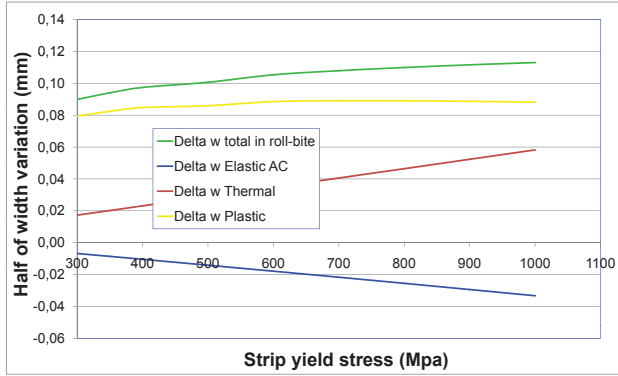


Figure 8.16: Effect of σ_0 on Δw - narrow strip (E16).

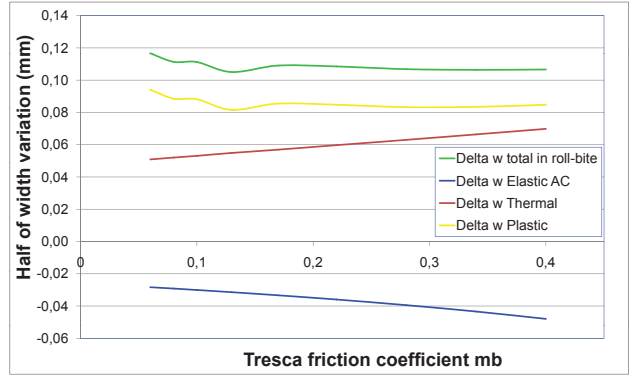


Figure 8.17: Effect of m on Δw - narrow strip (E16).

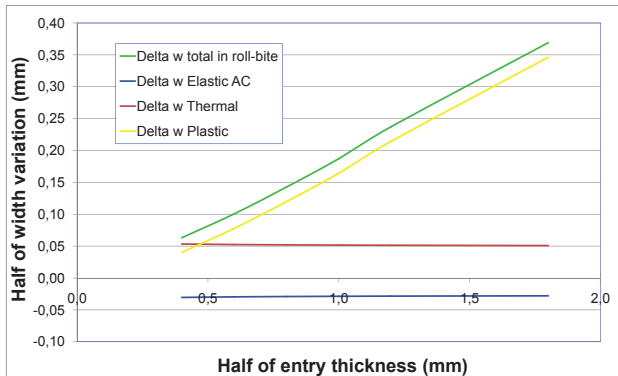


Figure 8.18: Effect of h_e on Δw - narrow strip (E16).

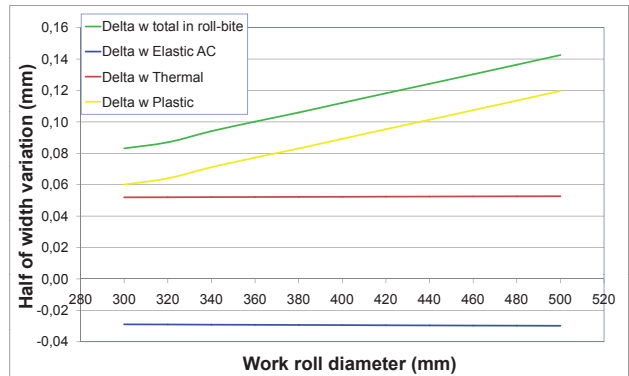


Figure 8.19: Effect of $2R$ on Δw - narrow strip (E16).

Chapter 9

General conclusions and perspectives

9.1 Conclusions

The development of predictive width variation model for automotive cold rolling is achieved

In the current industrial context where the width variation in cold rolling is important but not predicted, the main objective of the present thesis is to develop a predictive width variation model for automotive cold rolling process. Such a model need to be accurate and rapid to be used in real-time process control. For bar rolling process, the width variation topic has been studied largely and an important number of developed models were based on *FEM*, *UBM* as well as empirical methods. The *UBM* provides a good comprise between the accuracy and computing time. Nevertheless, in automotive rolling condition, the strip is large and the elastic width variation is no longer negligible. This elastic deformation is reversible but it has important impact on the plastic one. Moreover, due to the friction and plastic deformation powers the strip is heated up significantly. It is, therefore dilated in the width direction but it can not because of the contact friction with the roll. That creates compression plastic deformation - called thermal contraction. The modelling of width variation becomes more complicated and requires thermo-mechanical understanding. In this domain, there exist very few models. They are based on *FEM* and stream lines *FDM* and by consequence have important computing time.

We have, in the present thesis, carried out a deep analysis based on *Lam3-Tec3* simulations and brought out all the phenomena involved in the width variation. Since the analysis, the most important simplifying assumptions have been found. According to these assumptions, the elastic deformation as well as the thermal dilatation of the strip in the roll-bite create a plastic deformation of a same amplitude but with an opposite sign. In other words, the total width variation in the roll-bite of a thermo-elasto-plastic strip is the same as that of a rigid-plastic one. By consequence, we proposed a formula that computes the plastic width variation as a combination of three terms: the total width variation in the roll-bite, the elastic and thermal width variations between the first and last points of plastic deformation. In order to determine these three terms, we developed simplified models for the entry, exit and inside the roll-bite.

The simplified models for the entry and exit of the roll-bite are based on the assumption of a homogeneous stress and deformation across the strip thickness (slab method). They give approximations of the stress solution before and after the roll-bite allowing to determine the elastic width variation term between the first and the last points of the plastic deformation zone. As for the roll-bite model, it is the rigid-plastic *UBM* with 3D "simple" velocity field. The boundary conditions (longitudinal stress tensor) at the roll-bite entry and exit are given by the roll-bite entry and exit models instead of entry and exit tensions initially imposed. In addition, as the model allows to determine the plastic deformation and friction dissipation powers, the increase of strip temperature and the thermal width variation term can be computed. The simplified width variation model is thus completed and called the **UBM-Slab combined model**.

A comparison has been performed and showed a very good agreement between the UBM-Slab combined model and *Lam3-Tec3*. The difference of the total plastic width variations obtained with the two models is less than 6% for a stand that does relatively high reduction and 10% for a stand with very small reduction. The UBM-Slab combined model allows predicting the influence of rolling parameters on the final width variation and the results match really

well the tendencies observed in industrial data presented by some studies existing in the literature. Furthermore, as the model for roll-bite entry is completely analytical and the exit one is quasi-analytical, the main computing time is related to the roll-bite model - the rigid-plastic *UBM*. Thanks to the analytical development of the powers computation the total computing time of the width variation model (in C++) is less than 0.05s (CPU: Intel Core I5-4200M, 250GHz) enabling online applications such as preset or dynamic control.

The *UBM* is always efficient method to develop rapid model for rolling process

The *UBM* formulated by [91] have been for a very long period a method that was largely used to obtain approximate solutions strip drawing, extrusion, forging, rolling, drawing, cutting processes. Indeed, the method require to pre-assume a velocity field pattern (family) that can be described thanks to a certain number of parameters which are as well the unknowns of the optimization problem. In comparison to *FEM* where the number of unknowns depends in the freedom degree and number of elements which is usually very important, the *UBM* is thus advantageous. The quality of the *UBM* results depends, therefore strongly on the choice and the construction of velocity fields. During the second haft of 20th century, there were studied many rigid bodies motion velocity fields such as unitriangular and multitriangular. Several other continuous velocity fields have been as well proposed as the "eccentric", elliptical or "simple" and circular ones. But indeed, all these mentioned continuous velocity fields are closed each from the other. That makes an impression that despite the existence of sophisticated mathematical methods (Dual Stream Function...) for constructing kinematically admissible velocity fields, it is still difficult to go further than the simple velocity field to describe more deeply the mechanical fields in rolling process. Nevertheless, throughout the thesis we proved that the *UBM* remains powerful to approach the rolling process if we based on a *FEM* to better understand the velocity field behavior.

The first example is the 2D oscillation velocity field that allows to take into account the heterogeneity of the velocity, strain rate fields across the strip thickness, a domain very little investigated. We presented a method for constructing kinematically admissible velocity fields based on the DSF method where any kinematically admissible velocity field is expressed as a sum of the "simple" (or elliptical) one and an additional term. By observing that the equations of kinematically admissible conditions of the additional term are closely similar to the wave propagation ones, we proposed a new family of "oscillating" velocity fields. And the *UBM* using this new velocity family results to an optimum velocity that oscillates spatially throughout the roll-bite with pseudo-period equal to the local strip thickness. The rolling power obtained is smaller than the one with the "simple" (elliptical) velocity field. The results of this model match very well those obtained by *Lam3-Tec3* in terms of velocity field, plastic deformation zone and flow lines. As a result of the *UBM* model as well as *Lam3-Tec3*, the mechanical fields heterogeneity is non-linear, quasi-sinusoidal across the strip thickness.

The second example illustrating the interest of the *UBM* for rapid approach of rolling is the 3D width variation model for a crown strip. We developed a new *UBM* approach for cold rolling where the strip initial thickness has non-constant profile while the work-roll is considered rigid and perfectly cylindrical. As the geometry of the strip is more complex than the case of flat strip rolling, the roll bite is divided into three areas in which the velocity field is different. As a result, the model shows that the width variation decreases with an increase in the strip initial crown and the *UBM* results match very well those obtained with *Lam3-Tec3*.

9.2 Perspectives

Industrial applications

Having now a rapid model of width variation, it is possible to apply it to predefine the necessary width at the entry of the cold rolling mills that would give the customer desired width at the exit - specification. The only necessary thing is to build a good database which requires two width measurements at the entry and the exit of the concerned tandem mill. In addition, the temperature and the tension need to be measured the same places (as closed as possible to the width measurement places) allowing to quantify the real plastic width variation of the strip. The off-line and online collection of data database will allow to tune and correct (online adaptation) the model in order to get and keep a good

predictive performance during time. An analysis of the error of the predictive model needs to be done to define a over-width strategy that ensure the minimum total over-cost due to over-width for the most of cases and the under-width for the few remaining cases.

Furthermore, as a result the model is fast enough to be used for online control. Nevertheless many works need accomplishing. The choice of control parameters requires not only an analysis of the efficiency of all process parameters (similar to the parametric study done in the section 8.3) as well as an analysis of all industrial constrains concerning each parameter. The control strategy should also be suitable to all other existing controls.

Other proposals of velocity fields for 3D *UBM* analysis ¹

Polynomial velocity fields family: The new method for construction the kinematically admissible velocity fields presented in the section 4.2 opens actually divers solutions of kinematically admissible velocity fields for rolling. In addition to the oscillating velocity field, another family has been introduced in the section 4.2.2 - the polynomial one. This velocity family would allow especially to have higher strip speed on the contact before the neutral point and lower strip speed on the contact afterward. That would reduce the friction power and may lead to interesting results in term of rolling power optimization.

Perturbation of velocity field around the neutral point: The neutral point is the point where the contact shear stress (friction stress) is discontinuous which should create a discontinuity the strain rate. All the previous continuous velocity fields (eccentric, simple-elliptical and oscillating) are not able to model this phenomenon. In order to model that, it is necessary to separate the roll-bite into two areas with a discontinuity surface at the neutral point. On the other hand, it was observed that the *UBM* under-estimates the forward slip in comparison with *Lam3-Tec3* although the neutral point obtained by *UBM* is quite closed to *Lam3-Tec3*. Inversely, the unitriangular over-estimate it. This fact is not a random and can be explained by the existing of a neutral zone - sticking area (but not a point).

The oscillating velocity with advantage of low deformation power and the multitriangular with advantage of neutral zone modeling can be combined together to create the new one. The idea is to model the neutral zone as a rigid curvilinear triangular. This triangular rotates around the work-roll center with a same angular velocity. Before and after this neutral zone the velocity is modelled by the two oscillating ones. This idea is described in Figure 4.35.

3D *UBM* with deformed work-roll: Similarly to the *UBM* model approaching the width variation for the crown strip with the straight work-roll, it is possible to develop another one for a rectangular strip and crown work-rolls. When the work-roll crown is positive, *i.e* the center diameter is more important than the work-roll ends, the strip center is, same as the case with positive strip crown and straight roll, in contact with the work-roll before the strip edges. The geometry problem would be treated in a resembling way.

¹See more details in section 4.6.2

Appendix A

Numerical Gauss-Legendre integration

Contents

A.1 Principle	179
A.1.1 2-point Gaussian Quadrature Rule	179
A.1.2 Higher-point Gaussian Quadrature Rule	180
A.1.3 Values arguments and weighing factors for n-point Gaussian Rule	181
A.2 Applications	181

A.1 Principle

A.1.1 2-point Gaussian Quadrature Rule

The integration of 1-variable function is defined as the determination the area under a curve as showed in the figure A.1 symbolised by

$$I = \int_a^b f(x) \, dx \tag{A.1}$$

where $f(x)$ is integrand, a and b are the lower and upper limits of integration. The two-point Gauss Quadrature Rule is an extension an approximation where the arguments of the function are not predetermined but as unknowns x_1 and x_2 and the integral is approximated as

$$I = \int_a^b f(x) \, dx \approx c_1 f(x_1) + c_2 f(x_2). \tag{A.2}$$

The four unknowns x_1, x_2, c_1 and c_2 are found by assuming that the formula gives exact results for integrating a general third order polynomial

$$f(x) = a_0 + a_1 x + a_2 x^2 + a_3 x^3 \tag{A.3}$$

of which the integral is

$$I = \int_a^b f(x) \, dx = a_0 (b - a) + a_1 \left(\frac{b^2 - a^2}{2} \right) + a_2 \left(\frac{b^3 - a^3}{3} \right) + a_3 \left(\frac{b^4 - a^4}{4} \right). \tag{A.4}$$

On the other hand, the Gauss's integration is

$$\begin{aligned} I &= c_1 f(x_1) + c_2 f(x_2) \\ &= c_1 (a_0 + a_1 x_1 + a_2 x_1^2 + a_3 x_1^3) + c_2 (a_0 + a_1 x_2 + a_2 x_2^2 + a_3 x_2^3) \\ &= a_0 (c_1 + c_2) + a_1 (c_1 x_1 + c_2 x_2) + a_2 (c_1 x_1^2 + c_2 x_2^2) + a_3 (c_1 x_1^3 + c_2 x_2^3). \end{aligned} \tag{A.5}$$

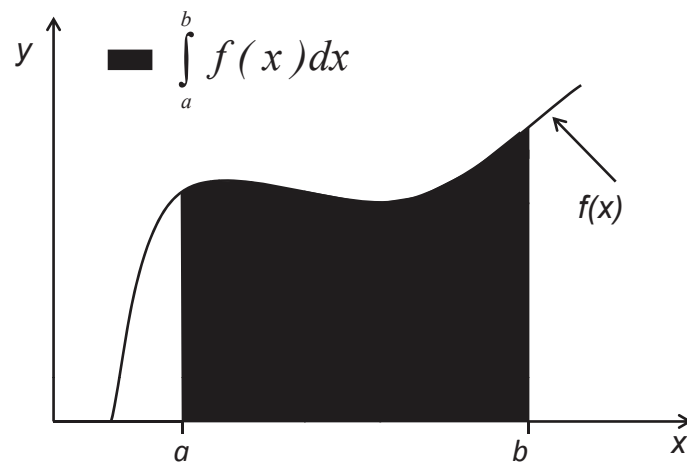


Figure A.1: Definition of integration of 1-variable function from a to b .

So that the two previous expressions are equal for any arbitrary constants a_0, a_1, a_2 and a_3 the following conditions need be verified:

$$\begin{cases} c_1 + c_2 = b - a \\ c_1x_1 + c_2x_2 = \frac{b^2 - a^2}{2} \\ c_1x_1^2 + c_2x_2^2 = \frac{b^3 - a^3}{3} \\ c_1x_1^3 + c_2x_2^3 = \frac{b^4 - a^4}{4}. \end{cases} \tag{A.6}$$

Then

$$\begin{cases} c_1 = \frac{b - a}{2} \\ c_2 = \frac{b - a}{2} \\ x_1 = \frac{b + a}{2} - \frac{1}{\sqrt{3}} \frac{b - a}{2} \\ x_2 = \frac{b + a}{2} + \frac{1}{\sqrt{3}} \frac{b - a}{2}. \end{cases} \tag{A.7}$$

A.1.2 Higher-point Gaussian Quadrature Rule

Similarly, the 3-point Gaussian Quadrature Rule is defined by

$$I = \int_a^b f(x) dx \approx c_1f(x_1) + c_2f(x_2) + c_3f(x_3). \tag{A.8}$$

The coefficients $c_1, c_2,$ and $c_3,$ and the functional arguments $x_1, x_2,$ and x_3 are calculated by assuming the formula gives exact expressions for integrating a fifth order polynomial

$$f(x) = a_0 + a_1x + a_2x^2 + a_3x^3 + a_4x^4 + a_5x^5. \tag{A.9}$$

And the general n-point rules would approximate the integral by

$$I = \int_a^b f(x) dx \approx \sum_{i=1}^n c_i f(x_i) \tag{A.10}$$

which gives exact expressions for integrating any $2n - 1$ -order polynomial.

A.1.3 Values arguments and weighing factors for n-point Gaussian Rule

The table A.1 gives the coefficients and arguments given for n-point (with n=2, 3, 4, 5, 6) Gauss Quadrature Rule given for integrals $I = \int_{a=-1}^{b=1}$.

Points	Weighting factors	Function arguments
2	$c_1 = 1$ $c_2 = 1$	$x_1 = -0.577350269$ $x_2 = 0.577350269$
3	$c_1 = 0.555555556$ $c_2 = 0.888888889$ $c_3 = 0.555555556$	$x_1 = -0.774596669$ $x_2 = 0$ $x_3 = 0.774596669$
4	$c_1 = 0.347854845$ $c_2 = 0.652145155$ $c_3 = 0.652145155$ $c_4 = 0.347854845$	$x_1 = -0.861136312$ $x_2 = -0.339981044$ $x_3 = 0.339981044$ $x_4 = 0.861136312$
5	$c_1 = 0.236926885$ $c_2 = 0.478628670$ $c_3 = 0.568888889$ $c_4 = 0.478628670$ $c_5 = 0.236926885$	$x_1 = -0.906179846$ $x_2 = -0.538469310$ $x_3 = 0$ $x_4 = 0.538469310$ $x_5 = 0.906179846$
6	$c_1 = 0.171324492$ $c_2 = 0.360761573$ $c_3 = 0.467913935$ $c_4 = 0.467913935$ $c_5 = 0.360761573$ $c_6 = 0.171324492$	$x_1 = -0.932469514$ $x_2 = -0.661209386$ $x_3 = -0.2386191860$ $x_4 = 0.2386191860$ $x_5 = 0.661209386$ $x_6 = 0.932469514$

Table A.1: Values of the coefficients and arguments for 2-point, 3-point, 4-point, 5-point and 6-point Gauss Quadrature Rules.

A.2 Applications

Gauss-Legendre integration formulas are extremely accurate to approximate the integrals. They are usually recommended when many integrals of a similar nature are to be evaluated. In this case, we can proceed as follows. Pick a few representative integrals, including some with the worst behavior that is likely to occur. Determine the number of sample points N that is needed to obtain the required accuracy. Then fix the value N , and use the Gauss-Legendre rule with N sample points for all the integrals.

There will be appeared in this thesis many integrals of a certain function on arbitrary bounds:

$$I_1 = \int_{x_{min}}^{x_{max}} f(x) dx \tag{A.11}$$

while the weighting factors and function arguments of Gauss-Legendre rule are defined for interval of integration $[-1, 1]$. We need a variable change for each such integral. In order to simplify the utilization of Gauss-Legendre integration in usual problems, we introduce an operator denoted $IGauss_{1D}^N(f, x_{min}, x_{max}, n_{ele})$ is N-point Gauss integration of a function f on the interval $[x_{min}, x_{max}]$ divided into n elements on which the integral is approximated by N-point Gauss integration. The size of each element is $\Delta x = \frac{x_{max}-x_{min}}{n_{ele}}$. The i^{th} elements is between two nodes

$x_{i-1}^{node} = x_{min} + (i-1)\Delta x$ and $x_i^{node} = x_{min} + i\Delta x$. The operator $IGauss_{1D}^N(f, x_{min}, x_{max}, n_{ele})$ is defined by:

$$IGauss_{1D}^N(f, x_{min}, x_{max}, n_{ele}) := \sum_{i=1}^{n_{ele}} \frac{\Delta x}{2} \sum_{j=1}^N \omega_j f(x_{ij})$$

(A.12)

where $x_{ij} = x_{i-1}^{node} + \Delta x \frac{\xi_j + 1}{2}$

An other application needed in this thesis is the 2D integral in a area where the bound of the second variable can depend on the first one. We are interested in the following integral of a function f on the area delimited by $x = x_{min}$, $x = x_{max}$, $y = y_{min}(x)$ and $y = y_{max}(x)$:

$$I_2 = \int_{x_{min}}^{x_{max}} \int_{y_{min}}^{y_{max}} f(x, y) dy dx. \tag{A.13}$$

We introduce an operator $IGauss_{2D}^N(f, x_{min}, x_{max}, y_{min}, y_{max}, n_x^{ele}, n_y^{ele})$ to approximate this integral. On x direction, there are n_x^{ele} elements of the same size

$$\Delta x = \frac{x_{max} - x_{min}}{n_x^{ele}}.$$

And on y direction there are n_y^{ele} elements of the size

$$\Delta y(x) = \frac{y_{max}(x) - y_{min}(x)}{n_y^{ele}}.$$

The i^{th} element in x direction is defined by two nodes $x_{i-1}^{node} = x_{min} + (i-1)\Delta x$ and $x_i^{node} = x_{min} + i\Delta x$. If we consider a function

$$g(x) = \int_{y_{min}}^{y_{max}} f(x, y) dy$$

and use approach A.12 the integral I_2 can be rewritten as:

$$I_2 \approx IGauss_{1D}^N(g, x_{min}, x_{max}, n_x^{ele}) = \sum_{i=1}^{n_x^{ele}} \frac{\Delta x}{2} \sum_{j=1}^N \omega_j g(x_{ij})$$

(A.14)

with $x_{ij} = x_{i-1}^{node} + \Delta x \frac{\xi_j + 1}{2}$.

By applying A.12 for $g(x_{ij})$, noting that the l^{th} element in y direction is defined two nodes $y_{l-1}^{node}(x_{ij}) = y_{min}(x_{ij}) + (l-1)\Delta y(x_{ij})$ and $y_l^{node}(x_{ij}) = y_{min}(x_{ij}) + l\Delta y(x_{ij})$ we have:

$$g(x_{ij}) = \int_{y_{min}(x_{ij})}^{y_{max}(x_{ij})} f(x_{ij}, y) dy = \sum_{l=1}^{n_y^{ele}} \frac{\Delta y(x_{ij})}{2} \sum_{k=1}^N \omega_k f(x_{ij}, y_{lk})$$

with $y_{lk} = y_{l-1}^{node}(x_{ij}) + \Delta y(x_{ij}) \frac{\xi_k + 1}{2}$

Finally, I_2 can be approximately evaluated by the following operator

$$IGauss_{2D}^N(f, x_{min}, x_{max}, y_{min}, y_{max}, n_x^{ele}, n_y^{ele}) := \sum_{i=1}^{n_x^{ele}} \frac{\Delta x}{2} \sum_{j=1}^N \omega_j \sum_{l=1}^{n_y^{ele}} \frac{\Delta y(x_{ij})}{2} \sum_{k=1}^N \omega_k f(x_{ij}, y_{lk})$$

(A.15)

with $x_{ij} = x_{i-1}^{node} + \Delta x \frac{\xi_j + 1}{2}$

and $y_{lk} = y_{l-1}^{node}(x_{ij}) + \Delta y(x_{ij}) \frac{\xi_k + 1}{2}$.

Appendix B

Calculation of powers

Contents

B.1 Calculation of power of plastic deformation $J_{\dot{\epsilon}}$ for the simple 2D velocity field	183
B.2 Calculation of powers for the simple 3D velocity field	185
B.2.1 Power of plastic deformation $J_{\dot{\epsilon}}$	185
B.2.2 Power of the discontinuity of velocity $J_{\Delta u}$	187
B.2.3 Power of friction J_{fric}	187

B.1 Calculation of power of plastic deformation $J_{\dot{\epsilon}}$ for the simple 2D velocity field

Tensor of deformation rate $\underline{\dot{\epsilon}}$

Given by equation 3.61, the velocity field depends only on x and z and moreover the component $u_y = 0$, there are only 4 components of the deformation rate tensor are different from zero. These are the components in the xz plan :

$$\begin{cases} \dot{\epsilon}_{xx} = \frac{\partial u_x}{\partial x} = -\frac{h_e v_e h'}{h^2} \\ \dot{\epsilon}_{xz} = \dot{\epsilon}_{zx} = \frac{1}{2} \left(\frac{\partial u_x}{\partial z} + \frac{\partial u_z}{\partial x} \right) = \frac{1}{2} z h_e v_e \left(\frac{h'}{h^2} \right)' = \frac{1}{2} z h_e v_e \left[\frac{h''}{h^2} - \frac{2h'^2}{h^3} \right] \\ \dot{\epsilon}_{zz} = -\dot{\epsilon}_{xx}. \end{cases}$$

Power of plastic deformation $J_{\dot{\epsilon}}$

The power of plastic deformation in roll bite is given by

$$\begin{aligned}
 J_{\dot{\epsilon}} &= \int_{\Omega_{emprise}} \sigma_0 \sqrt{\frac{2}{3} \dot{\underline{\epsilon}} : \dot{\underline{\epsilon}}} d\Omega \\
 &= \int_{\Omega_{emprise}} \sigma_0 \sqrt{\frac{2}{3} (\dot{\epsilon}_{xx}^2 + \dot{\epsilon}_{zz}^2 + 2\dot{\epsilon}_{xz}^2)} d\Omega \\
 &= \int_{-L}^0 \int_0^b \int_0^h \sigma_0 \sqrt{\frac{2}{3} \left(\frac{h_e^2 v_e^2}{2h^4} \left[4h'^2 + \left(h'' - \frac{2h'^2}{h} \right)^2 z^2 \right] \right)} dx dy dz \\
 &= \int_{-L}^0 \frac{\sigma_0}{\sqrt{3}} \frac{h_e b_e v_e}{h} \left(\frac{1}{h} \int_0^h \sqrt{4h'^2 + \left(h'' - \frac{2h'^2}{h} \right)^2 z^2} dz \right) dx \\
 &= \int_{-L}^0 \frac{\sigma_0}{\sqrt{3}} \frac{C_{vol}}{h} I dx
 \end{aligned}$$

with

$$\begin{aligned}
 I &= \frac{1}{h} \int_0^h \sqrt{4h'^2 + \left(h'' - \frac{2h'^2}{h} \right)^2 z^2} dz \\
 &= \int_0^1 \sqrt{4h'^2 + (hh'' - 2h'^2)^2 z^{*2}} dz^*
 \end{aligned}$$

where $z^* = \frac{z}{h}$.

We introduce an useful mathematic formula which is used frequently in our calculations :

$$\boxed{\int_0^1 \sqrt{a^2 + c^2 t^2} dt = \frac{1}{2} \left(\sqrt{a^2 + c^2} + \frac{a^2}{c} \ln \frac{c + \sqrt{a^2 + c^2}}{a} \right)}. \quad (B.1)$$

In using B.1 for $a = 2|h'|$, $c = |hh'' - 2h'^2|$ and in noting

$$\begin{cases} I_1 = c = |h.h'' - 2h'^2| \\ I_2 = \sqrt{a^2 + c^2} = \sqrt{4h'^2 + I_1^2} \end{cases}$$

we obtain

$$I = \frac{1}{2} \left(I_2 + \frac{4h'^2}{I_1} \ln \frac{I_1 + I_2}{2|h'|} \right).$$

Therefore,

$$\boxed{J_{\dot{\epsilon}} = \frac{\sigma_0}{2\sqrt{3}} C_{vol} \int_{-L}^0 \left[I_2 + \frac{4h'^2}{I_1} \text{Ln} \left(\frac{I_1 + I_2}{|2h'|} \right) \right] \frac{dx}{h}}. \quad (B.2)$$

B.2 Calculation of powers for the simple 3D velocity field

As a reminder, the simple 3D velocity field is expressed by 5.3 as follows

$$\begin{aligned} u_x(x, y) &= C_{vol} \frac{1}{h(x)\varphi(x)} \\ u_y(x, y) &= C_{vol} \frac{\varphi'(x)y}{h(x)\varphi^2(x)} \\ u_z(x, z) &= C_{vol} \frac{h'(x)z}{h^2(x)\varphi(x)}. \end{aligned} \quad (\text{B.3})$$

B.2.1 Power of plastic deformation $J_{\dot{\underline{\underline{\epsilon}}}}$

Tensor of deformation rate $\underline{\underline{\dot{\epsilon}}}$

Corresponding to this velocity field, all components of $\underline{\underline{\dot{\epsilon}}}$ are :

$$\dot{\epsilon}_{xx} = \frac{\partial u_x}{\partial x} = -\frac{C_{vol}}{h\varphi} \left[\frac{h'}{h} + \frac{\varphi'}{\varphi} \right] \quad (\text{B.4a})$$

$$\dot{\epsilon}_{yy} = \frac{\partial u_y}{\partial y} = \frac{C_{vol}}{h\varphi} \frac{\varphi'}{\varphi} \quad (\text{B.4b})$$

$$\dot{\epsilon}_{zz} = \frac{\partial u_z}{\partial z} = \frac{C_{vol}}{h\varphi} \frac{h'}{h} \quad (\text{B.4c})$$

$$\dot{\epsilon}_{xy} = \dot{\epsilon}_{yx} = \frac{1}{2} \left(\frac{\partial u_x}{\partial y} + \frac{\partial u_y}{\partial x} \right) = \frac{C_{vol}}{2h\varphi} \left[\varphi'' - \frac{h'\varphi'}{h} - \frac{2\varphi'^2}{\varphi} \right] \frac{y}{\varphi} \quad (\text{B.4d})$$

$$\dot{\epsilon}_{xz} = \dot{\epsilon}_{zx} = \frac{1}{2} \left(\frac{\partial u_x}{\partial z} + \frac{\partial u_z}{\partial x} \right) = \frac{C_{vol}}{2h\varphi} \left[h'' - \frac{h'\varphi'}{\varphi} - \frac{2h'^2}{h} \right] \frac{z}{h} \quad (\text{B.4e})$$

$$\dot{\epsilon}_{yz} = \dot{\epsilon}_{zy} = 0. \quad (\text{B.4f})$$

Thus, the power of plastic deformation is calculated as

$$\begin{aligned} J_{\dot{\underline{\underline{\epsilon}}}} &= \int_{\Omega_{emprise}} \sigma_0 \sqrt{\frac{2}{3} \dot{\underline{\underline{\epsilon}}} : \dot{\underline{\underline{\epsilon}}}} d\Omega \\ &= \int_{\Omega_{emprise}} \sigma_0 \sqrt{\frac{2}{3} (\dot{\epsilon}_{xx}^2 + \dot{\epsilon}_{yy}^2 + \dot{\epsilon}_{zz}^2 + 2\dot{\epsilon}_{xy}^2 + 2\dot{\epsilon}_{xz}^2 + 2\dot{\epsilon}_{yz}^2)} d\Omega \\ &= \int_{-L}^0 \int_0^b \int_0^h \sqrt{\frac{2}{3}} \sigma_0 \frac{C_{vol}}{h\varphi} \sqrt{Q^2 + f^2 \left(\frac{y}{b}\right)^2 + g^2 \left(\frac{z}{h}\right)^2} dx dy dz \\ &= \frac{2}{\sqrt{6}} \sigma_0 C_{vol} \int_{-L}^0 \int_0^b \int_0^h \sqrt{Q^2 + f^2 \left(\frac{y}{b}\right)^2 + g^2 \left(\frac{z}{h}\right)^2} dx \frac{dy}{b} \frac{dz}{h} \frac{b}{\varphi} \\ &= \frac{1}{\sqrt{6}} \sigma_0 C_{vol} \int_{-L}^0 \frac{b}{\varphi} \left(2 \int_0^1 \left(\int_0^1 \sqrt{Q^2 + f^2 y^{*2} + g^2 z^{*2}} dz^* \right) dy^* \right) dx \\ &= \frac{\sigma_0}{\sqrt{6}} C_{vol} \int_{-L}^0 P_x dx \end{aligned}$$

where

$$\begin{aligned}
 Q &= \sqrt{2\frac{h'^2}{h^2} + 2\frac{\varphi'^2}{\varphi^2} + 2\frac{h'\varphi'}{h\varphi}} \\
 f &= \frac{1}{\sqrt{2}} \left| \varphi'' - \frac{h'\varphi'}{h} - 2\frac{\varphi'^2}{\varphi} \right| \frac{b}{\varphi} \\
 g &= \frac{1}{\sqrt{2}} \left| h'' - \frac{h'\varphi'}{\varphi} - 2\frac{h'^2}{h} \right|.
 \end{aligned}
 \tag{B.5}$$

We calculate now the P_x in using the formula B.1 for $a = \sqrt{Q^2 + f^2y^{*2}}$ et $c = g$:

$$\begin{aligned}
 P_x &= 2\frac{b}{\varphi} \int_0^1 \left(\int_0^1 \sqrt{Q^2 + f^2y^{*2} + g^2z^{*2}} dz^* \right) dy^* \\
 &= \frac{b}{\varphi} \int_0^1 \left[\sqrt{Q^2 + f^2y^{*2} + g^2} + \frac{Q^2 + f^2y^{*2}}{g} \ln \frac{g + \sqrt{Q^2 + g^2 + f^2y^{*2}}}{\sqrt{Q^2 + f^2y^{*2}}} \right] dy^*
 \end{aligned}$$

For the first term in the integral, we could also apply the formula B.1 for $a = \sqrt{Q^2 + g^2}$ et $c = f$. And for the second, we use two following formulas :

$$\begin{aligned}
 I_1(a, b, c) &= \int_0^c \ln(\sqrt{a^2 + x^2} + b) dx \\
 &= c \ln(b + \sqrt{a^2 + c^2}) - c + \ln \frac{c + \sqrt{a^2 + c^2}}{a} + 2\sqrt{a^2 - b^2} \arctan \left(\frac{\sqrt{a-b} \sqrt{a^2 + c^2} - a}{a+b} \right)
 \end{aligned}
 \tag{B.6}$$

and

$$\begin{aligned}
 I_2(a, b, c) &= \int_0^c x^2 \ln(\sqrt{a^2 + x^2} + b) dx \\
 &= \frac{1}{3} \left[c^3 \ln(b + \sqrt{a^2 + c^2}) + (a^2 - b^2)c - \frac{c^3}{3} + \frac{bc}{2} \sqrt{a^2 + c^2} \right. \\
 &\quad \left. - 2(a^2 - b^2)^{\frac{3}{2}} \arctan \left(\frac{\sqrt{a-b} \sqrt{a^2 + c^2} - a}{a+b} \right) - \frac{b}{2} (3a^2 - 2b^2) \ln \frac{c + \sqrt{a^2 + c^2}}{a} \right]
 \end{aligned}
 \tag{B.7}$$

We obtain finally

$$J_{\dot{\epsilon}} = \frac{\sigma_0}{\sqrt{6}} C_{vol} \int_{-L}^0 P_x(x) dx
 \tag{B.8}$$

with

$$\begin{aligned}
 P_x &= \frac{b}{\varphi} \left\{ \frac{2}{3} \sqrt{Q^2 + f^2 + g^2} + \frac{Q^2 + \frac{1}{3}f^2}{g} \text{Ln} \left(\frac{g + \sqrt{Q^2 + f^2 + g^2}}{\sqrt{Q^2 + f^2}} \right) + \frac{Q^2 + \frac{1}{3}g^2}{f} \text{Ln} \left(\frac{f + \sqrt{Q^2 + f^2 + g^2}}{\sqrt{Q^2 + g^2}} \right) \right. \\
 &\quad \left. + \frac{4Q^3}{3fg} \left[\arctan \left(\frac{Qg}{(\sqrt{Q^2 + f^2} + f)(\sqrt{Q^2 + f^2 + g^2} + \sqrt{Q^2 + f^2})} \right) - \arctan \left(\frac{g}{\sqrt{Q^2 + g^2} + Q} \right) \right] \right\}
 \end{aligned}$$

B.2.2 Power of the discontinuity of velocity $J_{\Delta u}$

$$\begin{aligned}
 J_{\Delta u} &= \int_{S_{discontinues}} \frac{\sigma_0}{\sqrt{3}} [|\underline{V}|] dS \\
 &= \frac{\sigma_0}{\sqrt{3}} \int_0^{b_e} \int_0^{h_e} \sqrt{u_y^2(x = -L, y) + u_z^2(x = -L, z)} dydz \\
 &= \frac{\sigma_0}{\sqrt{3}} \int_0^{b_e} \int_0^{h_e} \sqrt{v_e^2 \frac{\varphi'^2(-L)y^2}{b_e^2} + v_e^2 \frac{h'^2(-L)z^2}{h_e^2}} dydz \\
 &= \frac{\sigma_0}{\sqrt{3}} C_{vol} \int_0^1 \int_0^1 \sqrt{\varphi'^2(-L)y^{*2} + h'^2(-L)z^{*2}} dy^* dz^*.
 \end{aligned}$$

The calculation is performed similarly to that of P_x and we receive :

$$J_{\Delta u} = \frac{\sigma_0}{\sqrt{3}} C_{vol} \left[\frac{\sqrt{\varphi_e'^2 + h_e'^2}}{3} + \frac{h_e'^2}{6|\varphi_e'|} \text{Ln} \left(\frac{|\varphi_e'| + \sqrt{\varphi_e'^2 + h_e'^2}}{|h_e'|} \right) + \frac{\varphi_e'^2}{6|h_e'|} \text{Ln} \left(\frac{|h_e'| + \sqrt{\varphi_e'^2 + h_e'^2}}{|\varphi_e'|} \right) \right] \quad (\text{B.9})$$

B.2.3 Power of friction J_{fric}

$$\begin{aligned}
 J_{fric} &= \int_{S_{contact}} \tau [|\underline{V}|] dS \\
 &= \int_{-L}^0 \int_0^b \frac{m\sigma_0}{\sqrt{3}} \sqrt{\left(\sqrt{u_x^2(x) + u_z^2(x, z = h)} - V_c \right)^2 + u_y^2(x, y)} dy \sqrt{1 + h'^2} dx \\
 &= \int_{-L}^0 \int_0^b \frac{m\sigma_0}{\sqrt{3}} \sqrt{\left(\sqrt{1 + h'^2} \frac{C_{vol}}{h\varphi} - V_c \right)^2 + \left(\frac{C_{vol}}{h\varphi} \frac{\varphi' y}{\varphi} \right)^2} dy \sqrt{1 + h'^2} dx \\
 &= \frac{m\sigma_0}{\sqrt{3}} C_{vol} \int_{-L}^0 \frac{b}{\varphi} \frac{\sqrt{1 + h'^2}}{h} \int_0^1 \sqrt{\left(\sqrt{1 + h'^2} - \frac{h\varphi V_c}{C_{vol}} \right)^2 + \frac{b^2}{\varphi^2} \varphi'^2 y^{*2}} dy^* dx
 \end{aligned}$$

In noting $J = \left| \sqrt{1 + h'^2} - \frac{h\varphi V_c}{C_{vol}} \right|$ and in using the formula B.1 for $a = J$ et $c = b'$, we have

$$J_{fric} = \frac{m\sigma_0 C_{vol}}{2\sqrt{3}} \int_{-L}^0 \frac{b}{\varphi} \frac{\sqrt{1 + h'^2}}{h} \left[\sqrt{\varphi'^2 + J^2} + \frac{J^2}{|\varphi'|} \text{Ln} \left(\frac{|\varphi'| + \sqrt{\varphi'^2 + J^2}}{J} \right) \right] dx. \quad (\text{B.10})$$

Appendix C

Experiment on narrow strips

Contents

C.1 Rolling parameters	189
C.2 Lam3-Tec3 modeling	190

C.1 Rolling parameters

Two types of steel are experimented, one has low flow stress and the other has very high flow stress. We present all the rolling parameters in the two following tables C.1 and C.2.

DWI					
Roll diameter	400	mm			
Limit of elasticity	280	Mpa			
Roll speed	25	m/min			
<i>EXPERIMENT</i>					
Samples	E1	E3	E5	E6	E7
Entry tension (kg/mm ²)	1.210	1.214	8.290	8.235	7.830
Exit tension (kg/mm ²)	2.025	2.187	10.571	12.029	12.954
Entry thickness measured (mm)	3.182	3.175	3.146	3.165	3.161
Exit thickness measured (mm)	2.749	2.233	2.755	2.383	2.213
Entry width measured (mm)	75.350	75.250	75.150	75.200	75.150
Exit width measured (mm)	75.450	75.750	75.200	75.350	75.350
Longitudinal friction (Coulomb)		0.0349	0.0595	0.0420	0.0423
Transverse friction (Coulomb)		0.1396	0.2380	0.1680	0.1692
<i>Width spread measured</i> in mm	0.10	0.50	0.05	0.15	0.20
<i>Forward slip measured</i> (%)	1.40	0.56	1.79	1.37	1.47
<i>Lam3-Tec3</i>					
COULOMB longitudinal friction coefficient	0.0520	0.0382	0.0600	0.0428	0.4260
COULOMB transverse friction coefficient	0.1405	0.1032	0.1622	0.1712	1.7040
Width spread calculated by <i>Lam3-Tec3</i> (mm)	0.179	0.659	0.052	0.165	0.232
<i>UBM</i>					
Tresca isotropic friction coefficient	0.105	0.080	0.085	0.065	0.063
Width spread calculated by UBM (mm)	0.134	0.571	0.053	0.160	0.211

Table C.1: Experiment and results obtained by different methods for **DWI** steel trials.

Soldur							
Roll diameter	400	mm					
Limit of elasticity	933	Mpa					
Roll speed	25	m/min					
<i>EXPERIMENT</i>							
Samples	E16	E18	E19	E20	E22	E23	E24
Entry tension (kg/mm ²)	3.804	7.620	7.843	7.551	2.534	3.170	5.860
Exit tension (kg/mm ²)	3.735	5.786	7.794	8.902	5.226	5.009	21.359
Entry thickness measured (mm)	1.310	1.308	1.312	1.320	1.310	1.309	1.304
Exit thickness measured (mm)	0.872	1.139	0.987	0.824	1.133	0.981	0.898
Entry width measured (mm)	60.20	60.20	60.25	60.20	60.25	60.25	60.20
Exit width measured (mm)	61.40	60.70	61.10	61.35	60.80	61.05	61.00
<i>Width spread measured</i> (mm)	1.20	0.50	0.85	1.15	0.55	0.80	0.80
<i>Forward slip measured</i> (%)	4.86	1.79	3.85	4.86	2.38	3.84	3.79
<i>Lam3-Tec3</i>							
COULOMB longitudinal friction coefficient	0.04961	0.0564	0.0569	0.04879	0.05698	0.05272	
COULOMB transverse friction coefficient	0.0992	0.1128	0.1138	0.09758	0.1139	0.0701	
Width spread calculated by <i>Lam3-Tec3</i> (mm)	1.29	0.87	1.06	1.36	0.89	1.13	
<i>UBM</i>							
Tresca isotropic friction coefficient	0.085	0.060	0.085	0.075	0.070	0.080	0.043
Width spread calculated by UBM (mm)	1.136	0.204	0.587	1.343	0.228	0.655	0.914

Table C.2: Experiment and results obtained by different methods for **Soldur** steel trials.

C.2 Lam3-Tec3 modeling

In order to verify the validity of *Lam3-Tec3* we model these trials with *Lam3-Tec3* and compare the results with the measurement. For the soldur steel, the strips are rectangular *i.e* flat. The old modeling *Lam3-Tec3* previously performed is credible. The results are presented in the tables C.2. However, for the **DWI** steel, they are crowned *i.e* their entry profiles are not rectangular. Therefore, we remodel these trails in taking into account the entry profile of the strips. We note that, the rheology of the steel is measured and the only unknown is the friction which can be isotropic or not.

In observing that the longitudinal friction coefficient μ_x influence only the forward slip and the transversal one μ_y has an important impact on the exit profile of the strips. Therefore, the μ_x is obtained when it gives a good forward slip and the μ_y is determined by comparison of the exit profile calculated by *Lam3-Tec3* with the measured. We present here the entry and exit profile in modeling *Lam3-Tec3* in compare with the measured ones for all the trials on the **DWI** steel.

In modeling *Lam3-Tec3*, the entry profile is devised into two parts. At the centre of the strip, the thickness is modeled constant and equal to the average of the measured thickness in this part. While at the edge part the profile is complicated, coming from the operation of edge cutting, and therefore, we have to approach the measured points by a polynomial of degree 8 and use this polynomial in *Lam3-Tec3* calculation. They are showed in the left hand side of the following figures.

We determine next the longitudinal friction coefficient μ_x by the way mentioned previously in concerning that the friction is isotropic. The details are not necessary to be presented. Only the results obtained are given the tables C.1 and C.2. Then we vary the transversal friction coefficient μ_y to obtain the best exit profile of the strips. The figures in the right hand side show the relative thickness, *i.e* the centre thickness is normalized to 1, calculated by *Lam3-Tec3* with the best value of the μ_y which give the best exit profiles in comparison with experiment. The final results on these trials are presented in the table C.1.

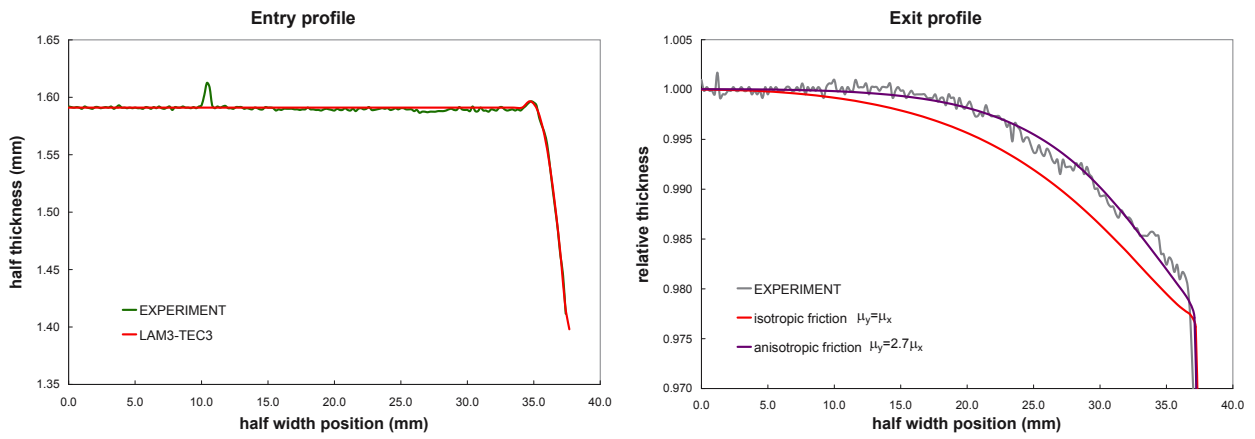


Figure C.1: Sample E1. Comparison between *Lam3-Tec3* and experiment.

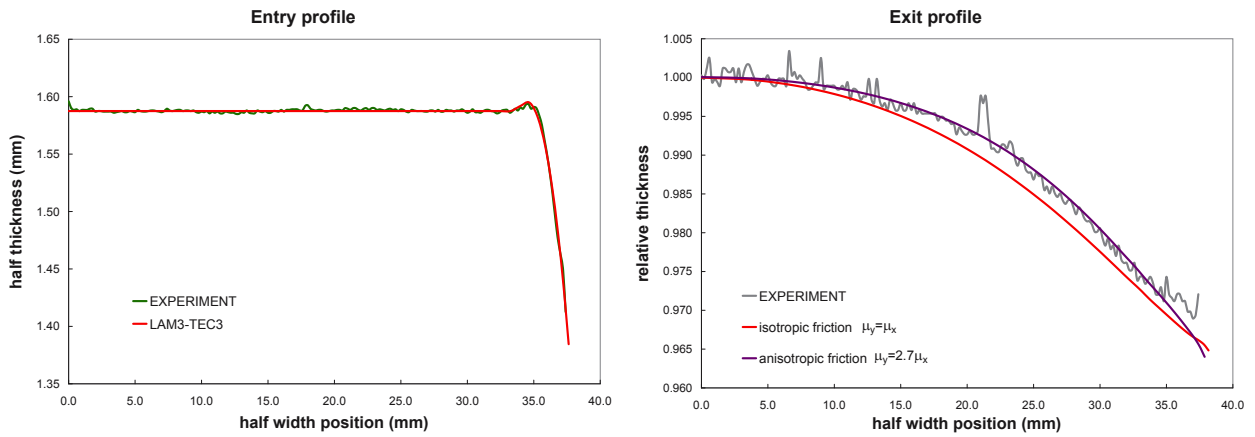


Figure C.2: Sample E3. Comparison between *Lam3-Tec3* and experiment.

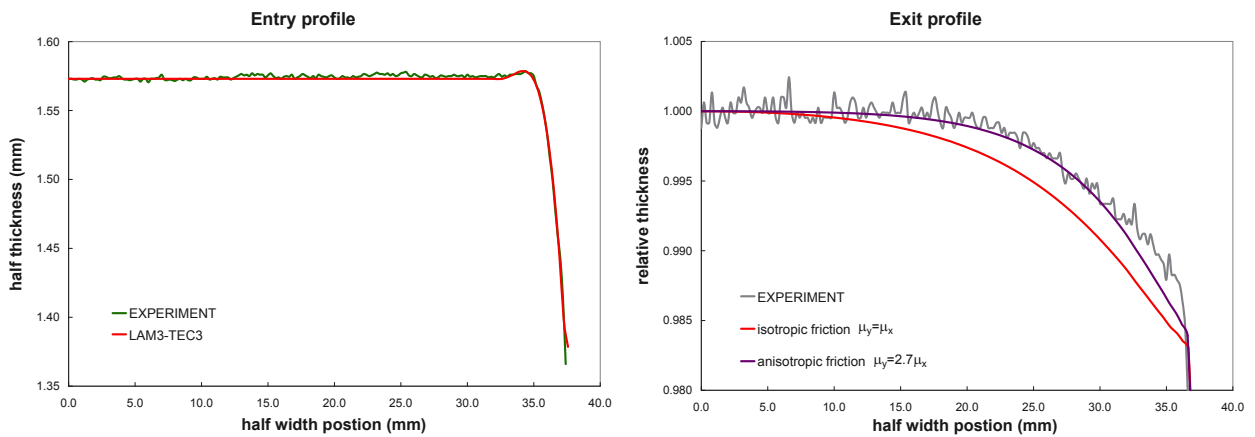


Figure C.3: Sample E5. Comparison between *Lam3-Tec3* and experiment.

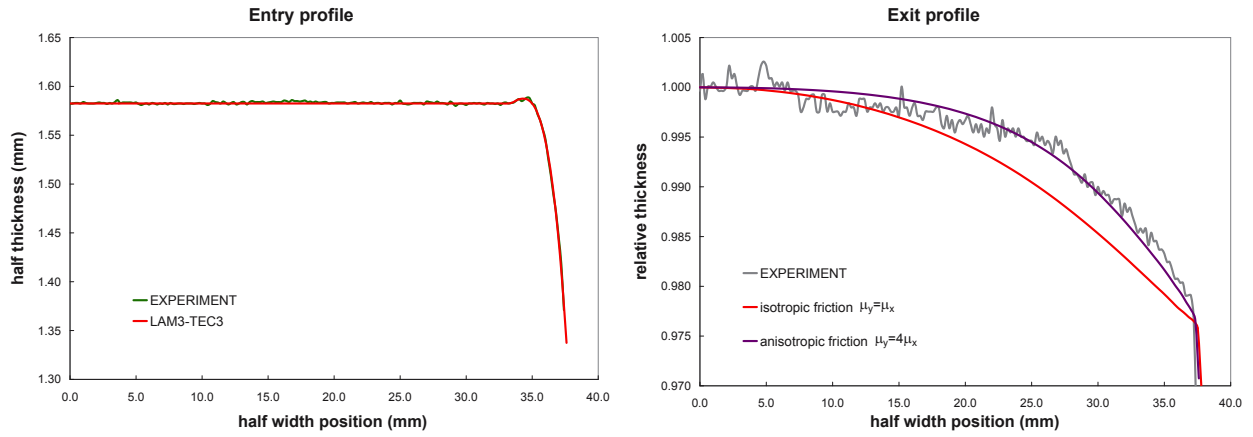


Figure C.4: Sample E6. Comparison between *Lam3-Tec3* and experiment.

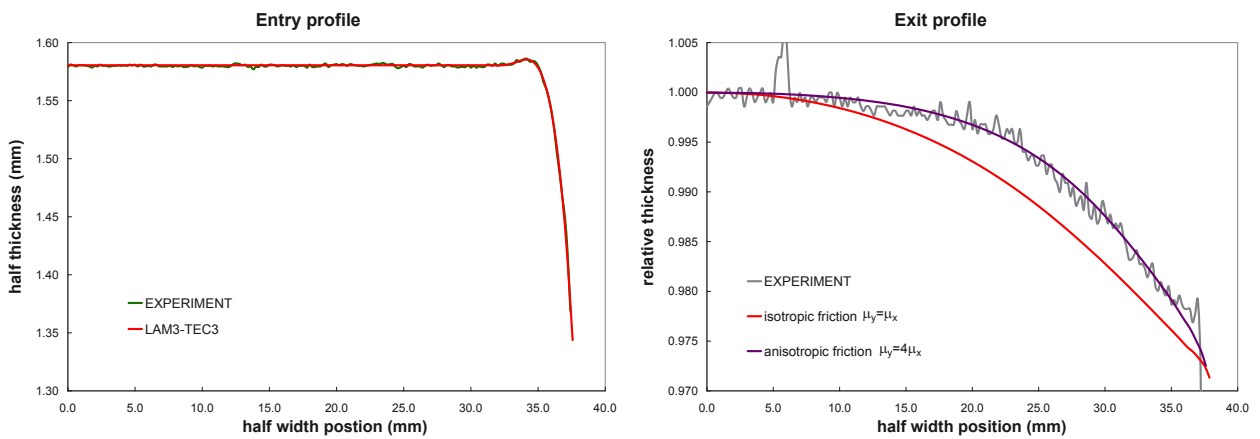


Figure C.5: Sample E7. Comparison between *Lam3-Tec3* and experiment.

Bibliography

- [1] K. Abrinia et A. Fazlirad. Three-dimensional analysis of shape rolling using a generalized upper bound approach. *journal of materials processing technology*, 209:3264–3277, 2009.
- [2] J. M. Alexander. On the theory of rolling. *Proc. R. Soc. Lond., A*, 326:535–563, 1972.
- [3] J. M. Allwood. A hybrid 2.5 dimensional elastoviscoplastic model of hot strip rolling for practical applications. *Simulation of Materials Proc: Theory, Methods and Appl*, pages 519–525, 2001.
- [4] S. Andersson, A. Söderberg et S. Björklund. Friction models for sliding dry, boundary and mixed lubricated contacts. *Tribology International*, 40:580–587, 2007.
- [5] B. Avitzur. Maximum reduction in cold strip rolling. *Proc. Inst. Mech. Engrs.*, 174:865–884, 1963.
- [6] B. Avitzur. Power analysis of cold strip rolling. *ASME Journal of Engineering for Industry*, 85:77–88, 1963.
- [7] B. Avitzur. An upper bound approach to cold strip rolling. *ASME Journal of Engineering for Industry*, 86:31–48, 1964.
- [8] B. Avitzur. *Metal Forming: Process and Analysis, Article Nos. [5], [15]*. 1968.
- [9] B. Avitzur. *Metal Forming: Application of Limit Analysis*. 1980.
- [10] B. Avitzur et W. Pachla. The upper bound approach to plan strain problems using linear and rotational velocity fields - part i: Basic concepts. *Journal of Engineering for Industry*, 108:295–306, 1986.
- [11] B. Avitzur et W. Pachla. The upper bound approach to plan strain problems using linear and rotational velocity fields - part ii: Applications. *Journal of Engineering for Industry*, 108:307–316, 1986.
- [12] B. Avitzur, S. Talbert et W. Gordon. Analysis of strip rolling by the upper bound approach. *J. Engineering for Industry*, 109(4):338–346, 1987.
- [13] M. J. M. Barata-Marques et P. A. F. Martins. The use of dual stream functions in the analysis of three dimensional metal forming process. *Int. J. Mech. Sci.*, 33:313–323, 1991.
- [14] J. G. Beese. Nomograms for predicting the spread of hot rolled slabs. *AISE Yearly Preceddings*, pages 251–252, 1972.
- [15] D. R. Bland et R. B. Sims. *Proc. Inst. Mech. Engrs*, 167:371, 1953.
- [16] D. Bland et H. Ford. The calculation of roll force and torque in cold strip rolling with tensions. *Proc. Instn. Mech. Eng*, 159:144–153, 1948.
- [17] D. Bland et H. Ford. Part iii - an approximate treatment of the elastic compression of the strip in cold rolling. *J. Iron Steel Inst*, 171:245–249, 1952.
- [18] S. Bouharaoua, G. Deffrennes, L. Lampin et M. Rivallain. A la recherche d'une modélisation simplifiée du laminage. Master's thesis, Ecole Nationale des Ponts et Chaussées, 2006.

- [19] G. F. Bryant et R. Osborn. Derivation and assessment of roll force models. *The iron and steel institute, London*, Chap. 12:245, 1973.
- [20] G. F. Bryant et R. Osborn. Derivation and assessment of simplified models for torque, slip and neutral angle. *The iron and steel institute, London*, Chap. 13:279, 1973.
- [21] J. Campas, S. Terreaux, L. V. des Roches, B. Bonvier et D. Janczak. New online gage for edge drop measurement and effect of tapered work rolls. *Iron and Steel Engineer*, pages 27–32, December 1995.
- [22] C. Camurri et S. Lavanchy. Application de la théorie des lignes de glissement au laminage à froid de tôle. *Journal de Mécanique Théorique et Appliquée*, 3(5):747–759, 1984.
- [23] C. Counhaye. *Modélisation et contrôle industriel de la géométrie des aciers laminés à froid*. PhD thesis, UNIVERSITE DE LIEGE, 2000.
- [24] A. S. Chai. Simulation. 10:221–233, 1968.
- [25] J.-L. Chenot, P. Montmitonnet, A. Bern et C. Bertrand-Corsini. A method for determining free surfaces in steady state finite element computations. *Comp. Meth. Appl. Mech. Eng.*, 92,2:245–260, 1991.
- [26] M. S. Chun, J. J. Yi et Y. H. Moon. Application of neural networks to predict the width variation in a plate mill. *Journal of Materials Processing Technology*, 111:146–149, 2001.
- [27] P. Cosse et M. Economopoulos. Mathematical study of cold rolling,. *C.N.R.M.*, 17:15–32, 1968.
- [28] R. Courant. *Differential and integral calculus*. Vol. I, Nordeman Publishing CO., New York, 1945.
- [29] M. Cozijnsen, A. Dixon et W. Y. D. Yuen. Development of a shape model that includes edge spread for cold rolling. *Steel rolling International conference; 9th, Steel rolling; 56*, Paris June 2006.
- [30] A. Dixon et W. Y. D. Yuen. An analytical model for the lateral spread and shape defects from the rolling of a ridge profile or edge drop. *44th MWSP Conf. Proc., Vol. XL, ISS, September 8-11, Orlando, USA*, pages 267–278, 2002.
- [31] A. N. Dogruoglu. On constructing kinematically admissible velocity fields in cold sheet rolling. *Journal of Materials Processing Technology*, 110:287–299, 2001.
- [32] H. Dusser, J. L. Larrodera et N. L. P. Francois. Improved cooling on cold tandem mills. *Rolling conference - Paris*, 2006.
- [33] W. J. Edwards. Width contraction in cold rolling. *Metals Technology*, page 86, 1975.
- [34] S. Eklund. *Jernkontorets*, 111:39, 1927.
- [35] K. E. H. A. El-Kalay et L. G. M. Sparling. Factors affecting friction and their effect upon load, torque and spread in hot flat rolling. *JISI*, 2:152–163, 1968.
- [36] N. A. Fleck et K. L. Johnson. Towards a new theory of cold rolling thin foil. *J. Mech. Sci*, Vol 29, No7:507–524, 1987.
- [37] H. Ford, F. Ellis et D. R. Bland. *J. Iron Steel Inst*, 168:57, 1951.
- [38] A. Fouratier, A. Lucas, J. H. Bianchi, P. Vescovo, F. Dionisi et P. D. Putz. Control of sheet surface defects and deep drawing in final strips production steps. Technical report, European Commission, technical steel research, 2007.
- [39] I. J. Freshwater. Simplified theories of flat rolling - i: The calculation of roll pressure, roll force and roll torque. *Int. J. Mech. Sci.*, 38, No. 6:633–648, 1996.
- [40] A. Hacquin. *Modélisation thermomécanique 3D du laminage: couplage bande-cylindres (3D thermomechanical modelling of rolling processes strip-roll coupling)*, PhD Dissertation. PhD thesis, Ecole des Mines de Paris, 1996.

- [41] J. Hadamard. Sur les problèmes aux dérivées partielles et leur signification physique. *Princeton University Bulletin*, pages 49–52, 1902.
- [42] H. Hartung, F. W. Hollmann et R. Holz. A new way to reduce the edge drop. *Steel research* 69, pages 143–147, 1998.
- [43] A. Helmi et J. M. Alexander. Geometrics factors affecting spread in hot flat rolling of steel. *Journal of the Iron and Steel Institute*, 206:1110–1117, 1968.
- [44] R. Hill. A comparative study of some variational principles in the theory of plasticity. *J. Appl. Mech.*, 17:64–66, 1950.
- [45] R. Hill. *The Mathematical theory of Plasticity*. Clarendon Press, 1950.
- [46] J. H. Hitchcock. Roll neck bearings. *A.S.M.E Report of Special Research Committee*, 1935 June.
- [47] T. Hoang. Asymmetric rolling analysis - energy saving and ski effect. Master's thesis, Ecole Nationale des Ponts et Chaussées, 2006.
- [48] Y. M. Hwang et H. H. Hsu. An investigation into the plastic deformation behavior at the roll gap during plate rolling. *Journal of Materials Processing Technology*, 88:97–104, 1999.
- [49] Z. Y. Jiang et A. K. Tieu. A 3-d finite element method analysis of cold rolling of thin strip with friction variation. *Tribology International*, 37:185–191, 2004.
- [50] K. L. Johnson et R. H. Bantall. The onset of yield in the cold rolling of thin strip. *Mech. Phys. Solids*, 17:253, 1969.
- [51] W. Johnson et P. B. Mellor. *Engineering Plasticity*. 1973.
- [52] D. Jortner, J. F. Osterle et C. F. Zorowski. An analysis of cold strip rolling. *Int. J. Mech. Sci. Pergamon Press*, 2:179–194, 1960.
- [53] M. Kazeminezhad et A. K. Taheri. A theoretical and experimental investigation on wire flat rolling process using deformation pattern. *Materials and Design*, pages 99–103, 2005.
- [54] N. Kim, T. Altan et S. Kobayashi. Three-dimensional analysis and computer simulation of shape rolling by the finite and slab element method. *International Journal of Machine Tools Manufacture*, 31:553–563, 1991.
- [55] S. Y. Kim et Y. T. Im. Three dimensional finite element analysis of non-isothermal shape rolling. *Journal of Materials Processing Technology*, 127:57–63, 2002.
- [56] K. Kitamura, T. Nakanishi, I. Yarita, N. Sugauma et K. Toyoshima. Edge-drop control of hot and cold rolled strip by tapered-crown roll shifting mill. *Iron and Steel Engineer*, pages 27–32, 1995.
- [57] M. Kiuchi et B. Avitzur. Limit analysis of flow through inclined converging planes. *ASME J. Engrg. Ind.*, 102(2):109–117, 1980.
- [58] K. Komori. Rigid-plastic finite element method for analysis of three dimensional rolling that requires small memory capacity. *Int. J. Mech. Sci.*, 40:479–491, 1998.
- [59] K. Komori. An upper bound method for analysis of three-dimensional deformation in the flat rolling of bars. *International Journal of Mechanical Sciences*, 44:37–55, 2002.
- [60] D. Lafontaine. Première approche sur le rétreint au cours du laminage à froid. Technical report, Internal report, Sollac Ste Agathe 02/70 DL, 2002.
- [61] G. D. Lahoti, S. N. Shah et T. Altan. Computer-aided analysis of deformations and temperatures in strip rolling. *ASME J. Engrg. Ind.*, 100:159–166, 1978.
- [62] A. C. W. Lau, R. Shivpuri et P. C. Chou. An explicit time integration elastic-plastic finite element algorithm for analysis of high speed rolling. *Int. J. Mech. Sci.*, 31(7):483–497, 1989.

- [63] H. C. Lee et S. Kobayashi. New solution to rigid-plastic deformation problems using a matrix method. *ASME J. Engrg. Ind.*, 95:865–873, 1973.
- [64] N. Legrand, B. Becker et C. Roubin. Towards a better width control in cold rolling of flat steel strips. *Steel rolling 2006 Congress, June 19-21, 2006, Paris, La Défense*, 2006.
- [65] N. Legrand et Q. T. Ngo. Rfcs rapport de l'étude sur la variation de largeur en usine à froid. Technical report, ArcelorMittal, 2011.
- [66] G. J. Li et S. Kobayashi. Rigid-plastic finite element analysis of plane strain rolling. *ASME J. Engrg. Ind.*, 104:55–64, 1982.
- [67] Y. H. Li, A. Randall, W. J. Lawrence et C. A. Fryer. Roll force model for online application in hot strip rolling with varying friction conditions. *Steel rolling 2006 Congress, June 19-21, Paris, La Défense*, 2006.
- [68] C. Liu, P. Hartley, C. E. N. Sturgess et G. W. Rowe. Analysis of stress and strain distributions in slab rolling using an elastic-plastic finite-element method. *International Journal for Numerical Methods in Engineering*, 25:55–66, 1988.
- [69] H. M. Liu, J. Dan et Y. R. Wang. Strip layer method for simulation of the 3d deformations of plate and strip rolling. *Comm. Numer. Methods Engrg*, 20:183–191, 2004.
- [70] A. A. Markov. On variational principles in the theory of plasticity (russian). *Prikladnaia Matematika i Mekhanika*, 11:339–350, 1947.
- [71] P. A. F. Martins et M. J. M. Barata-Marques. Upper bound analysis of plane strain rolling using a flow function and the weighted residuals method. *Int. J. Numer. Meth. Eng*, 44:1671–1683, 1999.
- [72] H. Matsumoto. Elastic-plastic theory of cold and temper rolling. *The Japan Society for Technology of Plasticity*, 49 no 565, 2007.
- [73] H. Matsumoto et T. Kawanami. Mechanism of material deformation related to shape and crown phenomena. *Proc. 4 th Int. Steel Rolling Conf., Deauville*, 6:1–12, 1987.
- [74] Y. Mitai et H. Iribe. Analysis of strip rolling by three-dimensionnal rigid plastic fem. *Nippon Steel Technical report n°52*, pages 1–5, 1992.
- [75] P. Montmitonnet. Laminage - objectifs et modélisation. *Technique de l'ingénieur*, MC1(Ref. Number M 3 065):M 3065, 2002.
- [76] P. Montmitonnet, J. Chenot, C. Bertrand-Corsini, C. David, T. Iung et P. Buessler. A coupled thermomechanical approach for hot rolling by a 3d finite element method. *Transactions of ASME Journal of Engineering for Industry*, 114:336–344, 1992.
- [77] K. Mori et K. Osakada. Simulation of three-dimensional deformation in rolling by the finite element method. *Int. J. Mech. Sci*, 26 (9-10):515–525, 1984.
- [78] K. Mori et K. Osakada. Finite element simulation of three-dimensional deformation in shape rolling. *International Journal for Numerical Methods in Engineering*, 30:1431–1440, 1990.
- [79] K. Mori et K. Osakada. Non-steady-state simulation of three-dimensional deformation around front and rear ends in shape rolling by the finite element method. *Transactions of NAMRI/SME*, 19:9–14, 1991.
- [80] A. Nadai. *Plasticity*. McGraw-Hill, New York and London, 1931.
- [81] A. Nadai. The forces required for rolling steel strip under tension. *Appl. Mech. ASME*, 1939.
- [82] T. Oda, N. Satou et T. Yabuta. Adaptive technology for thickness control of finisher set-up on hot strip mill. *ISIJ International*, 35, No. 1:42–49, 1995.

- [83] S. I. Oh et S. Kobayashi. An approximate method for a 3d analysis of rolling. *Int. J. Mech. Sci*, 17:293–305, 1975.
- [84] T. Okamoto, H. Kimura, K. Nakagowa et M. Ando. Measurement and estimation of mean flow stress and coefficient of friction in tandem mills. *IFTAC 8th Triennial World Congress*, pages XVIII–112–117, August 24-28, 1981, Kyota Japan.
- [85] A. Orban, D. Steinier et C. Counhaye. Shape control in cold rolling. in: *Proc. 6th Int. Rolling Conf. (METEC)*, pages 257–265, 1994.
- [86] E. Orowan. The calculation of roll pressure in hot and cold flat rolling. *Proc. Instn. Mech. Engrg*, 150:146–167, 1943.
- [87] J. Z. Pan, W. Pachla, S. Rossenberg et B. Avitzur. The study of distorted grid pattern for flow through conical converging dies by the multi-triangular velocity field. *ASME J. Engrg. Ind*, 106(2):150–160, 1984.
- [88] M. J. Peretic, J. Seidel et S. Kraemer. Coordinated application of roll gap lubrication, work roll cooling and antipeeling systems in hot rolling mills. *Iron and Steel Technology*, pages 27–36, May 2004.
- [89] V. Piispanen. Plastic deformation of metal: theory of simulated sliding. *wear*, 38(1):43–72, 1976.
- [90] D. Pirus. Modèle d'élargissement d'une bande laminée en emprise sous traction dans une cage de train finisseur par la méthode borne supérieure. Master's thesis, Institut supérieur d'informatique et d'automatique de Lorraine, 1992.
- [91] W. Prager et P. G. Hodge-Jr. *Theory of perfectly plastic solids*. 1951.
- [92] L. Prandtl. *Zeitschrift für angewandte Mathematik und Mechanik*, 3:401, 1923.
- [93] Z. Quan. Deformation characteristics of the cross shear cold rolling (cscr) of ultra thin strip and the theory of the "elastic plug". *Proc. Adv. Technol. Plastic*, 2:1173, 1984.
- [94] A. B. Richelsen et V. Tvergaard. 3d analysis of coldrolling using a constitutive model for interface friction. *International Journal of Mechanical Sciences*, 46:653–671, 2004.
- [95] M. A. Sadowsky. A principle of maximum plastic resistance. *J. Appl. Mech*, 10:A65–68, 1943.
- [96] Y. Saito, Y. Kusumoto, T. Hattori et K. Kato. Deformation analysis in shape rolling using an upper bound method. *Journal of Advanced Technology of Plasticity*, 11:1190–1199, 1984.
- [97] R. Schrodter et al. Roll lubrication trials at eko stahl's hot strip mill. *La Revue de Metallurgie-CIT*, pages 1033–1044, Nov 2001.
- [98] R. Schwarz et D. Vallet. Etude de la variation de largeur au tandem 4 cages de sollac blanche. *Revue de la métallurgie*, pages 83–87, 12-1994.
- [99] S. Serek, B. Aksakal et Y. Can. Analysis of cold and hot plate rolling using dual stream functions. *Materials and Design*, 29:584–596, 2008.
- [100] E. Siebel. *Stahl und Eisen*, 45:1563, 1925.
- [101] E. Siebel. Die formgebung in bildsame zu-stande (forming in plastic stage). page 91, 1932.
- [102] E. Siebel et W. Lueg. *Mitteilungen aux dem Kaiser Wilhelm Institut für Eisenforschung, Düsseldorf*, 53 - Part 1:346, 1933.
- [103] R. B. Sims. The calculation of roll force and torque in hot rolling mills. *Proc. Inst. Mech. Engrs*, 108:191–200, 1954.
- [104] L. G. M. Sparling. Formula for spread in hot flat rolling. *Proc. Instn. Mech. Engrs*, 17-1, 1961.

- [105] D. Steiner et al. Optimization of work roll lubrication at the hot strip mill. *La Revue de Metallurgie-CIT*, pages 1046–1053, Nov 2001.
- [106] A. Stephany. Contribution à l'étude numérique de la lubrification en régime mixte en laminage à froid. Master's thesis, Université de Liège, ArcelorResearch, 2006.
- [107] R. Stribeck. Die wesentlichen eigenschaften der gleit- und rollenlager. *Z Ver Dtsch Zucker-Ind*, 45(36), 1902.
- [108] S. TIMOSHENKO et J. N. GOODIER. *Theory of Elasticity*. McGraw-Hill, New York, 1951.
- [109] Y. Tozawa, T. Ishikawa et N. Iwata. Predicting the profile of rolled strip. *Steel Rolling Conference, Swansea*, pages 787–796, 1982.
- [110] A. I. Tselikov. Effect of external friction and tension on the pressure of the metal on the roll in rolling. *Metallurg*, 6, 1939.
- [111] R. Venter et A. Abd-Rabbo. Modelling of the rolling process - i: Inhomogeneous deformation model. *Int. J. Mech. Sci.*, 22:83–92, 1980.
- [112] R. Venter et A. Abd-Rabbo. Modelling of the rolling process - ii: Evaluation of the stress distribution in the rolled material. *Int. J. Mech. Sci.*, pages 93–98, 1980.
- [113] T. von. Karman. Beitrag zur theorie des walzvorgangesbeitrag zur theorie des walzvorganges. *Zeitschrift für angewandte mathematik und mechanik*, 5:139–141, 1925.
- [114] J.-P. Wanga, W.-C. Koa, H.-D. Leea et J. Wang. Analysis of 3d rolling forming with generalized rigid-plastic boundaries approach. *journal of materials processing technology*, 204:425–433, 2008.
- [115] Z. Wusatowski. Hot rolling. *Iron and Steel*, pages 89–94, 1955.
- [116] S. W. Xiong, J. M. C. Rodrigues et P. A. F. Martins. Application of the element-free galerkin method to the simulation of plane strain rolling. *Eur. J. Mech. A/Solids*, 23:77–93, 2004.
- [117] C. S. Yih. Stream functions in three dimensional flows. *La Houille Blanche*, 12:445, 1957.